DOE Office of Nuclear Energy

Fuel Resources
Uranium from Seawater Program

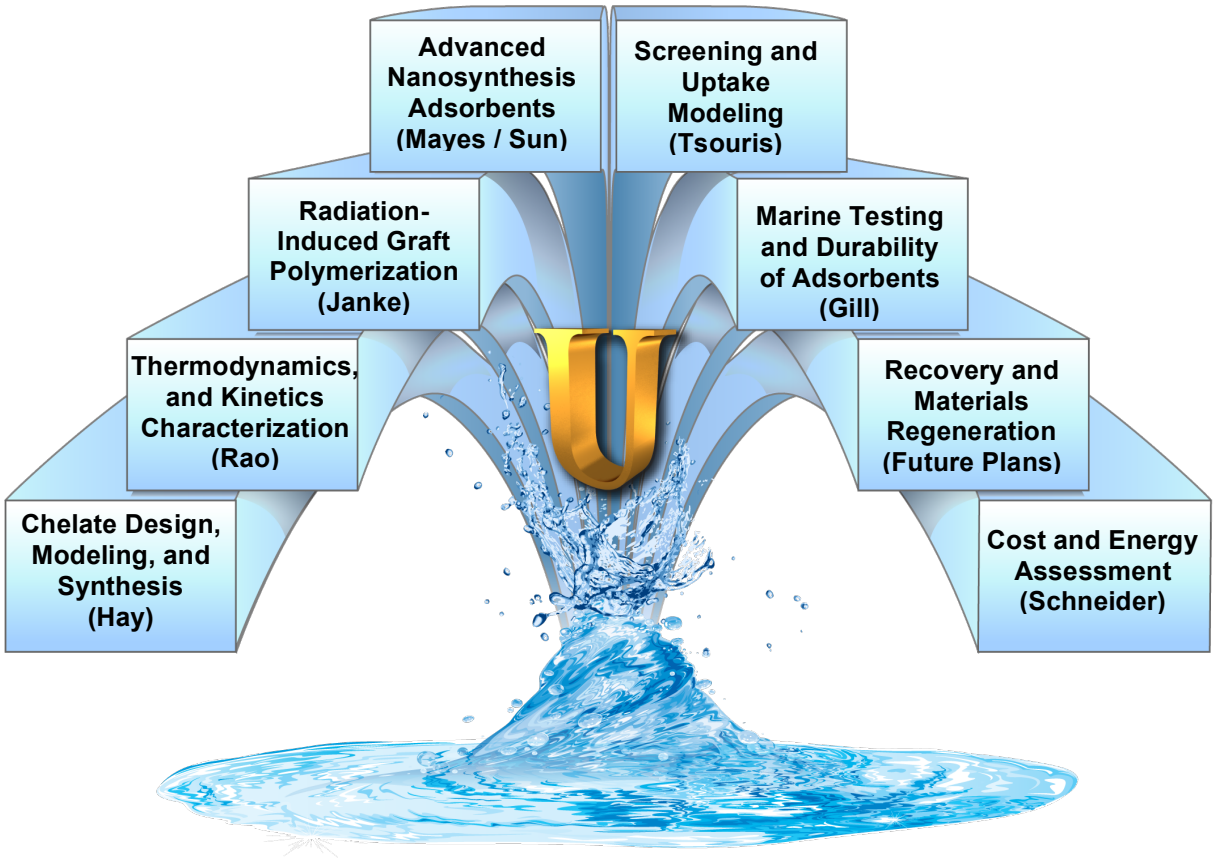

PROGRAM REVIEW DOCUMENT

June 13, 2013
Oak Ridge National Laboratory

ABSTRACT

For nuclear energy to remain sustainable in the United States, economically viable sources of uranium beyond terrestrial ores must be developed. The goal of this program is to develop advanced adsorbents that can extract uranium from seawater at twice the capacity of the best adsorbent developed by researchers at the Japan Atomic Energy Agency (JAEA), 1.5 mg U/g adsorbent. A multidisciplinary team from Oak Ridge National Laboratory, Lawrence Berkeley National Laboratory, Pacific Northwest National Laboratory, and the University of Texas at Austin was assembled to address this challenging problem. Polymeric adsorbents, based on the radiation grafting of acrylonitrile and methacrylic acid onto high surface-area polyethylene fibers followed by conversion of the nitriles to amidoximes, have been developed. These poly(acrylamidoxime-co-methacrylic acid) fibers showed uranium adsorption capacities for the extraction of uranium from seawater that exceed 3 mg U/g adsorbent in testing at the Pacific Northwest National Laboratory Marine Sciences Laboratory. The essence of this novel technology lies in the unique high surface-area trunk material that considerably increases the grafting yield of functional groups without compromising its mechanical properties. This technology received an R&D100 Award in 2012. In addition, high surface area nanomaterial adsorbents are under development with the goal of increasing uranium adsorption capacity by taking advantage of the high surface areas and tunable porosity of carbon-based nanomaterials. Simultaneously, *de novo* structure-based computational design methods are being used to design more selective and stable ligands and the most promising candidates are being synthesized, tested and evaluated for incorporation onto a support matrix. Fundamental thermodynamic and kinetic studies are being carried out to improve the adsorption efficiency, the selectivity of uranium over other metals, and the stability of the adsorbents. Understanding the rate-limiting step of uranium uptake from seawater is also essential in designing an effective uranium recovery system. Finally, economic analyses have been used to guide these studies and highlight what parameters, such as capacity, recyclability, and stability, have the largest impact on the cost of extraction of uranium from seawater. Initially, the cost estimates by the JAEA for extraction of uranium from seawater with braided polymeric fibers functionalized with amidoxime ligands were evaluated and updated. The economic analyses were subsequently updated to reflect the results of this project while providing insight for cost reductions in the adsorbent development through “cradle-to-grave” case studies for the extraction process.

This report highlights the progress made over the last three years on the design, synthesis, and testing of new materials to extract uranium for seawater. This report is organized into sections that highlight the major research activities in this project: (1) Chelate Design and Modeling, (2) Thermodynamics, Kinetics and Structure, (3) Advanced Polymeric Adsorbents by Radiation Induced Grafting, (4) Advanced Nanomaterial Adsorbents, (5) Adsorbent Screening and Modeling, (6) Marine Testing, and (7) Cost and Energy Assessment. At the end of each section, future research directions are briefly discussed to highlight the challenges that still remain to reduce the cost of extractions of uranium for seawater. Finally, contributions from the Nuclear Energy University Programs (NEUP), which complement this research program, are included at the end of this report.

CONTENTS

Page

LIST OF FIGURES

Figure **Page**

LIST OF TABLES

Table **Page**

LIST OF SCHEMES

Scheme **Page**

1. INTRODUCTION

For nuclear energy to remain a sustainable energy option for the United States, there must be assurance that economically viable resources of nuclear fuel are available. Currently, the primary natural resource for nuclear energy production is uranium, and almost all the commercial reactors in the world operate with a uranium fuel cycle. One goal of the US Department of Energy (DOE), Office of Nuclear Energy (NE) is to develop sustainable nuclear fuel cycles that improve uranium resource utilization, maximize energy generation, minimize waste generation, improve safety, and limit proliferation risk. Thus, the availability of fuel resources for each potential fuel cycle and reactor deployment scenario must be well understood. This area is most relevant for once-through approaches, but even modified open-cycle or full-recycle strategies will require comparable levels of natural resources for the foreseeable future. As stated in the US DOE NE Roadmap, the most appropriate place for federal involvement in this area would be research and development (R&D) to support investigation of long-term, "game-changing" approaches, such as recovering uranium from seawater.[1] To address this challenge, a workshop was held on October 13–15, 2010, to evaluate the emerging research areas that have the potential to ensure the availability of natural uranium resources for global nuclear expansion. The workshop report[2] evaluated the state of the art in uranium exploration, estimation, and extraction technologies and identified the R&D opportunities, science and technology challenges, and future research directions to overcome these challenges. The workshop also evaluated the extraction of uranium from seawater, the largest but most challenging unconventional resource, and identified future research directions to make the collection of uranium from seawater economically competitive. This alternative source of uranium would provide stability to the supply and market price of this fuel resource and allow for a sustainable expansion of nuclear energy in the United States and worldwide.

1.1 Extraction of Uranium from Seawater

The world's oceans represent a vast and as yet untapped source of uranium that is readily available to the United States.[2] Uranium, at approximately 3.3 ppb, is a conservative element in seawater and its concentration varies in direct proportion to changes in salinity. Since seawater is slightly basic (pH 8.0±0.4), uranium exists primarily as $[UO_2(CO_3)_3]^4$. It is estimated that the total sum of uranium in seawater is approximately 4.5 billion metric tons.[3] This amount is approximately 1000 times larger than the known amount of uranium from mineral reserves on land.[4] This reserve, combined with a suitable production cost for the extraction of uranium, can contribute to the growing international nuclear industry. Researchers in many countries—including the United States,[5-7] Japan,[8-10] Great Britain,[3] Germany,[11,12] Russia, China,[13] India,[14] South Korea,[15] Turkey,[16] and others—have been inspired to develop adsorbents to recover this untapped supply of uranium contained in world's oceans since the 1960s.

It was clear to scientists 60 years ago, just as it is today, that to exploit the ocean's reserves of uranium, a high-performance adsorbent was needed. A successful cost-effective extractant must have a very high distribution coefficient, very high selectivity, high loading capacity, rapid adsorption and elution kinetics, low losses of extractant, and low cost.[5] Thus, solvent extraction is not considered to be suitable for large-scale extraction of uranium from seawater because of the complex and expensive engineering aspects, the large amounts of chemicals and volatile solvents needed, and the loss of reagents by entrainment and dissolution. Extractants based on

solid-state adsorbents appear to be the most promising, but they need to be stable at slightly basic pH and high ionic strength, and they need to be extremely insoluble and durable in seawater.

1.1.1 Inorganic materials

In 1964, British researchers reviewed published studies on uranium extraction from seawater, including some based on solvent extraction techniques, and evaluated several solid sorbents.[3] They judged adsorption on solids to be the most sound extraction method. Various inorganic materials have been studied as potential adsorbents for uranium recovery from seawater. These include magnesium silicate, titania, manganese oxyhydroxide, silicate, nanoporous alumina, and iron (III) oxide.[13,17,18] Hydrous titanium oxide ($TiO_2 \cdot nH_2O$) has been the most studied inorganic adsorbent in uranium recovery from seawater. From 1981–1988, the first experimental plant for the collection of uranium from seawater with hydrous titanium dioxide was operated in Japan. However, with an adsorption capacity of only about 0.1 g of uranium per kg of sorbent, the method was regarded as too inefficient for industrial application and the adsorption capacities needed to be improved at least 10 times to make the process economical. Also, the low mechanical resistance of the sorbent and the consumption of electricity for pumping seawater increased the collection cost. Generating pelletized adsorbents using organic binding agents improved the mechanical resistance; however, the intraparticle mass-transfer resistance increased as a result of the pelletization due to the inability to easily access the inner portions of the monoliths/pellets derived from using organic binders.

1.1.2 Biopolymers

Biological adsorbents have been used for the uptake of radionuclides for pollution control. Furthermore, biological adsorbents such as grafted DNA aptamer, starch-based hydrogels, unicellular cyanobacteria, algae, chitosan, microorganisms, conifer barks, biomass, and plant wastes have been tested as potential adsorbents for the recovery of uranium from seawater.[19] Experimental data with spiked uranium solutions or simulated seawater have shown the feasibility of biological adsorbents for uranium uptake from seawater, but capacities are typically low and the kinetics can be slow. The capabilities of biological adsorbents were also demonstrated by several adsorption studies using real seawater. One of the advantages of biological adsorbents could be high selectivity for metal ions.[19]

1.1.3 Nanoporous carbon-based adsorbent

Nanoporous carbons are intriguing supports due to their broad chemical and thermal stability, ease of functionalization, potential for high surface area, and well-established industrial processes for production of various forms of carbon such as fibers and fabrics. Various functional groups, i.e., oxime, benzoylthiourea, carboxymethylated polyethyleneimine, and diarylazobisphenol, were applied to change the surface chemistry of nanoporous carbon adsorbents, demonstrating the feasibility of optimizing affinity and capacity by engineering the surface chemistry.[20-22] Superior physical properties, i.e., large pore size, spacious pore volume, and high surface area, provide an expansive area for functionalization and uranyl binding. Immobilization of chelating polymers inside the pores of the nanostructured carbon materials can be applied to increase selectivity and capacity of uranium.[20-22] While no seawater testing has been performed using nanoporous carbon materials (other than these studies), interesting results under other conditions exist. The high surface areas may result in high ligand densities, which may translate to high uranium capacities.

1.1.4 Polymeric adsorbents

In the early 1980s, scientists at the Nuclear Research Center in Jülich, Germany, conducted a systematic evaluation of 200 ion-exchange resin materials. The resins were tested at both laboratory scale and large field scale (100 g sorbent) with seawater (German North Sea and in the Gulf Stream near Miami). The team found that among all the materials tested, only amidoxime-based (Fig. 1.1) compounds, specifically cross-linked poly(acrylamidoximes), met the requirements for chemical stability and selective uptake of uranium under typical marine conditions. The uranium could be eluted from the poly(acrylamidoximes) resin by 1M HCl, but the uranium uptake decreased (ca. 6%) with increasing sorption-elution cycles. Although a number of other uranium extraction materials and methods have been studied, their various shortcomings have kept the focus on amidoxime-based adsorbents.

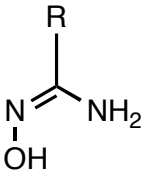

Fig. 1.1. Amidoxime ligand.

For the last three decades, Japan has been a leader in the extraction of uranium from seawater using amidoxime-based polymeric adsorbents, and it has conducted both laboratory and marine experiments in the Pacific Ocean. Initial experiments were conducted with polymer beads containing cyano groups, which were reacted with hydroxylamine to form the amidoxime groups.[23] However, the beads were not practical because they need packaging for deployment and effective contact with seawater. Thus an amidoxime fiber was prepared by reacting a commercially available poly(acrylonitrile) (PAN) fiber with hydroxylamine. Although the goal was to deploy this directly into seawater and utilize the ocean current and wave motion to circulate the seawater, the mechanical strength of the fibers was poor. To overcome this problem, graft polymerization was used to functionalize a strong polymer fiber (i.e., the trunk polymer) with PAN, which could then be converted to poly(acrylamidoxime). Graft polymerization is a powerful method to functionalize the surface of any polymer to make a copolymer that generally consists of a linear backbone of one composition (trunk) and randomly distributed branches of a different composition. The Japanese selected polyethylene non-woven fabric as the trunk polymer because of its mechanical strength and because it had previously been used in marine applications. The fabric was irradiated under nitrogen to generate free radical defects on the polymer surface. The reactive fabric was then placed in a solution of acrylonitrile to graft PAN chains from the free radical sites on to the trunk polymer. To increase the hydrophilicity of the polymer fibers and the adsorption rate, methacrylic acid was copolymerized with acrylonitrile in a 2:8 ratio, respectively. The cyano groups of the PAN were then converted to the poly(acrylamidoxime) by reacting with hydroxylamine (Fig. 1.2). Finally, the fabric was conditioned with KOH, which deprotonates the carboxylic acids and swells the fabric to facilitate contact with water.

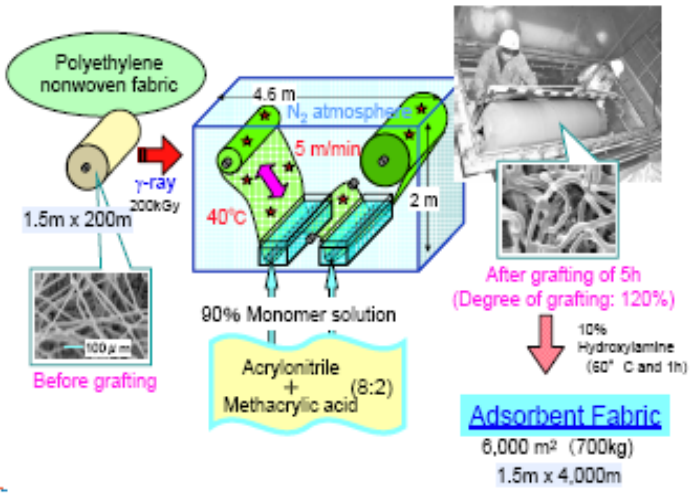

Fig. 1.2. Mass production of adsorbent fabric.[23]

The largest field test was a 2-year-long effort between 1999 and

2001 led by Noriaki Seko and Masao Tamada of Japan Atomic Energy Research Institute, now known as Japan Atomic Energy Agency (JAEA). The team prepared nonwoven sheets of amidoxime-functionalized polyethylene-polypropylene blend fabric (as described above) and loaded stacks of the sheets—separated by spacer nets—into three large connected cages that were lowered from a floating frame into the Pacific Ocean several miles from Japan's coastline in the Aomori Prefecture (Fig. 1.3). The truck-sized rig contained a total of 52,000 adsorbent sheets that weighed nearly 800 lb when dry. The team withdrew the adsorption beds every few weeks to analyze the sorbent for uranium uptake (by fractionally eluting the adsorbed uranium with 0.5M HCl). In total, the group submerged the adsorption beds for 240 days and recovered more than 1 kg of uranium from ocean currents flowing through the cages, thereby avoiding the need to pump seawater. With this setup, the Japanese team extracted, on average, 0.5 g of uranium per kilogram of sorbent in a 30-day period[24] and the uranium adsorption was found to correlate with seawater temperature and wave height.

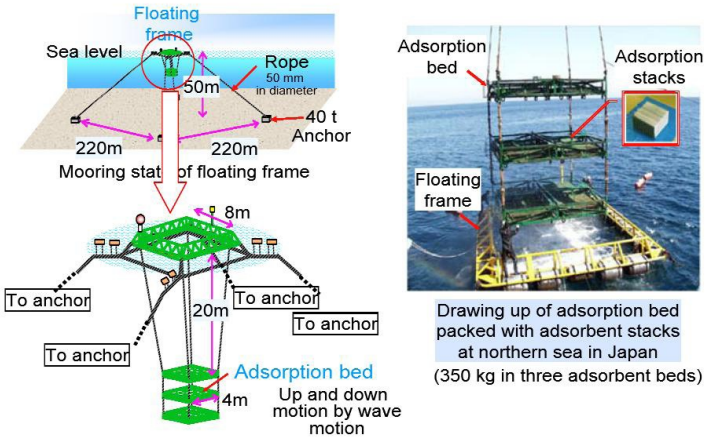

Fig. 1.3. Collection of uranium from seawater using the adsorbent stacks.[23]

Having firmly established that uranium can be extracted from the oceans in appreciable quantities, Seko, Tamada, and coworkers turned to lowering the cost of collecting uranium from seawater. They determined that 40% of the cost of retrieving metal from the sea was associated with the adsorption stacks, the frame, and other mechanical components. So, the group took a different approach; fashioning long seaweed-like braids of amidoxime-functionalized polyethylene fiber and attached the braids via remotely controlled fasteners to anchors that were lowered to the ocean floor (Fig. 1.4). The 60 m amidoxime functionalized braided adsorbent was evaluated in marine tests in the Okinawa area of Japan, and it was found that the average adsorbent collected was1.5 g of uranium per kg of sorbent in 30 days.[2,25] Thus, it was concluded that the braided-type adsorbent had a higher ability to adsorb uranium than the stacks of nonwoven fabric owing to the better contact between the seawater and the adsorbent.

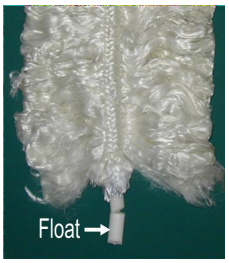

Fig. 1.4. Picture of the braided fiber.[23]

1.2 Economic Analysis

Economic analysis is key to determining the feasibility of technologies for uranium recovery from seawater. Several studies have reported economic analyses of actively pumped systems and passive, current-driven systems.[26-28] However, For actively pumped systems, increasing requirements of pumping power does not have an one-to-one relationship with the uranium production cost, and could be offset offset by a high adsorption capacity.[29] It has been reported that a passive, current-driven system is desirable due to its lower cost and simplicity compared to the more complex, actively pumped system.[28] An extended economic analysis of the production

cost for the extraction of uranium from seawater, based on the amidoxime braided fiber system described above, was developed by JAEA. This analysis confirmed that increased adsorption capacity is one of the most important factors in decreasing uranium costs.[26] In addition to adsorption capacity, the recycling frequency and the number of recycles are important parameters for reducing cost. These economic analyses provided motivation to develop robust adsorbents of high capacity, which can be regenerated and recycled many times.

The technical feasibility of uranium recovery from seawater has been proven. If 1% of the uranium in seawater were recovered, the available resources for nuclear power plants would increase by more than tenfold. The availability of terrestrial ores may diminish over time, should new discoveries of accessible, secure, environmentally tenable deposits not keep pace with extraction. Uncertainty in the sustainability of the conventional resource base can erode confidence in the long-term viability of the energy source, especially given the very long capital plant lifetimes that are in other respects a strength of the nuclear power industry. Nuclear fuel cycle research and development decision makers consider even longer time scales and are consequently strongly hampered by uncertainties surrounding the long term availability of the resource. Taken together, these factors imply that the costs – in nuclear build decisions not taken due to uncertainty around security of uranium supply and in R&D pursued as a hedge against scarce, expensive uranium – of not knowing how much uranium is available and at what cost are high. For its potential to eliminate this uncertainty and secure an indefinite supply of uranium at moderate cost, technology for the recovery of uranium from seawater will play a vital role in securing future energy resources. Furthermore, an effective uranium-recovery technology from seawater, based on selective adsorbents, can be extended to obtain other valuable materials present in seawater, such as energy-critical materials.

1.3 Objectives

Research and development efforts on uranium uptake technologies from seawater have progressed during the past six decades. However, for these efforts to lead to a viable technology for the production of uranium from seawater, additional breakthroughs are needed. Economic viability requires the development of the next generation of adsorbents that will exhibit higher adsorbent capacity, faster loading kinetics, and lower degradation over multiple loading/elution cycles. Equally important, uncertainties surrounding the performance and environmental impact of the technology must continue to be reduced. Both experimentation and modeling/simulation have a role to play in developing the technology to the point where its credibility as a viable large-scale source of uranium is beyond doubt.

The 2010 Workshop on Nuclear Fuel Resources, which was sponsored by US DOE NE, reviewed past efforts and evaluated emerging research areas that can potentially lead to the development of new technologies for the economic recovery of uranium from seawater. Advances in the following five research directions have been identified by the workshop participants in order to achieve economically competitive recovery of uranium: (1) molecular-level understanding of coordination modes, thermodynamics, and the kinetics and mechanism of uranium extraction; (2) design and synthesis of functional ligands; (3) advanced sorbents of high-surface-area polymer and hybrid supports; (4) new polymer sorbents via surface grafting techniques; and (5) innovative elution processes.[2] Based on the recommendations of the workshop, a research team was formed with scientist from ORNL, LBNL, PNNL and UT Austin to address these research challenges as highlighted in Fig. 1.5. ***The 3-year goal of this project is to build off the JAEA studies, which developed an amidoxime braided fiber adsorbent that extracted 1.5 g U/kg adsorbent from seawater, and develop advanced adsorbents that can at***

least double the adsorbent capacity of the JAEA adsorbent for extraction of uranium from seawater.

In this report, the progress over the last 3 years on our efforts to double the adsorption capacity of uranium from seawater will be summarized and plans for future research directions will be discussed. This study builds off the JAEA studies on grafted poly(acrylamidoxime) fibers, but it also investigates more fundamental questions such as how does the amidoxime ligand bind uranium, how can new ligands be designed with higher selectivity, what are the kinetics and thermodynamics of binding, and can new adsorbents be prepared that take advantage of the high surface areas of nanomaterials. These fundamental studies will produce new insight that can be used to produce transformational new materials with high capacities, fast kinetics, and high stabilities. The experimental studies will continue to be guided by economic analysis that highlights the key parameters that will lower the cost of extracting uranium from seawater. Finally, the new adsorbents prepared in this study are tested for uranium adsorption in laboratory experiments using real seawater. This experimental data feeds back into the economic analysis and plays a key role in reducing the uncertainty associated with the uranium production cost estimate.

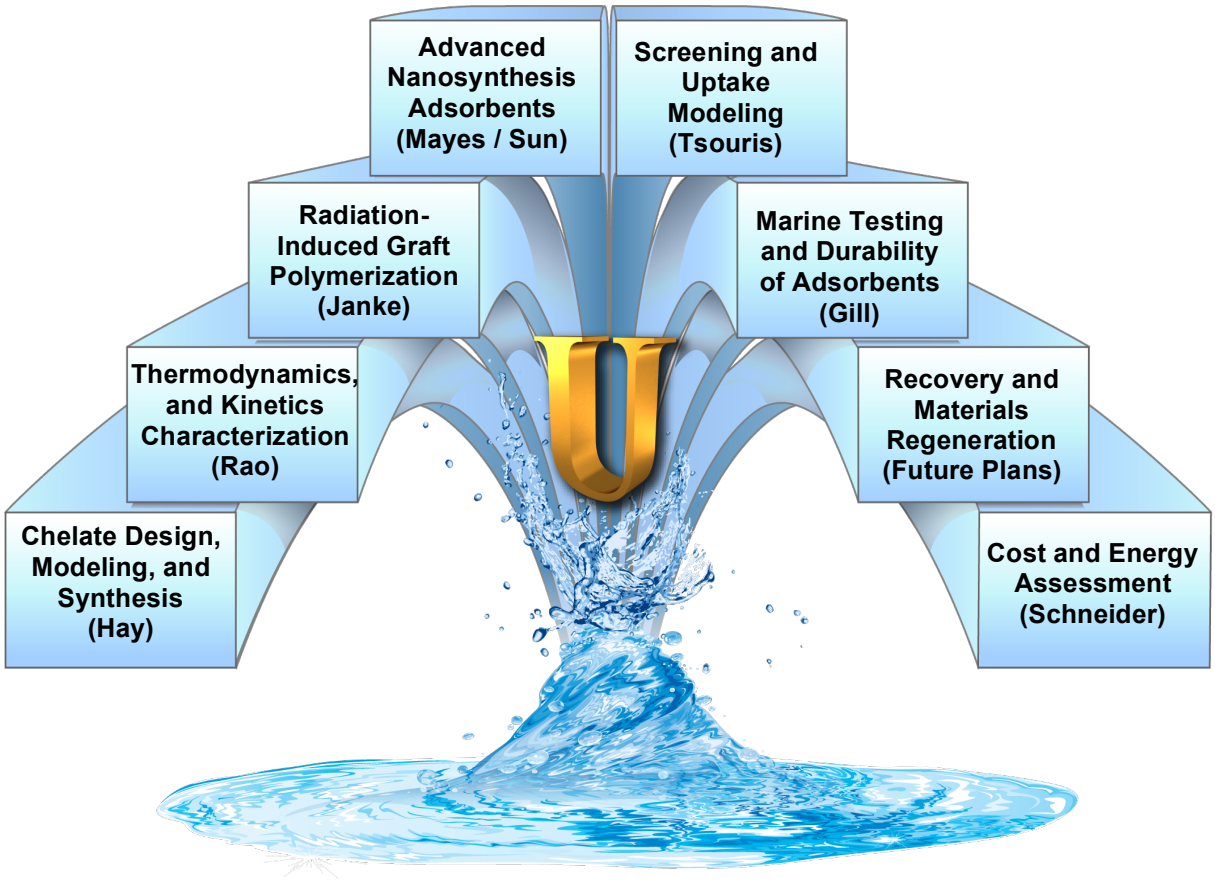

Fig. 1.5. The Uranium from Seawater Program.

1.4 References

(1) *Nuclear Energy Research and Development Roadmap*, US Department of Energy, Office of Nuclear Energy, 2010.

(2) *Technology and Applied R&D Needs for Nuclear Fuel Resources*, Oak Ridge National Laboratory, October, 2010.

(3) Davies, R. V.; Kennedy, J.; McIlroy, R. W.; Spence, R.; Hill, K. M. *Nature* **1964**, *203*, 1110.

(4) *Uranium 2011: Resources, Production and Demand*, OECD Nuclear Energy Agency and the International Atomic Energy Agency, 2012.

(5) Kelmers, A. D. *Sep. Sci. Technol.* **1981**, *16*, 1019.

(6) Kim, Y. S.; Zeitlin, H. *Anal. Chem.* **1971**, *43*, 1390.

(7) Kim, J.; Tsouris, C.; Mayes T., R.; Oyola, Y.; Saito, T.; Janke J., C.; Dai, S.; Schneider, E.; Sachde, D. *Sep. Sci. Technol.* **2013**, *48*, 367.

(8) Okamoto, J.; Sugo, T.; Katakai, A.; Omichi, H. *Radiat. Phys. Chem.* **1985**, *25*, 333.

(9) Tabushi, I.; Kobuke, Y.; Nakayama, N.; Aoki, T.; Yoshizawa, A. *Ind. Eng. Chem. Prod. Res. Dev.* **1984**, *23*, 445.

(10) Kanno, M. *J. Nucl. Sci. Technol.* **1984**, *21*, 1.

(11) Heide, E. A.; Wagener, K.; Paschke, M.; Wald, M. *Naturwissenschaften* **1973**, *60*, 431.

(12) Schenk, H. J.; Astheimer, L.; Witte, E. G.; Schwochau, K. *Sep. Sci. Technol.* **1982**, *17*, 1293.

(13) Fan, F.; Ding, H.; Bai, J.; Wu, X.; Lei, F.; Tian, W.; Wang, Y.; Qin, Z. *J. Radioanal. Nucl. Chem.* **2011**, *289*, 367.

(14) Saxena, A. K. *BARC Newsl.* **2004**, *249*, 226.

(15) Choi, S. H.; Choi, M. S.; Park, Y. T.; Lee, K. P.; Kang, H. D. *Radiat. Phys. Chem.* **2003**, *67*, 387.

(16) Donat, R.; Esen, K.; Cetisli, H.; Aytas, S. *J. Radioanal. Nucl. Chem.* **2009**, *279*, 253.

(17) Comarmond, M. J.; Payne, T. E.; Harrison, J. J.; Thiruvoth, S.; Wong, H. K.; Aughterson, R. D.; Lumpkin, G. R.; Müller, K.; Foerstendorf, H. *Environ. Sci. Technol.* **2011**, *45*, 5536.

(18) Sadeghi, S.; Sheikhzadeh, E. *J. Hazard. Mater.* **2009**, *163*, 861.

(19) Gupta, C. K.; Singh, H. *Uranium Resource Processing*; Springer-Verlag: Heidelberg, 2003.

(20) Tian, G.; Geng, J.; Jin, Y.; Wang, C.; Li, S.; Chen, Z.; Wang, H.; Zhao, Y.; Li, S. *J. Hazard. Mater.* **2011**, *190*, 442.

(21) Zhao, Y.; Liu, C.; Feng, M.; Chen, Z.; Li, S.; Tian, G.; Wang, L.; Huang, J. *J. Hazard. Mater.* **2010**, *176*, 119.

(22) Kim, J.; Lee, H.; Yeon, J.-W.; Jung, Y.; Kim, J. *J. Radioanal. Nucl. Chem.* **2010**, *286*, 129.

(23) Tamada, M. *J. Jpn. Inst. Energy* **2009**, *88*, 249.

(24) Seko, N.; Katakai, A.; Hasegawa, S.; Tamada, M.; Kasai, N.; Takeda, H.; Sugo, T.; Saito, K. *Nucl. Technol.* **2003**, *144*, 274.

(25) Rao, L. LBNL-4034E: 2011.

(26) Sachde, D. J., The University of Texas at Austin, 2011.

(27) Tamada, M.; Seko, N.; Kasai, N.; Shimizu, T. *Nihon Genshiryoku Gakkai Wabun Ronbunshu* **2006**, *5*, 358.

(28) Driscoll, M. J.; Best, F. R. *Systems studies on the extraction of uranium from seawater*, Massachusetts Inst. Technol., 1981.

(29) Best, F. R.; Driscoll, M. J. *Prospects for the recovery of uranium from seawater*, Massachusetts Inst. Technol., 1980.

2. CHELATE DESIGN, MODELING, SYNTHESIS, AND CHARACTERIZATION

Ben Hay, Christopher Grant, Sung-Ok Kang, Sinisa Vukovic
Oak Ridge National Laboratory

This project seeks to increase the uranium adsorbent capacity through the development of novel adsorbents that contain chelating sites with higher uranium binding affinity and selectivity than exhibited by those in the current amidoxime-based adsorbents. A combined theoretical and experimental approach has been pursued (1) to better understand how current amidoxime-based adsorbents function; (2) to identify novel chelating agents on the computer using state-of-the-art *de novo* structure-based design methods; (3) to synthesize, characterize, and evaluate the performance of promising candidates in the laboratory; and (4) to develop synthetic methods to allow chelate attachment to polymeric and high-surface-area materials.

2.1 R&D Progress/Status

Over the past 3 years, research efforts have been focused on the development of synthetically accessible uranium chelates containing two or three donor groups. The design approach involved selecting a set of donor groups and identifying how to covalently connect them to achieve optimal interaction with uranyl carbonate species. The selection of donor groups was based on previous successes reported in the literature for a copolymer containing roughly 50% amidoxime and 50% carboxylate groups. Although there is no direct evidence as to how uranium is bound by this copolymer, it is known that the amidoxime donor group is necessary, and chelating interactions with two or more donor groups generally yield stronger complexation than interactions with single-donor groups. The composition of the copolymer suggests there are three types of chelate present that could complex the uranyl ion and involve the amidoxime group (Fig. 2.1). The first is a tridentate cyclic imide dioxime, which forms when two adjacent amidoximes condense to eliminate hydroxylamine. It is believed that some of this chelate is formed during synthesis of the adsorbent, but the conversion is not quantitative, and the exact amount produced is not well characterized.[1] The second chelate contains two amidoxime groups, bridged by a three-carbon-atom linkage. The third bidentate chelate contains one amidoxime and one carboxylate donor, also bridged by a three-carbon linkage. Design, synthesis, and characterization of improved uranium receptors based on each of these donor group sets, discussed separately below, have led to the development of two promising chelate structures. The development of methods for generating novel adsorbent materials by covalently attaching the new chelates to grafted polymers is presented at the end of this section.

2.1.1 Cyclic imide dioxime chelates

The possible role of cyclic imide dioxime as a uranium chelator in amidoxime-based polymers was first proposed by Astheimer et al. in 1983.[1] Recent studies have confirmed that glutarimide dioxime, **1**, forms strong tridentate complexes with uranyl ion in aqueous solution (Fig. 2.2).[2] This result suggested that the performance of existing amidoxime-based adsorbents might be enhanced simply by adjusting conditions to favor the maximum formation of cyclic imide dioxime. It is known that treatment of poly(acrylamidoximes) with 0.5 M KOH solution prior to its submersion in seawater enhances uranium uptake.[3] Although it has been proposed that this enhancement is due to the conversion of open-chain amidoximes to cyclic imide dioximes,[3] there is no direct evidence to support base-induced cyclization. On examination of

glutaro bis(amidoxime), **2**, we found that exposure to base does not induce cyclization, but instead causes hydrolysis to glutaric acid, **3**.[4] We also demonstrated that this compound was quantitatively converted to the glutarimide dioxime, **1**, simply by heating for 3 hours at 130 °C in dimethylsulfoxide (DMSO) solvent, suggesting a simple and cost-effective way to maximize the amount of imide dioxime in the amidoxime-based adsorbent.

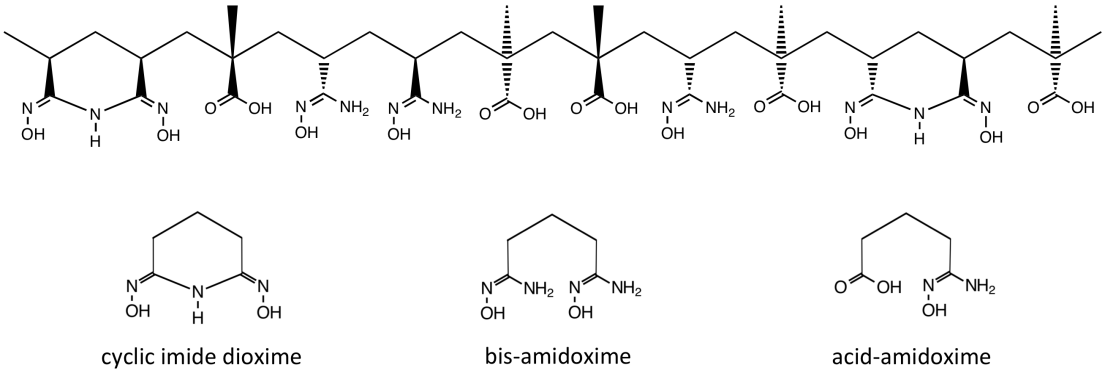

Fig. 2.1. The amidoxime-based polymer obtained by copolymerization of methylacrylic acid and acrylonitrile followed by treatment with hydroxylamine contains three chelate types that involve amidoxime.

Although a good uranyl chelator, the cyclic imide dioxime suffers from a serious flaw – instability toward acid. Amidoxime-based adsorbents are washed with 1 M HCl solution to elute adsorbed metals. This procedure is reported to decrease the extraction efficiency (6%) per cycle in amidoxime-based adsorbents, and it has been proposed that this decrease is due to the degradation of the cyclic imide dioxime binding sites present in the adsorbent.[3b] Even though it is known that cyclic imide dioximes are unstable under acidic conditions,[5] the rate of degradation had not been reported. We found that the glutarimide dioxime, **1**, is irreversibly hydrolyzed on exposure to 1 M HCl with a pseudo-first-order half-life of 0.9 h at room temperature.[4] This suggests that unless care is taken to minimize the acid exposure time during metal elution, most of the imide dioxime present in the polymer would be destroyed in the first elution step. In contrast to **1**, acetamidoxime is stable to acid hydrolysis, showing no degradation for a week under the same conditions.

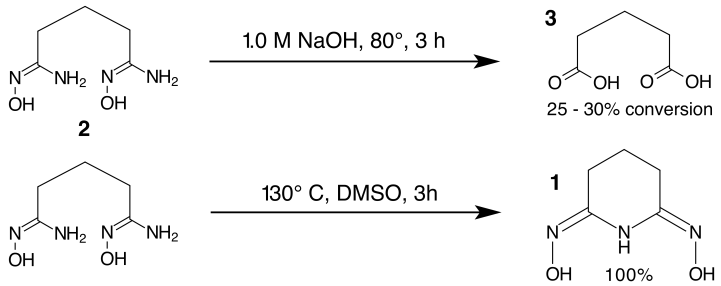

Fig. 2.2. Heating in base causes hydrolysis of glutaro bis(amidoxime), 2, to glutaric acid, 3. Heating at higher temperature in DMSO causes cyclization to form glutarimide dioxime, **1**.[4]

We proposed that improved resistance toward acid hydrolysis might be achieved by using aromatic imide dioxime derivatives. One such compound, phthalimide dioxime, **4**, was readily prepared from commercially available starting material. This aromatic derivative, shown in Fig. 2.3, was orders of magnitude more stable to acid hydrolysis, hydrolyzing on exposure to 1 M HCl with a half-life of 147 h at room temperature. The results of these hydrolysis studies, including the synthesis and characterization of **4**, have been published in *Industrial and Engineering Chemistry Research*.[4] Although soluble enough to allow hydrolysis studies, the solubility of **4** in aqueous solution needed to be increased to allow further characterization. A hydrophilic derivative was obtained by substituting the NH_2 group with the ethylsulphonic acid. The sodium salt of this compound, **5**, was sent to Lawrence Berkeley National Laboratory (LBNL) for uranyl binding affinity measurements (see Section 3.2.1).

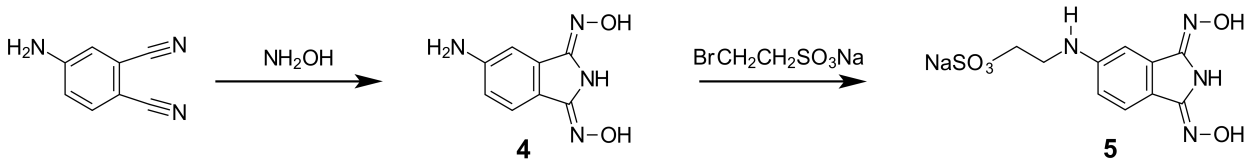

Fig. 2.3. One-step synthesis of cyclic phthalimide dioxime, 4, from commercial starting material and hydrophilic derivative, 5, isolated as the sodium salt of ethylsulphonate.

Electronic structure calculations were used to evaluate the uranium binding affinity for a series of aliphatic and aromatic cyclic imide dioxime architectures for 5-, 6-, and 7-membered ring sizes. The structures for this series of chelates and predicted ΔG values for uranyl complexation are summarized in Fig. 2.4. Although the model predicts that the 5-membered ring analogs should show decreased binding, the 6- and 7-membered ring analogs all exhibit comparable uranyl binding affinities. The calculated ΔG values systematically overestimate the binding strength when compared with known experimental values. However, we found that the calculated ΔG values are linearly correlated with experimental log K values, providing a method for predicting the experimental binding affinity for the proposed chelate. The validity of this predictive capability was confirmed for the dianion of the phthalimide dioxime derivative, **5**: predicted log K = 13.8, measured log K = 14.3 ± 0.8 (personal communication, Linfeng Rao, LBNL).

The 6-membered ring aromatic imide dioxime derivative, **6** in Fig. 2.5a, was synthesized by collaborator Professor David Jenkins (University of Tennessee), and a crystal structure was obtained showing the mono-deprotonated form bound to the uranyl cation in a tridentate fashion, Fig. 2.5b. This compound was not soluble in water, so it could not be tested for acid stability or uranium binding affinity. The synthesis of a water-soluble derivative was undertaken at Oak Ridge National Laboratory (ORNL). It proved to be challenging but was eventually achieved on a gram scale with the strategy shown in Fig. 5c. Full details of this synthesis have been submitted as an article to the *Journal of Organic Chemistry*.[6] This water-soluble derivative, **14**, proved to be the most acid-stable imide dioxime to date, showing no detectable reaction after 1 week of exposure to 1 M HCl at room temperature. The theoretical prediction that **14** should exhibit uranyl binding affinities comparable to that measured for **1** remains to be confirmed by experiment. Uranyl ion binding affinity measurements for **14** are now in progress by Professor Dale Ensor (Tennessee Technological University).

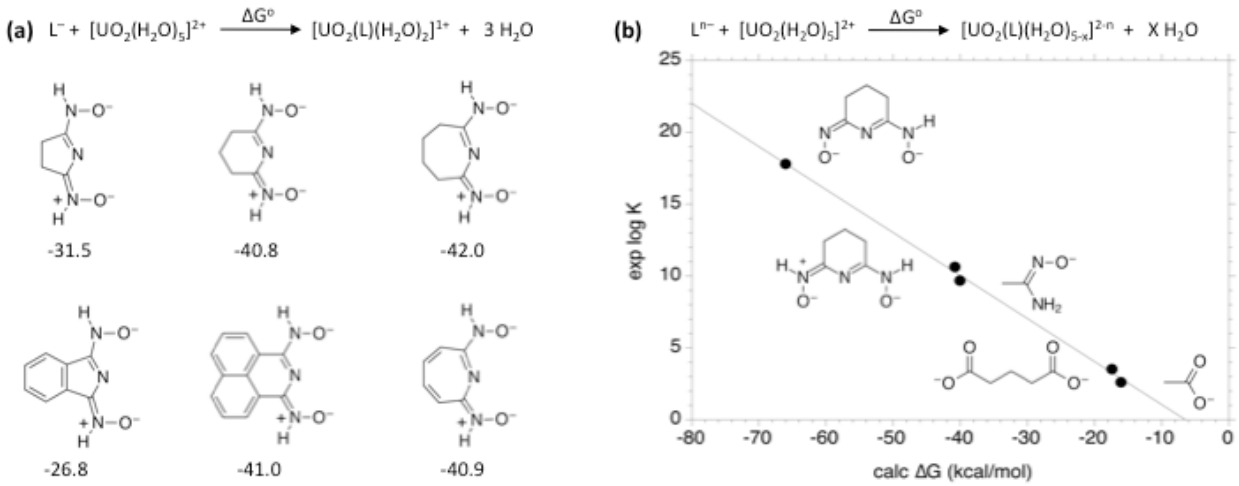

Fig. 2.4. (a) Calculated ΔG values (kcal/mol) for the reaction where a mono-deprotonated chelate displaces three water ligands from the uranyl pentaaqua ion are given below each structure.(b) Plot of experimental log K values versus calculated ΔG values for a series of chelates gives a linear correlation that can be used to estimate binding affinities for unknown chelates. Calculations: B3LYP/6-31+G(d) and ECP/SSD60, solvation IEFPCM model.

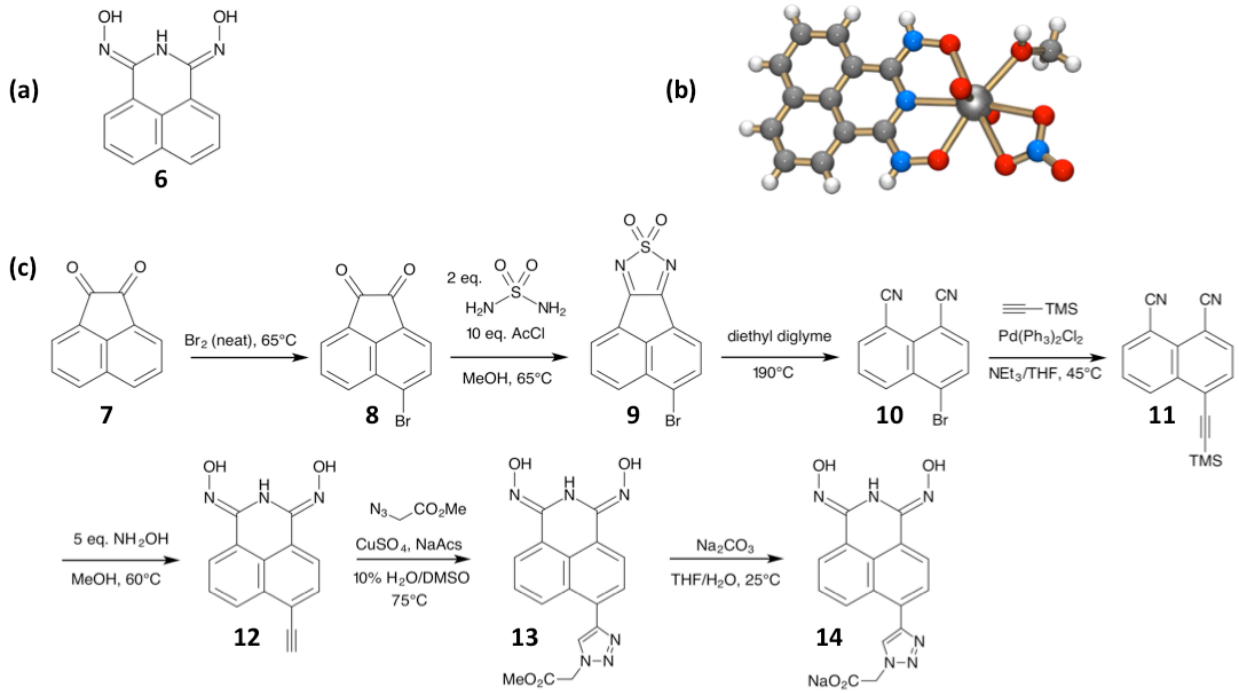

Fig. 2.5. (a) 6-membered ring aromatic imide dioxime, 6, based on naphthalene scaffold was prepared by David Jenkins (University of Tennessee). (b) Crystal structure of $[UO_2(\mathbf{6})OH_2NO_3]$. (c) Synthesis of water-soluble derivative **14**.[6]

2.1.2 Bis(amidoxime) chelates

Although amidoxime-based adsorbents have been studied extensively, at the start of this project, it was unclear how the amidoxime functional group interacted with the uranyl ion. It is known by potentiometric titrations with prototype compounds, acetamidoxime[7a] and benzamidoxime,[7 b] that amidoximes deprotonate to form charge-neutral bis-amidoximato uranyl complexes. Consistent with these solution studies, amidoxime-based polymers are observed to release 2 equiv of H^+ per uranyl adsorbed, leading researchers to propose the two possible binding motifs shown in Fig. 2.6.[3a-d,8] In the first motif, uranium is bound to the oxygen atoms of two amidoxime and two amidoximate donors.[8] In the second motif, uranium forms five-membered chelate rings by coordinating an oxygen atom and an NH_2 nitrogen atom of two amidoximate donors.[3a-d] Such structures have never been experimentally observed, and the exact nature of the binding motif of uranium species in amidoxime-based polymers remains obscure.

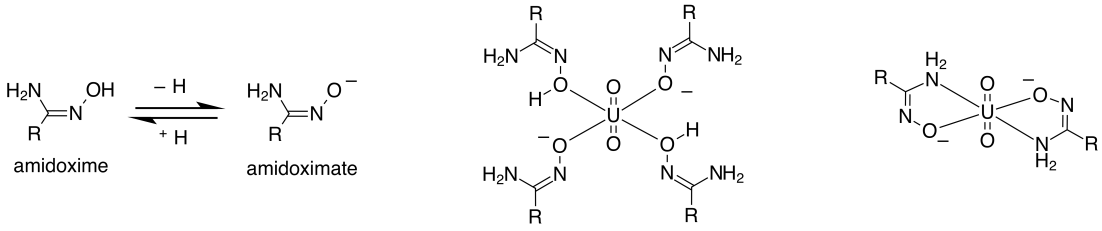

Fig. 2.6. Structure of amidoxime and amidoximate, and UO_2^{2+} binding motifs proposed to occur in amidoxime-based polymers. Solvent molecules complementing fifth and/or sixth coordination sites on the uranyl cation are not shown.

To identify how the amidoximate anion binds the uranyl ion, we performed density functional theory (DFT) calculations on a series of $[UO_2(\text{acetamidoximato})_x(OH_2)_y]^{2-x}$ (x = 1−3) complexes. These motifs included monodentate binding to either the oxygen or the nitrogen atom of the oxime group, bidentate chelation involving the oxime oxygen atom and the amide nitrogen atom, and η^2 binding with the N−O bond. The theoretical results establish the η^2 motif to be the most stable form. This prediction was confirmed when we obtained the first single-crystal X-ray diffraction structures for UO_2^{2+} complexes with amidoximate anions, both showing η^2 binding (Fig. 2.7a). These results were documented in a 2012 article published in *Inorganic Chemistry*.[9] A third crystal structure showing the η^2 binding motif has been obtained at the University of Alabama (Fig. 2.7b) from one of our Nuclear Energy University Program (NEUP) partners.[10]

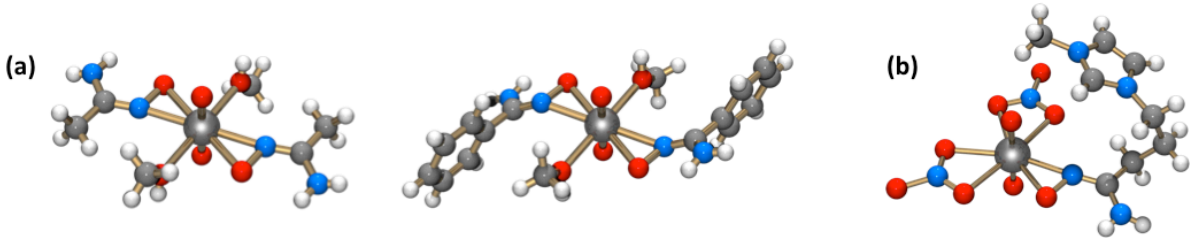

Fig. 2.7. (a) First crystal structures for uranyl amidoximate complexes confirm the η^2 binding motif predicted by theory.[9] (b) Third crystal structure example of the η^2 binding motif.[10]

Building upon the knowledge of how amidoximate binds the uranyl cation, design efforts focused on how to covalently connect two amidoxime groups to get the best chelating structure for binding the uranyl ion. Linking two groups together constrains their position in space. The design goal was to identify linkages that position both groups so that they can simultaneously

engage the uranyl ion with the most stable η^2 binding motif. The computational design process required an extended molecular mechanics model capable of predicting and evaluating the structures of amidoxime and uranyl-amidoxime complexes. To this end, an extended MM3 force field model was developed based on DFT calculations of amidoximate – uranyl cation complexes as well as the single-crystal x-ray diffraction structures for amidoximate complexes determined at ORNL and structures of related oximate metal complexes taken from the Cambridge Structural Database. This model was used both to generate structural input for the de novo design software, HostDesigner, as well as to evaluate candidates identified by the design code. After identifying candidates that scored well in terms of structural organization for uranyl complexation, additional criteria were applied to select candidates for potential synthesis and testing. These criteria included synthetic accessibility, chemical stability, and ability to chemically functionalize the candidate to allow covalent attachment to a polymer support. Details of the design process are documented in an article that has been accepted for publication in *Inorganic Chemistry*[11]

Because of their synthetic accessibility, simple $-(CH_2)_n-$ (n = 1–5) linkages are of interest. Fig. 2.8 summarizes the predicted MM3 geometries of the free chelates and $[UO_2(\text{chelate})CO_3]^{4-}$ complexes, as well as the free energy change in the chelate on going from the free to the bound form. It can be seen that propyl-linked structure, n = 3, which is a model for the bis-amidoxime chelate present in the amidoxime-based adsorbents, is able to achieve a bis-η^2 configuration with the uranyl ion, suggesting that such chelation could occur in the adsorbent. However, this chelate architecture is far from optimal with a 7.1 kcal/mol penalty associated with chelation. The best member of this series is the butyl linkage, n = 4, which lowers the penalty to 4.3 kcal/mol.

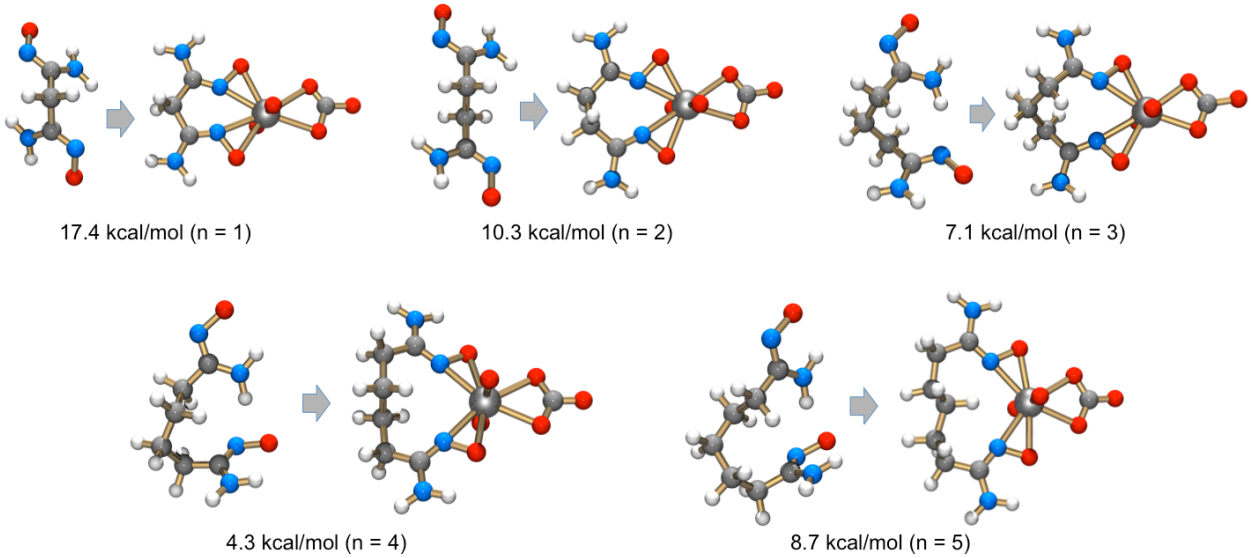

Fig. 2.8. MM3 optimized geometries for free chelates and $[UO_2(\text{chelate})CO_3]^{4-}$ complexes for simple $-(CH_2)_n-$ linked bis-amidoxime chelates. The free energy change in the chelate structure on going from free to bound is given below each compound.

Additional linkages were also evaluated. With a reorganization penalty of 2.2 kcal/mol, one of the top scoring bis-amidoxime candidates identified by the design process was **15** (Fig. 2.9). A synthetic strategy for this previously unknown compound was developed at ORNL (Fig. 2.9). The NH_2 group placed on the backside of the structure was substituted with an ethyl sulfonate group in order to make a water-soluble, acid-stable derivative, **19**. Uranyl ion binding affinity

measurements for **19** are now in progress by Robert Hancock (University of North Carolina–Wilmington).

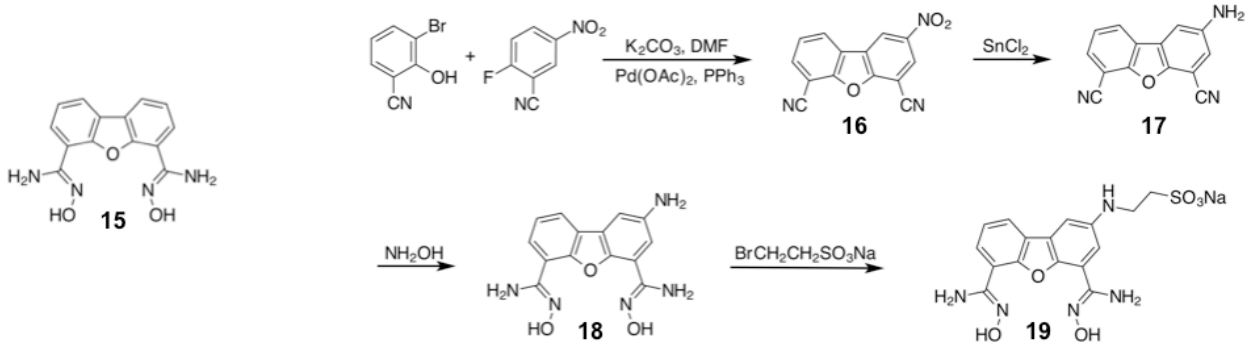

Fig. 2.9. One of the best scoring bis-amidoxime candidates, 15, and synthesis of water-soluble derivative, 19.

2.1.3 Amidoxime + carboxylate chelates

Using the same design methods described in the preceding section, we have also evaluated how to covalently connect one amidoxime group with one carboxylate group to get the best chelating structure for binding the uranyl ion. To do this, the MM3 force field model was further extended to handle calculations on uranyl carboxylate complexes based on extensive crystal structure data and DFT-generated potential energy surfaces. As before, the extended MM3 model was used both to generate structural input for de novo design as well as to evaluate candidates identified by the design code. As with the bis-amidoxime chelates (Fig. 2.8), synthetically accessible chelates formed from $–(CH_2)_n–$ (n = 1–5) linkages were evaluated (Fig. 2.10). In contrast to the bis-amidoximes, chelates formed by linking an amidoxime with a carboxyl group exhibit significantly lower reorganization penalties. For example, the 4.0 kcal/mol penalty for the propyl linkage, n = 3, is almost half that observed with the bis-amidoxime. This result suggests that propyl-linked carboxyl + amidoxime groups, which are the most prevalent chelates in the Japanese adsorbent, are capable of chelating the uranyl ion without excessive strain in the structure. In this series, the ethyl linkage, n = 2, gives the lowest reorganization penalty.

Synthetic efforts have been focused on cyclic imide dioximes and bis-amidoximes, rather than amidoxime + carboxylate chelates. The reason for this decision is that carboxylate is known to be a much weaker donor than amidoximate. This can be seen in Fig. 2.4b, where the simple acetamidoxime exhibits a log K for uranyl complexation that is >5 orders of magnitude stronger than acetic acid. Thus although amidoxime + carboxylate chelates may bind the uranyl ion, one would expect the resulting complexes to be orders of magnitude less stable than those formed by chelates containing two amidoxime donors.

2.1.4 Incorporating chelates in adsorbents

Since the beginning of the project, consideration has been given to how novel chelates would be incorporated into polymer-based adsorbents. One strategy is to functionalize the chelate with a vinyl group and use graft polymerization techniques to polymerize the monomer onto polyethylene fibers. An alternate strategy is to graft a reactive monomer onto polyethylene fibers and covalently attach the chelate by treating the fiber after grafting has taken place. Both of these strategies have been investigated.

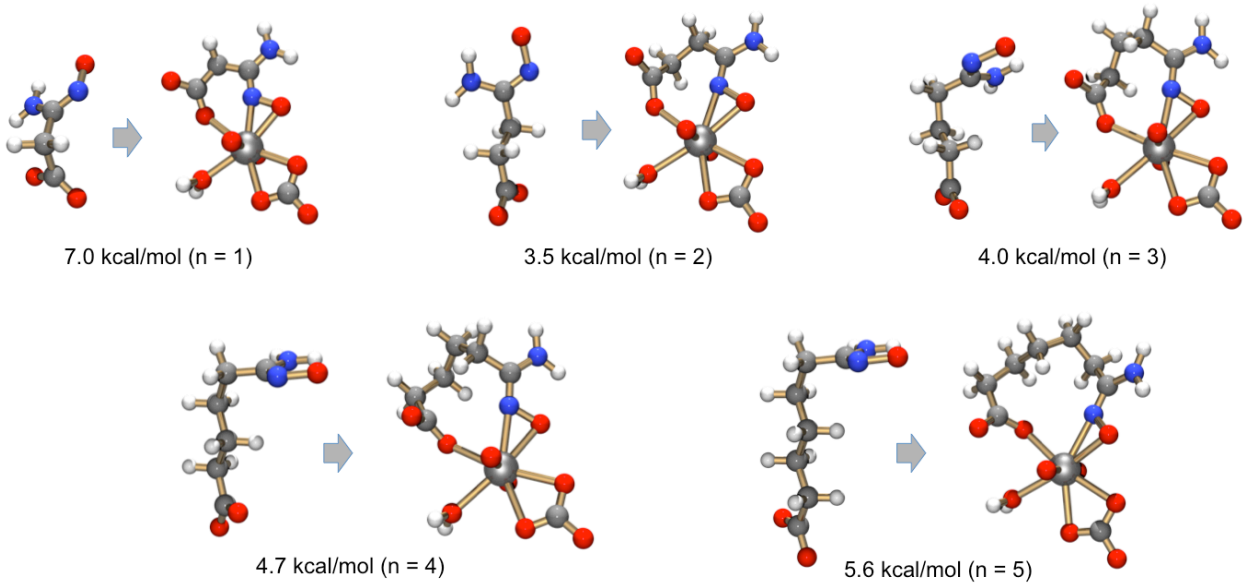

Fig. 2.10. MM3 optimized geometries for free chelates and $[UO_2(chelate)OH_2CO_3]^{4-}$ complexes for simple $-(CH_2)_n-$ linked amidoxime + carboxylate chelates. The free energy change in the chelate structure on going from free to bound is given below each compound.

Initial experiments focused on incorporation via vinyl polymerization. Because of its ease of preparation, initial experiments were made with the phthalimide dioxime chelate, **4**. The NH_2 substituent on this chelate provided a ready route to prepare in gram scale two derivatives that were functionalized with vinyl substituents, **20** and **21** (Fig. 2.11). However, repeated attempts under radical polymerization conditions failed to produce polymer from these monomers. We conclude that functionality in the chelate is quenching the radical polymerization, but it is not clear whether it is the amine or the cyclic imide dioxime functionality that is causing the problem. Given that cyano groups do not suppress polymerization, an alternative approach that should be successful would be to attempt to use the vinyl-substituted dicyano precursor as the monomer and then generate the chelate by subsequent treatment with hydroxylamine after polymerization. This requires the development of synthetic routes to the requisite vinyl-substituted dicyano precursors in the gram scale. Synthesis of one of the required precursors, **23**, should be possible in one step from an existing Br-substituted intermediate (**10**, Fig. 2.5c) and is now under investigation.

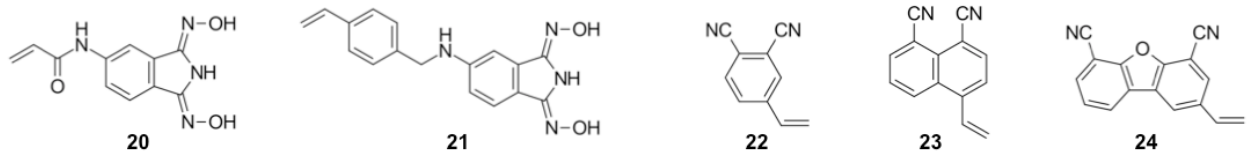

Fig. 2.11. Attempted polymerization of vinyl-substituted derivatives 20 and 21 was unsuccessful. An alternative concept, involving the polymerization of vinyl-substituted dicyano precursors, such as **22**– **24**, followed by hydroxylamine treatment is under investigation.

An alternate strategy developed to use an NH_2 substituent to connect the chelate to a polymer is shown in Fig. 2.12a. This strategy involved post-functionalization of chloromethylstyrene that had been grafted onto the fiber. It is known that chloromethylstyrene will undergo nucleophilic substitution with amines, replacing -Cl with –NHR. Because chloromethylstyrene is not

hydrophilic, we decided to enhance the hydrophilicity by first attaching a sodium ethylsulfonate group to the amine so that every attached chelate would be accompanied by a hydrophilic group, thereby yielding water-soluble polymer. Reaction conditions were optimized to attach **5** (Fig. 2.3) to chloromethylstyrene. Unfortunately, even under forcing conditions, this reaction would not go to completion; and the maximum degree of functionalization achieved was a disappointing 35% yield by elemental analysis. An alternate strategy to obtain hydrophilic product via a nucleophilic substitution approach, shown in Fig. 2.5b, is to react an NH_2-substituted chelate with a copolymer containing ester groups that can be subsequently hydrolyzed. This was attempted with the NH_2-substituted derivative **4** (Fig. 2.3), but in this case, yields obtained were <5%.

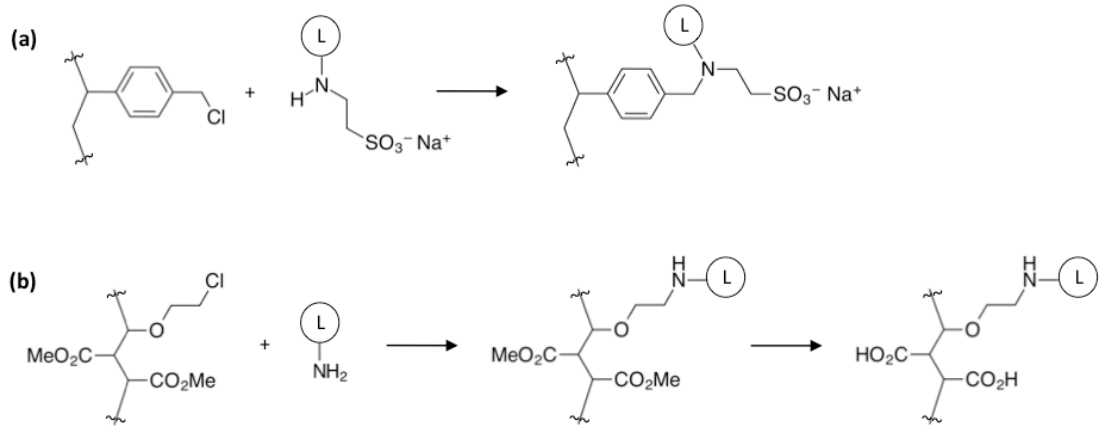

Fig. 2.12. Two strategies for attaching a chelate by nucleophilic substitution to obtain a hydrophilic product: (a) reaction of a hydrophilic chelate with a hydrophobic homopolymer and (b) reaction of a hydrophobic chelate with a copolymer that can be subsequently hydrolyzed to a hydrophilic form.

After failure to achieve sufficient yields with nucleophilic substitution, an alternate approach, using click chemistry, is now under investigation (Fig. 2.13). In this approach, chloromethylstyrene is converted to an azidomethylstyrene in near quantitative yield. The chelate is functionalized with an alkyne substituent instead of an NH_2 substituent. In the presence of a copper catalyst, the functionalized chelate reacts with the azidomethylstyrene in near-quantitative yield to form a 1,2,3-triazole linkage covalently attaching the chelate to the polymer. In preliminary experiments with a fiber that was grafted from a solution containing 30% methacrylic acid and 70% chloromethylstryene, we have been able to attach chelate **12** in up to ~80% yield, as determined by gain in mass and estimated polymer composition. Initial capacity testing of this material at the University of Tennessee gave a low uranium uptake, only 7.4 g U/kg absorbent, while the Japanese adsorbent gives 20 g/kg under the same test conditions, which at this point we attribute to insufficient hydrophilicity. We are planning to accompany the grafting team, led by Chris Janke (ORNL), to the e-beam facility to prepare a series of grafted fibers with differing blends of chloromethylstryene and a variety of acid monomers with the goal of preparing a more hydrophilic polymer.

2.2 Future Work

2.2.1 Adsorbent materials based on designed chelates

Initial efforts have led to the design and synthesis of two chelate architectures, **6** (Fig. 2.5) and **15** (Fig. 2.9), that are anticipated to exhibit high affinity for the uranyl ion. Adsorbents containing these chelates have the potential to exhibit significantly increased uranium capacity

and uptake kinetics. A priority in future work is to prepare and test such adsorbents. This will involve the optimization of synthetic methods for incorporating the chelates within polymers or high-surface-area support materials. Two approaches that will be further investigated are (1) copolymerization of vinyl-substituted dicyano chelate precursors with hydrophilic monomers and (2) use of click chemistry to attach alkyne-substituted chelates to azide functionalized polymers.

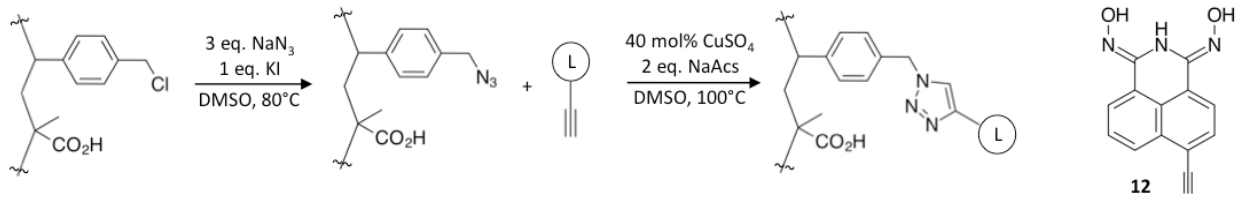

Fig. 2.13. Initial results using click chemistry; the Cu-catalyzed reaction of an azide with an alkyne, gave promising results, allowing the attachment of 12 to a copolymer of chloromethylstyrene + methylacrylic acid with an 80% yield.

2.2.2 Design of alternate chelating sites

Although initial efforts have focused on amidoxime and imide dioxime chelates, alternate types of donor groups may yield effective uranyl chelators under seawater conditions. One donor of interest is the basic aromatic hydroxyl group that occurs in strong chelates such as 8-hydroxyquinoline, salicylic acid, and maltol. Another family of donor groups are the organophosphorus acids (phosphates, phosphonates, and phosphinates). Computer-aided design methods will be used to identify optimal chelating architectures based on these donors. Synthetically tractable candidates will be prepared, characterized, and functionalized for incorporation in adsorbent materials.

2.2.3 Design monomers that co-polymerize to yield improved chelating sites

Some monomer pairs, A and B, polymerize in an alternating fashion to yield polymers of the form ABABABAB…. In such cases, it is possible to predict the local molecular structure of an AB subunit. By proper choice of monomer structure, it should be possible to form improved chelating arrangements of adjacent donor groups during polymerization. The benefits of this approach are that the monomers would be simpler molecules and, therefore, less costly to prepare; and the chelating sites would be directly formed during polymerization, removing the need for post-polymer functionalization.

2.2.4 Design of receptors for recognition of $[UO_2(CO_3)_3]^{4-}$

Competition with other metal ions present in seawater results in decreased uptake by adsorbents that form inner sphere metal complexes. Selectivity for uranium, and therefore the capacity of the adsorbent, could be greatly enhanced by developing receptors designed to work by binding the unique shape of the tris-carbonate complex rather than by displacing carbonate. HostDesigner, would be used to design the outer-sphere receptors that would be based on hydrogen bond donating groups. After identifying candidates that scored well in terms of structural organization for uranyl tricarbonate complex, additional criteria would be applied to select candidates for potential synthesis and testing.

2.3 References

(1) a) Schenk, H. J.; Astheimer, L.; Witte, E. G.; Schwochau, K. *Sep. Sci. Technol.* **1982**, *17*, 1293. b) Astheimer, L.; Schenk, H. J.; Witte, E. G.; Schwochau, K. *Sep. Sci. Technol.* **1983**, *18*, 307.

(2) Tian, G.; Teat, S. J.; Zhang, Z.; Rao, L. *Dalton Trans.* **2012**, *41*, 11579.

(3) a) Zhang, A.; Asakura, T.; Uchiyama, G. *React. Funct. Polym.* **2003**, *57*, 67. b) Katragadda, S.; Gesser, H. D.; Chow, A. *Talanta* **1997**, *45*, 257. c) Zhang, A.; Uchiyama, G.; Asakura, T. *React. Funct. Polym.* **2005**, *63*, 143. d) Zhang, A.; Uchiyama, G.; Asakura, T. *Sep. Sci. Technol.* **2003**, *38*, 1829. e) Zhang, A.; Uchiyama, G.; Asakura, T. *Adsorpt. Sci. Technol.* **2003**, *21*, 761. f) Seko, N.; Katakai, A.; Tamada, M.; Sugo, T.; Yoshii, F. *Sep. Sci. Technol.* **2005**, *39*, 3753. g) Kobuke, Y.; Tanaka, H.; Ogoshi, H. *Polym. J.* **1990**, *22*, 179.

(4) Kang, S. O.; Vukovic, S.; Custelcean, R.; Hay, B. P. *Ind. Chem. Eng. Res.* **2012**, *51*, 6619.

(5) a) Eloy, F.; Lenaers, R. *Chem. Rev.* **1962**, *62*, 155. b) Elvidge, J. A.; Linstead, R. P.; Salaman, A. M. *J. Chem. Soc.* **1959**, 208.

(6) Grant, C. D.; Kang, S. O.; Hay, B. P. *J. Org. Chem.* **2013**, submitted.

(7) a) Hirotsu, T.; Katoh, S.; Sugasaka, K. *J. Chem. Soc., Dalton. Trans.* **1986**, 1609. b) Tomiyasu, H.; Nogami, M.; Ikeda, Y. *J. Nucl. Sci. Technol.* **2000**, *37*, 344.

(8) Choi, S. H.; Nho, Y. C. *Radiat. Phys. Chem.* **2000**, *57*, 187.

(9) Vukovic, S.; Watson, L. A.; Kang, S. O.; Custelcean, R.; Hay, B. P. *Inorg. Chem.* **2012**, *51*, 3855.

(10) Barber, P. S.; Kelley, S. P.; Rogers, R. D. *RSC Advances* **2012**, *2*, 8526.

(11) Vukovic, S.; Hay, B. P. *Inorg. Chem.* **2013**, in press

3. COORDINATION OF UO_2^{2+} WITH AMIDOXIME-RELATED LIGANDS: THERMODYNAMICS, KINETICS, AND STRUCTURE

Linfeng Rao, Guoxin Tian, Xiaoqi Sun, Francesco Endrizz
Lawrence Berkeley National Laboratory

3.1 Background and Significance

Though the amidoxime-based sorption system has been demonstrated in Japan to be significantly better than other systems such as TiO_2(s) sorption or solvent extraction in the extraction of uranium from seawater, the cost of the marine extraction process is still much higher than that of uranium mining from terrestrial sources.[1-4] To substantially reduce the cost, fundamental thermodynamic, kinetic, and structural studies are needed to improve the sorption efficiency for uranium, the selectivity of the sorbents for uranium over other metal elements, and the stability of the sorbents under the conditions in seawater as well as in the elution (or desorption) process where strong acid or carbonate solutions are used.[1] At present, the following fundamental chemistry questions remain unanswered.

- What are the possible ligand functionalities that could have formed in the grafting/reaction process? Among the possible ligand configurations, which one has the strongest binding ability toward uranium?
- How is the uranium sorption affected by temperature variations?
- How strongly do the major transition metal ions [e.g., Fe(III)] compete with U(VI) for the sorption and how can the selectivity of the sorbents be improved?
- What are the coordination modes in the complexes between the ligands and uranium or major competing transition metal elements in seawater?
- How fast do the amidoxime-related ligands interact with uranium under seawater conditions?

Answers to these questions could have a number of significant scientific and technological impacts on the extraction of uranium from seawater: (1) the process for preparing the sorbents can be optimized to obtain high yields of the most preferred ligand configuration, thus increasing the sorption efficiency for uranium; (2) a structure-property relationship serves as guidance to modify the ligand structure to achieve the strongest binding with uranium and/or the highest selectivity for uranium over competing elements; (3) a better understanding of the effect of temperature on the sorption of uranium helps with the decision making as to the location of the marine sorption facility and the seasonal timing of the marine operation; (4) the kinetic information helps to identify the rate-determining step and leads to ways for improving the sorption rate. Ultimately, answers to the above questions help to reduce the cost of uranium collection from seawater and make the process economically more competitive.

3.2 Research Progress/Status

Searching for answers to the above questions, we have conducted systematic thermodynamic, kinetic, and structural studies in five areas, and the progress made to date is summarized in the following sections. A better fundamental understanding of the thermodynamics and kinetics of the interactions of amidoxime-related ligands with uranium and major transition metals in seawater, as well as the coordination modes, provides the guidance to improve the process for the extraction of uranium.

3.2.1 Quantifying the binding strength of UO_2^{2+} with structurally related amidoxime ligands

A few possible configurations of amidoxime-related ligands could form in the radiation grafting process, as discussed in Section 2 (Fig. 3.1): cyclic imide dioxime (H_2A) and open-chain diamidoxime (H_2B, also called "bis-amidoxime"), and cyclic carbonyl imidoxime (HC). If their binding strengths with UO_2^{2+} and chemical stability differ, the yields of each configuration in the grafting process will affect the efficiency of uranium collection and the reusability of the sorbents, thus having a significant impact on the cost of the process for the collection of uranium from seawater.

The cyclic imidedioxime and open-chain diamidoxime ligands were each synthesized in high yields by controlling the reaction temperature in the reaction with hydroxylamine (80–90 °C for the cyclic imidedioxime and room temperature for the open-chain diamidoxime). Thermodynamic studies were conducted to quantify their binding strengths with UO_2^{2+} in 0.5 M NaCl solutions (equivalent to ~ 3% NaCl as in seawater).[5,6] The study of the cyclic carbonyl imidoxime ligand (HC) has not been started in the first phase of the project and is planned for the next period.

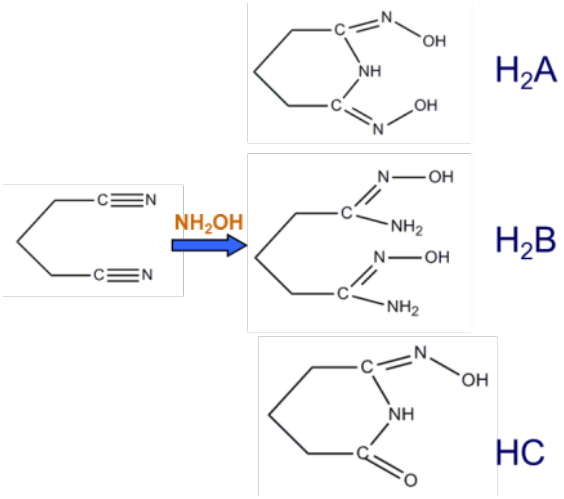

Fig. 3.1. Structurally related ligand configurations that could form in the grafting/reaction process for the preparation of amidoxime-based sorbents.

Potentiometric and spectrophotometric titrations were jointly used to determine the stability constants of the complexes between UO_2^{2+} and the two structurally related ligands: glutarimidedioxime (the cyclic imidedioxime H_2A) and glutardiamidoxime (the open-chain diamidoxime H_2B). Representative potentiometric titrations for the complexation of UO_2^{2+} with H_2A and H_2B are shown in Fig. 3.2. The stability constants obtained are summarized in Table 3.1. Data for the complexation of UO_2^{2+} with another ligand, synthesized at ORNL,[7] were also determined in this work and included for comparison in Table 3.1. This ligand—structurally similar to H_2A except that it has an aromatic ring fused with the cyclic imidedioxime structure—has been found to be more stable in strong acid solutions. [7]

Data in Table 3.1 indicate that the cyclic imidedioxime (H_2A) is a stronger ligand than the open-chain diamidoxime (H_2B). As the structural analysis shows, the high binding strength of ligand H_2A originates from the coordination with UO_2^{2+} in its equatorial plane through a conjugated O-N=C-N-C=N-O system where the electron density is delocalized due to the

rearrangement of protons.[5] On the other hand, the ligand with a fused aromatic ring is weaker than either H_2A or H_2B; computational studies may help to reveal the distribution of electron density on this ligand with a fused aromatic ring and help to interpret its lower binding strength with U(VI).

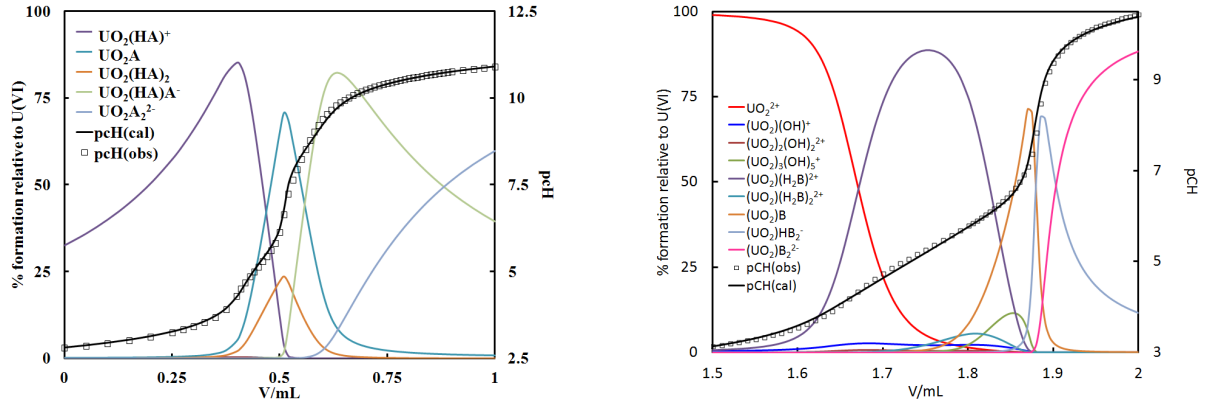

Fig. 3.2. Potentiometric titrations for the complexation of H_2A (left) and H_2B (right) with U(VI).[5,6]

Under the conditions of seawater (pH ~ 8.3), the predominant species of uranium is the very stable tricarbonate U(VI) complex, $UO_2(CO_3)_3^{4-}$. Therefore, to be effective, cationic sequestering agents such as the amidoxime-based sorbents must be capable of replacing the carbonate in $UO_2(CO_3)_3^{4-}$. Spectrophotometric experiments were conducted to evaluate the ability of ligands H_2A and H_2B to compete with carbonate for complexing UO_2^{2+} under seawater pH. The optical absorption spectra of U(VI) in the presence of carbonate and H_2A or H_2B are shown in Fig. 3.3.

Table 3.1. Stability constants of U(VI) complexes with structurally related amidoxime ligands (25 °C and 0.5 M NaCl ionic strength).[5,6]

Reaction	logβ				
	H_2A 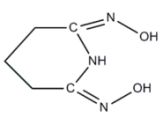		H_2B 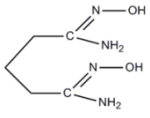		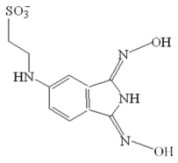
	logβ	ΔH, kJ/M	logβ	ΔH, kJ/M	logβ^*
$UO_2^{2+} + L^{2-} = UO_2L$	17.8 ± 1.1	-59 ± 8	17.3 ± 0.3	-49 ± 6	15.3 ± 0.5
$H^+ + UO_2^{2+} + L^{2-} = UO_2(HL)^+$	22.7 ± 1.3	-71 ± 6			19.5 ± 0.8
$2H^+ + UO_2^{2+} + L^{2-} = UO_2(H_2L)^{2+}$			29.2 ± 0.3	-102 ± 6	
$UO_2^{2+} + 2L^{2-} = UO_2L_2^{2-}$	27.5 ± 2.3	-101 ± 10	26.1 ± 0.3	-123 ± 7	25.1 ± 0.2
$H^+ + UO_2^{2+} + 2L^{2-} = UO_2(HL)L^-$	36.8 ± 2.1	-118 ± 6	36.4 ± 0.3	-133 ± 8	34.6 ± 0.2
$2H^+ + UO_2^{2+} + 2L^{2-} = UO_2(HL)_2$	43.0 ± 1.1	-154 ± 25			39.9 ± 0.2
$4H^+ + UO_2^{2+} + 2L^{2-} = UO_2(H_2L)_2^{2+}$			56.3 ± 1.0	-207 ± 16	

*Preliminary data to be further evaluated and finalized for this ligand.

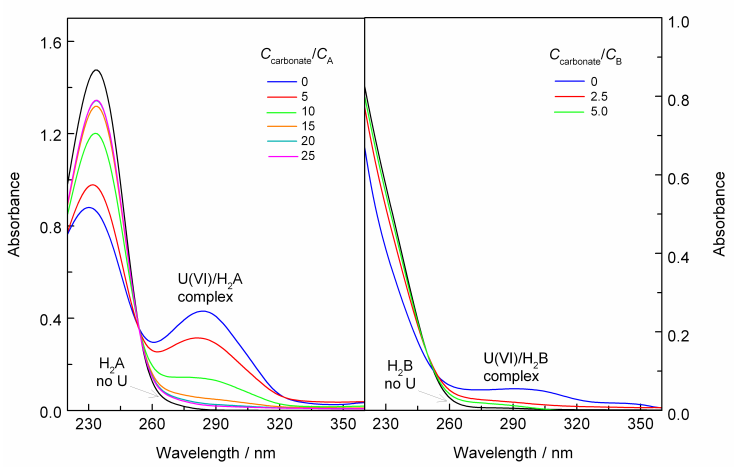

Fig. 3.3. Absorption spectra showing the competition of H_2A (left) and H_2B (right) with carbonate for complexing uranium. C_U = 0.05 mM. (left) C_A= 0.10 mM, $C_{carbonate}/C_A$ = 0 – 25; (right) C_B = 0.10 mM, $C_{carbonate}/C_B$ = 0 – 5.[6]

At the same concentration of the ligands ($C_A = C_B$ = 0.1 mM), the left figure shows that when the ratio of $C_{carbonate}/C_A$ is as high as 10, the intensity of the band for the U(VI)/H_2A complexes (at ~290 nm) is still significant. On the contrary, the right figure shows that the bands for the U(VI)/H_2B complexes (at ~300 nm and 350 nm) are barely identifiable when the ratio of $C_{carbonate}/C_B$ is as low as 2.5. Obviously, the cyclic imidedioxime (H_2A) is a much stronger competing ligand with carbonate for complexing U(VI) than the open-chain diamidoxime ligand (H_2B) under these conditions.

With the stability constants of U(VI) complexes with H_2A and H_2B from this work,[5,6] and with carbonate from the literature,[8] the speciation of U(VI) under seawater conditions (C_U = 3.3 ppb, $C_{carbonate}$ = 0.0023 M) is calculated and shown in Fig. 3.4. At the seawater pH (8.3) and in the presence of 0.001 M H_2A (left figure), more than 95% U(VI) is complexed by glutarimidedioxime (86% $UO_2HA_2^-$, 8% $UO_2A_2^{2-}$, 2% UO_2A), whereas $UO_2(CO_3)_3^{4-}$ accounts for only 2% U(VI). On the contrary, in the presence of 0.001 M H_2B (right figure), nearly all U(VI) is complexed by carbonate (98.6% $UO_2(CO_3)_3^{4-}$ and 1.1% $UO_2(CO_3)_2^{2-}$). The speciation indicates that the cyclic imidedioxime H_2A is a much stronger complexant that can compete with carbonate to complex U(VI) at the seawater pH.

The cyclic imidedioxime (H_2A) is a stronger complexing ligand than the open chain diamidoxime (H_2B) and can effectively compete with carbonate for U(VI) under seawater pH. Therefore, these studies indicate the cyclic imidedioxime (H_2A) is the preferred configuration on the sorbent for the collection of uranium from seawater. However, the stability of the cyclic imidedioxime ligand in the acidic elution is poor (Section 2.1.1) and alternative eluting conditions need to be evaluated.

3.2.2 Evaluating the effect of temperature on U(VI)/ligand binding

The temperature of seawater varies with location, depth, season, and time, which could have significant impact on the efficiency of U(VI) sequestration from seawater if the sequestration reaction has a strong temperature dependency. Therefore, the enthalpy of complexation is an important thermodynamic parameter that allows the evaluation of the effect of temperature on the collection of uranium under seawater conditions and helps in making decisions on the location and operation season/time of the marine collection facility.

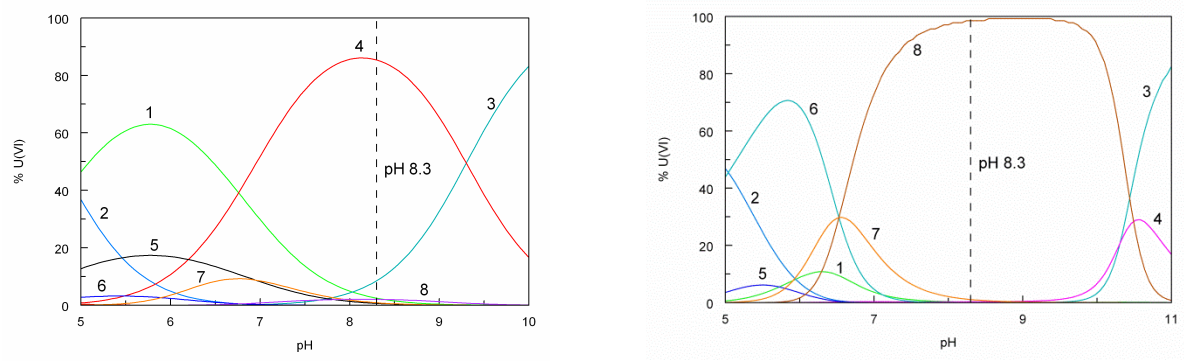

Fig. 3.4. Speciation of U(VI) as a function of pH (C_U = 3.3 ppb, $C_{carbonate}$ = 0.0023 M). (left) C_A = 0.001M. 1 - UO_2A, 2 - UO_2HA^+, 3 - $UO_2A_2^{2-}$, 4 - $UO_2HA_2^-$, 5 - $UO_2H_2A_2$, 6 - $UO_2(CO_3)$, 7 - $UO_2(CO_3)_2^{2-}$, 8 - $UO_2(CO_3)_3^{4-}$. (right) C_B = 0.001M. 1 – UO_2B, 2 - $UO_2H_2B^{2+}$, 3 - $UO_2B_2^{2-}$, 4 - $UO_2HB_2^-$, 5 - $UO_2H_4B_2^{2+}$, 6 - $UO_2(CO_3)$, 7 - $UO_2(CO_3)_2^{2-}$, 8 - $UO_2(CO_3)_3^{4-}$.[5,6]

Microcalorimetric titrations were conducted at 25 °C to determine the enthalpy of complexation between UO_2^{2+} and amidoxime-related ligands (H_2A and H_2B). The results are shown in Table 3.1. Based on the thermodynamic parameters on the speciation of carbonate,[9] the cyclic imidedioxime ligand and its complexes with U(VI) (Table 3.1), the dominant species under seawater pH, are HCO_3^-, H_2A, $UO_2(CO_3)_3^{4-}$, and $UO_2(HA)A^-$, respectively. Therefore, the major overall reaction can be written as

$$UO_2(CO_3)_3^{4-} + 2\ H_2A = UO_2(HA)A^- + 3\ HCO_3^- \quad (1)$$

Using the enthalpy values for HCO_3^- and $UO_2(CO_3)_3^{4-}$ in the literature[8,9,10] and for H_2A and $UO_2(HA)A^-$ from this work (Table 3.1), the enthalpy of reaction (1) is calculated to be +16.7 kJ/mol. This means that the overall sequestration of U(VI) from seawater by the cyclicimidedioxime ligand is *endothermic*, and that the efficiency of sequestration should be enhanced at higher temperatures. This thermodynamic analysis confirms the observation in the marine experiments in Japan that the U(VI) extraction efficiency was higher from warmer seawater.[11,12] The marine experiments in Japan showed a 1.5 times increase in the efficiency when the seawater temperature increased by 10 °C. [11,12] In fact, using the van't Hoff equation and the enthalpy of reaction (1) (+16.7 kJ/mol), it is estimated that the equilibrium constant of reaction (1) at 20 °C would be 1.3 times that at 10 °C, which is in excellent agreement with the observations in the marine experiments.

From a thermodynamic point of view, the endothermic enthalpy of the overall complexation reaction implies that the efficiency of uranium collection with amidoxime-based sorbents is higher at higher temperatures.

3.2.3 Evaluating the competition between transition metal elements and uranium

The concentrations of some transition metal elements in seawater are higher than or comparable to the concentration of uranium (e.g., Fe, 0.03 ppb; Pb, 0.01 ppb; Ni 0.48, ppb; Cu, 0.15 ppb).[13] Therefore, they are capable of competing with uranium for sorption by the amidoxime-based sorbents. Consequently, such competition would reduce the sorption capacity and efficiency for uranium and increase the cost of uranium collection.

Determination of the equilibrium constants and enthalpy of complexation between transition metal elements and a series of structurally related amidoxime ligands can provide thermodynamic information that allows quantitative evaluation of the competition between transition metal elements and uranium and helps to optimize the process for uranium collection.

Complexation of the cyclic imidedioxime ligand (H_2A) with major transition metal elements in seawater, including Fe(III), Cu(II), Pb(II), and Ni(II), was studied by potentiometry, microcalorimetry, and X-ray crystallography. The potentiometric titrations for the complexation of ligand H_2A with Fe(III), Cu(II), Pb(II), and Ni(II) are shown in Fig. 3.5. From these, the complexation stability constants are calculated and summarized in Table 3.2.

The stability constants of UO_2^{2+} with the cyclic imidedioxime ligand are also shown in Table 3.2, in comparison with the data for transition metal elements. In general, the binding strength of the ligand with UO_2^{2+} and transition metal elements follows the order [14]

$$\text{Fe(III)} > \text{U(VI)} \sim \text{Cu(II)} > \text{Pb(II)} > \text{Ni(II)} .$$

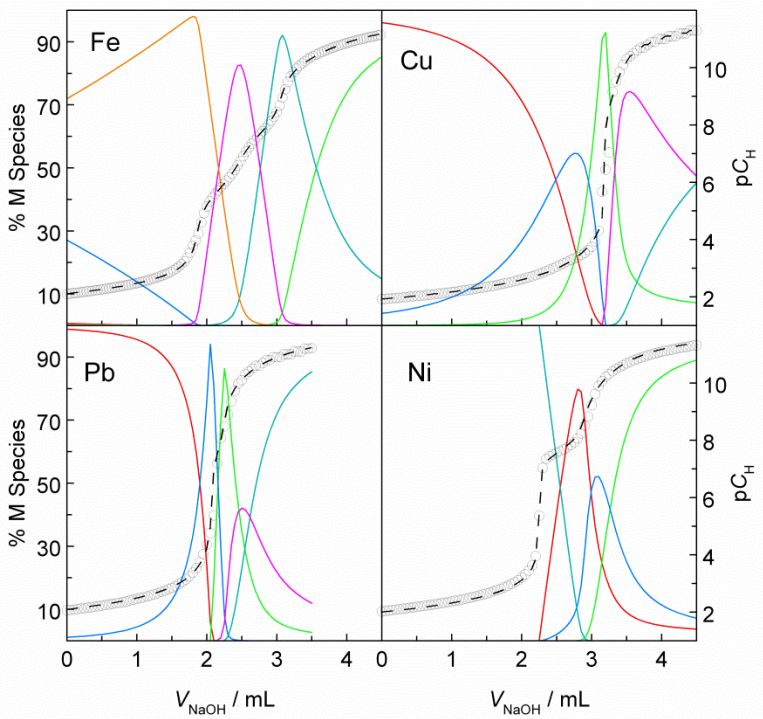

Fig. 3.5. Potentiometric titrations for the complexation of H_2A with transition metal elements. Solid color lines – the percentages of transition metal complexes with H_2A (left y-axis); gray circles – experimental pC_H; dashed black line – fitted pC_H (right y-axis). The titrations were conducted with metal/ligand solutions in the cup titrated with NaOH.[14]

Even though iron(III) concentrations vary in seawater, Fe(III) is a major competitor with U(VI) in the collection of uranium from seawater with amidoxime-based sorbents, because it binds with amidoxime-related ligands more strongly than U(VI). Improving the selectivity of the sorbent for uranium over iron and other metals through modifications of the amidoxime ligands and/or synthesis of new ligands guided by the computational studies outlined in Section 2, could increase the efficiency of uranium sorption and reduce the cost.

Table 3.2. Stability constants of the complexes between ligand H_2A and transition metals in comparison with UO_2^{2+} (ref. 14)

Reactions	logβ				
	UO_2^{2+}	Fe^{3+}	Cu^{2+}	Pb^{2+}	Ni^{2+}
$M^{j+} + A^{2-} = MA^{(j-2)+}$	17.8 ± 1.1		18.9 ± 0.2	14.3 ± 0.1	10.3 ± 0.1
$M^{j+} + H^+ + A^{2-} = M(HA)^{(j-1)+}$	22.7 ± 1.3	25.7 ± 1.1	22.7 ± 0.1	21.8 ± 0.1	
$M^{j+} + 2A^{2-} = MA_2^{(j-4)+}$	27.5 ± 2.3	36.0 ± 1.1	24.4 ± 0.1	19.4 ± 0.2	16.7 ± 0.1
$M^{j+} + H^+ + 2A^{2-} = M(HA)A^{(j-3)+}$	36.8 ± 2.1	43.9 ± 1.1	35.8 ± 0.1	30.0 ± 0.2	27.0 ± 0.1
$M^{j+} + 2H^+ + 2A^{2-} = M(HA)_2^{(j-2)+}$	43.0 ± 1.1	49.7 ± 1.1			
$M^{j+} + 2A^{2-} + H_2O = M(OH)A_2^{(j-4)+} + H^+$		25.7 ± 1.1			

3.2.4 Revealing the coordination modes in complexes with U(VI) and transition metal elements

Structural data on the complexes of amdioxime-related ligands with uranium and transition metal elements reveals the binding modes, helps to interpret the binding strength, and provides fundamental information that serves as the guidance to modify the ligand and improve the efficiency and selectivity of the collection of uranium from seawater.

3.2.4.1 Structure of the uranium complex with cyclic imidedioxime

The single-crystal structure of a 1:2 UO_2^{2+}/H_2A complex is shown in Fig. 3.6. The U(VI) complex, $UO_2(HA)_2H_2O$, crystalized in a highly symmetrical structure with the *Pccn* space group symmetry. The uranium atom is at the center of inversion. The two HA^- ligands coordinate to the uranium center in a tridentate mode *via* the equatorial plane. The HA^- ligands are almost coplanar except for the middle methylene groups. The O=U=O moiety is perfectly linear and symmetrical, with an angle of 180° and typical U=O distances of 1.7846 Å.

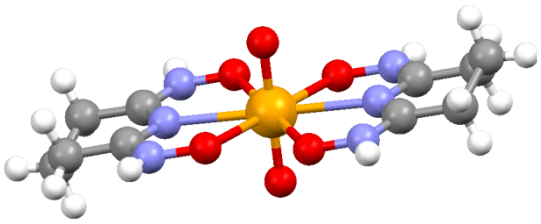

Fig. 3.6. Crystal structure of $UO_2(HA)_2 \cdot H_2O$. The H_2O molecule is not shown for clarity.[5]

Two unusual and remarkable features are observed in the structure of the $UO_2(HA)_2$ complex: (1) the protons of both oxime groups (-CH=N-O**H**) are rearranged from the oxygen atom to the nitrogen atom; (2) the middle imide group (-CH-**N**H-CH-) is deprotonated, resulting in a -1 charged HA^{-1} ligand that coordinates to UO_2^{2+} in a tridentate mode (*via* the two oxime oxygen atoms and the imide nitrogen atom). With such a configuration, the electron density on the HA^- ligand could actually be delocalized on –O-N-C-N-C-N-O-, forming a conjugated system that strongly coordinates to UO_2^{2+}. In fact, the bond length of the N-O bond of the oxime group is actually shortened, instead of being elongated as observed in many complexes, due to the complexation: 1.42 Å in the free H_2A molecule compared with 1.35/1.36 Å in the $UO_2(HA)_2$ molecule. The significant shortening of the N-O bond upon complexation with UO_2^{2+} supports

the above arguments for a conjugated ligand system with delocalization of electron density on –O-N-C-N-C-N-O-.[5]

DFT calculations were performed to optimize the geometry of the complex and obtain the electronic information on the coordination bonds in the complex. Two bonding molecular orbitals are shown in Fig. 3.7. The DFT analysis indicates large donation of electron density from the imidedioxime ligand to UO_2^{2+} and strong covalent bonding. Contrary to the structures of U(VI)/amidoxime complexes (where the nitrogen atom does not participate in the coordination) in the literature, our results (both experimental and computational) have unambiguously demonstrated the critical role of the orbitals on the imide nitrogen atom on the cyclic imidedioxime—particularly the orbitals with π character perpendicular to the ligand plane—in binding the uranyl cation. Therefore, maximizing the electron donating ability of the imide nitrogen atom should result in stronger interactions with the uranyl cation.

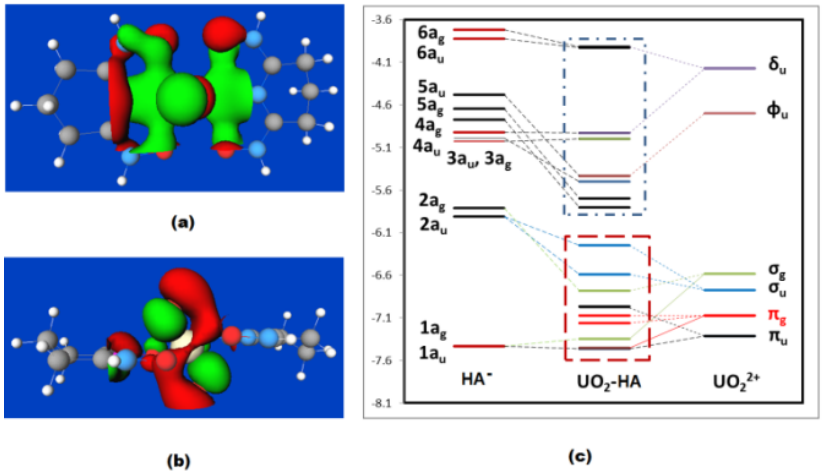

Fig. 3.7. Selected bonding orbitals in $UO_2(HA)_2$. (a) A strong bonding orbital between the uranyl σ_u and ligand $2a_u$; (b) a bonding orbital involving strong hybridization of the occupied σ and π orbitals on uranyl and hybridization between the nitrogen *p* orbitals in and perpendicular to the ligand plane; (c) molecular orbital diagram.[5]

3.2.4.2 Structure of iron complexes with cyclic imidedioxime

To gain insight into how to improve the selectivity between iron and uranium, the structures of a 1:1 and 1:2 Fe^{3+}/H_2A complexes, $Fe(HA)Cl_2$ and Fe(HA)A, were investigated. As shown in Fig. 3.8, for $Fe(HA)Cl_2$, the HA^- ligand coordinates to the iron atom in a tridentate mode (the two oxime oxygen atoms and the imide nitrogen atom) *via* the equatorial plane. The protons of both oxime groups are rearranged from the oxygen atom to the nitrogen atom, and the middle imide group is deprotonated (HA^-) to coordinate to Fe^{3+}. In Fe(HA)A, the two ligand units are not identical: one is HA^- and the other is A^{2-}. Both HA^- and A^{2-} are tridentate with two oxime oxygens and one imido nitrogen coordinating to the center iron atom. Similar to the coordination mode in the $UO_2(HA)_2$ complex,[5] the HA^- ligand coordinates to Fe^{3+} through a conjugated system with delocalization of electron density on –O-N-C-N-C-N-O-, resulting in very strong complexes.

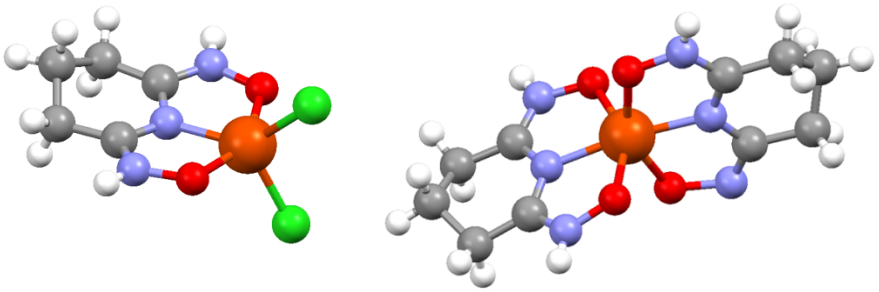

Fig. 3.8. Crystal structures of $Fe(HA)Cl_2$ (left) and Fe(HA)A (right).[14]

Structural information indicates that amidoxime-related ligands coordinate to both UO_2^{2+} and Fe^{3+} as tridentate ligands. Maximizing the electron-donating ability of the imide/amide nitrogen atom would result in stronger interactions with both cations, which may have little effect on the selectivity. From a structural point of view, developing ligands that could take advantage of the difference in shape of the two cations (the linear $O=U=O^{2+}$ and the spherical Fe^{3+}) could help to improve the selectivity for uranium over iron.

3.2.5 Investigating the kinetics of the complexation between U(VI) and the cyclic imidedioxime

Because seawater is in constant motion and the ocean current travels at fast speeds (e.g., 50–300 cm/s for the "Black Current" near the coast of Japan),[3,4] the efficiency of collecting uranium from seawater depends on, in addition to the thermodynamic binding strength, the rate of sorption. Therefore, it is of great importance to investigate the kinetics of the interactions between uranium and the amidoxime-related ligands.

As described previously, under the seawater conditions (pH 8.3, total inorganic carbon 2.3 mmole·L^{-1}), the major complexation reaction between U(VI) and cyclic imidedioxime is expressed as reaction (1). It is a competition reaction between the dominant U(VI) species in seawater, $UO_2(CO_3)_3^{4-}$, and the cyclic imidedioxime. Preliminary experiments have indicated that this reaction is relatively fast, so that conventional techniques for kinetic studies are not suitable. Instead, the stopped-flow technique is appropriate for such studies. Using this technique, the two reactants, $UO_2(CO_3)_3^{4-}$ and H_2A, were raplidly mixed (>99% mixing within milliseconds) and the absorption spectra in the UV region were collected, where the decrease of the absorpton band of H_2A is accompanied by the increase of the absorption band of $UO_2(HA)A^-$ (Fig. 3.9). Analysis of the spectra as a function of time gives the apparent rate constants for reaction (1). The values are summarized in Table 3.3.

Two features of the reaction kinetics are observed: (1) in general, the competition reaction between $UO_2(CO_3)_3^{4-}$ and H_2A is moderately fast; (2) the reaction becomes faster as the pH is increased from 5.4 to 8.8. At the seawater pH (8.3), k_1 is estimated to be ~ 1 s^{-1}, meaning that the reaction lifetime is about 1 second.

Results show that the overall competition reaction (1) is relatively fast compared with the rate of sorption of uranium on amidoxime-based sorbents, implying that the diffusion of uranium species in seawater into the sorbent might be the rate-determining step in the sorption process (see discussions in Section 6). Facilitating the diffusion process (e.g., by making the sorbents more hydrophilic and more accessible) would have the most significant impact on the rate of uranium sorption from seawater.

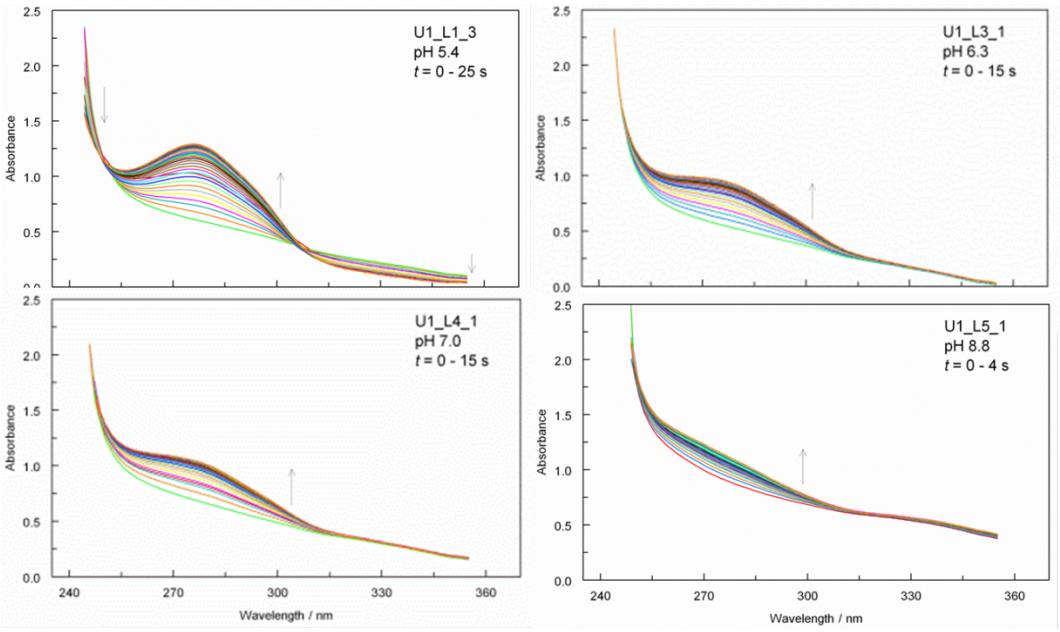

Fig. 3.9. Absorption spectra of the stopped-flow kinetic experiments for the reaction $UO_2(CO_3)_3^{4-} + 2\ H_2A = UO_2(HA)A^- + 3\ HCO_3^-$ (in 0.5 M NaCl).

Table 3.3. Apparent pseudo first-order rate constant for the reaction $UO_2(CO_3)_3^{4-} + 2\ H_2A = UO_2(HA)A^- + 3\ HCO_3^-$ (in 0.5 M NaCl)

pH	k_1, s^{-1}
5.4	0.205 ± 0.001
6.3	0.483 ± 0.003
7.0	0.674 ± 0.003
8.8	1.300 ± 0.010

3.3 Future Work

Four research activities are planned for the next 3 years.

3.3.1 Completing thermodynamic studies of the complexation of amidoxime-related ligands with uranium to develop the structure-property relationship

Besides the cyclic imidedioxime ligand (H_2A) and the open-chain diamidoxime ligand (H_2B), formation of a third configuration (shown as HC in Fig. 3.1) is also possible in the grafting/reaction process to prepare amidoxime-based sorbents. The reaction conditions that facilitate the formation of this configuration will be determined. Thermodynamic measurements and structural characterization will be performed to obtain the binding strength of HC with UO_2^{2+} and the coordination mode(s) in the uranyl complexes. Combining the data for HC with previous data for H_2A and H_2B, a structure-property relationship will be developed and it serves as the guidance for (1) modifying the ligand structure to achieve stronger binding with UO_2^{2+} and (2) optimizing the grafting/reaction conditions (e.g., temperature, concentration ratio of reactants) to obtain sorbents with the preferred ligand configuration in high yields.

In addition, because carboxylic acids were used as the co-monomer in the preparation of amidoxime-based sorbents to improve the hydrophilicity of the sorbents, it is likely that carboxylic acid groups are present in the proximity of the amidoxime functionality and they could complex uranium as either binary U(VI)/carboxylate complexes or as ternary U(VI)/amidoxime/carboxylate complexes. In the literature, there are sufficient data on the binary U(VI)/carboxylate complexes, but few data on the ternary U(VI)/amidoxime/carboxylate complexes. We will design experiments to determine the thermodynamic values for the U(VI)/amidoxime/carboxylate complexes.

3.3.2 Quantifying the binding strength of vanadium with amidoxime-related ligands to evaluate the effect of vanadium sorption on the efficiency of uranium collection

Previous sorption studies in Japan as well as at ORNL and PNNL have shown that vanadium was strongly absorbed by amidoxime-based sorbents and that it was extremely difficult to elute vanadium from the sorbents by HCl. Obviously, the behavior of vanadium could result in adverse effects on the collection of uranium collection. On one hand, the strong sorption of vanadium could diminish the effective sites that are available for uranium, reducing the sorption capacity and efficiency. On the other hand, the difficulty in the elution of vanadium could reduce the number of repeated use of the sorbents, increasing the cost of uranium collection.

The chemistry of vanadium is complex. As shown by the Pourbaix diagram (Fig. 3.10), multiple oxidation states and hydrolyzed species could be present in solution and solids. Under the seawater conditions, vanadium probably exists as anionic $VO_2(OH)_2^-$ and VO_3OH^{2-} species. It is unknown why these species interact so strongly with the amidoxime-based sorbents.

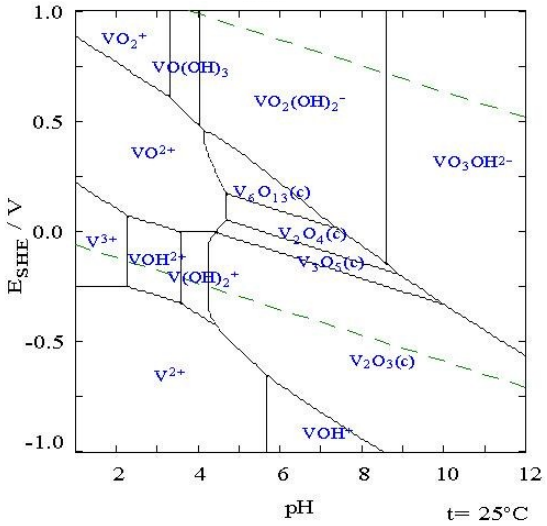

Fig. 3.10. Pourbaix diagram of vanadium (total concentration = 10 μM).[15]

At present, there are no thermodynamic data on the interaction of vanadium with amidoxime-related ligands. We plan to quantify the binding strength of amidoxime-related ligands with vanadium and investigate the coordination mode(s) in the vanadium complexes. The thermodynamic and structural data will help to evaluate the competition between vanadium and uranium in the sorption process, and provide guidance in developing an efficient elution process for vanadium.

3.3.3 Continuing the kinetic studies to determine the rate-determining step in the interaction of tricarbonato U(VI) with amidoxime-related ligands

The preliminary kinetic data described in a previous section only provide a general idea on the rate of the overall reaction (1). The overall reaction could consist of a number of elementary reactions, including the stepwise dissociation of $UO_2(CO_3)_3^{4-}$ (2), the stepwise deprotonation of H_2A (3), the complexation of UO_2^{2+} with the ligand (4), and the protonation of CO_3^{2-} (5), as shown below.

$$UO_2(CO_3)_3^{4-} \rightarrow \rightarrow \rightarrow UO_2^{2+} + 3CO_3^{2-} \text{ (stepwise)} \quad (2)$$

$$H_2A \rightarrow H^+ + HA^- \rightarrow 2H^+ + A^{2-} \quad (3)$$

$$UO_2^{2+} + A^{2-} + HA^- \rightarrow \rightarrow UO_2(HA)A^- \quad (4)$$

$$H^+ + CO_3^{2-} \rightarrow HCO_3^- \quad (5)$$

Further kinetic experiments are planned to determine which elementary reaction is the slowest, i.e., the rate-determining step of the overall reaction. At present, we hypothesize that the deprotonation of the ligand could be slow, because it involves the relocation of the proton(s) from the oxygen to the nitrogen in the oxime group and the deprotonation of the imide group upon complexation.[5] This hypothesis could be validated or refuted by determining the "kinetic isotope effect" in carefully designed experiments with H_2O/D_2O.[16] In conjunction with the studies of diffusion kinetics, information on the rate-determining step will help to improve the sorption rate and increase the efficiency of uranium collection.

3.3.4 Investigating the speciation of uranium in the presence of dissolved organic carbon and/or hydrogen peroxide under seawater conditions

Concerns have been raised recently about the effect of the presence of organic carbon and hydrogen peroxide on the speciation of uranium in seawater. Organic carbon materials, such as fulvic and humic acids, could form complexes with uranium. In particular, the complexes between U(VI) and humic acid could be moderately strong because the latter has both carboxylate and phenolate groups that are deprotonated to some degree at seawater pH.[17] Hydrogen peroxide, on the other hand, is known to exist in the ocean (mostly surface seawater) and form strong ternary complexes with UO_2^{2+} and carbonate, such as $UO_2(O_2)(CO_3)_2^{4-}$.[18,19] We plan to conduct a literature survey and collect the information on the concentrations of humic acid and hydrogen peroxide as a function of depth in the ocean and the thermodynamic data on their complexation with UO_2^{2+} and, using the most probable conditions in seawater, update the speciation of U(VI) that we have calculated previously. The results will show whether there are effects of the presence of organic carbon and/or hydrogen peroxide on the uranium speciation and, if there are any, how large the effects are. Such information is important to the development of the sorption and elution processes.

3.4 References

(1) Rao, L. Recent International R&D Activities in the Extraction of Uranium from Seawater, Report LBNL-4034E, Lawrence Berkeley National Laboratory, Berkeley, California, USA, March 15, 2010.

(2) Davies, R. V.; Kennedy, J.; McIlroy, R. W.; Spence, R.; Hill, K. M. Extraction of uranium from seawater, *Nature* **1964**, *203,* 1110-1115.

(3) Tamada, M. "Current Status of Technology for Collection of Uranium from Seawater," Japan Atomic Energy Agency, 2009.

(4) Seko, N.; Katakai, A.; Hasegawa, S.; Tamada, M.; Kasai, N.; Takada, H.; Sugo, T.; Saito, K. Aquaculture of uranium in seawater by fabric-adsorbent submerged system, *Nuclear Technology* **2003**, *144,* 274-278.

(5) Tian, G.; Teat, S. J.; Zhang, Z.; Rao, L. Sequestering uranium from seawater: Binding strength and modes of uranyl complexes with glutarimidedioxime, *Dalton Trans*. **2012**, *41* (38), 11579 - 11586. Cover article.

(6) Tian, G.; Teat, S. J.; Rao, L. Thermodynamic studies of U(VI) complexation with glutardiamidoxime for sequestration of uranium from seawater, *Dalton Trans*. **2013**, *42* (16), 5690 - 5696.

(7) Kang, S. O.; Vukovic, S.; Hay, B. Cyclic Imide Dioxime: Formation and Stability, *Ind. Eng. Chem. Res*. **2012**, *51*, 6619.

(8) Hummel, W.; Anderegg, G.; Puigdomenech, I.; Rao, L.; Tochiyama, O. "Chemical Thermodynamics of Compounds and Complexes of: U, Np, Pu, Am, Tc, Zr, Ni and Se with Selected Organic Ligands", Nuclear Energy Agency Data Bank, OECD, Ed., Vol. 9, Chemical Thermodynamics, North Holland Elsevier Science Publishers B.V., Amsterdam, The Netherlands, 2005.

(9) Martell, A. E.; Smith, R. M.; Motekaitis, R. J. NIST Critically Selected Stability Constants of Metal Complexes Data Base. NIST Stand. Ref. Database 46, US Department of Commerce, Gaithersburg, MD, 1998.

(10) Grenthe, I.; Fuger, J.; Konings, R. J.; Lemire, R. J.; Muller, A. B.; Nguyen-Trung, C.; Wanner, H. "Chemical thermodynamics of uranium", (H. Wanner and I. Forest, eds.), Amsterdam: Elsevier Science Publishers B.V., 1992.

(11) Shimizu, T.; Tamada, M. *Proceedings of Civil Engineering in the Ocean* **2004**, *20*, 617.

(12) Tamada, M.; Seko, N.; Kasai, N. Shimizu, T. *Transactions of the Atomic Energy Society of Japan* **2006**, *5*, 358.

(13) Values taken mostly from "The Periodic Table of the Elements in the Ocean." http://www.mbari.org/chemsensor/about.html

(14) Sun, X.; Tian, G.; Xu, C.; Rao, L. Complexation of glutarimidedioxime with transition metals: potentiometric, calorimetric and structural studies, *submitted for publication*.

(15) http://www.geocaching.com/seek/cache_details.aspx?guid=d987db33-569f-4271-a9f3-d5be8a1b059a, website visited on March 28, 2013.

(16) Espenson, J. H. Chemical Kinetics and Reactions Mechanisms, 2nd Edition, McGraw-Hill, Inc., New York, 1995.

(17) Stevenson, F. J. Humus Chemistry, Wiley, New York, 1982.

(18) Goff, G. S.; Brodnax, L. F.; Cisneros, M. R.; Peper, S. M.; Field, S. E.; Scott, B. L.; Runde, W. H. First Identification and Thermodynamic Characterization of the Ternary

U(VI) Species, $UO_2(O_2)(CO_3)_2^{4-}$, in UO_2-H_2O_2-K_2CO_3 Solutions, *Inorg. Chem.* **2008**, *47*, 1984-1990.

(19) Zanonato, P.; Di Bernardo, P.; Szabób, Z.; Grenthe, I. Chemical equilibria in the uranyl(VI)–peroxide–carbonate system; identification of precursors for the formation of poly-peroxometallates, *Dalton Trans*. **2012**, *41*, 11635.

4. ADVANCED ADSORBENT DEVELOPMENT EMPLOYING RADIATION-INDUCED GRAFT POLYMERIZATION

Yatsandra Oyola, Tomonori Saito, Suree Brown, Sheng Dai, Christopher J. Janke
Oak Ridge National Laboratory

4.1 Background and Significance

An extensive study conducted by German researchers in the 1980s concluded that amidoxime was the most effective functionality for the recovery of uranium from seawater.[1,2] The amidoxime structure was first elucidated in 1884 by Tiemann; however, the first amidoxime was prepared in 1873 by Lossen and Schifferdecker from the reaction of hydrogen cyanide with hydroxylamine.[3] Despite the dozen existing methods to generate amidoxime, the exclusive approach for polymeric adsorbent synthesis still is the original preparation from 1873, the functional group interconversion of nitriles with hydroxylamine (Scheme 4.1).

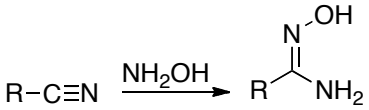

Scheme 4.1. Functional group interconversion of nitriles with hydroxylamine.

Initial research efforts on polymeric adsorbents focused on those containing the amidoxime group including poly(acrylamidoxime) fibers and polymeric beads; however, these approaches were later abandoned due to their low mechanical properties, poor durability, and practical handling issues.[4-9] To improve the durability and tensile properties of amidoxime-based fiber adsorbents, researchers at the Japan Atomic Energy Research Institute (JAERI), which is now part of the Japan Atomic Energy Agency (JAEA), studied the irradiation-induced graft polymerization (RIGP) of gaseous acrylonitrile (AN) on various trunk polymers, including tetrafluoroethylene-ethylene copolymer, polypropylene, polyamide, polyethylene, polyester, and carbon fiber.[10] By irradiating the materials, radicals were generated throughout the trunk polymer, which can initiate the graft polymerization. The grafting yield of the product was controlled by the irradiation dose, or in other words by the number of initial radicals, and the length of the graft chains. The efficiency for adsorption of transition metal ions was improved either by adding small amounts of acrylic acid (AA) or 4-vinylpyridine, or by restricting the distribution of amidoxime groups at the tetrafluoroethylene ethylene copolymer fiber surface.[11] The hydrophilicity increased the exchange rate between the external hydrated metal ions and the internal polymer hydrating water, allowing the interaction of the functional groups throughout the polymer, and induced the diffusion of hydrated metal ions. The co-grafting with hydrophilic monomers was effective in improving the adsorption rate of the uranium onto the resulting amidoximated adsorbent in seawater.

One of the challenges in RIGP is to maximize the grafting yields, i.e., the degree of grafting (DOG) determined gravimetrically from pre-irradiation and post-grafting weights, of AN groups onto the trunk polymer. The Japanese obtained a DOG of 130% by grafting AN to hollow fiber adsorbents. The material was reacted with hydroxylamine to convert the nitrile groups to the amidoxime, and was then conditioned with alkali. It was determined that the optimum alkaline treatment time was 1 h.[12,13] We have demonstrated that alkaline conditioning swells the adsorbent and increases its uranium adsorption capacity.

$$\%DOG = \frac{\left(wt_{AG} - wt_{BG}\right)}{wt_{BG}} x100$$

Equation 4.1. % DOG = % degree of grafting; wt_{AG} = dry weight after grafting; wt_{BG} = dry weight before grafting.

Other studies utilizing grafting mixtures of AN and AA or methacrylic acid (MAA) onto polyethylene films demonstrated the need for hydrophilic groups. A maximum adsorption of uranyl ions on polyethylene was obtained when a 50:50 mixture of AN:AA was randomly co-grafted onto the fibers.[14] For polypropylene fibers, an optimum DOG of 200% and 150% was obtained with a starting mixture of 80:20 AN:MAA or 70:30 AN:MAA, respectively, in dimethyl sulfoxide (DMSO).[15,16]

To synthesize a more durable deployable adsorbent, researchers from the JAEA attempted to use nonwoven polymeric fibers made from approximately 50/50 wt % of high-density polyethylene (sheath)/polypropylene (core).[17-21] These nonwoven fabrics were investigated for many years and are constructed using short, discontinuous, thermally spun-bonded fibers that have relatively poor mechanical strength compared with continuous fiber forms. Nonwoven fabrics were evaluated in several seawater experiments; however, due to their low mechanical properties, these materials had to be sandwiched into bulky stacks composed of nonwoven adsorbents, spacer nets, and stack holders that were placed on large, heavy floating frames which eventually proved too costly for deployment in the sea (see Section 1). In addition, the sandwich stacks that contained the nonwoven adsorbents prevented good accessibility to the seawater, resulting in much lower adsorption capacities compared with braided adsorbents.[22,23] Due to the high cost of the floating frames and the poor accessibility of the seawater for the nonwoven adsorbents, research efforts transitioned to braided fiber adsorbents.

The braided adsorbents were composed of continuous high-density polyethylene (HDPE) fibers that were braided around a porous polypropylene float that can be made into long lengths. The braided adsorbent was made from round, approximately 20-micron-diameter HDPE fibers. It is currently considered the material of choice for uranium adsorbents due to its outstanding balance of properties, including high mechanical properties, durability, low cost, chemical resistance (i.e., acids, bases, solvents) as well as ease of placement and retrieval from the sea.

A recent economic analysis performed by Schneider and Sachde (discussed in Section 8), assessed the current braid adsorbent process described by Tamada.[24,25] This analysis concluded that the uranium adsorption capacity, the recyclability of the adsorbent, and the cost of the chemicals used in the adsorbent manufacturing process were the most important cost drivers for extracting uranium from seawater. Possible options for increasing the recyclability and durability of the adsorbent include using a less damaging chemical process for the elution and reconditioning steps. In addition, the adsorbent manufacturing cost can be reduced by minimizing or recycling the various chemicals used in the process. The uranium adsorption capacity for Japan's most advanced braid adsorbent and its nonwoven adsorbent (non-sandwich stack configuration) has been reported to be 1.5 g U/kg adsorbent after 30 days of immersion in seawater (M. Tamada; N. Seko, personal communication) . However, these results could not be verified by ORNL or Pacific Northwest National Laboratory (PNNL) after conducting several seawater experiments using two different sets of nonwoven adsorbents that were provided by the JAEA and the capacity results for these adsorbents ranged from 0.74–1.1 g U/kg adsorbent. Nevertheless, the capacity value of 1.5 g U/kg-adsorbent is still considered to be too low to be

cost-effective for implementation; therefore, we began our development efforts to advance the existing Japanese technology and increase the adsorption capacity of fiber-based adsorbents.

The objective of this task was to develop polymeric adsorbents that have at least double the uranium adsorption capacity of the best adsorbent reported by the JAEA. Since adsorption capacities can vary with test conditions, our polymeric materials were tested under real seawater conditions along side the Japanese supplied nonwoven adsorbent.

4.2 R&D Progress/Status

Over the past 3 years we have focused our approach on increasing the adsorption capacity by increasing the surface area of the fiber adsorbents and optimizing the RIGP conditions and degree of grafting. Currently, our best polymeric materials have capacities of 2.8–3.4 g U/kg adsorbent in seawater tests, which is 2.5-4.5 times higher than the Japan's nonwoven fiber adsorbent (which has capacities of 0.74–1.1 g U/kg adsorbent). In our most recent seawater tests at PNNL, preliminary results on two of our newest adsorbents show even higher adsorption capacities of 4.6 g U/kg adsorbent (4–6 times higher capacity than the Japanese adsorbent). The enabling factors responsible for these capacity improvements resulted from the synergistic combination of high-surface-area fibers and optimized processing conditions.

4.2.1 High-surface-area polyethylene fibers

The current Japanese braided adsorbents are made from round, 20-micron-diameter HDPE fibers.[20] These fibers have relatively low surface area and cannot be made with fiber diameters less than approximately 15–20 microns due to inherent limitations in the melt-spinning process of polyethylene. However, we determined that one of the most effective methods to increase the uranium adsorption capacity is to increase the surface area of the adsorbent fibers. By using unique fiber technology developed and patented by Hills, Inc.,[26-32] we have achieved higher-surface-area fibers that show higher uranium adsorption capacities compared with commercially available 20-micron-diameter round fibers. This unique technology effectively increases the surface area of polyethylene fibers by reducing the diameter of the fibers and/or changing the shape of the fibers (see below). It has been determined that the surface area–to–weight ratio for adsorbent fibers can be increased substantially by reducing the diameter of the fiber or changing the cross-sectional shape of the fiber, or a combination of both. Fig. 4.1 below shows the increase in surface area as the fiber diameter is reduced.

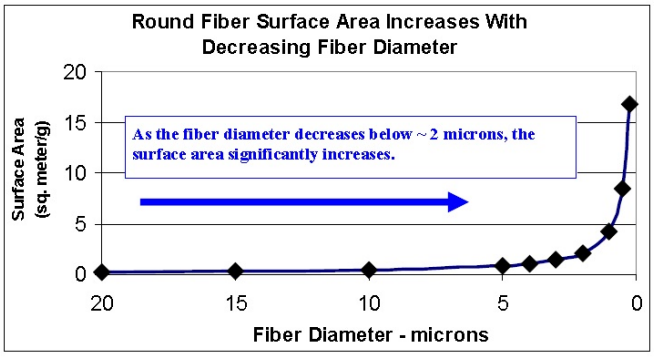

Fig. 4.1. Increase in surface area as fiber diameter is reduced.

One feature of their technology is called the islands-in-the-sea (I-S) method, wherein fibers as small as 0.25 micron in diameter can be made, resulting in a 6000% increase in surface area compared with commercially available 20-micron-diameter round fibers. In the I-S method,

polyethylene nanofibers, i.e. the islands, are embedded inside a larger diameter fiber made of a dissolvable polymer like polylactic acid (PLA), i.e. the sea. After the fibers are made, the sea polymer is dissolved away to expose the nanofibers. Using this manufacturing process, fibers with as many as 156,000 islands can be made.

Another unique aspect of the technology involves melt-spinning fibers that have non-round shapes. Round or circular cross-sectional shaped fibers have much lower surface areas than non-round shaped fibers of the same diameter. Fiber shapes that we have studied include solid or hollow flower shape, solid or hollow gear shape, solid or hollow trilobal shape, solid trilobal gear shape, and others (Fig. 4.2). In our research, we have evaluated several high-surface-area fibers including a range of small-diameter, round fibers (0.24–15 microns in diameter) and many non-round-shaped fibers that had surface areas about 2–60 times higher than the standard 20-micron-diameter round fiber. The Brunauer–Emmet–Teller (BET) surface areas of our high-surface-area fibers ranged from 0.36 to 11.5 m^2/g versus 0.18 m^2/g for the standard 20-micron-diameter round fiber. Fig. 4.2 shows some selected cross-sectional shapes of high-surface-area polyethylene fibers used to make our adsorbents, including the hollow gear-shaped fibers, which constitute one of our better adsorbents (38H).

Hollow gear shape | Solid gear shape | Flower shape | Caterpillar shape

Fig. 4.2. Selected cross-sectional shapes of some high-surface-area polyethylene fibers used to make our adsorbents.

4.2.2 Manufacture and synthesis of adsorbents

The adsorbent fibers were prepared by RIGP, as illustrated in Fig. 4.3, and involve four processing steps: electron beam irradiation of high-surface-area polyethylene fibers; co-grafting polymerizable monomers containing nitrile groups and hydrophilic groups to form grafted side chains throughout the fiber; conversion of nitrile groups to amidoxime groups; and alkaline conditioning of the grafted fibers. The resulting adsorbents are then tested for their capacity to bind uranium from seawater.

Each of the four processing steps discussed above has many parameters that can greatly influence the uranium adsorption capacity; therefore, much of our efforts were focused on systematically investigating the large number of experimental variables and preparing hundreds of adsorbent samples to determine which of these parameters were the most important. These parameters included trunk polymer fiber type, fiber diameter, fiber morphology, fiber surface area, and crystallinity. Irradiation conditions included dose, dose rate, irradiation time, atmosphere, and temperature. Graft conditions included solvent, co-monomers, concentration, co-monomer ratio, additives, and reaction temperature and time. Amidoximation conditions included solvent, solvent concentration, hydroxylamine concentration, and reaction temperature and time. Alkaline conditions included alkaline concentration and reaction temperature and time. Based on these results, additional experiments were conducted to better understand and optimize the key parameters in order to continuously improve the uranium adsorption capacity.

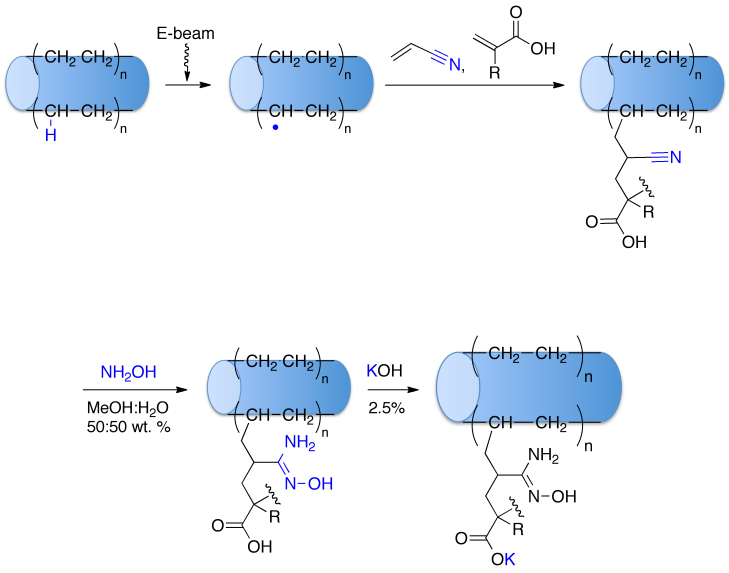

Fig. 4.3. Reaction scheme for ORNL's adsorbent fibers.

4.2.3 General synthesis approach

The general synthesis approach is described below followed by a discussion on the impact of the experimental parameters on the uranium adsorption capacity.

4.2.3.1 Irradiation of high-surface-area polyethylene fibers

Many different high-surface-area polyethylene fibers were made at Hills, Inc., using readily dissolvable PLA. The PLA was removed from the fibers prior to irradiation by submerging them in excess tetrahydrofuran (THF) at 60 °C overnight. This process was repeated three times, and the fibers were filtered and dried at 50 °C under vacuum.

Prior to irradiation, the high-surface-area polyethylene fibers were pre-weighed and placed inside a plastic glove bag and sealed under nitrogen in double-layered plastic bags. The bags were then put inside an insulated container and placed on top of a bed of dry ice and irradiated typically to a dose of 200 kGy using 4.9 MeV electrons and 1 mA current from an RDI Dynamitron electron beam machine. Due to the high reactivity of the free radical species that are generated during the irradiation of the polyethylene fibers, it is very important to irradiate them under low temperatures and inert conditions, and then add them as quickly as possible to the grafting solution. Irradiation in the presence of the monomers provides low grafting yields.

All irradiation and grafting activities were conducted off-site at Neo Beam— Mercury Plastics, Inc. in Middlefield, Ohio. Figure 4.4 shows the electron beam setup for irradiating the adsorbent fibers, which shows the sealed Styrofoam insulated box, containing dry ice and several fiber samples, positioned on top of a computer-controlled, screw-driven, translating table and underneath the 4-ft-wide scan horn of the electron beam machine that is contained within a concrete vault.

Fig. 4.4. Electron beam setup used for irradiating fiber samples.

4.2.3.2 Grafting of polymerizable monomers containing nitrile groups and hydrophilic groups

After irradiation, the fibers were immersed in a flask containing a previously de-gassed solution of AN and MAA in DMSO and placed in an oven at 60–70 °C for about 6–18 h for grafting. After the grafting reaction was complete, the fibers were drained from the solution and washed with dimethylformamide (DMF) to remove any monomers or co-polymer by-products. The fibers were then washed with methanol to remove the DMF and dried at 50–60 °C under vacuum. The grafted fibers were weighed to determine the % DOG.

4.2.3.3 Conversion of nitrile groups to amidoxime groups

Approximately 150 mg of each type of high-surface-area, grafted polyethylene fiber was placed in a flask containing 15 mL of 10% hydroxylamine hydrochloride in 50/50 (w/w) water/methanol at 80 °C for 24 h. The fibers were filtered, and the process was repeated two more times. The fibers were then washed with deionized water followed by a methanol rinse and allowed to dry at 50 °C under vacuum.

4.2.3.4 Alkaline conditioning of grafted fibers

For uranium screening experiments, typically 15–30 mg of each fiber type was added to a flask containing 15 mL of 2.5 wt % KOH and heated for 3 h at 80 °C. The fibers were then filtered using a vacuum filtration system with a low extractable borosilicate glass holder through a hydrophilic polyethersulfone membrane with low extractable and washed with at least 400 mL of deionized water until the pH of the excess water in the fiber was neutral. The fibers were kept wet at all times during this process and it was found that if the fibers dried out, their capacity would significantly decrease.

4.2.3.5 Laboratory screening of adsorbents

To understand the effects of the many synthesis and processing variables on the uranium adsorption capacity, it was necessary to prepare and screen hundreds of adsorbent samples. Typical seawater contains 140 ppm bicarbonate ions, 10,500 ppm sodium ions, 19,000 ppm chloride ions, and 3.3 ppb uranium dioxide as the tricarbonate complex $\{[UO_2(CO_3)_3]^{4-}\}$ with a pH of 7.5–8.4.[33-35] Since typical screening experiments with real seawater take 30–60 days to reach equilibrium, a rapid screening protocol was developed that contains a higher level of uranium to quickly and efficiently determine the correlation between the adsorbent synthesis variables and the uranium adsorption capacity. The test solution contained 140 ppm bicarbonate ions from sodium bicarbonate (193 mg, 2.3 mmol), 10,516 ppm sodium ions and 16,136 ppm chloride ions from sodium chloride (26.5 g, 453.5 mmol), and 6–7 ppm uranium ions from

dissolving (17.00 mg, 0.034 mmol) uranyl nitrate hexahydrate in nanopure water for a final pH of 7.97. From chemical equilibrium modeling, using the MINEQL equilibrium software package, the uranium speciation and composition were obtained, for a closed system, as follows: $UO_2(CO_3)_3^{4-}$ (42%), $UO_2(CO_3)_2^{2-}$ (39.2%), $(UO_2)_2(OH)_2CO_3^{-}$ (17.1%), UO_2CO_3 (1.4%), and $(UO_2)OH_2(s)$ (0.3%).

The wet fibers were placed in a new trace metal polypropylene container filled with the uranium solution described above using a graduated pipette or volumetric flask. A sample of the solution was collected prior to sorbent addition to determine the initial uranium concentration before the adsorption experiment. The solution was shaken at 500 rpm for 24 h at room temperature. It was determined that these conditions were sufficient for the fibers to reach equilibrium. The adsorbent was then filtered, and an aliquot of the solution was put into a 12 mL plastic cap vial for uranium analysis via inductively coupled plasma optical emission spectroscopy (ICP-OES). To avoid introducing large particles into the ICP, the solution was then filtered through a Teflon syringe filter (0.45 μm). If the adsorption analysis was performed on the metals eluted from the fibers, the fibers were filtered from the solution using the same vacuum filtration system with a low extractable borosilicate glass holder, through a hydrophilic polyethersulfone membrane with low extractable. The initial and final solutions were then analyzed using a Perkin Elmer Optima 2100 DVICP-OES. Using the difference in uranium concentration of the solution, theuranium adsorption capacity is determined, using Eq. (4.2).

$$\textit{Uranium adsorption capacity} = \left(\frac{\textit{initial Uranium conc. (mg/L)} - \textit{final Uranium conc. (mg/L)}}{\textit{g of dry adsorbent}} \right) \textit{x L solution}$$

Equation 4.2. With the initial and final uranium concentrations determined for each sample, we calculated the uranium adsorption capacity (mg Uranium/g adsorbent).

The ICP-OES was calibrated using 5–10 standard solutions ranging from 0.05–20 ppm, which were prepared from a 1000 ppm uranium in 5% nitric acid stock solution, and a linear calibration curve was obtained. In addition, a blank solution of 2–3% nitric acid was prepared and washouts were monitored between samples. To ensure accuracy and reproducibility of the measurements (and no sample carryover), the following protocol was used after calibration.

A. Analysis of the uranium solution (described above) before fiber was added.
B. Analysis of the corresponding solution before the fiber was added but after shaking with the membrane filter for 24 h (to determine if the membrane filter had any effect on the uranium concentration in the solution).
C. Analysis of the sample solutions were then conducted, and between each sample, blank solution was analyzed to ensure no uranium was carried over into the next analysis.
D. The analysis was then repeated on the samples as described in Steps A and B.
E. The last analysis was conducted on deionized water.

Since uranium dioxide in the laboratory screening solution does not predominantly exist as a tricarbonate complex $\{[UO_2(CO_3)_3]^{4-}\}$,[36] as in the case of seawater, it was found that the amount of uranium adsorbed out of the solution needed to be kept relatively constant (about half the uranium in solution) to obtain reproducible results. This was accomplished by varying the volume of the solution. Thus the laboratory screening method successfully correlated with the adsorption capacity when tested in real seawater (Fig. 4.5).

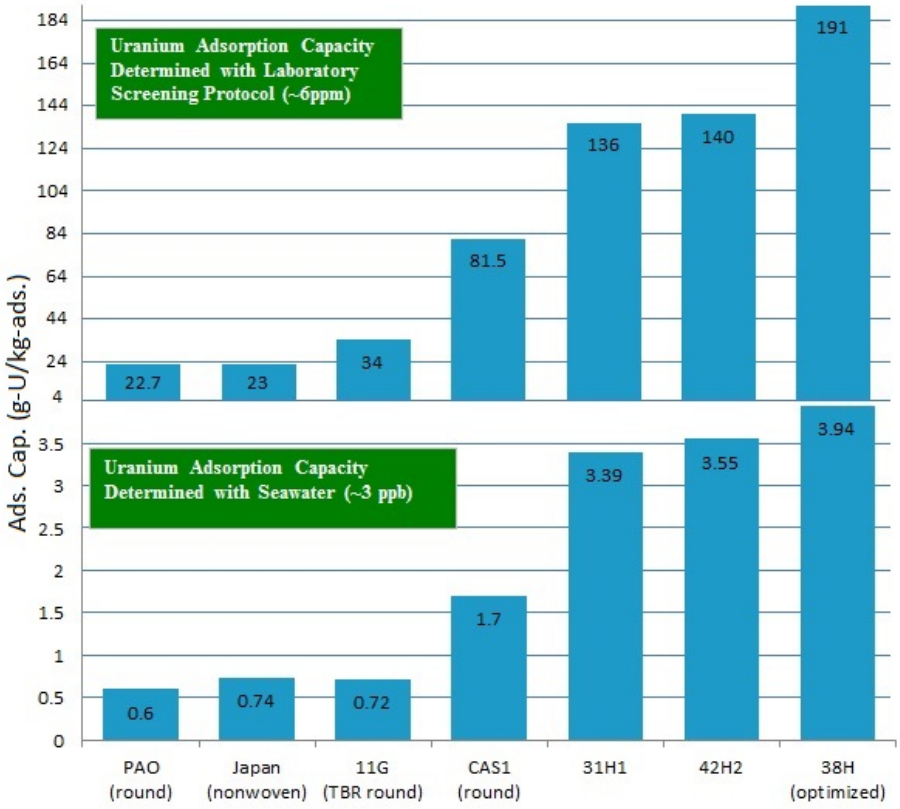

Fig. 4.5. The results of the laboratory screening method are in parallel to the results obtained in seawater, and it follows the same trend.

4.2.4 Key findings from the experimental studies relating synthesis condition to adsorption capacity for the RIGP of adsorbent fibers

In order to monitor the improvement in the uranium adsorption capacity of our adsorbents, we have concentrated our efforts on establishing a synthesis condition-adsorption capacity relationship rather than relying on the % DOG as previously used. The % DOG does not directly correlate with the weight increase of the fibers after grafting with an improvement in the adsorption capacity. Summarized below are the key findings from our experimental studies on relating synthesis condition and adsorption capacity.

4.2.4.1 Irradiation conditions

As discussed earlier, the optimum irradiation conditions for the irradiation of the fibers were under dry ice temperatures and an oxygen-free (N_2) atmosphere. This set of conditions was determined to be critical for preserving a high concentration of free radicals with long lifetimes, prior to the grafting step, and minimized the detrimental recombination and crosslinking reactions as well as any reactions with oxygen. Conducting irradiation experiments at room temperature decreased the adsorption capacity. Modifying the atmosphere of the fibers from fixed N_2 pressure to constant N_2 flow or constant vacuum did not appreciably affect the adsorption capacity. A total irradiation dose of 200 kGy was sufficient to maximize the adsorption capacity, and increasing the dose to 300 or 400 kGy did not increase capacity.

4.2.4.2 Grafting conditions

We determined that the optimum composition of the graft solution for preparing several of our high-surface-area adsorbent fibers was either 25% by weight DMSO and 75% by weight co-monomer (70/30 by weight AN/MAA) or 10% by weight DMSO and 90% by weight co-monomer (70/30 by weight AN/MAA). Varying the DMSO concentration, co-monomer concentration, and/or co-monomer ratios outside these preferred limits or eliminating the DMSO from the graft solution or eliminating the hydrophilic MAA monomer from the graft solution decreased the adsorption capacity. The optimum graft temperature and time were 60–70 °C for 6–18 h. Decreasing the graft temperature from 60 °C to room temperature or increasing the temperature from about 70–80 °C decreased adsorption capacity. No change was observed in the adsorption capacity by increasing the graft time from 6–18 h. In addition, changing the ***initial*** graft solution temperature from room temperature to about 40 °C did not appreciably change the adsorption capacity; however, using an initial graft temperature of 60 °C significantly decreased adsorption capacity. Adding sulfuric acid and/or changing the solvent from DMSO to DMSO/H_2SO_4(0.05M), DMSO/H_2O/H_2SO_4(0.05M), DMSO/DMF, or DMF/H_2O/H_2SO_4(0.05 M) did not increase the adsorption capacity. It was determined that shaking or stirring the graft solution or inputting ultrasonic energy into the graft solution during the grafting reaction decreases the adsorption capacity. We also conducted experiments on reducing the amount of grafting solution, in order to reduce the manufacturing cost of the adsorbent, and determined that reducing the solution from 500 mL per gram of fiber to 20 mL per gram of fiber did not change the adsorption capacity. We also conducted some preliminary experiments using Mohr's salt (ammonium iron (II) sulfate hexahydrate) as an additive in the grafting solution. This compound potentially reduces co-polymer formation, enhances grafting efficiency, and increases the amount of recyclable grafting solution. The adsorption capacities of adsorbents made with Mohr's salt were comparable to those same adsorbents made without Mohr's salt.

4.2.4.3 Amidoxime reaction conditions

A variety of parameters have been evaluated in optimizing the amidoximation reaction for our adsorbent fibers, including varying the solvent, solvent concentration, hydroxylamine hydrochloride concentration, reaction temperature, and reaction time. The best method so far uses 10% hydroxylamine hydrochloride in 50/50 (w/w) water/methanol that was previously neutralized with a 1:1 mole ratio of KOH to hydroxylamine hydrochloride. After the flasks were sealed, they were allowed to sit undisturbed at 80 °C for 24 h. The solutions were then drained, and the fibers were physically separated to maximize their surface area. The same amidoximation reaction was then conducted two more times in the same fashion. The solutions were then drained and the adsorbent fibers were washed with deionized water, washed with methanol, and dried under vacuum at 50 °C.

4.2.4.4 Alkaline conditioning

The optimum alkaline conditioning method determined thus far for our adsorbent fibers involves heating the fibers to 80 °C for 3 h in 2.5 wt% KOH solution (prepared from 18 ohm water). The fibers were then filtered and washed with deionized water until the eluted water attained a pH of about 7. The fibers were then kept wet until uranium adsorption testing was complete. After the KOH conditioning step, the fibers dramatically increased their hydrophilicity and swelled to 3–5 times their original size. We also determined that it was very important to keep the fibers wet prior to seawater immersion since drying out the fibers significantly

decreased the adsorption capacity. In addition, we have demonstrated that some of the amidoxime groups can degrade into carboxylic acid groups during KOH conditioning; however, if this conditioning is not performed, the capacity is decreased. It was also demonstrated that KOH conditioning is required after each acid elution recycling step; otherwise, the capacity is compromised.

The importance of the hydrophilic MAA monomer in the grafting solution was demonstrated by synthesizing a random copolymer of AN and MAA without the trunk polymer fiber. After the amidoximation reaction and KOH conditioning, the polymer completely dissolved in the water. This is in sharp contrast to films made with only amidoxime groups, which do not dissolve in water. This finding underlined the importance of the hydrophilic monomer and its significant effect on increasing the wettability and hydrophilicity of the adsorbent.

4.2.4.5 Summary of uranium adsorption capacities using Laboratory Screening Method

Figure 4.6 summarizes the uranium adsorption capacities determined with the laboratory screening method for some of our selected high-surface-area adsorbents. Our adsorbents have shown continuous improvement over the course of the project and exceed Japan's adsorbents as well as other adsorbents made with lower-surface area round fibers. It is worth noting that this plot represents only a small sampling of the hundreds of adsorbent samples that were synthesized and tested in this project.

Figure 4.7 shows how the adsorbent fiber shape and fiber surface area affect the uranium adsorption capacity using the laboratory screening method. It is clear from this data that there is not always a direct relationship between fiber surface area and capacity, although in each case the higher-surface-area fibers have significantly higher capacities than conventional round fibers.

4.2.5 Other important findings from our experimental research

4.2.5.1 Adsorbent shelf life

The uranium adsorption capacities of approximately 20 different ORNL adsorbents were determined using our laboratory screening method immediately after their preparation. After storing these adsorbents for 4 months at room temperature in deionized water, the adsorption capacities did not change over time as long as the fibers were kept wet.

4.2.5.2 Adsorbent mechanical properties

The tensile strength and percent elongation properties of our hollow gear 38H adsorbent fibers were determined on "dry" and "wet" fiber tow samples, including unirradiated baseline samples and samples irradiated at total doses of 100, 200, 300, and 400 kGy. The peak tensile load and percent elongation for the "dry" and "wet" baseline tow samples containing 288 filaments/tow were about 700 g and 600%, respectively. The irradiated samples were processed using our conventional method discussed above; then after KOH conditioning half the samples were dried at 40 °C ("dry") and the other half were placed in seawater ("wet") at room temperature for 6 days prior to tensile testing. The resulting tensile strengths for the "dry" samples were equivalent to or increased in strength as dose increased and retained about 97–133% of their "dry" baseline strength. The "wet" samples lost about 10–30% of their "wet" baseline strength as dose increased from 0–400 kGy. The resulting percent elongation values for the "dry" samples retained about 6–20% of their "dry" baseline value, and the "wet" samples retained about 14–41% of their "wet" baseline value. Even though the fibers experienced a large decrease

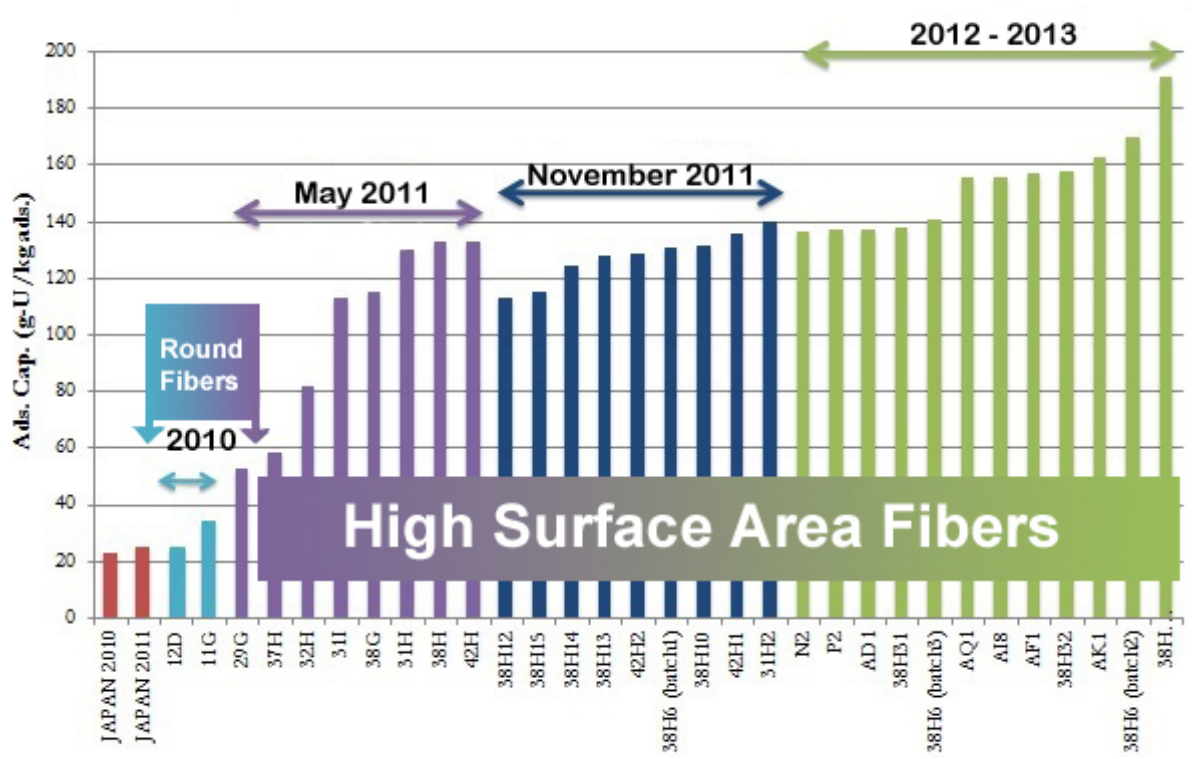

Fig. 4.6. Uranium adsorption capacities on selected high-surface-area adsorbent samples using the laboratory screening method (6 ppm U).

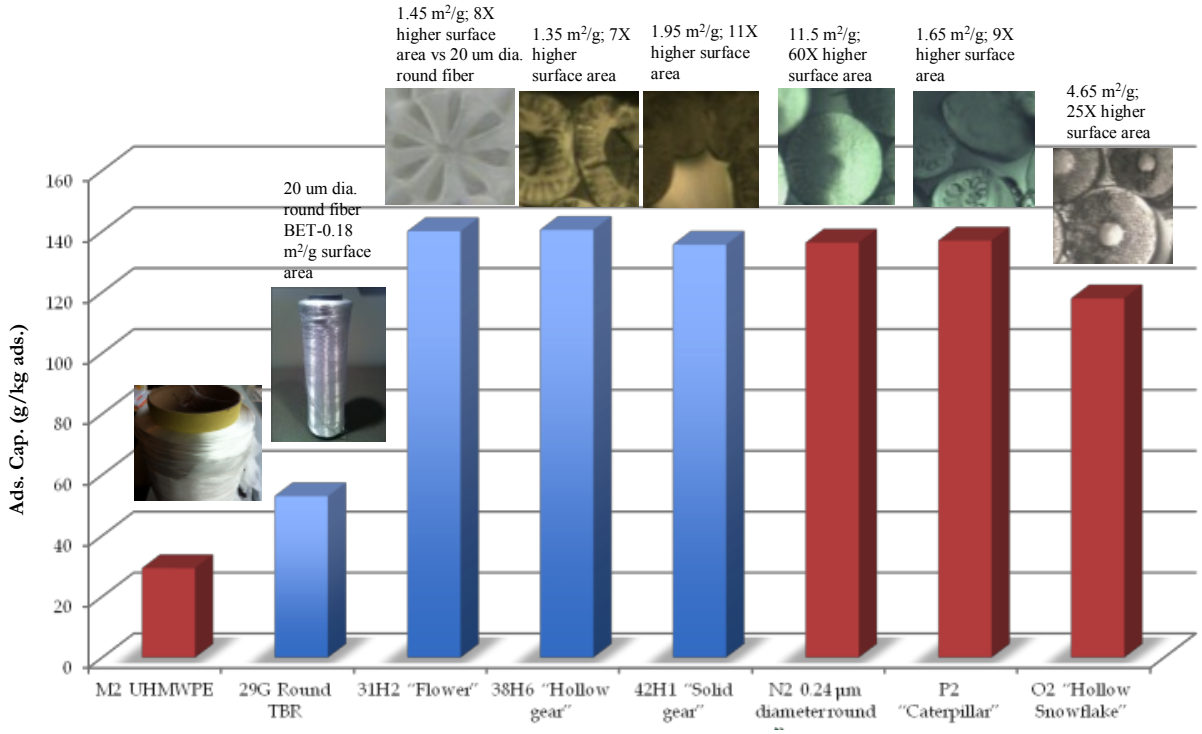

Fig. 4.7. Uranium adsorption capacity versus adsorbent fiber shape and surface area.

in percent elongation from their unirradiated baseline value of about 600% elongation, all samples still had percent elongation values greater than 35%. This area needs further research in the future in order to determine what levels of mechanical properties are necessary for surviving in the sea, including parameters such as immersion time, ocean current velocity, etc.

4.2.5.3 Cost reduction strategies for manufacturing adsorbents

Since the cost of the various chemicals used to manufacture our adsorbents is one of the major cost drivers in the entire manufacturing process (as discussed in Section 8), we have conducted experiments to determine whether it is possible to reduce, recycle, or eliminate these chemicals. For example, DMF is used to wash away copolymer by-products after the grafting step. DMF is one of the more expensive chemicals used in the manufacturing process, and it was determined that it can be eliminated from the process since all of the un-grafted, copolymer by-products become soluble in water after the alkaline conditioning step. We also envision that other chemicals including those making up the un-grafted solution (DMSO, AN, and MAA) as well as the hydroxylamine, methanol, THF, and polylactic acid can potentially be recycled and reused, thereby greatly reducing the manufacturing cost of the adsorbent.

4.2.5.4 ORNL's braided adsorbents

In a subcontract with Steeger USA, we successfully produced Japanese-like braid adsorbents using a variety of high-surface-area fibers that are potentially suitable for marine deployment. These braids were manufactured on a custom-modified braiding machine (Fig. 4.8), which offers the flexibility to vary the length and the density of the loops. A variety of braid styles have been constructed, and they are currently being processed into adsorbents for seawater testing and evaluation.

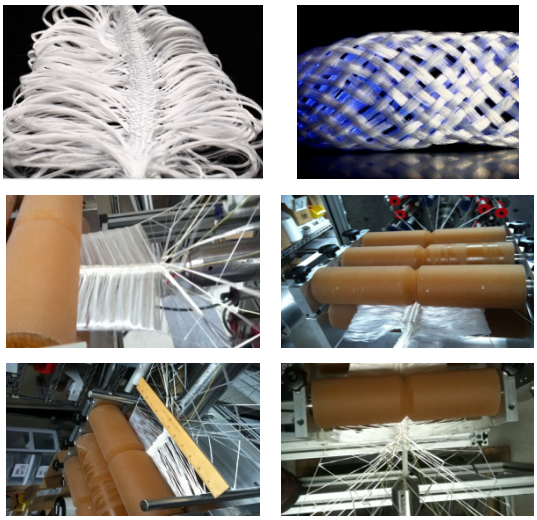

Fig. 4.8. Representative ORNL braid adsorbents and braiding machine.

4.2.5.5 Novel fiber adsorbents prepared by controlled radical polymerization

Since 2013, an alternative approach was investigated to prepare high-performance fiber adsorbents to better control the AN polymerization reaction, increase the capacity, and provide potential cost savings. The strategy utilizes atom-transfer radical polymerization (ATRP), a controlled radical polymerization method, to grow AN polymers from a halide functionalized

polymer.[37] ATRP can readily control the degree of polymerization, i.e., the length of a polymer brush on a fiber (theoretically unlimited length), and can create a controlled polymer topology such as the formation of multiblock copolymers. In addition, ATRP is a versatile methodology and applicable for the majority of monomers. Due to its mechanism, the occurrence of ungrafted polymer chains in solution is minimal. Thus, recycling monomer and catalyst is readily possible, which has a significant cost advantage.

The first strategy was to use ATRP to randomly copolymerize AN and *t*-butyl acrylate (*t*BA) on poly(vinylbenzyl chloride) grafted polyethylene (PVBC-*g*-PE) hollow gear fiber. PVBC-*g*-PE fiber was previously prepared via RIGP as described in the above section (96% DOG). The benzyl chloride site serves as an initiation point for ATRP to create PAN brushes on PVBC brush (Fig. 4.9). Due to its 3-dimensional structure, this topology might increase the access of the amidoxime ligand to the uranyl ions in seawater and thus increase the adsorbent capacity. After many attempts with carefully tuned reaction conditions, a reaction condition was identified that grafts PAN and P*t*BA in a high grafting yield. The P*t*BA is then hydrolyzed to polyacrylic acid to increase the hydrophilicity of the brushes. At constant reaction time (24 h), PAN-*co*-P*t*BA grafting achieved up to ~3000% DOG. Tuning the reaction time and condition will readily allow the % DOG to be smaller or larger. The fibers were converted to amidoxime by reaction with hydroxylamine and then conditioned in KOH following the procedure described above. Capacity measurements using the laboratory screening method (6 ppm U) achieved 141–179 g U/kg adsorbent, which is similar to some of our best fibers.

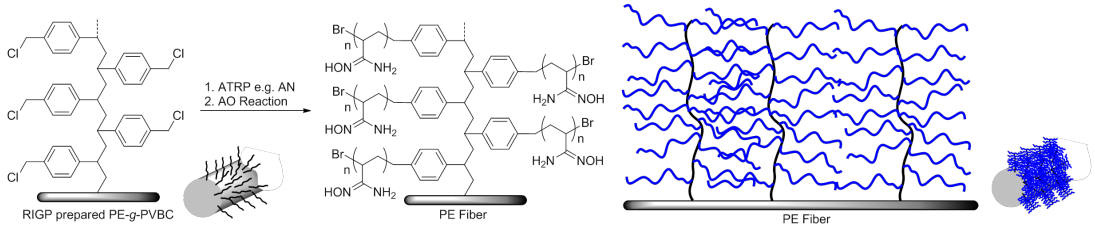

Fig. 4.9. Novel adsorbents prepared via ATRP.

The second strategy employs the same ATRP technology but completely eliminates RIGP, which potentially provides a significant advantage in cost and manufacturing. In the first step, polypropylene fibers were chlorinated through a radical chlorination reaction with bleach under a light source. This produces a polypropylene fiber with 19.3 wt% chloride. The PAN-*co*-P*t*BA brushes were grown from the halide-functionalized fiber via ATRP. In the first attempt, 439% DOG was obtained, and uranium adsorption capacity was 73 g U/kg adsorbent using the laboratory screening procedure (6 ppm uranium, see Fig. 4.6). We will continue to explore this method in the future.

4.3 Future Work

We have made significant progress over the past 3 years, including more than doubling the uranium adsorption capacity versus the Japanese adsorbents. Our best adsorbents have achieved capacities of 2.8–4.6 g U/kg adsorbent versus 0.74–1.1 g U/kg adsorbent for the Japanese adsorbent in actual seawater testing (2.5–6 times higher capacity). We have also conducted synthesis and testing of hundreds of adsorbent samples involving many different high-surface-area fibers and other textile forms, mono-dentate and multi-dentate ligands, irradiation conditions, grafting conditions, amidoximation reaction conditions, and alkaline conditions. We have also evaluated various cost-saving strategies for manufacturing adsorbents, including

recycling, reuse, or elimination of costly chemicals, and successfully manufactured several braided adsorbents that are potentially suitable for marine deployment.

In our future work, we will focus on increasing the uranium adsorption capacity of our polymeric adsorbents. Clearly increasing the capacity, selectivity and durability of the adsorbent will make extraction of uranium from seawater more cost effective (see Section 8). We will continue to rely on computational studies to define new more selective ligands for adsorption of uranium from seawater and determine methods to incorporate these ligands into the polymer trunks. We will investigate different hydroxylamine motifs, alternative amidoxime-like structures, and other hydrophilic monomers to increase the selectivity and capacity. We will covalently attach CN containing small molecules to previously grafted adsorbents with reactive functional ligands. We will make advancements in adsorbent processing technology (i.e., irradiation, grafting, amidoximation reaction, and KOH conditioning) to reduce cost and increase the performance. We will continue to develop and optimize the ATRP reactions to maximize capacity. Finally, the mechanical properties of the new ATRP polymers will be tested to determine if they are durable enough for seawater experiments.

We will also investigate strategies for reducing the adsorbent manufacturing cost and investigate the scalability of the process. As detailed in Section 8, capital costs for adsorbent production are driven by the chemical processes and e-beam equipment, while chemical and material inputs are the largest cost driver for adsorbent production. Surprisingly, electricity, to run the e-beam, is not an insignificant cost (see Figure 8.6). Thus, alternate approaches to prepare amidoxime functionalized fibers without using RIGP will be investigated. We will also evaluate recycling and reuse of costly chemicals and polymers used in adsorbent manufacture. Another cost driver is the number of uses of the adsorbent before its final disposal. Therefore, methods to increase the durability and recyclability of the adsorbent will be investigated. We will also optimize the stripping method. We will take advantage of the fact that other economically attractive metals are present in seawater and investigate recovering these co-products from seawater (i.e., vanadium). Finally, we will optimize the deployment design and focus on the braided fiber adsorbents (Fig. 4.8). The braid style can be changed by increasing the loop length, loop density, and the number of loops and these parameters will be varied to optimize the design.

4.4 References

(1) Schenk, H. J.; Astheimer, L.; Witte, E. G.; Schwochau, K. *Separation Science and Technology* **1982**, *17*, 1293–1308.

(2) Astheimer, L.; Schenk, H. J.; Witte, E. G.; Schwochau, K. *Separation Science and Technology* **1983**, *18*, 307–339.

(3) Eloy, F.; Lenaers, R. *Chem. Rev.* **1962**, *62*, 155–183.

(4) Sugasaka, K.; Katoh, S.; Takai, N.; Takahashi, H.; Umezawa, Y. *Separation Science and Technology* **1981**, *16*, 971–985.

(5) Zheng, B.; Cai, S.; Zhuang, M.; Jiang, L. *Haiyang Xuebao (Zhongwenban)* **1985**, *7*, 34–9.

(6) Kobuke, Y.; Tanaka, H.; Ogoshi, H. *Polym. J.* **1990**, *22*, 179–182.

(7) Egawa, H.; Kabay, N.; Jyo, A.; Hirono, M.; Shuto, T. *Ind. Eng. Chem. Res.* **1994**, *33*, 657–661.

(8) Kavakl, P. N. A.; G ven, O. *J. Appl. Polym. Sci.* **2004**, *93*, 1705–1710.

(9) Kago, T.; Goto, A.; Kusakabe, K.; Morooka, S. *Ind. Eng. Chem. Res.* **1992**, *31*, 204–209.

(10) Okamoto, J.; Sugo, T.; Katakai, A.; Omichi, H. *J. Appl. Polym. Sci.* **1985**, *30*, 2967–2977.

(11) Tabushi, I.; Kobuke, Y. *Mem. Fac. Eng., Kyoto Univ.* **1984**, *46*, 51–60.

(12) Saito, K.; Yamaguchi, T.; Uezu, K.; Furusaki, S.; Sugo, T.; Okamoto, J. *J. Appl. Polym. Sci.* **1990**, *39*, 2153–2163.

(13) Sugo, T.; Saito, K. *Nippon Kikai Gakkaishi* **1990**, *93*, 575–8.

(14) Choi, S.-H.; Nho, Y.-C. *Radiation Physics and Chemistry* **2000**, *57*, 187–193.

(15) Kawai, T.; Saito, K.; Sugita, K.; Kawakami, T.; Kanno, J.-I.; Katakai, A.; Seko, N.; Sugo, T. *Radiation Physics and Chemistry* **2000**, *59*, 405–411.

(16) Seko, N.; Katakai, A.; Tamada, M.; Sugo, T.; Yoshii, F. *Separation Science and Technology* **2004**, *39*, 3753–3767.

(17) Seko, N.; Katakai, A.; Hasegawa, S.; Tamada, M.; Kasai, N.; Takeda, H.; Sugo, T.; Saito, K. *Nucl. Technol.* **2003**, *144*, 274–278.

(18) Katakai, A.; Seko, N.; Kawakami, T.; Saito, K.; Sugo, T. *Journal of the Atomic Energy Society of Japan / Atomic Energy Society of Japan* **1998**, *40*, 878–880.

(19) Sekine, A.; Seko, N.; Tamada, M.; Suzuki, Y. *Radiation Physics and Chemistry* **2009**, *79*, 16–21.

(20) Tamada, M.; Seko, N.; Yoshii, F. *Radiation Physics and Chemistry* **2004**, *71*, 223–227.

(21) Sugo, T.; Tamada, M.; Seguchi, T.; Shimizu, T.; Uotani, M.; Kashima, R. *Journal of the Atomic Energy Society of Japan / Atomic Energy Society of Japan* **2001**, *43*, 1010–1016.

(22) Seko, N.; Tamada, M.; Yoshii, F. *Nuclear Instruments and Methods in Physics Research Section B: Beam Interactions with Materials and Atoms* **2005**, *236*, 21–29.

(23) Tamada, M.; Seko, N.; Kasai, N.; Shimizu, T. *Nihon Genshiryoku Gakkai Wabun Ronbunshu* **2006**, *5*, 358–363.

(24) Sachde, D. J. (2011). *Uranium Extraction from Seawater: An Assessment of Cost, Uncertainty and Policy Implications* (Master's Thesis). The University of Texas at Austin.

(25) Kim, J.; Tsouris, C.; Mayes, R. T.; Oyola, Y.; Saito, T.; Janke, C. J.; Dai, S.; Schneider, E.; Sachde, D. *Separation Science and Technology* **2013**, 48, 367-387.

(26) Hills, W.H. US Patent 5,162,074, 1992.

(27) Talley, Jr. A. et. al. US Patent 6,767,498, 2004.

(28) Hills, W.H. US Patent 5,551,588, 1996.

(29) Hills, W.H. US Patent 5,562,930, 1996.

(30) Hills, W.H. US Patent 5,344,297, 1994.

(31) Hills, W.H. US Patent 4,406,850, 1983.

(32) Hills, W.H. US Patent 5,466,410, 1995.

(33) Sodaye, H.; Nisan, S.; Poletiko, C.; Prabhakar, S.; Tewari, P. K. *DES* **2009**, *235*, 9–32.

(34) Favre-Reguillon, A.; Lebuzit, G.; Foos, J.; Guy, A.; Draye, M.; Lemaire, M. *Ind. Eng. Chem. Res.* **2003**, *42*, 5900–5904.

(35) Gupta, C.; Singh, H. *Uranium Resource Processing*; Springer Verlag, 2003.

(36) Saito, K.; Miyauchi, T. *Journal of Nuclear Science and Technology* **1982**, *19*, 145–150.

(37) Matyjaszewski and Xia; *Chem. Rev.* **2001**, 101, 2921-2990.

5. ADVANCED NANOSYNTHESIS ADSORBENTS

Richard T. Mayes, Xiao-Guang Sun, Sheng Dai, Suree Brown, Joanna Górka, Yanfeng Yue
Oak Ridge National Laboratory

5.1 Background

Although polyethylene fibers have arisen as the support of choice for seawater extractions because of their strength, durability, and ability to graft a variety of ligands, they have low surface area, which ultimately limits its capacity. The use of high-surface-area nanomaterials has received considerable attention since it can increase the graft density and consequently extraction capacity.[1] These nanomaterials achieve their high surface areas not due to particle size or fiber diameter as in the case of polyethylene fibers, but due to the void volume in the particle itself. The void volume arises from either templating or self-assembly that results in void spaces after thermal annealing. The diameters of these void spaces can range from sub-2 nm (micropores), 2-50 nm (mesopores), or larger than 50 nm (macropores) based on International Union of Pure and Applied chemistry nomenclature. Hierarchical materials have a combination of pore sizes, often spanning multiple size regimes. Activated carbons, for example, have tremendous microporosity with some mesoporosity. Mesoporous materials are attractive for seawater applications due to their high surface areas, tailorable porosity, and regular network of large pores, which can facilitate mass transport throughout the particle. Of the nanomaterials available for study, silicates are not suitable since they are not stable under oceanic conditions (high salinity, high pH). Although hydrous titania and nanostructured titania has received significant attention,[2] it is not of interest due to its low selectivity and lower capacity than the polyethylene fiber-based amidoxime adsorbents. Of the nanomaterials available, carbon-based materials, e.g. activated carbons or carbon fibers, are the material of choice for seawater applications due to their inherent chemical stability in high salinity and basic pH conditions. This stability, coupled with the high surface areas possible (250–3000 m^2/g) provide promise for effective sorbents with high capacities. Although the use of carbon in seawater applications is somewhat limited, the vast majority of the cases use oxidized activated carbon, i.e. a carboxylated surface, to adsorb materials from seawater or utilize the excellent capillary effect and retention of substrates in the porosity.

The bulk of the nanoporous composite literature dealing with cases in which pores are impregnated with other materials involves total pore filling, with no indication of final use or attention paid to pore accessibility.[3] This represents the primary challenge of using any porous material, especially porous carbon materials. Other materials, such as silicates and metal oxides, have been utilized to collect fission products in which small-molecule functionalized silanes were loaded into self-assembled monolayers on mesoporous supports (SAMMS).[4] Although uranium was not investigated in this report, other radionuclides were found to have Log K_D values in the 3–6 range. An oxime-functionalized mesoporous CMK-5 carbon adsorbent was produced to study adsorption uranium and other simulated nuclear industry effluents.[1a] Here, diazonium chemistry was used to graft 4-aminoacetophenone oxime onto the carbon surface with isoamyl nitrite. A grafting yield of 28.9% was obtained, determined by thermal gravimetric analysis (TGA), and the uranyl loading was determined to be approximately 65 mg U/g adsorbent at pH ≈ 4.5. Although the grafting yields were moderate, the adsorption capacity was relatively high. This highlights the challenge of grafting onto chemical stable carbon surfaces but also highlights the potential of high capacity.

One of the challenges in working with nanoporous materials is grafting inside the pores, where confinement effects can dominate nanoscale phenomena. This is vastly different from grafting onto the exterior of surfaces such as carbon nanotubes. In surface grafting, spatial proximity in 2 dimensions is key, as optimizing the density of the graft sites will determine the grafting yield. Inside a pore, the spatial proximity of two molecules is dictated in 3 dimensions, where not only is the density of graft sites in 2 dimensions critical, but also a third dimension involving the pore curvature will play a critical role in the graft density. This relates to the size of the grafts; when confined in a pore, two grafts growing on opposite ends will begin to interact sterically and stop growing. When the graft density (molecules per nm^2) inside the pore is optimized, this effect of curvature is enhanced as the distance available before steric interactions between different graft sites may decrease. Optimizing the grafted polymer, while optimizing the steric packing of the polymer chains inside the pore, constitutes the second challenge for functional porous materials.

5.2 R&D Progress/Status

This task seeks to take advantage of the high surface areas of nanoporous materials to generate a new class of high-capacity adsorbents that can be functionalized with ligands to selectively bind uranium. Our approach toward a nanostructured alternative to polyethylene fibers focuses on two classes of material: (1) carbon-based nanostructures and (2) polymeric nanostructures. Three carbon-based nanostructured materials have been utilized: (1) mesoporous carbon, (2) carbon nanotubes, and (3) carbon fibers. The mesoporous carbons are prepared via a soft-templating method where the porosity is controlled by a sacrificial polymer. In addition to the polymer, silicate spheres with low size dispersions can be used to introduce porosity to enhance the mass-transport through the carbon material. This generates highly porous carbon materials with surface areas from 250 to 700 m^2/g. When coupled with high temperature activation by alkali hydroxides, steam, carbon dioxide, or ammonia, microporosity can be introduced to yield high-surface-area (> 2000 m^2/g) materials. AN and hydrophilic monomers, such as MAA and AA, are then polymerized inside the pores of the nanostructured materials. Carbon nanotubes were also investigated due to the high aspect ratios of the tubular carbon material resulting in high surface areas ($\geq$ 250 m^2/g). Carbon fibers, generated from pitch-derived sources or pyrolized PAN fibers, have also received attention. These materials are fibers with small diameters that exhibit enhanced stability over non-pyrolized polymer fibers while maintaining strength and flexibility. Other carbon materials investigated include activated carbon fabric, typically derived from pyrolizing Rayon fabric under inert atmospheres, and commercial activated carbon materials, each with surface areas > 1000 m^2/g. The activated carbon and fabric are predominately microporous with little mesoporosity. The commercial nature of these two products provides an appealing case for their use; however the lack of significant porosity larger than 2 nm creates a challenge in that polymerization in the pores may block access, thus lowering the achievable capacity.

The grafting methods utilized include irradiation-based methods and chemical grafting. Electron beam irradiation was carried out in collaboration with Chris Janke at Neo Beam along with the electron beam irradiation facility at the University of Maryland, overseen by Dr. Mohamad Al-Sheikhly, a US DOE Nuclear Energy University Program (NEUP) participant. Here, the carbon materials were irradiated at low temperature in a dry ice bath with an electron beam to induce radicals. The carbon materials were then placed in a monomer solution while maintained in an inert atmosphere. The induced radicals polymerized the monomers with grafting onto the carbon material. Gamma irradiation, another irradiation technique utilized at the

University of Maryland, uses a cobalt-60 source to induce radicals. The irradiation can occur at room temperature due to the lower radiation-induced heating that occurs during irradiation, but the irradiation also requires more time due to the lower flux. Chemical methods have the advantage that they are less expensive and do not require highly specialized equipment. Utilizing radical initiators such as 4,4'-azobisisobutryonitrile (AIBN) or benzoyl peroxide (BPO), free radicals are generated that polymerize the monomers while grafting the polymer to the surface. Thermal radical initiation is the most popular method of radical generation with chemical initiators; however, recently sonication has received attention since it can generate radicals by the intense pressures and temperatures generated at the interface of the cavitation bubbles. For example, graphene was functionalized with polystyrene using ultrasonication.[5] With sonication-induced polymerization, the transport through porous media can be facilitated while simultaneously grafting the monomers onto the surface. This is expected to lower the possibility of surface polymerization dominating the grafting process in porous materials.

Carbon materials, aside from being relatively chemically inert, provide functional versatility since they can be produced in a variety of structural motifs and should be easily produced industrially with current equipment available in the industrial sector (e.g. Mast Carbon; Chemviron Carbon; Clorox Corp., Brita Division). Activated carbon fiber can be woven similarly to polymer fibers and Rayon fabric can be carbonized and activated with steam to introduce microporosity, producing activated carbon fabric. In addition to this, templated mesoporous materials provide a route to multiple material motifs from powder to monoliths and membranes. In the following sections, the grafting of chelation polymers to carbon-based nanomaterials will be investigated by irradiation (electron beam and γ-irradiation), and chemical methods (radical initiator or controlled living polymerization) and the effect of sonication on the grafting will be discussed.

5.2.1 Electron beam and ^{60}Co γ-irradiation of carbon materials

Electron beam irradiation of mesoporous carbon materials was carried out at Neo Beam in Middlefield, OH, or at the University of Maryland's Department of Materials Science and Engineering irradiation facility in conjunction with Dr. Mohamad Al-Sheikhly. Due to the short lifetime of radicals formed on the carbon materials, it was discovered that in situ polymerization during irradiation was required. The in situ polymerization was performed neat, i.e. solvent-less, and in conjunction with a solvent. Multiple monomer systems were attempted, primarily with glycidyl methacrylate, AN, and MAA. Carbon materials were mesoporous carbon, activated mesoporous carbon, C-Tex 20 (MAST) activated carbon fabric, fluorinated mesoporous carbon, and carbon nanotubes. Mesoporous carbon materials (2 nm < pore diameter > 50 nm) were chosen due to their high surface area and uniformity of the pore size distribution compared to commercially available carbons. The activated mesoporous carbons were produced via base activation at high temperature to increase the surface area through the addition of micropores (pore diameters less than 2 nm). The C-Tex 20 activated carbon fabric represents a high-surface-area carbon material that is produced typically from the carbonization of Rayon fabric. The fabric retains its shape and dexterity after carbonization, and while losing some of its strength during the process, lamination to canvas fabric will provide the strength required for deployment. Fluorinated mesoporous carbons were explored briefly under electron beam irradiation due to the radical generation properties of fluorinated mesoporous carbon materials. Using the fluorine as a radical generator under e-beam irradiation could increase the radical density and thus increase grafting of the chelation polymer onto the surface of the carbon material. Fluorinated materials

are typically hydrophobic and thus not desired for deployment in seawater, unless the hydrophilicity could be modulated through the irradiation process. Oxidation of several materials, i.e. mesoporous carbon, activated carbon, carbon nanotubes, and carbon fibers, was performed to introduce defect sites on the carbon surface along with reactive surface oxygenate functional groups (carboxylic acids, alcohols, ketones). Oxidation also increases the hydrophilicity of the carbon surface. This was performed through acid oxidation, typically sonication in 70% nitric acid for 5 hours or a mixture of sulfuric acid and nitric acid (3:1 ratio respectively).

Carbon nanotubes represent a cylindrical carbon alternative to polymer fibers that exhibit a high length-to-diameter aspect ratio with lengths of millimeters and diameters in the 50 nm range. This results in a high-surface-area material that can be functionalized in a variety of ways. Several functional forms have been produced for other applications such as Buckypaper, a flexible nanotube-based paper used in advanced battery research. An advanced carbon nanotube-based material tested was the "nano hybrid shish-kabob" polyethylene-carbon nanotubes composite produced by Dr. Christopher Li at Drexel University. This material was selected for screening due to its combination of crystalline polyethylene supported by carbon nanotubes.[6] This combination should have the advantages of the stability of carbon materials and the ease of radiation-induced grafting of polyethylene fibers through incorporation into one motif. Unfortunately, this material is hard to produce, as the polyethylene must crystallize on the carbon nanotubes and currently is only prepared in small milligram quantities.

Electron beam irradiation of the carbon materials, 200 kGy dose at Neo Beam in collaboration with the Radiation Induced Graft Polymerization Subtask, resulted in low grafting yields, typically around 30%. This translated into low capacities for acrylonitrile-based systems, with laboratory screening (6 ppm [U]) capacities often less than 5 mg U/g adsorbent. Due to the nature of the grafting process, there was no agitation during the irradiation and during the thermal treatment after irradiation. Thus little could be done to facilitate monomer transport through the pores, other than capillary effects, which should decrease crosslinking of the monomers outside the pores. One alternative to increase the capacity was to graft epoxides, such as glycidyl methacrylate, onto the carbon surface and react them with amines to introduce nitrile functional groups, which can be convert to amidoximes. This approach provided capacities of 13 mg U/g adsorbent under laboratory screening conditions (6 ppm U) with carbon nanotube materials and iminodipropionitrile, a bis-nitrile that can be converted to the bis-amidoxime, compared to 20 mg-U/g-adsorbent for the Japanese nonwoven fiber. However, the ester functional group in poly(glycidyl methacrylate) (GMA) may have stability issues under seawater conditions, i.e. pH ≈ 8 and high salinity that may result in cleavage of the ester bond in GMA to form a carboxylic acid while losing the amidoxime functionality. In addition, the standard conditioning step used for the polymeric adsorbents, involving treatment with 2.5% KOH, may further degrade the ester linkage in the GMA-based polymer. There have been some attempts to use sodium carbonate instead of KOH to condition the polymer, and higher capacities have been observed on some GMA-based composites; however the capacity increases are not consistent. Efforts to understand the capacity of GMA-based composites are still under way with a focus on determining the stability with respect to conditioning and seawater conditions.

Gamma irradiation of the mesoporous carbon materials was performed at the University of Maryland in collaboration with Dr. Mohamad Al-Sheikhly. The gamma irradiation was less intense than the electron beam irradiation, with dose rates of 10 kGy/hr, and the monomers did not require cooling to prevent volatilization or thermal degradation. The samples were irradiated

for 3 h and a total dose of 30 kGy. Significant crosslinking occurred during irradiation, resulting in solidified polymer surrounding the carbon material. The capacities were low as with the electron beam irradiation materials, with most below 2 mg U/g adsorbent; hierarchically porous (macroporous + mesoporous) carbon rods generated via soft-templating and spinodal decomposition exhibited capacities of 0.36 mg U/g adsorbent. Commercial oxidized carbon fibers (Toho Pyromex) procured from Toho Tenax America, Inc. (Rockwood, TN) were also tested. These fibers were utilized after it was discovered that oxidation resulted in slightly higher capacities for the mesoporous carbon materials during chemically induced radical polymerization. Under γ-irradiation, the Toho Pyromex fibers exhibited a higher capacity at 5.6 mg U/g adsorbent. While this was not comparable to the Japanese adsorbent, the capacity was higher than any other sample tested. This could be due to the possibility that the carbon fibers were not carbonized which would introduce surface oxygenates and provide reactive functionalities on which to graft the polymers. However, the lack of carbonization also diminishes some of the chemical stability associated with the pyrolysis. Balancing the grafting efficiency and resulting capacity with the chemical stability of the fiber in seawater requires further study.

5.2.2 Chemically initiated grafting of chelation polymers onto carbon materials

Several methods have been utilized to chemically functionalize the carbon materials. The first is diazonium chemistry, in which a diazonium salt is prepared in situ through the reaction of amyl nitrite and an amine and grafted onto the carbon material (Scheme 5.1). This was initially believed to take advantage of the high surface area of the carbon material and graft functional ligands or nitrile-containing ligands that can be converted to amidoxime groups onto the surface. This method did not provide a high grafting yield and the capacity was lower than the adsorbent supplied by Japanese researchers in side-by-side testing.

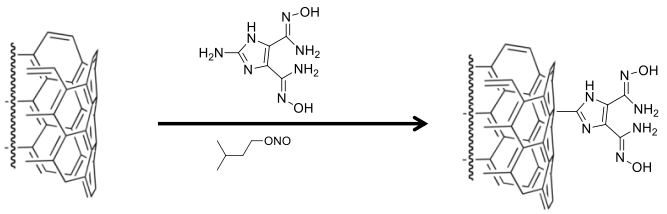

Scheme 5.1. Example of diazonium-based grafting onto a carbon material.

Thermally initiated polymerization of chelation polymers, namely PAN, was attempted with mesoporous carbon that had a maximum average pore size of 10 nm (i.e. mesoporous carbon, surface area of 400–600 m^2/g) and activated mesoporous carbon (mesoporous carbon with micropores added through base activation, surface area 1700 m^2/g) in an attempt to increase the capacity. The carbon materials were oxidized by either nitric acid or sulfuric/nitric acid mixtures to provide a hydrophilic surface and to provide surface defect sites on which to grow the polymer. The grafting yields, as determined by TGA, were found to be low. However, it has been found that PAN does not cleanly pyrolyze under inert atmosphere. This leaves a carbon residue so the grafting yields are underestimated. The PAN was converted to poly(acrylamidoxime) by reaction with hydroxylamine. Although the uranium adsorption capacities were found to improve with surface oxidation, they were not significantly. The optimized results for thermally grafting PAN to the carbon materials are provided in Fig. 5.1. In an attempt to understand why the large surface areas were not resulting in high grafting yields and capacities, the capacity was expressed in terms of uranium adsorbed per surface area (m^2), where the capacity (μg U/g adsorbent) is divided by the surface area (m^2/g

adsorbent). This normalized surface area led to the realization that pore size is an issue. In the mesoporous, activated, and oxidized activated mesoporous carbon samples (18a-64), there was essentially no difference in the capacity, although the activated carbon samples were slightly higher (Fig. 5.2). This suggests that the pore size is having a negative effect on the capacity.

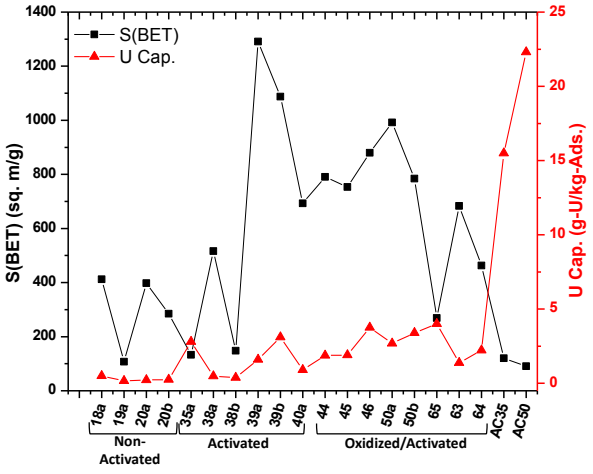

Fig. 5.1. Surface area vs. capacity for PAN functionalized mesoporous carbon materials.

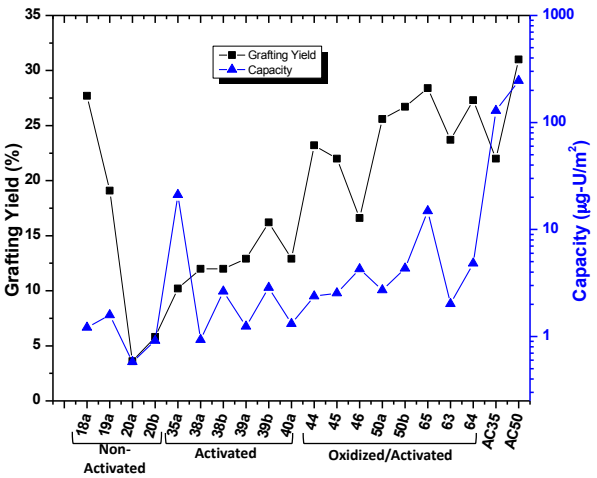

Fig. 5.2. Grafting yield vs. specific capacity for the PAN functionalized mesoprous carbon material materials.

Thus larger pores were introduced into the mesoporous carbons to determine the effect of pore size on the capacity. Using silicate spheres (35, 50, or 85 nm diameter) as the sacrificial template, mesoporous carbons were produced with varying levels of porosity. This resulted in a large increase in capacity with the inclusion of 35 nm pores (AC35 in Fig. 5.2) in addition to the microporosity and 10 nm mesopore. Further increasing the pore size to 50 nm (AC50 in Fig. 5.2) resulted in higher capacities. Surprisingly, the 85 nm pore sample showed a decrease in capacity, from 245 µg U/m^2 for the 50 nm pores sample to 80 µg U/m^2; however the capacity was similar at 20.9 vs. 22.3 mg U/g adsorbent, respectively.

Optimization of the pore structure requires knowledge of the effect of the porosity on adsorption capacity. Table 5.1 illustrates the effect of pretreatment condition and pore structure on the 85 nm macroporous carbon sample. The pretreatment condition was either the standard 2.5% KOH at 80 °C for 3 h that was used for the polymer samples described in Section 4, or a pretreatment at 120 °C for 3 h in DMSO, which should produce the cyclic imidoxime as described in Section 2. Optimization of the grafting method and the pore structure resulted in a material that adsorbs 400 µg U/m^2, correlating to a capacity of 41.9 mg U/g adsorbent. Ultimately, the effect of porosity is complex, and understanding it requires more in-depth study. However, it appears that, while micropores were believed to be required for grafting, i.e. as anchor points for the polymer within the mesopore, the data suggest that micropores are actually detrimental to the capacity. This is most likely due to the micropores filling with polymer, thus blocking access to those pores. A pore regime consisting of the uniform mesopores in addition to the 85 nm macropores resulted in the highest capacity. This is believed to be due to an interconnected network of mesopores that in turn connect the 85 nm macropores together. This would provide effective transport through the material while decreasing the possibility of complete pore blockage. Thus, in general KOH conditioning is either similar to or a more

effective method to increase the capacities and this pretreatment is adopted for the rest of the study.

Table 5.1. Effect of pretreatment on capacity of hierarchically porous carbon materials. Capacity derived from laboratory screening protocols using 6 ppm U solutions.

Sample	Pore Regime	S_{BET} (m^2/g)	Grafting (%)	Uranium Adsorption Capacity (mg-U/g-ads)		
				No Conditioning	DMSO (120 °C/3 hrs)	KOH (80 °C/3 hrs)
85a-AO	2/10/85	260	19.1	4.8	20.9	20.5
85b-AO	2/85	283	16.2	10.3	13.4	6.5
85c-AO	85	-	10.0	6.4	33.0	37.8
85d-AO	10/85	103	14.0	7.0	28.9	41.9

To increase the grafting yields and capacity for uranium adsorption onto carbons, sonochemically assisted radical generation was attempted based on work from Suslick's group at Illinois on the functionalization of graphene with polystyrene.[5] Sonochemistry generates cavitation bubbles that have extreme temperatures and pressure at the bubble/solvent interface, which can help generate radicals. In addition to the sonochemical effect on radical generation, it is believed that mass transport is enhanced by the ultrasonic action and facilitates transport of the monomer throughout the pores. Two types of sonication were utilized, the standard laboratory sonication bath (100 W, 42 kHz) and a variable-power, high-intensity ultrasonic probe (700 W max, 25 kHz). By using sonication, the polymerization reaction was accelerated and the reaction was completed in 3 h rather than 48 h for the thermally assisted radical generation. Since differences in the grafting yields between the two sonication methods were minimal, the high-intensity ultrasonic probe was used for most of the studies. Overall, sonication increased the grafting yields by approximately 20 to 30% compared with the thermally assisted radical generation, and the uranium capacities increased from the low 20s to approx. 40 mg U/g adsorbent. This work was recently published in the *Journal of Materials Chemistry A*.[7]

Carbon fibers represent a viable replacement for the polyethylene trunk fiber used by Japanese researchers. These are flexible, high-strength fibers that can be woven and deployed in a similar scenario to the current technology with higher chemical and thermal stability. The fibers have similar chemical reactivities to the mesoporous carbon fibers and can be activated to introduce porosity. The carbon fibers investigated were procured from Hexcel (activated carbon fibers) and Toho Tenax 344. The Toho Tenax 344 (Toho America, Inc.) fibers were grafted with PAN both thermally and sonochemically. Low grafting yields were obtained, i.e., 1–3% grafting, which produced capacities of 4 mg U/g adsorbent. This capacity is abnormal compared with the previous results wherein low grafting resulted in very low capacity (<0.1 mg-U/g-adsorbent). Efforts to increase the capacity of the fibers through higher grafting yields is currently on-going.

5.2.3 Mesoporous carbon-polymer composite adsobents

Currently, we have not been successful at finding a method to graft polymer chains or functional ligands onto a carbon surface in high yields. Therefore, we explored an alternate approach where functional monomers are polymerized and crosslinked inside the pores of a mesoporous carbon, locking into place without the need to graft to the carbon surface (Fig. 5.3). The polymers were synthesized using AN and AA with divinylbenzene (DVB) as a crosslinking

agent. Through this route, the pores of the carbon materials are impregnated with monomers, followed by polymerization to crosslink the copolymer inside the mesopores of the carbon support. This "one-pot" synthetic route using DVB is straightforward, and stable polymer-carbon nanocomposites can be obtained in large quantity. The carbon-supported polymeric sorbents were synthesized by a thermal polymerization method in which the activated carbon was immersed into varying amounts of monomer while the ratio of AN, AA, and DVB was held constant at 7:2:1 (w/w). After polymerization, the composite sorbents were washed with dichloromethane and dimethylformamide to remove excess monomers and homopolymers, respectively, followed by treatment with hydroxylamine to generate the amidoxime sorbents and drying at ambient temperature.

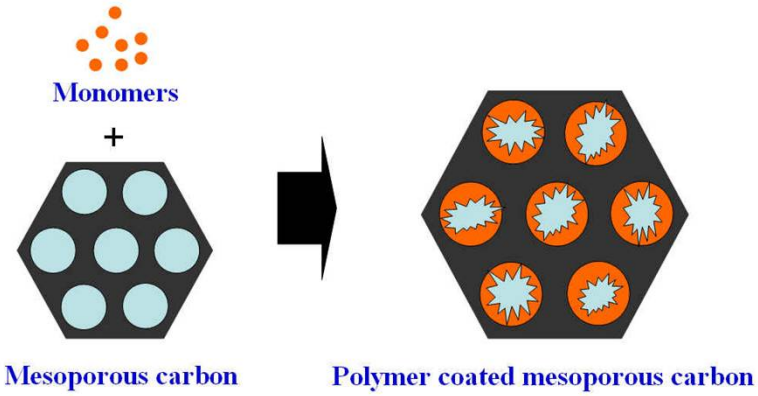

Fig. 5.3. Impregnation scheme for activated mesoporous carbon materials.

The BET surface areas of the composite materials were calculated from the N_2 adsorption at 77 K. The specific surface areas, along with total pore volume, were observed to gradually decrease as the monomer-to-carbon ratio was increased (Table 5.2) compared with the original carbon. The broadening of the calculated pore size distributions (PSDs), calculated according to the improved KJS-method, suggest that pores on the carbon support are filling and being partially blocked as more polymer is coated on the surface. Further evidence to support the surface coating of the particles arises from the lack of a shift in the peak maximum of the PSD. This indicates that while some porosity is utilized, the available surface area arising from the particle size is a determining factor for the capacity of the impregnated adsorbents.

This series of composite sorbents (described by an acronym based on CP-carbon-to-total monomer ratio [i.e., CP-1:2] in which the total monomer ratio is the sum of AN to AA at a 7:2:1 ratio of AN, AA, and divinylbenzene, respectively) were screened with simulated seawater consisting of a high uranyl concentration (~ 6 ppm) brine to identify ideal samples for marine testing. The uranium adsorption capacity increases as the ratios of monomers and carbon increase in the composites. The highest capacity of 62.7 mg U/g adsorbent was obtained for the sample of CP-1:12. The capacity decreases slightly with further increases of the monomers/carbon ratio, indicating that there is a saturation effect for the nanocomposite, which is due to pore filling or pore blocking which reduces the surface area for uranyl adsorption.

Table 5.2. The porosity and uranium adsorption capacities for the polymer coated carbon composites MC and MC-A represent mesoporous carbon and activated mesoporous carbon, respectively; CP-*x* represents the carbon polymer composite where *x* is the carbon to total monomer ratio (i.e., 7:2:1 mixture of acrylonitrile, acrylic acid and divinylbenzene monomers) of 1:*x* by weight, respectively

Sample	V_{SP} (cm^3/g)[a]	S_{BET} (m^2/g)[b]	V_{mi} (cm^3/g)[c]	S_{mi} (m^2/g)[d]	DOG (%)[e]	Capacity (mg/g)	K_d (mL/g)
MC	0.84	373	0.04	91	–	–	–
MC-A	1.55	1609	0.45	985	–	–	–
CP-1:3	0.58	592	0.15	333	87.1	24.8	5667
CP-1:4	0.49	504	0.13	288	89.0	14.6	2931
CP-1:5	0.45	465	0.12	267	95.4	23.7	5293
CP-1:7	0.37	347	0.08	180	95.4	35.4	9524
CP-1:12	0.21	161	0.03	64	97.2	62.7	29978
CP-1:15	0.15	108	0.02	41	97.3	48.9	16984
CP-1:20	0.10	91	0.03	59	96.0	59.6	28579
CP-1:25	0.07	55	0.01	26	95.5	57.2	25676

[a]Single point pore volume taken at p/p_0~0.98. [b]Specific surface area calculated in the p/p_0 range of 0.05 – 0.20. [c]Micropore volume and [d]micropore surface calculate using carbon black STSA equation within the 0.50–0.60 nm thickness range. [e]Degree of grafting (DOG) was calculated from thermogravimetric analysis data obtained under nitrogen atmosphere for a nonporous reference carbon material, i.e. carbon black. The broadening of the calculated pore size distributions (PSDs) suggests the filling and partial blocking of the pores in the carbon support as more polymer is coated on the surface. Further evidence to support the surface coating of the particle arises from the lack of a shift in the peak maximum of the PSD. This indicates that while some porosity is utilized, the available surface area arising from the particle size is a determining factor for the capacity of the impregnated adsorbents.

To determine the uranyl capacity in seawater, CP-1:12 sorbent was immersed in a tank filled with 5 gal. of seawater and shaken for 5 weeks. Five separate tanks were utilized to understand the capacity as a function of time. After each week, the adsorbent was collected and eluted with a 3:1 mixture (by volume) of 12 M hydrochloric acid to 16 M nitric acid, respectively (Fig. 5.4). The gravimetric capacity is low for the carbon sorbents (0.55 mg U/g adsorbent). Pore blockage is undoubtedly the culprit for the low capacities, as the polymerization was not controlled and significant polymer was observed on the exterior of the particles. During conversion and conditioning, the polymer swells further decreasing the surface area available for transport through the pores and effectively leaving only the external surface of the polymer available as the primary adsorbent. This is an inherent disadvantage to free radical polymerization, and thus led to efforts to control the polymerization.

5.2.4 Controlled living polymerization growth of PAN onto carbon materials

Although the nanomaterials have lower grafting yields than the polymers studied in Section 4, their uranium adsorption capacities are higher than expected, indicating that the nanomaterials are utilizing the grafted ligands more efficiently or the ligands have better access to the solution (Fig. 5.5). Thus, if grafting yields can increase, big increases in capacity could be gained. In an attempt to increase the effective grafting yields in the nanomaterials, controlled radical polymerization was investigated. This method utilizes chain growth initiators, such as pendant bromides or chlorides covalently anchored onto the nanomaterial surface, and a metal catalyst consisting of an organometallic complex such as a copper(II) chloride-bipyridine or an

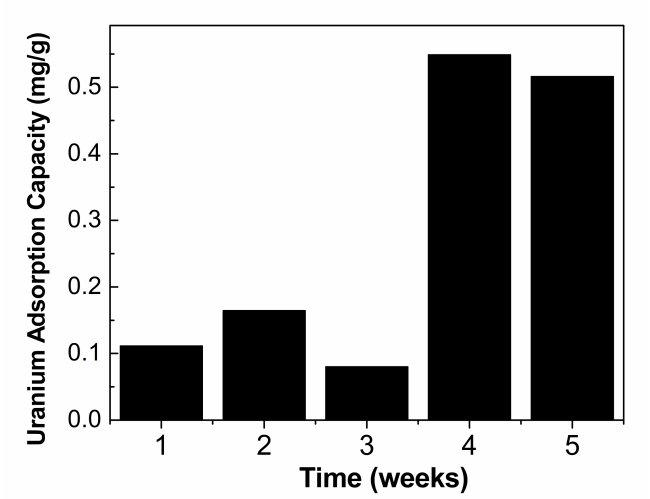

Fig. 5.4. Transient seawater capacity for the impregnated activated mesoporous carbon CP-1:12.

iron(III) chloride-iminodiacetic acid complexes, to initiate the polymer growth off the substrate. This method has the advantage that less homopolymer is formed in solution, so the chains can grow without competition for free monomers; however, this method is dependent on the density of initiator sites on the support surface. To avoid copper or iron catalysts coordinating to the acidic monomers (AA or MAA) that are being grafted into the polymer, the corresponding esters are used, which can be converted to the corresponding acid through base hydrolysis.

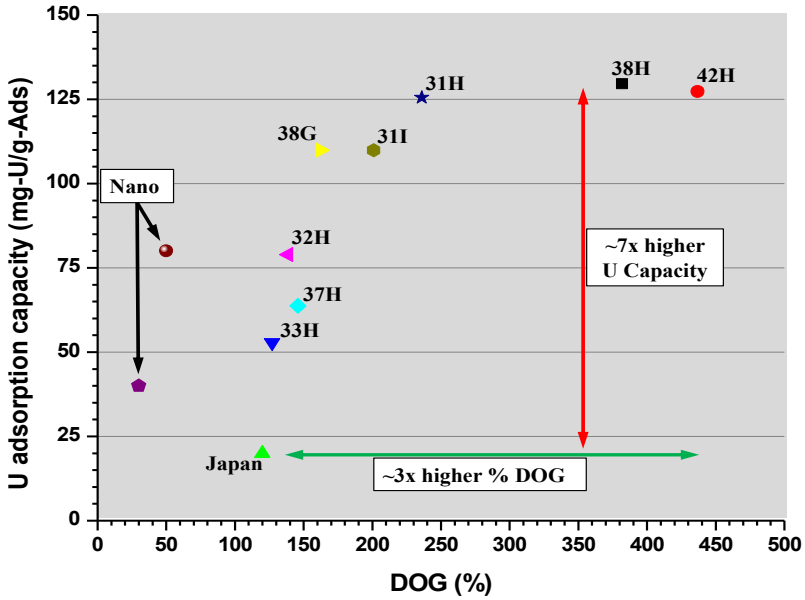

Fig. 5.5. Degree of grafting vs screening capacity for the nanoporous and polymeric adsorbents.

Oxidation of the carbon surface provides sites, i.e. surface hydroxyl functional groups, on the surface to anchor initiators, such as α-bromoisobutyryl bromide for ATRP (Scheme 5.2). Initially, low grafting yields were obtained on the 85 nm mesoporous-carbon–containing 10 nm mesopores and the Pyromex carbon fibers. One method to overcome the lower grafting yields was to direct the monomer to the substrate surface through suspension polymerization of the hydrophobic monomers in water. The monomers will concentrate on the surface in close

proximity to the initiator and catalyst complex. In some instances, the surfactant cetyltrimethylammonium chloride was added to enhance the suspension formation while coupling ATRP to sonication polymerization. Initial attempts at ATRP with the iron catalyst system were promising with moderate grafting yields. However, capacities for the large-pore hierarchical mesoporous carbon were not high, on the order of 2–4 mg U/g adsorbent. This suggests accessibility issues through pore blockage, since the grafting yield was consistently on the order of 50%. Switching to carbon fibers resulted in higher capacities, with similar grafting yields compared to the sonication polymerization reactions. While the work is ongoing, the grafting yields have plateaued at approximately 30% on the carbon fibers with capacities under laboratory screening conditions plateaued at 30 mg U/g adsorbent for grafting onto carbon fibers. This is most likely due to the surface density of the initiator sites, which is an active focus of the subtask.

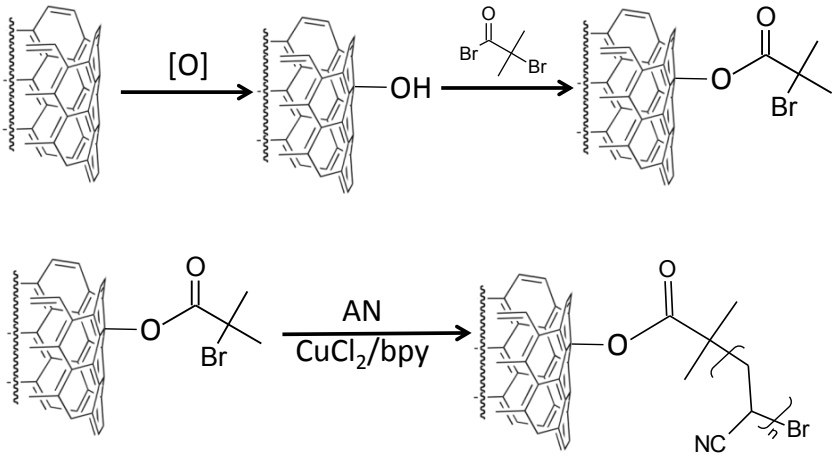

Scheme 5.2. Grafting of the ATRP initiator onto the carbon surface (top) followed by polymerization of acrylonitrile (bottom).

5.2.5 PAN adsorbent based on ATRP reaction with mesoporous copolymer substrate

With the density of initiator sites on carbon materials low, high-surface-area porous polymer materials with a high density of initiator sites were synthesized from divinylbenzene and vinylbenzyl chloride. The rationale for this porous polymeric materials arose from a recent report on the preparation of a stable mesoporous polymeric solids by copolymerization of DVB with sodium *p*-styrene sulfate under a simple solvothermal method without surfactant templating.[8] A series of mesoporous copolymers were synthesized under similar reaction conditions, using 4-vinylbenzyl chloride (VBC) instead of sodium *p*-styrene sulfate, hereafter referred to as poly(DVB-VBC)/*x* (where *x* stands for the molar ratio of VBC to DVB). The BET surface area, pore volume and active site concentration of the copolymers can be tuned by varying the ratio of the reactants. For example, a gradual decrease in both the specific surface areas and total pore volume was observed as the DVB-to-VBC ratio was increased. Balancing the VBC content with surface area and mesopore formation is vital. PAN was grafted via ATRP onto the poly(DVB-VBC). Degrees of grafting for the PAN onto the porous polymer was high, (280, 509, 310% for poly(DVB-VBC)/*1,* (DVB-VBC)/*2*, and poly(DVB-VBC)/*3*, respectively) indicating the synergistic effect of the nanostructuring coupled with the density of the initiator sites for the grafting under the same condition.

The above PAN-grafted porous polymers were screened with simulated seawater (6 ppm U) with capacities approaching 80 mg U/g adsorbent and capacities tracking with the grafting yields. As a reminder, the supplied Japanese adsorbent capacity was 20 mg U/g adsorbent under identical conditions. It is important to note that no hydrophilicity has been incorporated in these polymers. Acidic functionality can be added by copolymerization of an ester, such as tert-butyl acrylate, with AN followed by base hydrolysis to the acid. While work is ongoing, initial experiments suggest that the copolymerization of PAN and tert-butyl acrylate, under conditions similar to the grafting PAN polymer above, resulted in a 20% drop in grafting yield but only a 12.5% drop in uranium capacity under screening conditions. Optimization of the polymerization parameters is ongoing for the copolymerization. In addition to the reaction optimization, these materials are undergoing initial marine testing at this time.

5.3 Future Work

Although carbon-based nanomaterials have promise for the extraction of uranium from seawater because of their high surface areas, tailored porosity, and stability, the challenge is to obtain high grafting yields. We will continue to focus efforts on this core hurdle that is preventing the realization of high capacities for carbon-based nanomaterials.

5.3.1 Increasing the ATRP initiator concentration on the surface of carbon nanomaterials

The primary limitation for controlled growth of polyacrylonitrile via ATRP on the surface of nanomaterials is the initiator density. This applies to both the carbon and polymer materials. Tailoring the oxidation protocols for carbon materials can provide higher densities of specific oxygen functional groups, i.e. predominately hydroxyls or acids instead of a distribution of functional groups. Alternatively, more stringent oxidation methods could be utilized to influence the type of oxygenates on the surface and tailor it toward grafting the ATRP initiator onto the surface. Concurrent to this is eliminating the ester linkage found in the preliminary work. Covalent grafting of more stable functional groups, with respect to seawater, will eliminate one inherent weakness in this approach. While the oxidation experiments are on-going, other grafting methods will be explored to increase grafting density of the ATRP initiator onto the surface.

5.3.2 Optimization of the mesoporous polymer capacity with ATRP

In continuation of the porous polymer nanomaterials research,[8] there are two directions that can assist in understanding the effect of amidoxime-acid copolymers on uranyl capacity. First is introduction of hydrophilicity into the hydrophobic polymer. This represents a challenge as the porosity is dependent upon the divinylbenzene:monomer ratio. High amounts of divinylbenzene are required to produce a rigid polymer, which negatively affects the capacity, as the divinylbenzene does not contribute to the overall capacity of the adsorbent. Primary methods would suggest replacing a portion of the vinylbenzyl chloride with styrene sulfonate. However, this results in a drop in capacity as the vinylbenzyl chloride is crucial for polymer grafting. Therefore, functionalization of the polymer material through the introduction of hydrophilicity to divinylbenzene or replacement of divinylbenzene with a rigid, yet more hydrophilic monomer will be studied. Secondly, grafting the initiator onto the porous polymer will overcome the limitations of the vinylbenzyl chloride content. This will provide more flexibility in the type of initiator used while allowing for higher grafting and ultimately higher capacities.

5.3.3 Carbon fiber adsorbent development

Carbon fibers potentially represent the best carbon material as a consequence of their small fiber diameter coupled with their chemical resistance, they could supplant polyethylene fibers in deployment. The chemical stability is crucial for regeneration studies as the carbon fiber could be acid stripped of all monomers when the capacity reaches a certain level, then reused after polymerization of a new set of monomers on the surface. In revisiting the use of activated carbon fibers as trunk materials, more rigorous oxidation methods will be used to increase the grafting densities of ATRP initiators onto the surface thus increasing the grafting yield and capacity. This, coupled with suspension polymerization to lower the solvent usage, will provide a secondary fibrous material that can be instituted into current testing without the need for redesigned testing apparatus.

5.4 References

(1) (a) Tian, G.; Geng, J. X.; Jin, Y. D.; Wang, C. L.; Li, S. Q.; Chen, Z.; Wang, H.; Zhao, Y. S.; Li, S. J. *Journal of Hazardous Materials* **2011,** *190* (1-3), 442-450; (b) Li, X. L.; Song, Q.; Liu, B. J.; Liu, C. X.; Wang, H.; Geng, J. X.; Chen, Z.; Liu, N.; Li, S. J.; *Prog. Chem.* **2011,** *23* (7), 1446-1453; (c) Kim, J. H.; Lee, H. I.; Yeon, J. W.; Jung, Y.; Kim, J. M.; *J. Radioanal. Nucl. Chem.* **2010,** *286* (1), 129-133; (d) Jung, C. H.; Lee, H. Y.; Moon, J. K.; Won, H. J.; Shul, Y. G. *J. Radioanal. Nucl. Chem.* **2011,** *287* (3), 833-839; (e) Drisko, G. L.; Kimling, M. C.; Scales, N.; Ide, A.; Sizgek, E.; Caruso, R. A.; Luca, V. *Langmuir* **2010,** *26* (22), 17581-17588.

(2) (a) Davies, R. V.; Kennedy, J.; Hill, K. M.; McIlroy, R. W.; Spence, R.; *Nature* **1964,** *203* (495), 1110; (b) Hutchins, C. M.; Panther, J. G.; Teasdale, P. R.; Wang, F. Y.; Stewart, R. R.; Bennett, W. W.; Zhao, H. J. *Talanta* **2012,** *97*, 550-556; (c) Turner, G. S. C.; Mills, G. A.; Teasdale, P. R.; Burnett, J. L.; Amos, S.; Fones, G. R. *Anal. Chim. Acta* **2012,** *739*, 37-46.

(3) (a) Jung, Y.; Lee, H. I.; Kim, J. H.; Yun, M. H.; Hwang, J.; Ahn, D. H.; Park, J. N.; Boo, J. H.; Choi, K. S.; Kim, J. M. *J. Mater. Chem.* **2010,** *20* (22), 4663-4668; (b) Kruk, M.; Dufour, B.; Celer, E. B.; Kowalewski, T.; Jaroniec, M.; Matyjaszewski, K. *Macromolecules* **2008,** *41* (22), 8584-8591; (c) Aydin, B.; Bilodeau, S.; Hamidipour, M.; Larachi, F.; Kleitz, F. *Ind. Eng. Chem. Res.* **2008,** *47* (8), 2569-2578.

(4) Johnson, B. E.; Santschi, P. H.; Addleman, R. S.; Douglas, M.; Davidson, J. D.; Fryxell, G. E.; Schwantes, J. M. *Appl. Radiat. Isot.* **2011,** *69* (1), 205-216.

(5) Xu, H. X.; Suslick, K. S. *J. Amer. Chem. Soc.* **2011,** *133* (24), 9148-9151.

(6) Li, L. Y.; Wang, W. D.; Laird, E. D.; Li, C. Y.; Defaux, M.; Ivanov, D. A. *Polymer* **2011,** *52* (16), 3633-3638.

(7) Gorka, J.; Mayes, R. T.; Baggetto, L.; Veith, G. M.; Dai, S. *J. Mater. Chem. A* **2013,** *1* (9), 3016-3026.

(8) Liu, F. J.; Kong, W. P.; Qi, C. Z.; Zhu, L. F.; Xiao, F. S. *ACS Catal.* **2012,** *2* (4), 565-572.

6. ADSORBENT SCREENING AND ADSORPTION MODELING

Costas Tsouris, Jungseung Kim, Richard Mayes, Christopher J. Janke, Yatsandra Oyola,
Oak Ridge National Laboratory

6.1 Background and Significance

Uranium in seawater is present in multiple forms, including $UO_2(CO_3)_3^{4-}$, $UO_2(OH)_3^-$, $UO_2(CO_3)_2^{2-}$, UO_2^{2+}, $UO_2(OH)^+$, and $UO_2(OH)_2$, although the dominant form (84.9%) is the uranyl tricarbonate complex $UO_2(CO_3)_3^{4-}$.[1] Adsorption is widely accepted as the best method for uranium uptake from seawater because of simplicity in operation, low operating cost, low environmental risk, and high rate of uranium uptake, compared with other separation methods such as solvent extraction, membrane filtration, coagulation, and coprecipitation.[1] Because of the low uranium concentration and the complex nature of uranium speciation in seawater, the development of novel adsorbents with a promising capacity and a high selectivity for uranium has been the focus of our research.

A number of promising adsorbents are under development in this program at DOE and university laboratories (NEUP); therefore, a quick screening method was needed for the selection of the most promising adsorbents based on their performance in uranium adsorption from a synthetic seawater solution. It is difficult to make a direct comparison of adsorbents discussed in the literature because of the different initial uranium concentrations and chemical compositions of synthetic seawater solutions used. Since the speciation of uranium and the concentration of its various species change significantly with the solution concentration of various ions, pH, adsorbent mass per unit volume of the solution, and other thermodynamic conditions, the adsorbent performance is very sensitive to the analysis conditions.[1] On the other hand, if the screening solution chemistry was similar to that of seawater, adsorbent screening would need a considerable amount of time due to (1) the competition of other ions for the adsorption sites and (2) the high stability of uranyl tricarbonate in the solution. Thus it was important to define the initial uranium concentration, chemical composition in the solution, amount of adsorbent used, contact time, and operating conditions for the adsorbent screening method to have comparable results.

For the selection of the best adsorbents for field-testing, among the promising ones determined by the synthetic seawater screening experiments, it is necessary to use natural seawater without spiking the uranium concentration. Natural seawater is necessary in order to (1) keep the equilibrium speciation of uranium undisturbed and (2) allow other ions that are present in seawater to compete with uranium species for the adsorption sites. The key in this test is to keep a reasonable ratio of mass of adsorbent per volume of seawater, so that uranium is not completely depleted in seawater at the end of the test. If carefully designed as a well-mixed batch reactor, this seawater-screening test can provide the equilibrium uranium capacity of the adsorbent, as well as valuable kinetic information from uranium concentration measurements in seawater vs time.

Understanding the rate-limiting step of uranium uptake from seawater is essential to designing an effective uranium recovery system. Uranium uptake has been investigated mainly based on a reaction-limited assumption. For instance, linear-driving-force models, based on a single-species reaction mechanism, have frequently been used to describe the uranium adsorption behavior of amidoxime polymeric adsorbents.[2] Previous studies suggested that the decomplexation step of the uranyl tricarbonate complex [$UO_2(CO_3)_3^{4-}$] is the rate-limiting step in

uranium complexation by amidoxime functional groups from seawater.[2] The influence of transport of the uranyl complex on the uptake rate was also investigated by using an intraparticle diffusion model.[2] It was reported that intraparticle diffusion might also be the rate-limiting step for uranium uptake by amidoxime-based polymeric adsorbents.[3] In some cases for amidoxime-grafted polymeric adsorbents, intraparticle diffusion determined the overall rate of uranium uptake from seawater.[4] The influence of transport of uranium species on the overall uranium uptake process is supported from observations where the adsorption rate increased with increasing porosity and hydrophilicity of the polymeric adsorbents.[3b] The liquid-film mass-transfer model also described well the uranium adsorption behavior from seawater, indicating that the film resistance can also be the rate-limiting step in the overall process.[5] In another study, uranium uptake was reported as a process controlled by both the binding reaction between the amidoxime and uranyl species and the diffusion through hollow amidoxime-grafted polymer in a packed bed.[4a] Uptake rates of uranium from real seawater were reported for different reactor configurations, such as batch[5] and packed-bed.[4, 6] Previous reports recommended that the uptake performance should be described with reliable mathematical models under different regimes, with proper consideration of reactor design in order to reliably predict and improve the adsorption performance under realistic conditions.

Determining the rate-limiting mechanism in uranium adsorption is important because it can influence the adsorbent development and/or the deployment conditions. The following transport/reaction mechanisms are usually considered:[7] (1) transport of adsorbate from the bulk liquid phase to the exterior film of the adsorbent (interparticle diffusion); (2) transport of adsorbate from the film to the surface of adsorbent (liquid-film mass transfer); (3) transport of adsorbate in the interior of adsorbent fibers (intraparticle diffusion); and (4) binding reaction of adsorbate with the active sites of the adsorbent. These transport/reaction mechanisms are depicted in Fig. 6.1. If interparticle diffusion is the rate-limiting step, then the hydrophilicity of the adsorbent needs to increase in order to reduce aggregation. The seawater flow also affects transport steps (1) and (2), so if these steps control the rate of uranium uptake, this is an indication that a higher linear velocity of seawater is needed. If intraparticle diffusion is the rate-limiting mechanism, then smaller-diameter fibers can reduce the diffusion resistance. On the other hand, if complexation reaction is the rate-limiting step, then larger-diameter fibers can be used, if the degree of grafting can be preserved, to increase their strength. Because of the importance of the uptake rate-limiting mechanism in the design and deployment of the adsorbent, a systematic approach is needed to determine the limiting step of the overall uptake process.

6.2 R&D Progress/Status

6.2.1 Adsorbent screening

Batch laboratory experiments have been conducted to investigate the uranium adsorption kinetics and equilibrium by amidoxime-based polymeric adsorbents described in Section 4 with the objectives to determine the rate-limiting mechanism for uranium adsorption and screen various adsorbents with respect to their uranium adsorption capacity and rate. Japanese adsorbents were also tested at similar conditions for comparison with the performance of ORNL adsorbents. Two protocols have been used for adsorbent screening: (1) synthetic seawater solution in glass beakers and (2) natural seawater in 5 gal plastic tanks. Information on the sampling location

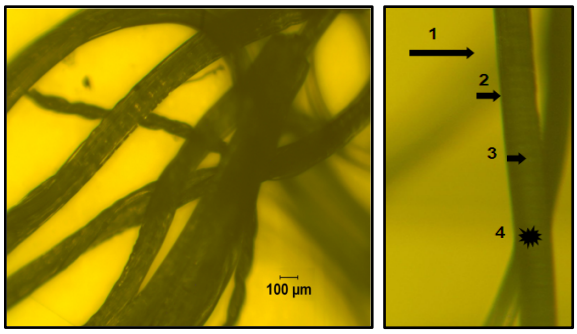

Fig. 6.1. Wet ORNL38H adsorbent fibers of 153-µm diameter (wet) fibers (left) and mechanisms involved in the adsorption process (right): (1) interparticle diffusion; (2) liquid-film mass transfer; (3) intraparticle diffusion; (4) binding reaction. Images were obtained using an optical microscope (Nikon Microphot-SA).

of the natural seawater is given below. For the synthetic seawater solution tests, sodium chloride (0.43 M) and sodium bicarbonate (2.29×10^{-3} M) were used, and the solution was spiked with uranyl nitrate at a uranium concentration of 6 ppm. From chemical equilibrium modeling, using the MINEQL equilibrium software package, the uranium speciation and composition were obtained, for a closed system, as follows: $UO_2(CO_3)_3^{4-}$ (42%), $UO_2(CO_3)_2^{2-}$ (39.2%), $(UO_2)_2(OH)_2CO_3^{-}$ (17.1%), UO_2CO_3 (1.4%), and $(UO_2)OH_2$(s) (0.3%). The ratio of uranyl bicarbonate to uranyl tricarbonate is approximately one, which makes the screening solution more favorable than seawater for uranium uptake. Therefore, the synthetic spiked solution allows a fast screening to determine the most promising adsorbents, which are subsequently screened further with natural seawater as discussed below. More information on screening tests with synthetic solution and results for various adsorbents is presented in Section 4.

For adsorbent screening tests with natural seawater, two different seawater batches were used: (1) coastal gulfstream seawater from a location 210 m deep, 75 miles east of Savannah, GA, collected in 5 gal tanks and (2) near-surface seawater from Charleston, SC, collected in 110 gal tanks. The salinities of the Charleston and Savannah seawater were measured with a CTD (conductivity, temperature, and depth) instrument, using Niskin bottles, at 34.5 and 35.5 ppt, respectively. The initial uranium concentration was measured by ICP-MS and found to range between 3.1 and 3.2 ppb for the Charleston seawater and 3.5 and 3.7 ppb for the Savannah seawater. Amidoxime-based polymeric adsorbent fibers were introduced into 5 gal plastic containers filled with seawater to initiate the screening tests. During the tests, which were run in batch mode, the seawater was well mixed using shakers, and seawater samples were collected periodically for uranium concentration analysis. Collected seawater samples were acidified with HNO_3 (Optima, Fisher Scientific, Hampton, NH, USA) to prevent biological activity and to keep the uranium dissolved for quantitative analysis. At the end of the tests, typically 6–9 weeks, the adsorbent fibers were recovered by membrane filtration using 200 nm pore-size membranes (Nylaflo™, Pall, Port Washington, NY, USA). The adsorbed uranium species were eluted using a highly concentrated acidic solution (mixture of HCl and HNO_3 at a ratio of 1:3, Fisher Scientific, Hampton, NH, USA), and samples were subsequently diluted with deionized water (Optima, Fisher Scientific, Hampton, NH, USA) prior to chemical analysis. Inductively coupled plasma with mass spectroscopy (ICP-MS, Thermo Scientific X-Series II) was used for quantitative analysis.

Selected results for uranium adsorption from seawater in 5 gal batch reactors are presented in Fig. 6.2. The uranium concentration vs time in seawater decreased fast initially and then approached a plateau region. The ORNL38H adsorbent showed the highest uranium uptake rate and capacity compared with ORNL42H and ORNL31H for the duration of the experiment (see

Section 4 for a description of the morphology of the fibers). As shown in Fig. 6.2, the capacity of ORNL38H was nearly double the amount observed for the Japanese adsorbent that was donated by JAEA, after 30 days of contact with seawater. From these tests, ORNL38H was selected for further seawater studies using adsorption columns for continuous flow. Results from batch experiments were also used in modeling studies as discussed below.

6.2.2 Adsorption modeling

Mechanistic studies have been performed to understand the underlying phenomena during adsorption and determine the rate-limiting step of the uptake process, among the four steps identified in Fig. 6.1. In this study, the first step, which is referred to as interparticle diffusion, is assumed to occur rapidly since the adsorbent is fluidized in single fibers in seawater. Thus this step is not considered the slowest step in batch experiments and can be neglected from the overall uptake process.[7] In some cases, however, the adsorbent forms aggregates in a confined space and, as a result, interparticle diffusion may become the controlling step.

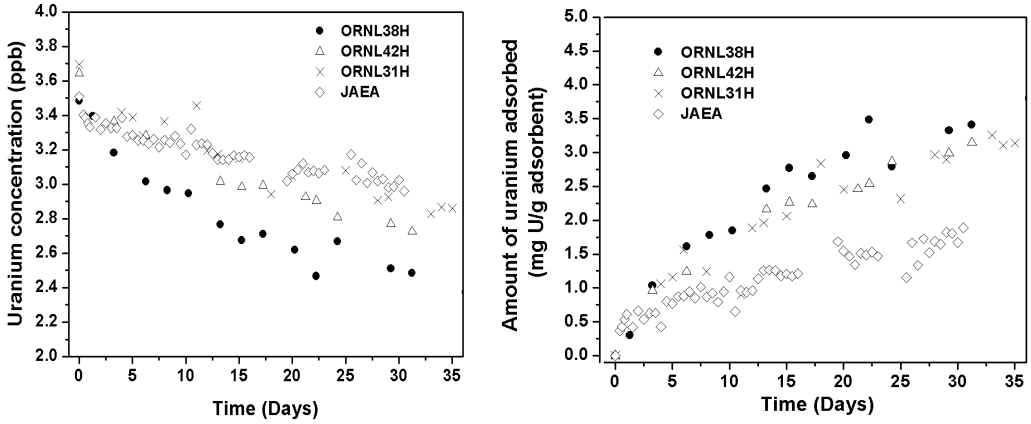

Fig. 6.2. Experimental results for adsorption of uranium from seawater in 5-gallon batch reactors. Agitation speed: 100 rpm.

In this investigation, the relative importance of liquid-film mass transfer, intraparticle diffusion, and binding reaction[4a] is evaluated for uranium adsorption by amidoxime-grafted polymeric adsorbent fluidized in a batch reactor. In the case in which the binding reaction is the rate-limiting step, the uptake rate is governed by interactions between the grafted functional ligand and uranium species. To evaluate the relative importance of each step, we employed dimensionless numbers, i.e., the Sherwood number and Thiele modulus, which are widely used in chemical engineering. The relative importance between liquid-film mass transfer and intraparticle diffusion can be evaluated by using the dimensionless Sherwood (*Sh*) number:

$$Sh = \frac{k_L \cdot L}{D} \tag{1}$$

Here, k_L is the liquid-film mass transfer coefficient and D is the diffusivity. The characteristic length L is considered the diameter of the adsorbent fibers. Liquid-film mass transfer is considered as the rate-limiting step if *Sh* is less than 1. On the other hand, if *Sh* is larger than 200, intraparticle diffusion is the rate-limiting step. If *Sh* is between 1 and 200, the liquid-film mass transfer resistance and intraparticle diffusion resistance are of the same order[5, 8]. Determination

of *Sh* through Eq. (1) requires values of the physical properties of the adsorbent, including the surface area and diameter. The surface area relevant to the external mass-transfer coefficient is the external surface area per unit mass of the fibers, which, for hydrated fibers of 153μm diameter (shown in Fig. 6.1), is 1.35 m^2/g (see Section 4). The corresponding value of *Sh* is over 10,000 suggesting that, between external-liquid-film mass-transfer resistance and intraparticle diffusion resistance, the intraparticle diffusion resistance is much higher. This result is consistent with experimental data shown in Fig. 6.3, where a comparison of uranium uptake is presented using the ORNL38H adsorbent at different agitation speeds. The amounts of uranium adsorbed vs time are similar for 100 and 200 rotations of the shaker per minute, indicating that both interparticle-diffusion and external-mass-transfer resistances are negligible under these experimental conditions.

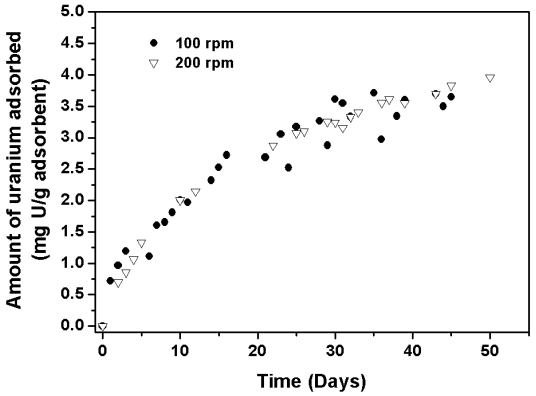

Fig. 6.3. Comparison of experimental results of amount of uranium adsorbed vs time (calculated from the uranium concentration decrease in seawater) in 5 gal batch reactors, using the ORNL38H adsorbent at different agitation speeds.

Subsequently, to determine the rate-limiting step in the uranium recovery from seawater process, it was required to evaluate the relative importance between intraparticle diffusion and binding reaction steps. In order to estimate the binding reaction rate constant, the experimental data were analyzed by the Azizian kinetic model.[9] A detailed mathematical description of the model is available in one of our publication.[10] The Thiele Modulus (ϕ_n) with a reaction order *n* has been employed to evaluate the relative importance between transport and binding reaction. The general equation is shown in Eq. (2).[11]

$$\phi_n = L_T \cdot \sqrt{\frac{(n+1) \cdot k_n \cdot C^{n-1}}{2D}} \qquad (2)$$

In this study, L_T is equal to half the radius of a cylinder,[11] *n* is the order of uranium binding reaction, k_n is the reaction rate constant for the binding reaction, and *D* is the diffusivity. Intraparticle diffusion is considered to be negligible when the Thiele modulus is smaller than 0.4. A Thiele modulus larger than 4 reveals a strong diffusion resistance (Fig. 6.4).

Batch results from the ORNL38H adsorbent, which showed the best performance with natural seawater, were used for the calculation of the Thiele modulus. The diffusion coefficient was obtained from the following mathematical model, where $q[t]$ is the amount of uranium adsorbed as a function of time and q_e is the amount of uranium adsorbed at equilibrium:

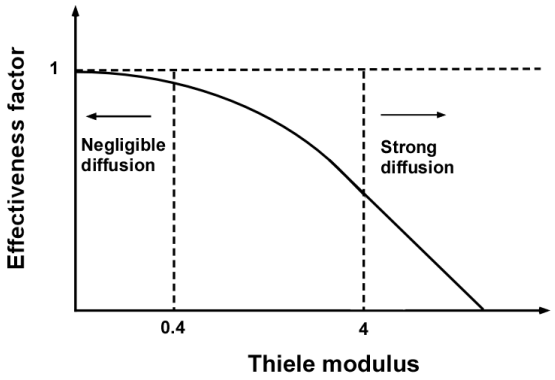

Fig. 6.4. Relationship between Thiele modulus and effectiveness factor for the comparison of transport and binding reaction kinetics effects.[11]

This relationship is the solution of the diffusion equation derived for the case of diffusion from a stirred solution of limited volume into a cylinder. The parameter α is the ratio between solution volume and cylinder volume. The diffusivity and the radius of cylindrical adsorbent fibers are expressed as D and r, respectively. This analysis considered amidoxime-grafted polymeric adsorbent fibers of a high aspect ratio having a cylindrical shape. The contribution of the intraparticle diffusion resistance can be evaluated by batch adsorption tests at good mixing conditions, which can minimize the effects of the liquid-film mass-transfer resistance and interparticle diffusion resistance.

$$\frac{q[t]}{q_e} = \frac{1+\alpha}{1+\frac{1}{4}\alpha} \cdot \left\{ 1 - exp\left[\frac{4\left(1+\frac{1}{4}\alpha\right)^2 \cdot D}{\alpha^2 \cdot r^2} \cdot t \right] \cdot erfc\left[\frac{2\left(1+\frac{1}{4}\alpha\right) \cdot \sqrt{D}}{\alpha \cdot r} \cdot \sqrt{t} \right] \right\} \tag{3}$$

For k_n in Eq. (2), the estimated value of the adsorption rate constant was employed in the calculation. With the assumption of a reaction-limited process, the experimental data were analyzed by the binding-reaction kinetic model presented by Azizian:[9]

$$A + L \underset{k_d}{\overset{k_a}{\leftrightarrow}} AL \tag{4}$$

Here A and L denote the adsorbate and functional ligand on adsorbent, respectively. AL is the complex of adsorbate and the ligand grafted on the adsorbent surface. k_a and k_d are the rate constants for adsorption and desorption, respectively. The initial amount of uranium adsorbed is assumed to be zero in all cases. Equation (5) applies for the rate of reaction:

$$\frac{d\theta}{dt} = v_a - v_d = k_a C(1-\theta) - k_d\theta \tag{5}$$

According to the theoretical analysis, the rate constants of the kinetic model combine the results of the complex binding reactions occurring during adsorption and desorption.[9] Experimental data were employed for the estimation of the rate constants of Eqs. (4) and (5). A nonlinear least-square regression method was used to determine the unknown parameters in the model equations, and results are shown in Fig. 6.5. The forward reaction-rate constant obtained

in this work is much lower than that reported by Rao in Section 3 of this document because, in his kinetic study, Rao had both reactants in the solution, while in this work the ligand is immobilized on the polymer.

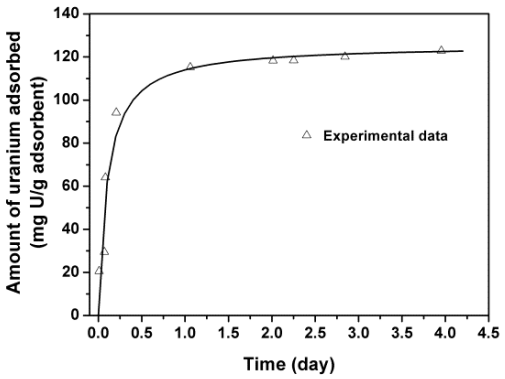

Fig. 6.5. Rate of amount of uranium adsorbed for uranium uptake in screening solution. The initial concentrations were 2.52×10^{-5} M uranyl nitrate corresponding to 6 ppm uranium, 2.29×10^{-3} M sodium bicarbonate, and 0.43 M sodium chloride.

The diffusion coefficient obtained from batch seawater experiments was used, and a value of 0.63 was calculated from Eq. (2) for the Thiele modulus. This value indicates that the overall adsorption process is near the limit where the process is reaction limited. It should be pointed out, however, that the diffusion coefficient was estimated under the assumption of a transport-limited process; therefore, the value of the diffusion coefficient obtained is the lowest possible. Furthermore, the kinetics obtained from batch experiments with the synthetic screening solution is much faster than the kinetics with natural seawater, which includes the competition effects from other ions in seawater. Thus the kinetic coefficient is expected to be smaller for seawater. For greater values of the diffusivity and lower values of the kinetic coefficient, the Thiele modulus becomes even smaller than 0.63, which means that the uptake process is controlled by the binding reaction.[10]

6.2.3 Flow-through tests and modeling

Prior to marine testing, it was important to demonstrate and optimize the engineering approaches, including adsorbent packing density and scaleup, using laboratory-scale flow-through tests. Flow-through adsorption columns have been used in these tests using 110 gal seawater tanks. Seawater was pumped from a tank through the columns and then recycled back to the tank. The ORNL38H adsorbent, which showed the best performance in batch experiments, was employed in the flow-through experiments. The temperature and flow rate were monitored during the experiments. Experimental data of uranium uptake from seawater obtained from three separate experiments at different temperature and flow rate conditions are presented in Fig. 6.6.

The amount of uranium uptake for the ORNL38H adsorbent was more than three times higher than the amount taken by the Japanese adsorbent for the same contact time. The uranium uptake after 6 weeks reached up to 3.3 mg U/g adsorbent, which is slightly lower than the maximum uranium uptake observed in batch experiments for the same contact time. This behavior may be attributed to temperature and water quality effects.

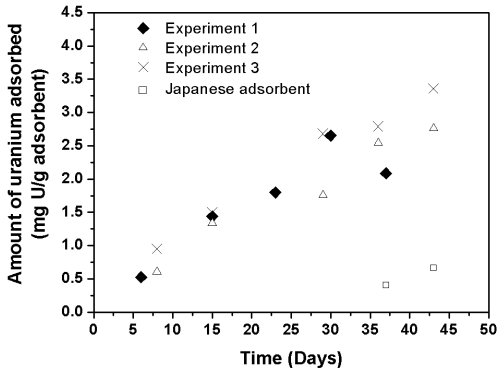

Fig. 6.6. Experimental data of uranium adsorption behavior obtained from flow-through adsorption experiments with the ORNL38H adsorbent. Temperature: 16.4±2.2 °C (Experiment 1), 23±2 °C (Experiments 2 and 3); Flow rates: 288.3±13.5 mL min^{-1} (Experiment 1), 273±23 mL min^{-1} (Experiment 2), and 231±11 mL min^{-1} (Experiment 3). The experiments were used as a guide for field experiments.

Field experiments were subsequently performed at the Marine Sciences Laboratory at PNNL, Sequim, WA. Figure 6.7 shows schematically experimental systems tested at PNNL, as well as experimental results from multiple experiments. Experiments were initially performed with the left top configuration in Fig. 6.7, which consisted of four parallel series of adsorbent beds. This design was used for two reasons: (1) it is a simple system that can provide kinetic information and (2) calculations based on batch data showed that the maximum concentration drop at the exit of each bed was less than 2.3%. In subsequent experiments, the left bottom manifold system in Fig. 6.7 was used to eliminate any error introduced by the series configuration of the left top system.

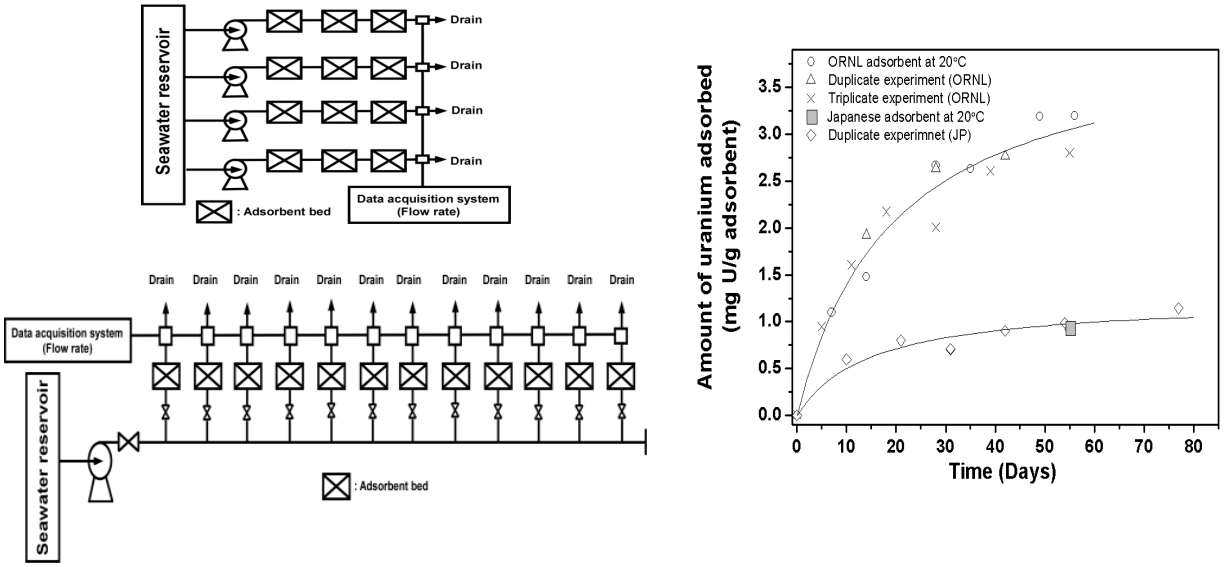

Fig. 6.7. Experimental systems (left) tested at PNNL and data (right) of multiple tests performed at the Marine Sciences Laboratory of PNNL at 20 °C.

In these tests, ORNL adsorbents have shown performance superior to that of Japanese adsorbents. These results are consistent with batch experimental results. Specifically, the ORNL adsorbent performed three times better than the Japanese adsorbent provided by JAEA in terms of amount of uranium uptake under similar experimental conditions. The initial uptake rate was also 2.6 times faster than that of the Japanese adsorbent, as shown in Fig. 6.8. The uptake rate decreased sharply during the first 3weeks for the ORNL adsorbent, while the uptake rate of the Japanese adsorbent decreased quickly during the first 2 weeks. Uranium uptake for the Japanese

adsorbent reached a plateau after approximately 4 weeks of contact with seawater, while the ORNL adsorbent accumulated uranium over a period of 60 days of contact with seawater.

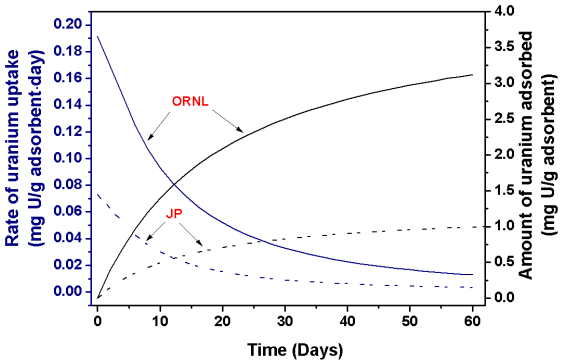

Fig. 6.8. Experimental information on amount and rate of uranium uptake vs time.

Data from different experimental setups and sample analyses were reproducible. No flow rate effects were observed when the linear velocity was higher than 0.78 m/min (0.013 m/s). This velocity is relatively low, as natural seawater currents in the Gulf Stream can reach up to 2 m/s. More details on the marine experiments are presented in Section 7.

In parallel to the experimental information, a simple mathematical model was used to provide a better understanding for the uranium uptake behavior in flow-through experiments. From the mass balance, Eq. (6) was derived for an adsorption column:

$$\frac{d(C \cdot V)}{dt} = Q_F \cdot C_F - Q \cdot C - M \cdot R \tag{6}$$

C_F and C are the concentrations [in ppb] of uranium in feed solution and in the adsorbent bed in flow-through experiments (initially 3.3 ppb) at any time, respectively. V is the volume of seawater in the adsorbent bed [L] and t is time [days]. Q_F and Q are the flow rates of seawater in feed solution and in outlet solution [L/day]. M is the weight of adsorbent [g] and R is the reaction term for uranium adsorption from seawater. In this study, the linear driving force model[2] is used to describe the uranium uptake rate from seawater and the following equations are incorporated into the mass balance to quantitatively describe the behavior of uranium uptake:

$$R = \frac{dq}{dt} = k \cdot (q_e - q) \tag{7}$$

$$q = q_e \cdot \left(1 - e^{-k \cdot t}\right) \tag{8}$$

$$\frac{d(C \cdot V)}{dt} = Q_F \cdot C_F - Q \cdot C - M \cdot k \cdot q_e \cdot e^{-k \cdot t} \tag{9}$$

$$\tau = \frac{V}{Q} \tag{10}$$

$$\frac{dC}{dt} = \frac{1}{\tau} \cdot (C_F - C[t]) - \frac{M \cdot k \cdot q_e}{V} \cdot e^{-k \cdot t} \tag{11}$$

$$C[t] = \frac{M \cdot k \cdot q_e \cdot \tau}{V \cdot (k - 1)} \cdot \left(e^{-k \cdot t} - e^{-\frac{t}{\tau}}\right) + e^{-\frac{t}{\tau}} \cdot (C_0 - C_F) + C_F \tag{12}$$

Here, k is the uptake rate constant [day^{-1}] in the linear-driving-force model. The model is similar to the first-order kinetic model, which was previously used to describe the uranium uptake from seawater.[2] The term q_e is the amount of uranium adsorbed at equilibrium [mg U/g adsorbent], and τ is the residence time of uranyl species in an adsorption bed [days]. Figure 6.9 shows the prediction using the linear-driving-force model for the experimental data with the ORNL adsorbent presented in Fig. 6.7. The model describes well the experimental data when the experimental value of q_e (i.e., amount of uranium uptake per unit mass of adsorbent at equilibrium) is used.

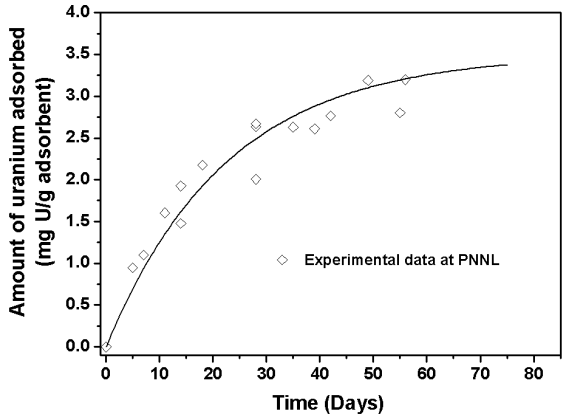

Fig. 6.9. Results for flow-through adsorption tests at PNNL using a linear driving force model.

Using Eq. (12), one can calculate the exit concentration of uranium from each column and estimate how much the uranium concentration drops from the entrance, where the feed concentration is 3.3 μg/L, to the exit of each column. Figure 6.10 shows a negligible drop in concentration of seawater passing through a column containing 100 mg of ORNL adsorbent. The maximum drop in concentration, which occurs in the beginning of the experiments, is 2.3% for 250 mL/min and 1.1% for 500 mL/min. This result demonstrates that the binding reaction rate of uranium is relatively slow. The reason for this behavior is probably due to the speciation of uranium in seawater and, specifically, the tendency of carbonate ions to keep uranyl ions in the solution instead of letting them bind to surface amidoxime groups. This result is also consistent with the finding that the binding reaction is the rate-limiting mechanism of uranium uptake.

6.3 Future Work

6.3.1 Experiments

Significant progress has been made in terms of amount and rate of uranium uptake from seawater in comparison with a previously developed Japanese adsorbent. A further scientific breakthrough is needed to make the technology of uranium recovery from seawater commercially competitive. Better understanding of various parameters in the uranium adsorption

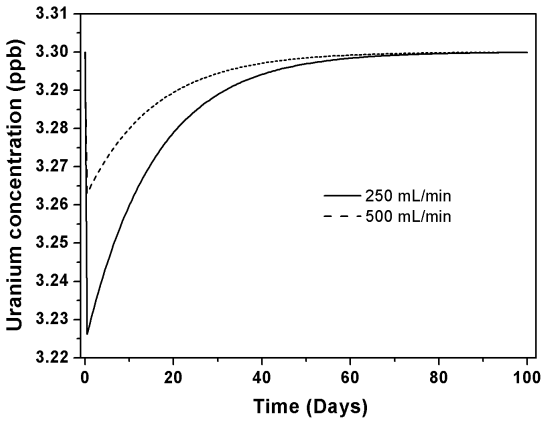

Fig. 6.10. Simulated uranium concentration history at the exit of a column containing 100 mg ORNL adsorbent, for 250 and 500 mL/min flow rates. The maximum drop in concentration, which occurs in the beginning of the experiments, is 2.3% for 250 mL/min and 1.1% for 500 mL/min.

process can lead to improvements not only in adsorbent design, but also in testing methodologies. Temperature is one of the most important parameters for uranium uptake from seawater. From our previous studies [10], the uranium binding reaction was found to be the rate-limiting step of the overall uptake process, so it is important to investigate the effect of temperature on binding kinetics. Positive values of enthalpy change of uranyl ion adsorption by either amidoxime resin or inorganic adsorbents have been observed in other studies,[10] including work performed under this program (see Section 3). This result suggests that the adsorption process is endothermic and driven by the change in entropy. This finding is consistent with previous reports suggesting that charge interactions, e.g., electrostatic or van der Waals are not the main driving force for solutions containing high concentrations of a mixture of ions, such as seawater.

It is also important to determine the influence of linear velocity, which has to do with testing the adsorbent performance in marine experiments, as well as in future deployment of the adsorbent in seawater. Specifically, adsorbent testing at different velocities of seawater is needed to determine the lower velocity limit, above which external mass-transfer limitations are negligible. Packing properties, such as porosity and adsorbent density, will also be investigated with the objective to minimize their effect on interparticle and film mass-transfer resistances.

Uranium speciation in seawater is another important parameter that significantly affects uranium adsorption. There is evidence in the open literature showing the influence of uranium speciation on uranium uptake.[12] Uranyl ions are known to form stable complexes with carbonate ions, such as uranyl mono-, di-, and tri-carbonate ions. Increasing amounts of these uranyl carbonate complexes lead to a decrease in the adsorption capacity.[12] Our hypothesis is that there also exists a relation between uranium speciation and transport properties through amidoxime-based polymeric materials. Spectroscopic analysis will be used to measure the permeation rate of uranyl compounds through an amidoxime-functionalized polyethylene membrane under various conditions to quantify the diffusivity of uranium species through the functionalized membrane. This part of the study is expected to provide insight into the influence of uranium speciation on transport properties and adsorption equilibrium. Diffusivity values are also needed in transport modeling of uranium species in the interior of adsorbent fibers.

6.3.2 Modeling

The objective of future modeling studies is to develop and validate mechanistic transport and kinetic models based on molecular-level understanding that can be employed to predict the uranium uptake rate. These models will be useful in many ways. (1) More effective adsorbents will be developed by delineating the mechanisms involved in uranium uptake by amidoxime. (2) A reliable prediction of the behavior of the adsorbent under various operating conditions, such as

temperature and linear velocity, will be important in the future selection of ocean deployment sites. (3) A reliable economic evaluation of the process cannot be accomplished without a reliable prediction of the adsorbent performance.

Modeling work will complement current efforts at ORNL, LBNL, and PNNL. Specifically, computational chemistry results at ORNL and experimental thermodynamic and kinetic information obtained at LBNL can be combined to establish possible reaction pathways of uranyl tricarbonate, which is the dominant species of uranium in seawater, as well as uranyl dicarbonate, with the amidoxime group. After possible chemical pathways are established based on molecular-level computational and experimental techniques, kinetic models based on real applications can be developed to describe the rate of uranium uptake as a function of independently obtained model parameters. Accurate prediction of the uranium uptake rate is needed to estimate the duration of possible deployment of the adsorbent to achieve target capacity. Predicting the amount of uranium adsorbed as a function of deployment duration and number of cycles has implications for the economics of the process.

An important finding from our studies so far is that the uranium uptake process is limited by the binding reaction rate. Experimental data obtained at LBNL (Section 3), on the other hand, have shown that the reaction of amidoxime in solution with uranyl ion is very fast. Furthermore, batch experimental data obtained at ORNL have shown that the speciation of uranium in seawater plays a controlling role in the adsorption process. In terms of transport, a diffusion coefficient in polyethylene fibers in the range of 10^{-6} m^2/day has been reported,[12] while ORNL batch experimental data can be explained by a diffusion coefficient in the range of 10^{-11} m^2/day. This large difference in diffusivity is probably a result of the speciation of uranium in the solution used in the experiments. Saito et al.[12] and Das et al.[12] used systems where UO_2^{2+} was the dominant species, while in our experiments, the dominant species is uranyl tricarbonate. Thus the hypothesis is that uranium speciation plays a significant role in both adsorption and transport rates of uranium and should be taken into consideration in transport and reaction kinetics modeling. Under high concentrations of the bicarbonate ion (HCO_3^-), uranyl tricarbonate is the dominant species of uranium in seawater. Uranyl tricarbonate is a very stable complex and competes effectively against the amidoxime ligand. This conclusion is supported by experimental observations using spiked solution of uranyl nitrate and sodium bicarbonate. In addition, computational chemistry calculations conducted at ORNL showed that, energetically, the binding reaction of uranyl dicarbonate with amidoxime is two orders of magnitude more favorable than the binding reaction of uranyl tricarbonate with amidoxime in aqueous solutions. Thus uranyl dicarbonate may contribute more to the adsorption of uranium than the uranyl tricarbonate species. The relative contribution of uranyl dicarbonate and uranyl tricarbonate to the uptake of uranium by the amidoxime ligand can be based on energetic calculations of reactions, through computational chemistry, combined with information on speciation. This hypothesis can explain (1) the low diffusivity obtained from our batch experiments compared with the values reported in the literature for uranyl nitrate and (2) the results of the reaction-limited process.[12] Modeling results can therefore provide insight into the transport and binding reaction mechanisms and aid in the performance and economic evaluation of the adsorbents and the uranium uptake process, respectively.

6.4 References

(1) Kim, J.; Tsouris, C.; Mayes, R. T.; Oyola, Y.; Saito, T.; Janke, C. J.; Dai, S.; Schneider, E.; Sachde, D., Recovery of uranium from seawater: A review of current status and future research needs. *Sep. Sci. Technol.* **2013,** *48*, 367-387.

(2) Das, S.; Pandey, A. K.; Athawale, A. A.; Manchanda, V. K., Exchanges of uranium (VI) species in amidoxime-functionalized sorbents. *J. Phys. Chem. B* **2009,** *113* (18), 6328-6335.

(3) (a) Hirotsu, T.; Katoh, S.; Sugasaka, K.; Takai, N.; Seno, M.; Itagaki, T., Adsorption of uranium on cross-linked amidoxime polymer from seawater. *Ind. Eng. Chem. Res.* **1987,** *26* (10), 1970-1977; (b) Hirotsu, T.; Katoh, S.; Sugasaka, K.; Takai, N.; Seno, M.; Itagaki, T., Effect of water content of hydrophilic amidoxime polymer on adsorption rate of uranium from seawater. *J. Appl. Polym. Sci.* **1988,** *36* (8), 1741-1752.

(4) (a) Sekiguchi, K.; Saito, K.; Konishi, S.; Furusaki, S.; Sugo, T.; Nobukawa, H., Effect of seawater temperature on uranium recovery from seawater using amidoxime adsorbents. *Ind. Eng. Chem. Res.* **1994,** *33* (3), 662-666; (b) Goto, A.; Kusakabe, K.; Morooka, S.; Kago, T., Test of uranium recovery from seawater with a packed bed of amidoxime fiber adsorbent. *Sep. Sci. Technol.* **1993,** *28* (6), 1273-1285.

(5) Omichi, H.; Katakai, A.; Okamoto, J., Simulation of adsorption of uranium from seawater using liquid film mass transfer controlling model. *Sep. Sci. Technol.* **1988,** *23*, 1133-43.

(6) Saito, K.; Uezu, K.; Hori, T.; Furusaki, S.; Sugo, T.; Okamoto, J., Recovery of uranium from seawater using amidoxime hollow fibers. *AIChE J.* **1988,** *34*, 411-16.

(7) (a) Vadivelan, V.; Vasanth Kumar, K., Equilibrium, kinetics, mechanism, and process design for the sorption of methylene blue onto rice husk. *J. Colloid Interface Sci.* **2005,** *286* (1), 90-100; (b) Choy, K. K. H.; Ko, D. C. K.; Cheung, C. W.; Porter, J. F.; McKay, G., Film and intraparticle mass transfer during the adsorption of metal ions onto bone char. *J. Colloid Interface Sci.* **2004,** *271* (2), 284-295.

(8) Sonetaka, N.; Fan, H. J.; Kobayashi, S.; Chang, H. N.; Furuya, E., Simultaneous determination of intraparticle diffusivity and liquid film mass transfer coefficient from a single-component adsorption uptake curve. *J. Hazard. Mater.* **2009,** *164* (2-3), 1447-1451.

(9) Azizian, S., Kinetic models of sorption: A theoretical analysis. *J. Colloid Interface Sci.* **2004,** *276* (1), 47-52.

(10) Kim, J.; Tsouris, C.; Mayes T., R.; Oyola, Y.; Saito, T.; Janke J., C.; Dai, S.; Schneider, E.; Sachde, D., Recovery of uranium from seawater:A review of current status and future research needs. *Sep. Sci. Technol.* **2013,** *48*, 367-387.

(11) Levenspiel, O., *Chemical reaction engineering*. 3rd ed.; John Wiley & Sons, Inc.: 1999.

(12) Saito, K.; Yamada, S.; Furusaki, S.; Sugo, T.; Okamoto, J., Characteristics of uranium adsorption by amidoxime membrane synthesized by radiation-induced graft polymerization. *J. Membr. Sci.* **1987,** *34* (3), 307-315.

7. MARINE TESTING PROGRAM, ADSORBENT DURABILITY, AND MARINE DEPLOYMENT ASSESSMENT STUDIES

Gary Gill, George Bonheyo, Tarang Khangaonkar,
Key-Young Choe, Robert Jeters, Li-Jung Kuo, and Jordana Wood
Pacific Northwest National Laboratory

7.1 Project Goals

A major goal of the PNNL effort for this program is to identify and address issues and concerns associated with the deployment of uranium adsorbent materials in the marine environment. The work effort to achieve this primary goal is broken into two main tasks described in detail below: (1) A marine testing program to characterize the adsorbent capacity and adsorption rate with natural seawater and (2) a research effort to assess the durability of adsorbent materials in marine conditions, in particular adsorbent reuse, toxicity, and biological fouling. Before marine deployment can be conducted, it will also be necessary to identify and characterize issues associated with deployment of adsorbent materials in the marine environment from an engineering and physical oceanographic perspective.

Testing the performance of adsorbent materials in natural seawater under controlled conditions is a necessary and critical step between laboratory investigations and ultimate deployment in the marine environment. Other participants in the program who are developing adsorbents are using testing protocols with synthetic seawater with elevated uranium concentrations as a rapid screening tool to identify candidate adsorbents. These candidate materials are then sent to PNNL for continued testing with realistic seawater conditions to verify and characterize the performance of the adsorbent material. This approach provides a common testing platform with which to assess and compare the various adsorbent materials being developed under this program. Moreover, deployment of adsorbent materials in the marine environment will require understanding optimal strategies and cost-effective approaches for many interrelated activities, including deploying the adsorbent, retrieving the adsorbent, extracting uranium from the adsorbent, re-using the adsorbent material, minimizing biofouling, identifying any toxicity issues, and locating a suitable deployment site.

7.1.1 Task 1. Marine testing program

The marine testing program was started at PNNL in October 2011 (FY 2012). The main goal of this task is to obtain information on the adsorbent capacity and the rate of uranium (and other element) uptake from samples prepared at ORNL and other DOE and DOE–NEUP partners. Testing involves exposure of the adsorbents to natural seawater using the Marine Sciences Laboratory (MSL) seawater system for periods of time ranging from several days to several (6–10) weeks and then determining the uranium and other elements (e.g., V, Zn, Cd, Fe, Cu) retained by the adsorbent material. In addition to the main testing program, MSL is collaborating with Costas Tsouris and other scientists at ORNL to design and conduct experiments to characterize the ORNL adsorbent material response to major environmental conditions such as temperature and flow rate. A related subtask is to characterize the ORNL adsorbent material with respect to its elution properties and reuse. This effort entails conducting controlled laboratory tests to understand the efficiency of uranium and other element response to varying extraction temperature, elutant composition, elutant strength, adsorbent reuse, and extraction time.

7.1.2 Task 2. Material testing and marine deployment assessment

The material testing and marine deployment assessment task was initiated at PNNL beginning in FY 2013. The main goal of this task is to identify the issues and the information needed for marine deployment of the adsorbent material. Subtasks include identification of adverse biological or chemical effects, assessment of adsorbent material to reuse (extraction/desorption cycles), assessment of the toxicological response of adsorbent materials, and identification of candidate deployment sites and engineering infrastructure needs for marine deployment.

PNNL is working with the various principle investigators who are developing sorbents or support structures to identify any adverse biological or chemical effects that the marine environment might have on the durability and efficiency of the adsorbent materials. The studies will be integrated with the marine testing program described in Task 1. The results will be used to select or inform the design of strategies to mitigate any observed impacts. This subtask is being led by Dr. George Bonheyo of MSL.

A second subtask effort is to develop an understanding of the physical, technical and engineering aspects associated with marine deployment of an adsorbent system to extract uranium from seawater. Initial efforts will focus on understanding the impact of the deployment of a farm of adsorbent materials on hydrodynamic flows. Subsequent efforts will identify technical deployment issues and also recommend oceanic regions where conditions (e.g. temperature, light, and currents) and logistic location are optimal for deployment. This effort is being led by Dr. Tarang Khangaonkar, a physical oceanographer at MSL.

7.2 Research and Development: Progress/Status

7.2.1 Ambient seawater exposure system

Marine testing is conducted using ambient seawater from Sequim Bay, WA. MSL has a seawater delivery system that can provide ambient seawater into our “wet laboratory” for scientific investigations. Briefly, ambient seawater is drawn by pump from a depth of 10 m from Sequim Bay through a plastic pipe and is passed through a sand filter to remove large particles. The seawater is then stored in a large-volume reservoir tank outside the laboratory. This seawater is fed into the laboratory facilities at MSL for use by gravity feed through PVC piping.

A depiction of the manifold system used for seawater exposure of adsorbent materials is given in Fig. 7.1. Seawater from the large outside tank is feed sequentially through 5 μm and then 1 μm cellulose filters and then collected in a 180 L fiberglass reservoir tank referred to as a “head tank.” Seawater in the head tank can be heated to the desired temperature using a titanium immersion heater. Temperature-controlled seawater is drawn from the head tank with a pump (nonmetallic pump head), passed through a 0.45 μm polyethersufone membrane cartridge filter (Memtrex MP, GE Power and Water) and into a 12-port PVC manifold. Water that is not used to expose adsorbent material and passes through the manifold is returned to the head tank. Pressure in the manifold is controlled with a gate valve at the outlet of the manifold. MSL has three separate 12-port manifolds, linked to two separate head tanks, permitting testing of 36 adsorbent materials simultaneously. Additional testing capacity can be achieved by building more manifolds or doubling up on the test cartridges attached to a single manifold port. All the major components of the MSL seawater delivery system are non-metallic (primarily PVC piping) to minimize metal contamination issues. The only major metallic component in the seawater system is the pump system used to draw raw seawater from Sequim Bay to fill the large outside storage tank.

Adsorbent materials for seawater exposure are packed into non-metallic (primarily Teflon, PVC, and polyethylene) columns or cartridges and mounted in one of the 12 positions on the seawater manifold (Figs. 7.1 and 7.2). Two types of systems were used to hold adsorbent material for exposure to flowing seawater. Typically, 50–100 mg of adsorbent material is packed into a column or cartridge and held in place using a combination of glass wool and/or glass beads (3–5 mm). Flow rates are determined at the outlet of each sample column or cartridge using a DigiFlow turbine flowmeter system. Flow measurements were made using either a hand-held system or an automated 8 or 36 channel recording system built on National Instruments software. Initial studies in FY 2012 were conducted using multiple peristaltic pumps to deliver water from the head tank to cartridges stacked in series containing absorbent.

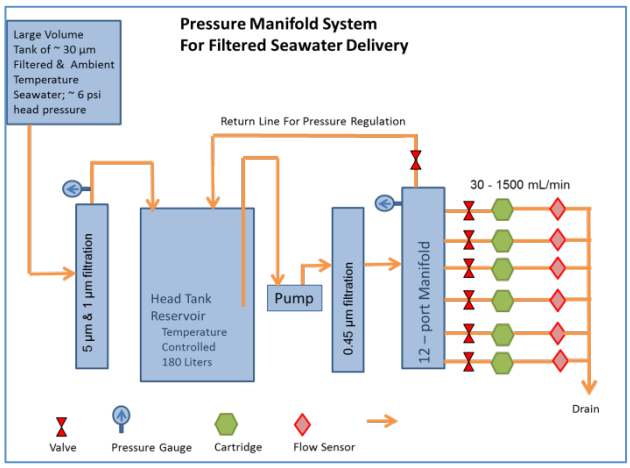

Fig. 7.1. Layout and components of seawater manifold system for exposing uranium adsorbents to ambient seawater.

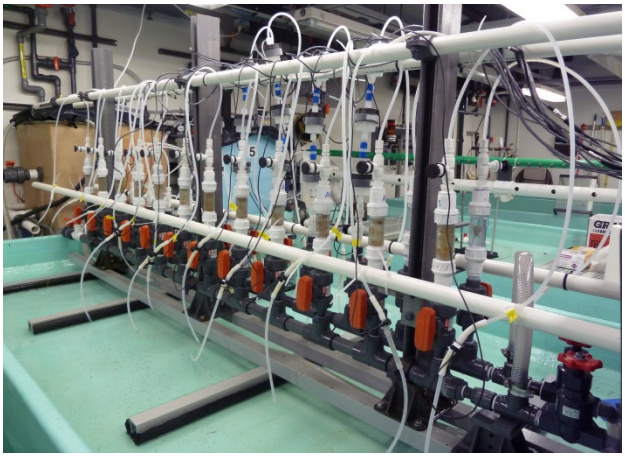

Fig. 7.2. Seawater manifold and PNNL style columns containing uranium adsorbent material.

7.2.2 Trace element and water quality measurements

Water quality and trace element measurements of the seawater used for marine testing are being conducted as part of the marine testing program. Water quality measurements include salinity, temperature, pH, and dissolved organic carbon. In addition to uranium, measurements of selected trace elements are also being conducted. Elements of interest include vanadium, iron, copper, nickel, zinc, manganese, and lead. This information is being used to help understand whether variations in seawater composition influence the performance of the adsorbent material. In Table 7.1 are measurements of the elemental concentrations observed in a saturated ORNL adsorbent material, ambient seawater, and seawater in exposure system. The table is organized relative to the abundance of trace elements found in the adsorbent material. This arrangement allows the affinity or selectivity of the ORNL adsorbent (38H) to be assessed by comparing the mass of adsorbent retained on the saturated adsorbent relative with seawater concentrations of these elements. The table also shows that, with a few minor exceptions (e.g., Zn, Cu, Ni, and Pb), the concentration of trace elements in ambient seawater does not get significantly contaminated during passage through the seawater delivery system to the manifold used to expose seawater to test adsorbents.

Table 7.1. Elemental concentrations in adsorbent material, ambient seawater, and seawater in exposure system

Element	µg Metal/ g adsorbent	Typical Total Surface Seawater Conc.[1] (ng/kg)	Filtered Sequim Bay Seawater (ng/kg)	Filtered Ambient Seawater Conc. in Test System (ng/kg)
V	5720	2000	1500	1480
U	2798	3300	2850	2840
Fe	1973	30		
Cu	1365	150	190	540
Ni	760	480	320	560
Zn	736	30	285	2100
Sr	313	8		
Cr	203	210	135	180
Mn	140	20		
Pb	111	10	3	25
Co	84.2	1	0.02	0.01
Sn	34.3	0.5		

[1] Values taken mostly from "The Periodic Table of the Elements in the Ocean." http://www.mbari.org/chemsensor/about.html

7.2.3 Analytical methods

7.2.3.1 Elemental analysis

Elemental analyses of uranium and trace elements in seawater and extracts from adsorbent materials are being conducted using ICP mass spectrometry and inductively coupled optical emission spectrometry. Seawater samples are pre-concentrated prior to analysis using borohydride reductive precipitation preconcentration from a mixture of Fe/Pd and ammonium pyrrolidine-dithiocarbamate (APDC). Seawater uranium measurements are determined without preconcentration using the method of standard additions to overcome the seawater matrix interference.

7.2.3.2 Water quality parameters

Determination of salinity is conducted using a hand held salinometer (YSI, model 30) and a continuous recording sonde (In-Situ, Inc.). pH measurements are being conducted using standard ion selective electrode systems calibrated with NIST buffers. Dissolved organic carbon measurements are conducted by high temperature catalytic combustion using a Shimadzu instrument.

7.2.3.3 Marine testing program

Table 7.2 provides a summary of the marine testing activities conducted to date. There are two general types of column or cartridge exposure experiments: (1) time series measurements to determine the kinetics of uranium and trace element uptake and (2) several-week-duration exposure experiments to determine the adsorption capacity of a uranium adsorbent material. The

ORNL adsorbent material used for the ORNL time series experiments 2 and the PNNL independent time series test was from a common formulation with the designation 38H. This material formulation has proved to have the highest adsorbent capacity of the materials tested to date in natural seawater, approximately 3500 μg U/g adsorbent. Additional details about this material are given below. Details associated with individual tests noted in Table 7.2 are described in other reports being submitted for the review process.

Table 7.2. Summary of Marine Testing Program at PNNL

Institution/PI Test Name	Start Date	Duration (days)	Temp (°C)	Flow rate (mL/min)	Number of Columns and Adsorbent	Description
FY 2012						
ORNL/Tsouris Time Series #1	1/4/2012	41	31	200/500	6–ORNL 6 -Japan	4 flow-lines with 3 ORNL cartridges in series
ORNL/Tsouris Time Series #2	3/28/2012	56	22	250/500	12-ORNL	4 flow-lines with 3 ORNL cartridges in series
PNNL/Gill Independent Time Series	5/17/2012	56	21	500	8-ORNL 1-Japan	PNNL manifold with PNNL columns; Combination of time series and adsorption capacity
ORNL/Tsouris Time Series #3	6/19/2012	42	21	500	11-ORNL	PNNL manifold; 10 ORNL cartridges and 1 PNNL column
ORNL/Tsouris Tea Bag Time Series			13/20	~ 1 L/min	12-ORNL “Tea Bags”	Time Series exposure of ORNL adsorbents in filtered and unfiltered water in aquaria
FY 2013						
ORNL/Janke Adsorbent Capacity #1A	10/17/2012	79	20	250-300	14-ORNL fibers	Adsorption capacity study of new ORNL amidoxime-based adsorbent fibers
ORNL/Janke Adsorbent Capacity #1B	10/18/2012	41/78	20	1-2 L/min	4-ORNL braids 2-Japan	Adsorption capacity study of new ORNL amidoxime-based adsorbent braids exposed in aquaria
ORNL/Tsouris Time Series and Adsorbent Capacity #4	10/17/2012	77	20	250-300	1–Chinese (F1) 6-Chinese (F2) 6 Japanese	Time series and adsorption capacity studies of Chinese and Japanese adsorbents
LBNL/Tian Time Series #1	12/10/2012	37	20	250-300	6-LBNL adsorbent sheets	Time series study of LBNL adsorbent material

Table 7.2. (continued)

Institution/PI Test Name	Start Date	Duration (days)	Temp (°C)	Flow rate (mL/min)	Number of Columns and Adsorbent	Description
ORNL/Tsouris Adsorption Capacity #5	1/23/2013	21/63	20	250-300	3-ORNL	
ORNL/Janke Adsorption Capacity #2	1/23/2013		20	250-300	4-ORNL Braid 2-ORNL Fiber	New variation of ORNL amidoxime-based adsorbent fibers and braids
CUNY/ Alexandratos Time Series #2	2/5/2013	38	20	250-300	4-RS02-S3 adsorbent	Time series with RS02-S3 adsorbent
ORNL/Janke Adsorption Capacity #3	3/22/2013	56/77	20	250-300	6-ORNL	New variation of ORNL amidoxime-based adsorbent fibers and braids
PNNL & ORNL/Gill & Tsouris Temperature Experiment	3/11/2013	56	10, 20, &30	250-300	15 –ORNL	Determine adsorption capacity as a function of temperature and time; 5 time points
ORNL/Tomonari Adsorption Capacity #1	3/9/2013	42	20	250-300	2-ORNL (Tomonari)	Adsorption capacity study of new ORNL amidoxime-based adsorbent fibers
ORNL/Tomonari Adsorption Capacity #2	3/26/2013	42	20	250-300	2-ORNL (Tomonari)	Adsorption capacity study of new ORNL amidoxime-based adsorbent fibers
Univ. of Maryland/Al-Sheikhly Adsorption Capacity	3/27/2013	7	20	250-300	1-U Maryland	Adsorption capacity study of U Maryland adsorbent material – initial scoping
PNNL & ORNL/Gill & Tsouris Flow rate Experiment	pending					Determine adsorption capacity as a function of flow rate

7.2.3.4 PNNL independent verification

Initial marine test experiments focused on conducting an independent test to validate the adsorption rate and capacity of the ORNL adsorbent material 38H6, which had high capacity in batch experiments with simulated seawater and enhanced uranium content at ORNL. Time series results from that test are shown in Fig. 7.3. Modeling of the adsorption rate using a one-site ligand saturation model is shown by the lines drawn through the data points. This modeling

effort predicts that the adsorbent has a maximum adsorption capacity at equilibrium saturation of 3330 μg U/g adsorbent and that the half-time for the saturation of the adsorbent is 12 days. These results agree well with ORNL experiment #2 (and the other ORNL tests, not shown) conducted by Costas Tsouris and co-workers at ORNL (see Fig. 7.4), verifying the capacity of the adsorbent in natural seawater. For comparison, the Japanese adsorbent material, which was included as a reference material in most of the tests, had an adsorption capacity of approximately 900 μg U/g of adsorbent (see Fig. 7.3).

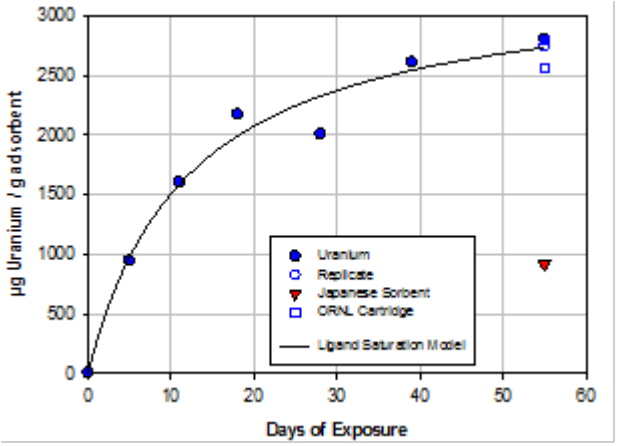

Fig. 7.3. PNNL independent test of the ORNL 38H6 adsorbent. Shown are time series measurements of uranium adsorption in natural filtered seawater at 20 °C. The Japanese adsorbent served as a reference material.

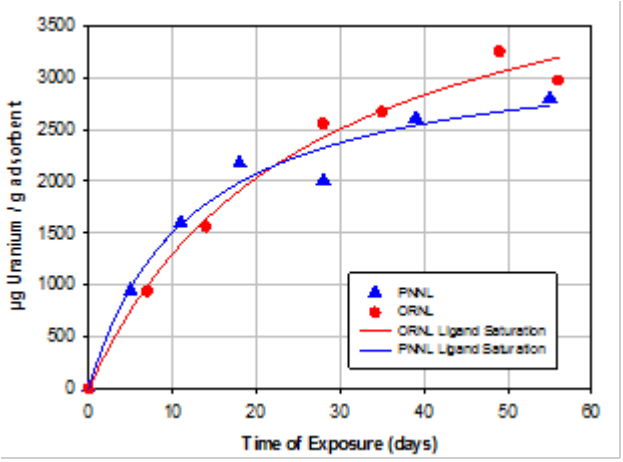

Fig. 7.4. PNNL independent test of the ORNL 38H6 adsorbent. Shown is a comparison of results from the PNNL independent test with results from the ORNL time series test #2.

It was noted previously (Table 7.2), that the amidoxime-based adsorbent materials are not exclusive for uranium but retain other trace elements. Fig. 7.5 shows the time course of the 38H6 adsorbent to sequester other trace elements from seawater. Most notably, the adsorbent has a higher capacity for extracting vanadium than it does for uranium. The uptake rate of vanadium and copper appear to occur at roughly the same rate as that observed for uranium. Zinc and nickel reached saturation much more rapidly. Several other elements also are retained, including rare earth elements, but at much lower levels. The ability of the adsorbent to retain other elements may provide a cost reduction for uranium extraction if the elements co-extracted can be recovered for use during uranium processing. The majority (~90%) of the adsorption sites on the amidoxime-based adsorbent are occupied by calcium and magnesium, a feature common to most chelating ion exchange resins used for extraction of trace elements from seawater.

7.2.3.5 Toxicity testing

Determination of potential toxicity of the adsorbent materials is initially being conducted using a Microtox assay system. The Microtox assay uses the bacteria *Aliivibrio fischeri* ATCC 49387 (formerly NRRL B-11177) to determine the toxicity of compounds such as metals, antibiotics, and phenols. In *A. fischeri,* there is a direct correlation between luminescence and bacterial respiration. In this assay, *A. fischeri* is exposed to the potential toxin for 30 minutes and then luminescence is measured. The level of toxic effect is determined by the amount of toxin added to *A. fischeri* to result in a 50% reduction of luminescence, EC_{50}.

Fibers and supernatant provided to PNNL-MSL have been tested via the Microtox assay via a commercially available freeze-dried cells (Modern Water Inc.) and living cells prepared at PNNL-MSL. The freeze-dried cells were reconstituted and diluted using Modern Water Inc. solutions and tested at 15 °C; the living cells were grown at 22 °C and tested at room temperature. Microtox test results from both the reconstituted cells and living cells resulted in no assay reaching the EC50. Test results were validated using a copper and zinc control that met and surpassed their EC50.

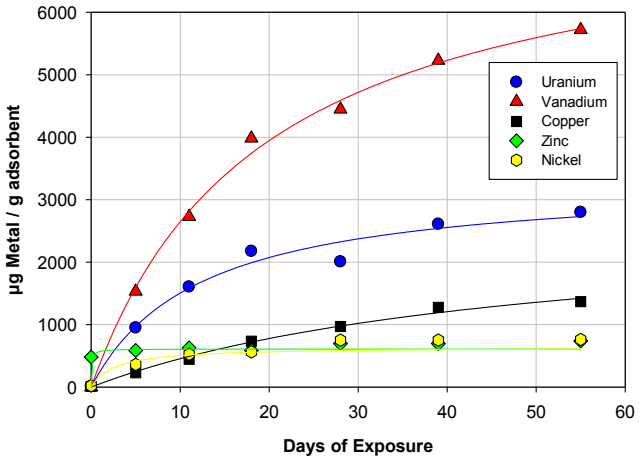

Fig. 7.5. PNNL independent test of the ORNL 38H6 adsorbent. Shown are time series measurements of adsorption of uranium and selected trace metals.

A second round of testing will be completed to determine if an increase in sample concentration will result in attaining an EC50 for the fiber samples. Since these fibers display a large amount of surface area once they get wet in the sample tube, and subsequently take up space, there may be a limit to the amount of fiber concentration one can place inside a tube. Once that point is reached, a final determination will be reached for Microtox toxicity of the Oak Ridge.

7.2.3.6 Chemical imaging

One approach to studying fouling of adsorbent material is chemical imaging. Illustrated in Fig. 7.6 is an x-ray microtomography 3-dimensional rendering of the ORNL 38H6 adsorbent material after exposure to fouling organisms. The dataset was acquired at Sector 2-BM of the Advanced Photon Source at Argonne National Laboratory. The color is related to the x-ray attenuation, and depends strongly on average atomic number and a bit less strongly on density. Based on the data, the red spots on the outside are probably higher Z. Larger eukaryotic cells or aggregates of cells are easier to visualize but all are fairly "transparent," and the samples may need to be treated with osmium to enhance the visualization of the cells.

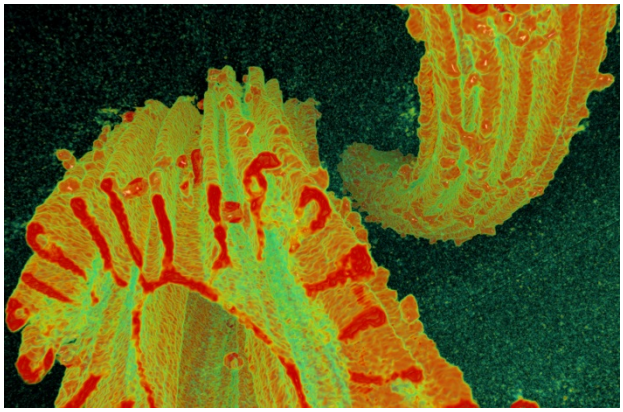

Fig. 7.6. X-ray microtomography of the ORNL 38H6 adsorbent material after exposure to fouling organisms. Dataset acquired at Sector 2-BM of the Advanced Photon Source at Argonne National Laboratory.

7.2.3.7 Marine deployment assessment

This effort was initiated in March of 2013 and is being led by Dr. Tarang Khangaonkar, the group manager for the Integrated Coastal Ocean Modeling Group at MSL. Initial efforts are focusing on understanding

how deployment of a "farm" of adsorbent material (as discussed in Section 8, Figure 8.5) in the marine environment will influence hydrodynamic flow in a coastal ocean environment. Concern has been expressed that a farm of adsorbent material might have a substantial impact on flow and thereby cause environmental harm. The "farm" concept of braided fiber material, woven into long "kelp-like" dimensional structures, is based on the previous work of Japanese scientists Seko and Tamada.[1,2] They envisioned the adsorbent as being placed below the surface by anchoring one end of the braided material to the ocean floor, allowing it to rise upward like a piece of kelp. The individual braid structures were spaced such to minimize contact between braids.

Hydrodynamic modeling is being conducted using an 3-dimensional finite volume coastal ocean model (FVCOM).[3] Details on the hydrodynamic model can be found at: http://fvcom.smast.umassd.edu/FVCOM/. Because information on hydrodynamic flow in a farm of adsorbent material does not exist, initial efforts will use information derived from flow through kelp beds as an analog.[4] This hydrodynamic feature is being incorporated into FVCOM code using a water column momentum sink approach. This approach allows incorporating the effect of the presence of kelp-like structures in the water column. For simplicity, the development work will be done on a simple rectangular channel with steady conditions and uniform incident channel flow (Fig. 7.7). Literature values and data from physical models and other numerical studies will be used to validate the performance of the incorporation of a kelp-like forest of braided uranium adsorbent extraction farm. Following model validation, PNNL will conduct a series of sensitivity tests to assess the hydrodynamic response to variation in physical parameters such as mooring height, braid deployment density, projected area (diameter), and ambient current.

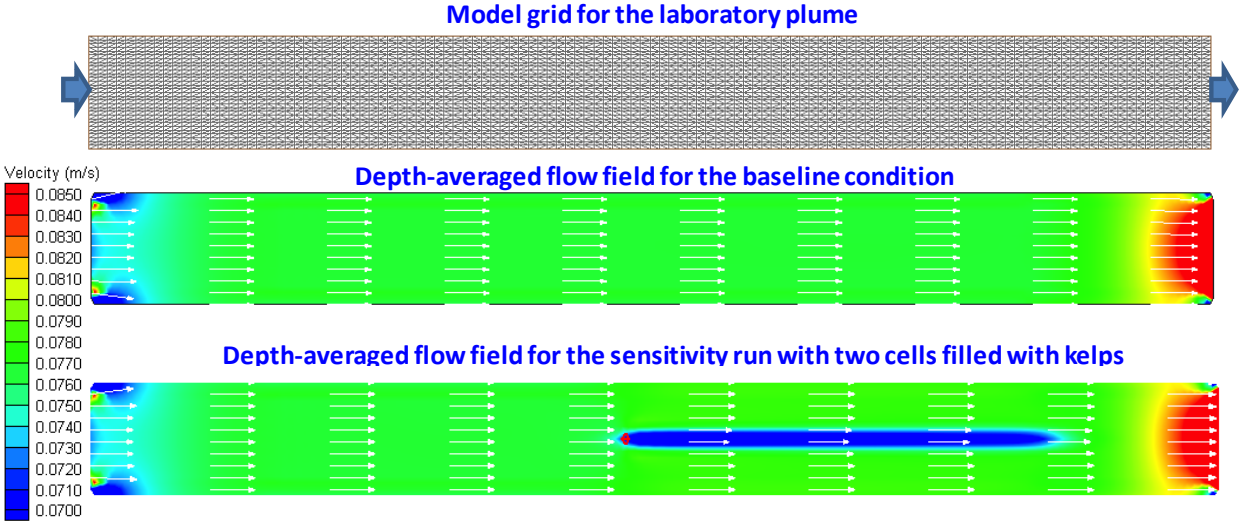

Fig. 7.7. Numerical flume experiment—model grid and comparison of depth averaged currents, baseline condition, and retardation due to momentum sink at the kelp cells

Once parameterized and validated, the model will be applied to the Puget Sound–Georgia basin coastal region where the PNNL coastal ocean model is already up and running. This region offers many sites that fit the typical braided farm description of over 100 m of water depth

supporting 60 m long braided moorings spread out over a 15 by 68 km^2 area. PNNL will then utilize the model to design and recommend an optimum spatial deployment configuration.

7.2.3.8 Stripping efficiency and durability

A series of laboratory experiments and exposure tests are under way to provide information on the desorption or stripping performance of the ORNL adsorbent. Initial results of the response of the adsorbent to acid strength and extraction time are shown in Fig. 7.8. These preliminary results for uranium extraction agree well with the previous work conducted by the Japanese and indicate that uranium can be removed from the ORNL 38H6 adsorbent with a short exposure (< 1 hr) to a mild acid (~ 1 M HCl). At these conditions, most other trace elements are also removed, with the exception of vanadium which requires a strong acid treatment (> 6 M HCl). Follow-on experiments are planned with sodium carbonate as the extraction medium. Once an optimum extraction media is identified, the reuse of the adsorbent (multiple extractions and regeneration cycles) will be investigated to determine adsorbent durability and efficiency in reuse.

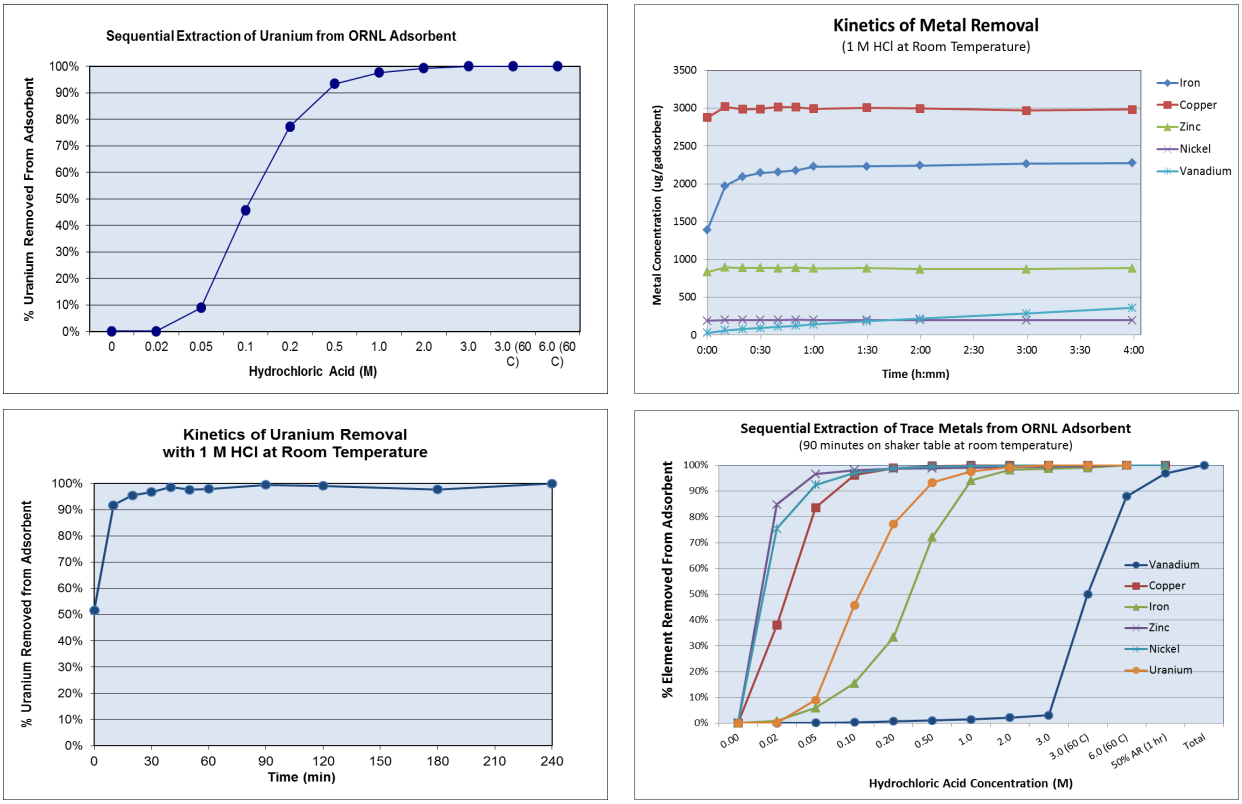

Fig. 7.8. Desorption characteristics of the ORNL 38H6 adsorbent for uranium and selected trace elements.

7.3 Work in Progress and Planned Future Work

Many of the planned efforts in each task and subtask have already been discussed. Specific planned experiments are described below.

7.3.1 Temperature experiment

Understanding how temperature influences adsorption capacity and adsorption rate is critical to identifying an optimal site and conditions for marine deployment. Research conducted by scientists at LBNL have suggested that the adsorption of the uranyl ion (UO_2^{2+}) is an endothermic process.[5] Hence, higher seawater temperatures should yield enhanced adsorption capacity. Tamada[2] also observed a higher adsorption capacity for an amidoxime functionalized adsorbent at 30 °C in braid format compared with a deployment at 20 °C with an adsorbent stack exposure.

Preliminary results were obtained in experiments conducted in FY 2012 indicating that the adsorption capacity of the ORNL 38H6 adsorbent may vary with temperature. PNNL, in collaboration with Dr. Costas Tsouris at ORNL, has designed an experiment to determine temperature influences. Preliminary time series tests are currently being planned at PNNL to address temperature effects on adsorption capacity and adsorption rate.

7.3.2 Flow-rate experiment

Another important characteristic of the adsorbent that must be clearly understood to choose an optimal deployment site in a marine system is the impact of current velocity on adsorption capacity and adsorption rate. To date, all marine testing experiments have been conducted using exposure flow rates between 250 and 500 mL/minute. Depending on the test column or cartridge configuration, these flow rates correspond to linear velocities in the exposure column of approximately 2–7 cm/sec. At these flow rates and corresponding linear velocities, we have not been able to observe any significant differences between adsorption rate and adsorption capacity, implying that the slow step in the adsorption of uranium by the adsorbent is not related to flow rate, at least not in the flow rate ranges used to date.

To better understand how flow rate (linear velocity) impacts the rate of uranium uptake, PNNL and ORNL (Costas Tsouris) have designed a "flow rate experiment." A time series experiment is planned for the latter half of FY 2013 to follow adsorption rate at four nominal linear velocities: 0.30, 1.0, 1.5, and 2.5 cm/sec. The upper end of these linear velocities is comparable to the lower end of the linear velocities used for a majority of the marine testing experiments to date. Variations in linear velocity will be achieved by varying flow rate through the column and using varying diameter columns. The upper range in this series represents the linear velocity used most frequently for marine testing.

The flow rates chosen for this experiment are on the low end of most near-surface currents in the ocean. Maximal surface water velocities occur in western boundary currents like the Gulf Stream or the Kurishio current and in tidally driven currents at the entrance to bays and estuaries. These currents can reach velocities of several meters per second. Typical wind-driven surface currents flow at about 2% of the wind speed that generated them. For example, a 25 mile per hour wind (11.2 m/sec) would produce a surface current of 22 cm/sec. The velocity of wind-driven surface currents diminishes rapidly with depth, so that velocities at 100 m are only a fraction of surface values. Because deployment of adsorbent material is likely to occur below the surface zone, the velocities chosen for this experiment are reasonable.

7.3.3 Characterization of braided adsorbent material

As the program progresses, marine testing of fiber material will shift to testing of the same adsorbent formulations in a braided material using small aquaria as the testing platform. Initial

tests will be with filtered seawater and then with unfiltered seawater. This is another interim step in the development of a deployable uranium adsorbent material for the marine environment.

7.4 References

(1) Seko, N.; Tamada, M.; Yoshii, F. *Nuclear Instruments and Methods in Physics Research Section B: Beam Interactions with Materials and Atoms* **2005**, *236*, 21–29.

(2) Tamada, M. "Collection of uranium from seawater. **2009**. Available at https://iaea.org/OurWork/ST/NE/NEFW/documents/RawMaterials/TM_Vienna2009/presentations/22_Tamada_Japan.pdf.

(3) Yang, Z.; Khangaonkar, T. P. Modeling the hydrodynamics of Puget Sound using a three-dimensional unstructured finite volume coastal ocean model. In Estuarine and Coastal Modeling, M.L. Spaulding (ed.), *Proceedings of the 10th International Conference (accepted for publication)*, American Society of Civil Engineers, Newport, RI, **2008**.

(4) O'Donohue, F. Physical and numerical modeling of impeded tidal flows: Effects of aquaculture structures on hydrodynamics and material transport. A thesis submitted in partial fulfillment of the requirements for the Doctor of Philosophy, in the College of Engineering and Informatics, **2012**.

(5) Tian, G.; Teat, S. J.; Zhang, Z.; Rao, L. Sequestering uranium from seawater: binding strength and modes of uranyl complexes with glutarimidedioxime, *Dalton Trans.* **2012**, *41*, 11579–11586.

8. COST AND ENERGY ASSESSMENT

Eric Schneider, Harry Linder, and Darshan J. Sachde
University of Texas at Austin

8.1 Background and Significance

An authoritative 2011 survey of world uranium resources published by the Organization for Economic Cooperation and Development identifies over 7 million tonnes of conventional uranium resources available at $260/kg U or less.[1] This resource base would suffice to meet some 110 years of uranium requirements at 2010 consumption levels. When estimated undiscovered resources are included, the potential conventional uranium supply rises to over 17 million tonnes. Following two decades of low prices induced in part by earlier oversupply and lower than expected demand, the uranium spot price rose above $100/kg U in 2006. After briefly reaching a peak of $335/kg U in 2007, the spot price has remained between $100 and $180/kg U since 2008.[2]

Cost analysis of systems for recovering uranium from seawater must be placed in the context of conventional resources that are expected to be adequate at moderate price for several decades. Seawater uranium may serve as a "backstop" to conventional uranium resources. A backstop provides an essentially unlimited supply of an otherwise exhaustible resource. A backstop may not be immediately commercially viable. Indeed it might never be deployed at large scale at all. Its role is to remove the uncertainty around the long-term sustainability of the exhaustible resource.

Reactors are being deployed today that will require uranium for six decades or longer, and R&D decisions in part based on nuclear fuel cycle uranium requirements over an even longer time frame are being taken as well. Therefore, the cost analysis of the braid adsorbent technology plays three key roles. First, it must demonstrate a uranium production cost that is sustainable for the nuclear power industry, with no insurmountable technical or environmental roadblocks to its large-scale deployment. Second, a backstop requires not only sustainable cost but also minimal uncertainty. Defining the cost uncertainties is thus at equal importance with establishing the expected system costs themselves. Finally, it guides further R&D for the braid adsorbent technology, identifying inputs and performance factors where further development would offer the greatest reduction in costs and/or their uncertainties.

The energy return on investment (EROI) is another technology metric that provides important insights into cost drivers. Defined here as the amount of useful energy, in this case electrical power, ultimately produced by an energy resource divided by the amount of energy consumed to produce it, the EROI is often more straightforward to quantify for a developing technology than its cost if brought to industrial scale.

This section describes the major steps in the adsorbent fabrication and grafting, mooring at sea and recovery, and elution and purification components from the standpoint of cost as well as the EROI. It summarizes the life cycle discounted cash flow methodology used to calculate the uranium production cost and its uncertainty from the component costs and the calculation of EROI. Next, it presents results with emphases on the key cost drivers as well as the progress this R&D campaign has made in reducing their impact and uncertainty. In conclusion, major ongoing and future R&D focus areas impacting cost are reviewed.

8.2 R&D Progress/Status

The point of departure for much of the R&D described in this document was the braided adsorbent system pioneered by JAEA.[3] The first task of the economic analysis group was to create an independent baseline uranium production cost estimate using data made public by JAEA. Since the high-level process flow and deployment concept remain similar in the state of the art DOE system, the description that follows is valid for both technologies.

The cost and EROI assessment methodologies applied to both the JAEA and DOE technologies draw upon widely accepted approaches that are in common use. This section summarizes them as well as the methods and data sources used to collect input data, such as equipment and commodity costs and energy intensities.

8.2.1 System description

The uranium production process consists of three basic steps: adsorbent synthesis, adsorbent deployment, and uranium elution and purification (Fig. 8.1). The adsorbent material is reusable, though not indefinitely, and it undergoes multiple deployment and elution cycles.

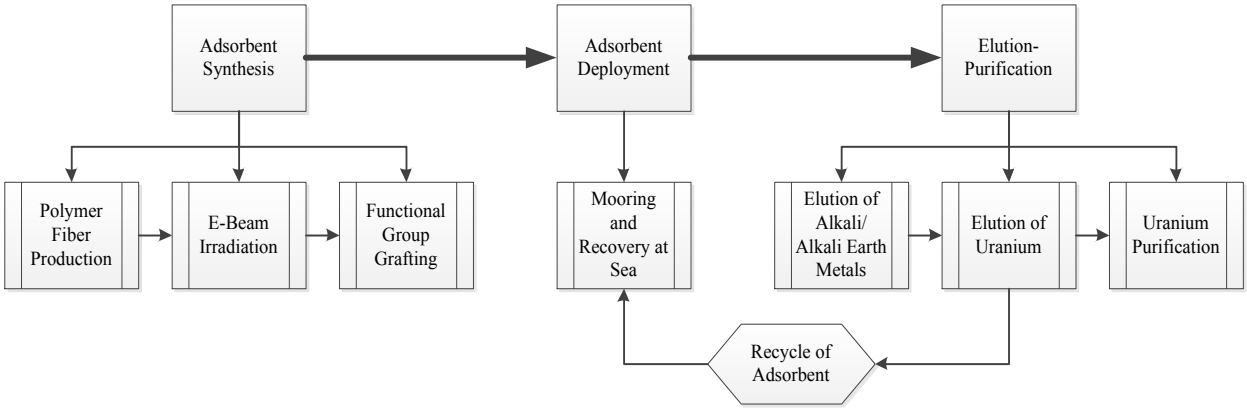

Fig. 8.1. Process overview.

Individual processes within each major step play an important role in the cost and EROI analyses. Fiber production requires purchase of the HDPE base polymer and its melt spinning and extrusion into fibers, with high-surface-area fibers offering superior performance (see Section 4). The fibers are irradiated to open grafting sites for amidoxime and hydrophilic functional groups. The chemicals used in the grafting process are shown in this section to be an important determinant of overall system costs.

The fibers are braided around a low-density core to result in positively-buoyant braids approximately 60 m in length. The material is carried to the deployment site by workboats and moored to the ocean floor with anchor chains as depicted in Fig. 8.2. At the end of the mooring period, the boats winch up the chains to recover the adsorbent material. The material is then returned to shore or a centrally located mother ship for recovery of uranium and any co-products. The adsorbent itself can be regenerated and used multiple times. The number of reuses and degree of retention of uranium adsorption capacity with reuse are not yet fully determined; multiple experiment campaigns of significant duration will be needed to do so. These parameters are key drivers of the uranium production cost and the dominant remaining contributors to its uncertainty.

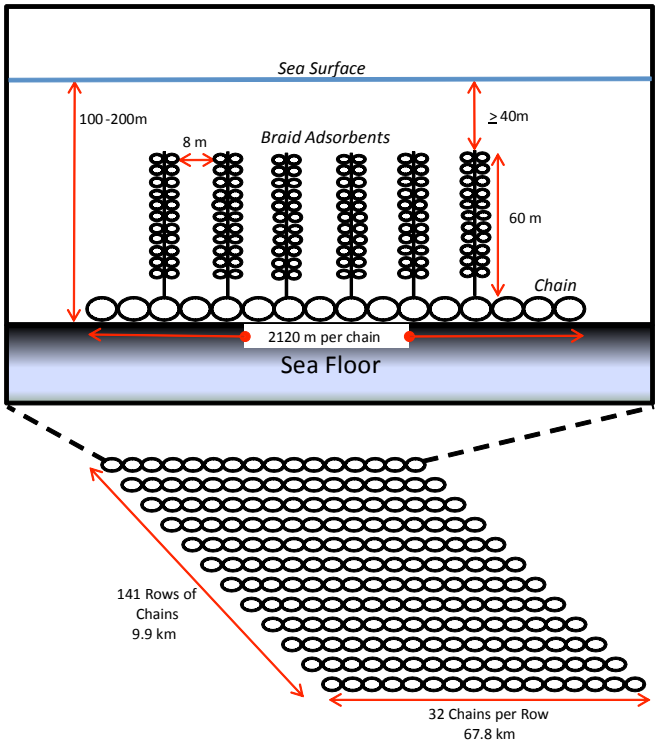

Fig. 8.2. Braid adsorbent and mooring system.

The adsorbent performance is characterized by capacity (kg U/tonne adsorbent), which in turn is a function of time immersed, temperature of the seawater, and (at very low velocities only) bulk seawater flow velocity (Section 7). Both capacity and durability—number of adsorbent uses prior to disposal, extent of capacity retention with reuse—are key performance-related drivers of the uranium production cost.

8.2.2 Methodology

The life cycle discounted cash flow (LCDCF) approach is used to synthesize the system component costs into a uranium production cost in $/kg U. Here, the approach is used to track cash flows over the life cycle of a unit mass of adsorbent. This widely used methodology is described in the Generation IV International Forum Economic Modeling Working Group (EMWG) cost estimation guidelines[4] and its application to the uranium recovery system is fully documented by Schneider and Sachde.[5,6]

The LCDCF approach requires cost estimates to be obtained for inputs, including capital and operating costs (e.g., capital equipment, labor, materials, utilities). Cost data was developed in accordance with the EMWG code of accounts (COA) system and cost estimation guidelines for nuclear fuel cycle facilities.[4] The COA approach systematizes the estimate by defining cost categories and an organizational structure for the analysis.

Two approaches were taken to develop the input cost data. When sufficiently detailed design information was available or could be developed (e.g. chemical consumption levels, equipment sizing and specifications), bottom-up cost data was developed using multiple publicly available cost data points and/or vendor quotes, with economies of scale accounted for and uncertainty and variability quantified. If such detail is not available, for instance for an industrial plant where an engineering design is premature, a standard top-down scaling methodology was used to estimate

plant costs from known major equipment item costs and sizes. Full documentation of cost inputs and methods is in Schneider and Sachde.[5,6]

Similar methods were used to collect data for the EROI calculations. Energy is used in direct and embodied forms in the uranium recovery system. Direct energy is defined as the energy content of energy carriers such as electricity and natural gas crossing into the system, where the system is the set of processes depicted in Fig. 8.1. Embodied energy is the energy used to fabricate material, equipment, or chemical inputs to the system. The EROI was then calculated as the ratio of the electricity ultimately produced from a unit mass of natural uranium in the once-through fuel cycle, divided by the direct plus embodied energy required to recover the uranium.

8.2.3 Results

Table 8.1 lists the key parameters defining the reference system for the cost and EROI analyses. The annual uranium production affects the scale economies, with a larger adsorbent field leading to somewhat reduced uranium production costs. The value given in the table was chosen for compatibility with the cost estimate for an early version of the technology developed by JAEA[3] and leads to a field with an undersea footprint of 670 km^2, as depicted in Fig. 8.2. Uncertainties are given where relevant and used to establish the uncertainty in the overall system cost. The capacity uncertainty was developed from statistical analysis of measured data and is taken to be normally distributed about the median value given in the table.

Table 8.1. Top level parameters of reference system

Parameter	Value	Unit	Source/comment
Annual Uranium Production	1,200	t/year	Establishes scale economies
Seawater Temperature	20-25	°C	See section 7
Adsorption Capacity	3.09 +/- 0.31	kg U/ t adsorbent	See section 4 and 6 – uncertainty established from 2nd order kinetic model fit to measured data
Length of Mooring Campaign	60	days	
Adsorbent Uses	6	N/A	HDPE sold as scrap after 6th use
Adsorbent Degradation Rate	5%**	per reuse	From data collected over 5 elution / use cycles and reported in Tamada et al.[3]

** Varied over 0% to 10% for within the cost uncertainty analysis.

If the mooring and deployment system proposed by JAEA is used, the expected uranium production cost for this system is $760/kg U.* This figure will be used as the reference cost for most of this section, but two significant modifications to the deployment system are under consideration. These are (1) conducting the elution and purification step at sea aboard a centrally located mother ship and (2) replacing the steel anchor chains with appropriately weighted polymer fiber ropes. Preliminary results indicate that if these changes were both adopted, the expected uranium production cost would drop to $610/kg U.

* This cost, and all others provided in this section unless otherwise noted, is given in year 2011 US dollars.

These figures can be compared against the uranium spot price range between 2006 and 2013, $100–$335/kg U. It may also be compared against a 2006 JAEA estimate of the Japanese system, which stood at approximately $1,000/kg U, and this group's independent analysis of the JAEA technology that placed the cost at $1,230/kg U.[†] Table 8.2 summarizes major changes in the cost.

Table 8.2. Major changes in the process and cost estimation and their tendency to increase or decrease uranium production costs

Update/modification that led to an increase	Update/modification that led to a decrease
Adsorbent braiding process updated for production of higher surface area fibers	Uranium adsorption capacity has increased from 2.0 kg U/t ads to 3.09 kg U/t ads
Hazardous chemical disposal costs added (not included in JAEA estimate)	Grafting flowsheet redesigned to recycle or identify substitutes for selected high-cost chemicals (e.g., hydroxylamine, dimethylformamide)
Financial model and parameters (cost of capital, discount rate) changed to reflect private-sector commercial operation in the USA	Elution process determined suitable for recovering part of the cost of HDPE through its sale as scrap
Seabed leasing costs included	Economies of scale effects taken into account
Costs of major equipment items (e.g. work boats, mooring chains) and labor needs generally found to be higher than JAEA estimates	Costs of chemical inputs generally found to be lower than JAEA estimates
Surfactant process replaced with dimethylsulfoxide solvent based process, hydrophilic monomer grafting step added (not present in JAEA cost analysis)	System-level updates to mooring strategy (replace steel mooring chains with polymer, move elution/recovery step offshore) shown to offer potential for dramatic reduction in cost
Initial inventories of chemicals and materials included (neglected in JAEA equilibrium analysis)	

8.2.4 Cost drivers

Table 8.3 lists the major components of the $760/kg U production cost. Capital investment costs for adsorbent production are driven by chemical process and e-beam equipment as well as capitalized costs of chemicals and materials needed for the initial adsorbent field. For the mooring and recovery stage, capital costs are dominated by workboat and anchor chain purchase. Mooring and recovery operating costs are driven by the 76 workboats needed to service the field. Chemical and material inputs to adsorbent production are seen to be the largest single cost driver, especially when the capitalized initial chemical stocks of recyclable materials mentioned in Table 8.2 are considered.

[†] These two estimates assessed the cost of the JAEA system as it was depicted by JAEA in the published literature. Subsequent development of the process in the USA has identified cost elements not originally considered by JAEA, for instance the cost of disposing of hazardous chemicals and used adsorbent. In addition, experimentation in the USA with the JAEA adsorbent and process could not systematically replicate the adsorbent capacity level (2 kg U/t adsorbent) upon which the JAEA cost analysis was based. It should be noted that JAEA did not directly measure the 2 kg U/t adsorbant capacity, but instead inferred it from their most favorable experimental trial, which collected 1.5 kg U/t adsorbent over 30 days of immersion.

When the capitalized initial inventory costs equivalent to $84/kg U are included, variable costs associated with adsorbent production account for $329/kg U or 43% of the $760/kg U production cost. Figure 8.3 shows that no single chemical or material input dominates this large cost component. Poly(lactic acid) and tetrahydrofuran are used in the fiber formation and spinning step (Section 4), while the other chemicals are all employed within the grafting process. Electricity is consumed by the electron beam accelerators whose role is to open grafting sites (Section 4).

Table 8.3. Cost components for 1200 tonne U/year system with uranium production cost of $760/kg U

	Capital Investment Cost		Annual Operating Costs	
	Total (Million $)	**Contribution to Production Cost ($/kg U)**	**Total (Million $/year)**	**Contribution to Production Cost ($/kg U)**
Adsorbent Production	1,223*	133	295	245
Mooring and Recovery	1,525	167	167	139
Elution and Purification	102	11	24	20
Interest During Construction			54	45
TOTAL	**2850**	**311**	**540**	**449**

* includes $770 million for initial chemical and material inventories.

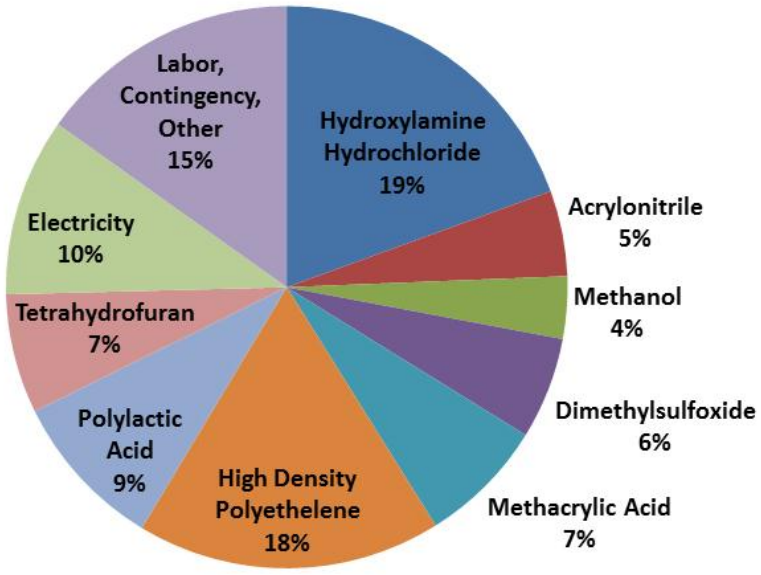

Fig. 8.3. Components of adsorbent production materials, labor, and utilities costs.

8.2.5 Energy return on investment

The predominance of material and utility inputs to adsorbent production is even more evident in the EROI results (Fig. 8.4). The figure plots the energy intensity components of the seawater technology against those of a representative average of conventional mines and mills.[7] The EROI values themselves are given for the uranium recovery step only, i.e. the electricity ultimately produced by the uranium in the once-through fuel cycle is divided by the respective energy intensities of uranium production. At 16, the EROI of the seawater uranium technology is a

factor of 10 lower than that of conventional mining. This result provides a degree of confirmation of the cost analyses in that both the uranium production cost and EROI are seen to

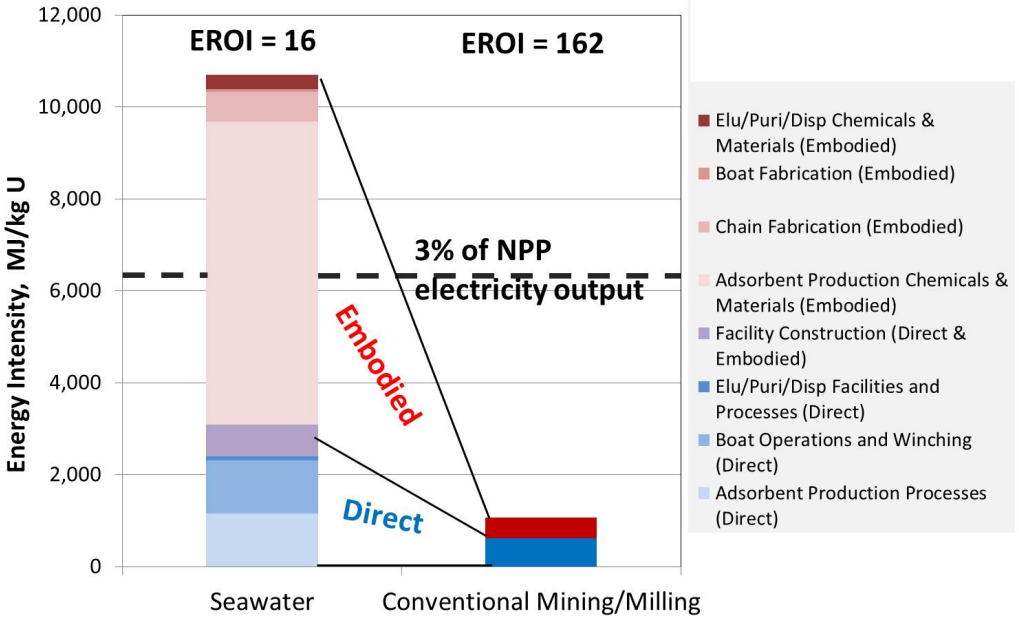

Fig. 8.4. Energy return on investment (EROI).

differ by roughly the same factor when present-day conventional and seawater uranium recovery are compared.

Embodied energy, notably in chemicals and materials consumed in adsorbent production, is seen to account for more than 70% of the total energy used in the process. This category encompasses the energy inputs to the production of the chemicals. Workboat operations and winching, direct energy consumers primarily of diesel fuel oil, are the second largest constituent of the energy use, followed closely by electricity directly consumed in e-beam accelerator operations. Further information on the EROI calculation can be found in Schneider and Lindner.[8]

8.2.6 Uncertainty analysis

As mentioned, uncertainties are attached to the baseline cost estimate. Three major uncertainty categories have been identified. First are the cost inputs themselves. Input cost uncertainties are reflected in, for example, commodity and equipment costs as well capital plant investment costs estimated through the top-down approach. In the latter case, 30% relative uncertainties were generally applied in accordance with standard engineering practice for projects in the pre-conceptual design stage. Second, there remains a degree of uncertainty in the uranium capacity of the fresh adsorbent. The capacity, defined here as the uranium adsorption over 60 days of immersion (a duration that has been shown to lead to near-optimal uranium production costs; see Schneider and Sachde[6]), continues to evolve with fiber design and grafting chemistry. Therefore, a limited set of field test data is available to inform the capacity estimate (see Sections 6 and 7). Statistical analysis of the data permits both the mean 60 day capacity and its uncertainty to be estimated. Finally, while upcoming experimentation at PNNL is expected to provide new data in connection with adsorbent durability (Section 7), the JAEA campaigns remain the main source of empirical data on adsorbent capacity loss with reuse when the adsorbent is placed in the ocean environment.

Table 8.4 provides 95% confidence intervals about the expected uranium production cost of $760/kg U for the three classes of uncertainties in turn, as well as for all uncertainty sources taken together. Since the major cost drivers are widely used industrial commodities and materials, the uncertainty associated with the cost inputs, while substantial, is not as large as might be expected for a technology early in its development cycle. The 95% confidence interval associated with 60 day adsorption capacity is similar in size but can by reduced by further experimentation. It represents a substantial tightening of the confidence interval from an earlier analysis of the Japanese system,[6] where capacity uncertainties alone led to a confidence interval of [$850, $2,370] about the then-expected production cost of $1,230/kg U. These large uncertainties reflected the limited, and highly variable, capacity data published by JAEA. Finally, durability uncertainties also give rise to uncertainty in the amount of uranium collected per unit of adsorbent fabricated. As will be discussed below, production costs would be significantly reduced if it proves feasible to use the adsorbent material more than six times with limited capacity loss per use. As the number of uses grows large, the durability comes to drive the production cost uncertainty. For example, if the adsorbent is used 18 times, the uranium production cost ranges from $530/kg U at a capacity loss of 0%/use to $770/kg U at 5%/use and $1,070/kg U at 10%/use.

Table 8.4. 95% confidence intervals on the nominal ($760/kg U) uranium production cost

Uncertainty Component	Distribution	95% confidence interval - low	95% confidence interval - high
Input costs (labor, equipment, utilities, etc.)	Varies with cost component	$640/kg U	$880/kg U
60 day capacity of fresh adsorbent	Normal: mean = 3.08, sd = 0.31 kg U/t adsorbent	$650/kg U	$930/kg U
Adsorbent durability: percent capacity loss per use	Uniform: lower bound 0%, upper bound 10%	$690/kg U	$850/kg U
Overall: include all three components	Assume independence	$630/kg U	$1,020/kg U

8.2.7 Sensitivity analysis

This section illustrates the sensitivity of the uranium production cost to major performance parameters and cost inputs. The three panels in Fig. 8.5 plot the uranium production cost versus number of uses of adsorbent prior to its final disposition. From top to bottom, the panels plot the expected cost at 0% capacity loss per reuse of adsorbent, 5% (the reference value), and 10%. At 5% and 10% capacity loss, there is a cost-minimizing number of adsorbent uses. Since a fixed mooring and deployment cost is incurred upon each reuse regardless of the amount of uranium recovered, as the adsorbent capacity degrades, the mooring and deployment cost *per kg of uranium recovered* is seen to increase. The cost-minimizing number of uses at 5% capacity loss lies between 10 and 15, and the uranium production cost in this range is near $720/kg U.[‡]

If the adsorbent proves very durable and 0% capacity loss upon reuse is demonstrated, the cost dynamic changes substantially. The top panel in Fig. 8.5 shows that outside of deployment and mooring, all cost components decline with reuse number when measured on a basis of kg of uranium recovered. As the uranium recovered over the adsorbent's lifetime increases, the contribution of the adsorbent fabrication investment to the cost per kg of uranium recovered

[‡] A conservative value of six uses was chosen for the reference case because the extant multi-use data from JAEA does not extend beyond this number of adsorbent uses. The JAEA cost analysis [3] also adopted six uses in its reference scenario.

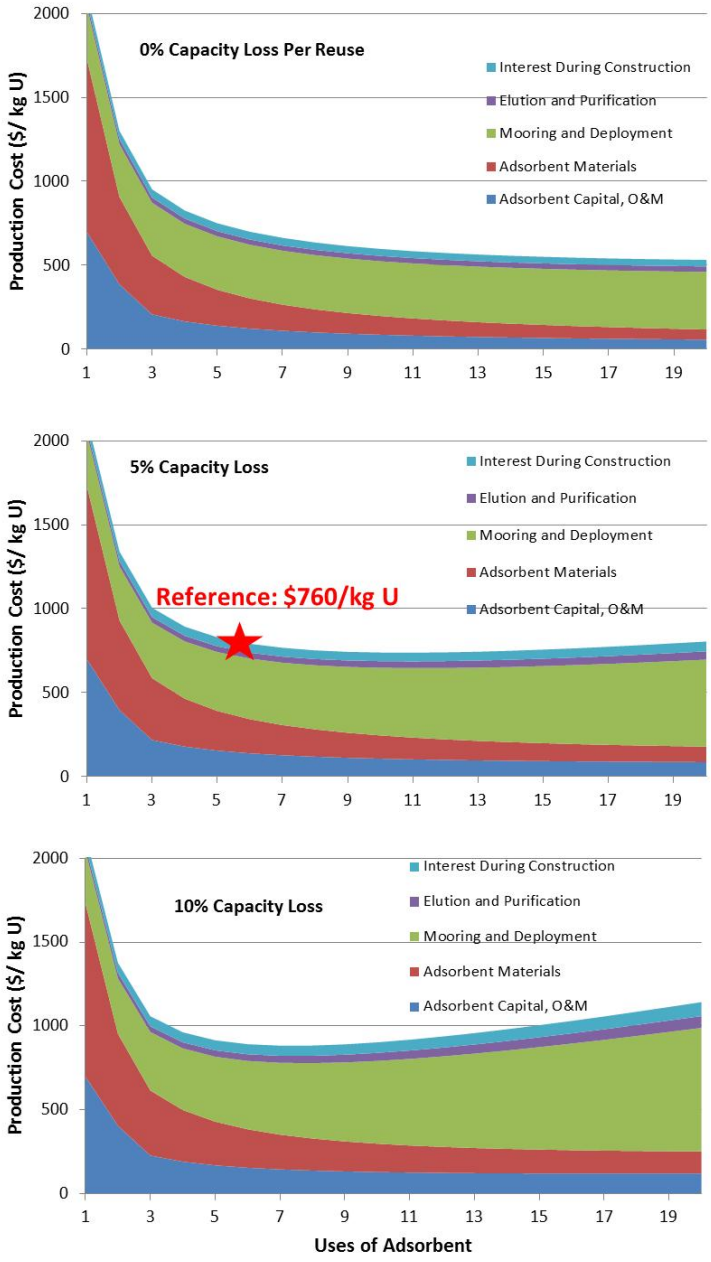

Fig. 8.5. Dependence of cost components on number of uses of adsorbent and durability.

decreases. Therefore, even if attaining very high durability requires an increase in the adsorbent fabrication cost from its current level of $4,700 per tonne of adsorbent, the uranium production cost itself would be little affected. For many adsorbent reuses, it is seen to be driven largely by mooring and deployment costs that are incurred each time the adsorbent is taken to sea. At the reference capacity of 3.09 kg U/t adsorbent, if a large number of reuses with no capacity loss can be demonstrated, the expected uranium production cost will drop to near $500/kg U.

Section 2 describes several potential causes of capacity degradation. Among these are damage to the ligands arising from the acid elution process and occupation of binding sites by competing elements. Section 7 shows that nearly 100% uranium elution efficiency has been demonstrated; 100% efficiency is assumed in the cost analysis. But the competing elements are in some cases difficult to elute without causing further degradation of the ligands. Physical attrition of the polymer fibers themselves while moored at sea must also be considered as a cause of capacity loss, as well as a source term for plastics pollution in the maritime environment.

The reduction in the expected uranium cost from levels exceeding $1,000/kg U reported in Tamada et al.[3] and Schneider and Sachde[5] has largely been driven by improvement of the fresh adsorbent capacity from approximately 2 kg U/t adsorbent to 3.09 kg U/t adsorbent. The 2 kg U/t adsorbent figure from the JAEA reference case was, moreover, based upon a degree of speculation, as it was not directly observed but instead based upon extrapolation from a data

point associated with a shorter immersion time. As mentioned, the 3.09 kg U/t adsorbent capacity upon which this base case rests is based upon multiple measurements and associated with a considerably smaller uncertainty than the starting-point value.

Figure 8.6 illustrates the dependence of the uranium production cost on the fresh adsorbent capacity. A 5% capacity loss per use is assumed in this figure, and the capacity and recycle

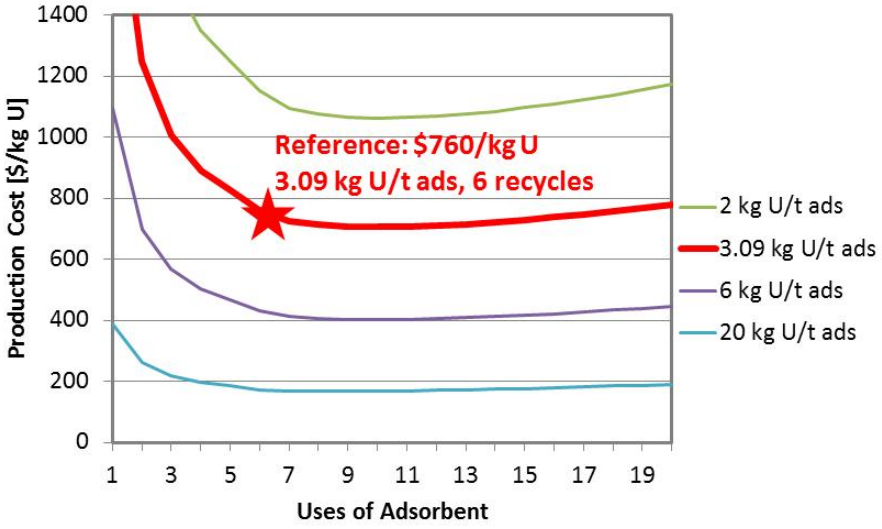

Fig. 8.6. Dependence of uranium production cost on fresh adsorbent capacity and number of adsorbent uses.

number are varied without modifying the adsorbent production process or other inputs. Therefore, the plot serves to illustrate the potential benefit that may be attained from higher capacity levels, with the caveat that the process costs themselves would likely increase. As described in Section 4, adoption of finer, higher-surface-area fibers played an important role in achieving the capacity gain reported in this document. The increased fiber length per unit fiber mass and chemical requirement (PLA and THF, mentioned above) associated with spinning the finer fibers did lead to an increment in the adsorbent production cost. This increment was more than offset by the capacity gain.

8.2.8 Mooring system design

As mentioned above, mooring and deployment costs are a significant contributor to the uranium production cost. Their contribution to the reference cost of $760/kg U approaches 40%. If adsorbent durability is improved and many reuses become feasible, mooring and deployment will likely dominate system costs, with costs incurred upon each maritime deployment cycle establishing a lower bound on the uranium production cost.

Mooring system analysis has not been a major R&D focus of the Fuel Resources Campaign. Engineering design of the deployment and mooring architecture would be a task undertaken by private industry should the technology be commercialized in the future. Nonetheless, to establish a uranium price backstop, that is, a good approximation of the lowest-cost system the technology can support, high-level optimization of the mooring strategy is appropriate. As mentioned at the beginning of this section, two deployment and mooring system design changes reduce the expected uranium production cost from $760/kg U to $610/kg U. This section describes those modifications.

One area of optimization is the deployment strategy. The reference deployment strategy calls for medium-sized (1000 DWT) workboats to service the adsorbent field. Each boat would remain at sea for the length of an adsorption campaign (60 days for the reference case). This strategy has two disadvantages. First, the boats must be rather large to hold the substantial inventory of adsorbent they will accumulate over 60 days of recovering loaded adsorbent braids. Second, the average adsorbent braid will spend a significant amount of time in a boat's cargo hold, producing no revenue.

An alternative strategy, then, calls for a mother ship with onboard elution and purification equipment to be located at the site of the adsorbent field. Smaller work boats (sized at 65 DWT) would service the field but return to the mother ship daily to offload collected adsorbent. A supply vessel would also be needed to replenish the mother ship and return uranium and spent adsorbent to shore.

Table 8.5 contrasts the boat costs for the reference, on-shore strategy to initial cost estimates for the offshore approach. Boat capital costs are seen to be reduced by almost two-thirds, with a commensurate reduction in operating costs not shown. The overall impact of the offshore strategy in this preliminary estimate is to reduce the uranium production cost by \$60/kg U, to \$700/kg U. While it is premature to adopt the offshore approach into the reference case,[§] it exemplifies the importance of cost drivers not directly impacted by the process chemistry.

Table 8.5. On-shore and offshore elution strategies: cost summary

Item	On-shore elution (reference)		Offshore elution	
	Boat capacity (DWT)	**Boat capital cost ($)**	**Boat capacity (DWT)**	**Boat capital cost ($)**
Mothership	N/A	N/A	10,000	\$44M
Work Boats	1,000 (76 boats)	\$320M	65 (76 boats)	\$41M
Supply Boat	N/A	N/A	5,900	\$30M
Summary	**Boat capital cost: \$320M U production cost: \$760/kg U**		**Boat capital cost: \$115M U production cost: \$700/kg U**	

The cost of the anchor chains may also be reduced. In the JAEA reference design, these are fabricated of extra-high-strength (Grade 3) steel with a linear density of 43 kg/m, and their purchase and maintenance contributes \$120/kg U to the uranium production cost. Schneider and Sachde[5] verifies that the self-weight of the steel during winching, as well as drag forces exerted on the chain and adsorbent braids, requires the use of a high-strength material. The design change therefore involves replacing the steel anchor chains with ultra-high molecular weight polyethylene (UHMWPE) fiber rope. But the rope and attached braids would be slightly positively buoyant and, even more restrictively, tangential skin drag on the braids by the ocean current would prevent the system from remaining moored on the seabed. It was found that 25% of the length of the original chain must be retained to provide the needed weight and frictional contact with the seabed. At the required working load calculated for each material, the cost of the co-polymer rope is one-third that of the steel chains.[9] Even given that 25% of the original steel chain must be retained, substituting the co-polymer rope for the chain is found to reduce the uranium production cost by a further \$90/kg U, from \$700/kg U to \$610/kg U.

[§] The strategy remains to be subjected to full peer review. One area that remains in doubt is winching power and load requirements, which (depending on the depth of the seabed at the location of the field) may prove to mandate larger work boats.

Figure 8.7 summarizes key uranium production cost sensitivities. The 95% confidence intervals, shown in blue, reflect input cost uncertainties alone. With the exception of the uppermost bar that recaps the US cost assessment of the JAEA process,[6] each case assumes that process costs are held fixed at current values while adsorbent performance is allowed to vary. The progression of the system cost from the JAEA value is shown in the second bar. The fourth and fifth bars depict two notional trajectories toward a lower uranium production cost: a

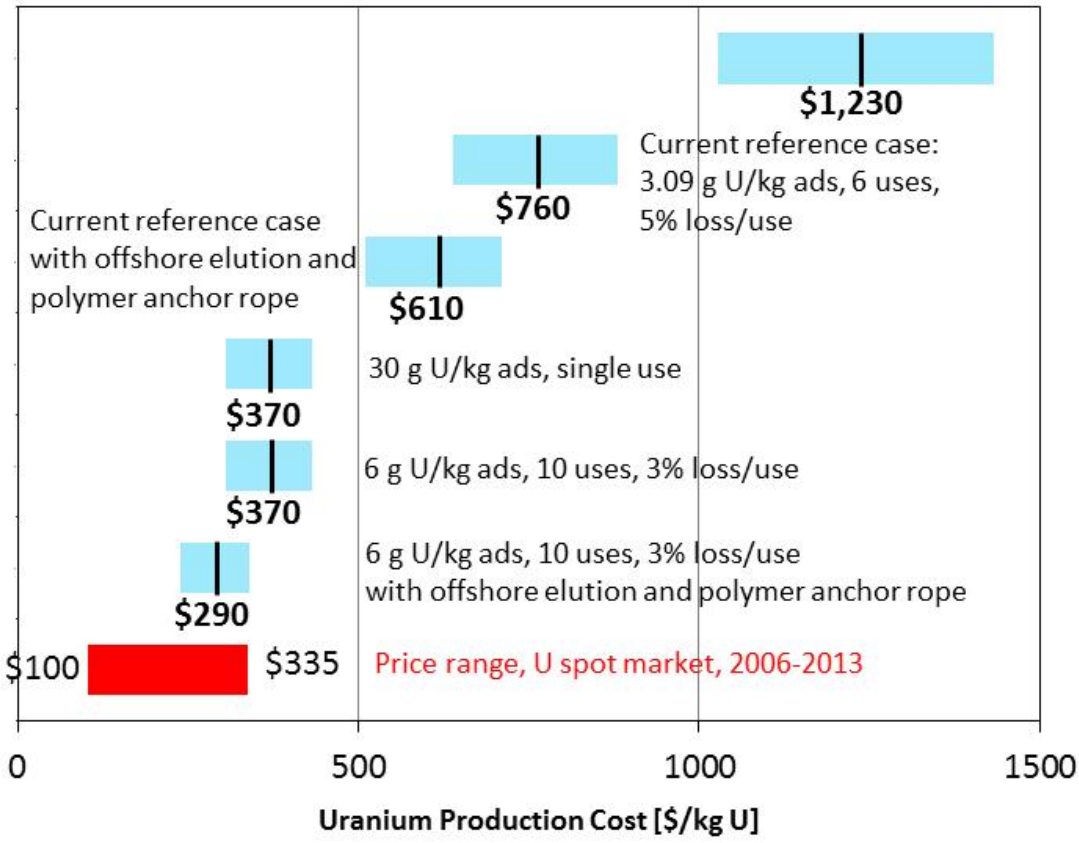

Fig. 8.7. Cost progression and notional performance milestones.

a very high capacity, single use material as well as moderate-capacity, highly durable adsorbent. Finally, the uranium spot price is illustrated to provide context for the cost figures.

8.2.9 Additional R&D recommendations

The cost and EROI analysis suggest a number of R&D directions that are aimed at high-leverage contributors to the uranium production cost or—of equal importance—reducing uncertainties associated with the present cost estimate. These include

1. Systematically vary acrylonitrile (AN) and methacrylic acid (MAA) usage during the grafting step in order to correlate AN and MAA usage to adsorbent capacity with the aim of optimizing the chemical usage for cost
2. Experimentally identify and demonstrate minimum DMSO solvent requirements per unit of AN/MAA
3. Experimentally demonstrate sustained hydroxylamine and methanol recycle (2 and 3 aim to minimize requirements for key chemical cost drivers)

4. Quantify adsorption rate and capacity dependence on number of reuses in order to optimize investment in durability and stability with respect to uranium production cost
5. Quantify the performance of novel elution strategies (e.g., CO_2, Na_2CO_3/H_2O_2) and associated cost-benefit trade-offs (initial experimental results from the Na_2CO_3/H_2O_2 leaching process indicated a capacity loss of just ~3% per recycle[10])
6. Improve the determination of potential co-product concentrations from the current order-of-magnitude level (V is an identified co-product but of minor economic benefit due to the difficulties associated with its elution, see Section 7)
7. Quantify the process and cost impacts of elution/recovery steps that would be needed to isolate promising co-products
8. Correlate fiber physical properties (diameter, shape, surface area to volume ratio) to performance and fabrication cost with the aim of optimizing fiber dimensions/design for cost
9. Enhance the kinetics models (Section 6) to focus on high-fidelity description of the time, temperature and possibly flow velocity dependence of adsorption rate with the aim of optimizing with respect to soaking time and temperature of the water environment.

8.3 References

1. OECD Nuclear Energy Agency, "Uranium: Resources, Production and Demand 2011 (Red Book)," OECD NEA and the International Atomic Energy Agency technical report, 2012.
2. The Ux Consulting Company, LLC, "Historical Ux Price Charts," http://www.uxc.com/, webpage accessed April 15, 2013.
3. Tamada, M., Seko, N., Kasai, N. and T. Shimizu. "Cost Estimation of Uranium Recovery from Seawater with System of Braid Type Adsorbent." *Transactions of the Atomic Energy Society of Japan*, 358-363, 2006.
4. The Economic Modeling Working Group of the Generation IV International Forum, *Cost Estimating Guidelines for Generation IV Nuclear Energy Systems*. Technical report, OECD Nuclear Energy Agency, 2007.
5. Schneider, E. A., and D. J. Sachde. *Review of JAEA Cost Analysis of Braid Adsorbent System for Recovery of Uranium from Seawater.* Technical report, Austin: The University of Texas at Austin, DOE sub-contract 00114954, 2011.
6. Schneider, E. A., and D. J. Sachde, "The Cost of Recovering Uranium from Seawater by a Braided Polymer Adsorbent System," *Science and Global Security*, in press, 2013.
7. Schneider, E. A., Carlsen, B., Tavrides, E., Phathanapirom, U. and C. van der Hoeven, "Measures of the Environmental Footprint of the Nuclear Fuel Cycle," *Energy Economics*, 2013.
8. Schneider, E. A. and H. Lindner, "Energy Balance for Uranium Recovery from Seawater," *Proceedings of GLOBAL 2013,* Salt Lake City, UT, September 2013. Under review.
9. Yale Cordage, "Ultrex Single Braided Rope," http://www.yalecordage.com/industrial-rope/single-braided-ropes/ultrex.html, webpage accessed May 10, 2013.

10. Wai, C., Liao, E., Pan, H. and N. Miyamoto, “Innovative Elution Processes for Recovering Uranium from Seawater,” presented at Fuel Resources Campaign Review Meeting, ORNL, January 2013.

9. INDICATORS OF PROJECT QUALITY AND PRODUCTIVITY

9.1 Publications

Górka, J.; Mayes, R. T.; Baggetto, L.; Veith, G. M.; Dai, S. Sonochemical functionalization of mesoporous carbon for uranium extraction from seawater. *Journal of Materials Chemistry A*, **2013**, 1(9), 3016-3026.

Górka, J., Dai, S. Adsorption by soft-templated carbons. in: *J.M.D. Tascon, Novel Carbon Adsorbents,* Elsevier Ltd, 2012, pp. 323–350.

Grant, C. D.; Kang, S. O.; Hay, B. P. Synthesis of a Hydrophilic Naphthalimidedioxime. *J. Org. Chem.* **2013**, submitted.

Kang, S. O.; Vukovic, S.; Custelcean, R.; Hay, B. P. Cyclic Imide Dioxime: Formation and Hydrolytic Stability. *Ind. Chem. Eng. Res.* **2012**, *51*, 6619-6624.

Kim, J.; Oyola, Y.; Tsouris, C.; Cole R., H.; Mayes T., R.; Janke J., C.; Dai, S., Characterization of uranium uptake kinetics from seawater in batch and flow-through experiments. *Ind. Eng. Chem. Res.* **2013,** *Submitted*

Kim, J.; Tsouris, C.; Mayes T., R.; Oyola, Y.; Saito, T.; Janke J., C.; Dai, S.; Schneider, E.; Sachde, D., Recovery of uranium from seawater:A review of current status and future research needs. *Sep. Sci. Technol.* **2013,** *48*, 367-387.

Kim, J., C. Tsouris, Y. Oyola, R.T. Mayes, C. Hexel, C.J. Janke and S. Dai, "Uranium from Seawater: Adsorption Tests," NEI Magazine, 2013, January, 34-35. www.neimagazine.com

Rao, L. Recent international R&D activities in the extraction of uranium from seawater, Report LBNL-4034E, Lawrence Berkeley National Laboratory, Berkeley, California, USA, March 15, 2010.

Rao, L. Application of radiation grafting: Progress and status of the extraction of uranium from seawater in Japan, *Journal of Isotopes*, 2012, *25* (3), 65 - 75.

Reed, W. A.; Oliver, A. G.; Rao, L. Tetra(tetramethylammonium) uranyltricarbonate octahydrate, *Acta Cryst*. **2011**, *C67*, m301–m303.

Schneider, E. A. and Saschde, D. J. Review of JAEA costa analysis of braid adsorbent system for recovery of uranium from seawater. Technical report, Austin: The University of Texas at Austin, DOE Subcontract 00114954, 2011.

Schneider, E. A. and Saschde, D. J. The cost of recovering uranium from seawater by a braided polymer adsorbent system. *Science and Global Security*, in press, **2013**.

G. Tian, G.; Teat, S. J.; Zhang, Z.; Rao, L. Sequestering uranium from seawater: Binding strength and modes of uranyl complexes with glutarimidedioxime, *Dalton Trans*., **2012**, *41* (38), 11579 - 11586. Cover article.

Tian, G.; Teat, S. J.; Rao, L. Thermodynamic studies of U(VI) complexation with glutardiamidoxime for sequestration of uranium from seawater, *Dalton Trans* **2013**, *42,* 5690-5696.

Vukovic, S.; Watson, L. A.; Kang, S. O.; Custelcean, R.; Hay, B. P. How Amidoximate Binds the Uranyl Ion. *Inorg. Chem.* **2012**, *51*, 3855-3859.

Vukovic, S.; Hay, B. P. De Novo Structure-Based Design of bis-Amidoxime Uranophiles. *Inorg. Chem.* **2013**, in press.

9.2 Patents/Invention Disclosures

Janke, C. J.; Dai, S.; Oyola, Y. "Fiber-based adsorbents having high adsorption capacities for recovering dissolved metals and methods thereof." US Patent Application 2013/0071659.

Dai, S.; Górka, J.; Mayes, R. T. "Surface-Functionalized Mesoporous Carbon Materials." US Patent Application 13/851,523.

9.3 Awards

2012 R&D100 Award: "HiCap Adsorbents" with Chris Janke, Yatsandra Oyola, Chris Bauer, Sheng Dai, Tomonori Saito, Xiao-Guang Sun, Costas Tsouris, & Hills, Inc (co-submitting industrial partner; Jim Brang & Jeff Haggard).

9.4 Outreach

Uranium from seawater program website: http://www.ornl.gov/sci/nuclearfuelresources/

Ben Hay (ORNL) and Sheng Dai (ORNL) with Robin Rogers (Univ. of Alabama) co-organized I&EC Symposium, Uranium from Seawater, 244th American Chemical Society National Meeting, Philadelphia, PA, August 2012.

Results from this work and the sponsored symposium was highlighted in an article entitled "Extracting Uranium from Seawater" that appeared in *Chemical and Engineering News*, Volume 90 (36), pp 60-63, September 3, 2012.

10. NUCLEAR ENERGY UNIVERSITY PROGRAM (NEUP) REPORTS

POLYMER-SUPPORTED PRIMARY AMINES FOR THE RECOVERY OF URANIUM FROM SEAWATER

Prof. Spiro D. Alexandratos (PI), Dr. Remy Sellin (post-doctoral associate)
Department of Chemistry, Hunter College of the City University of New York, 695 Park Avenue
New York, NY 10065

A manuscript on which this report is based has been submitted to Adsorption.

Abstract

The primary amine $–CH_2NH_2$ ligand bound to cross-linked polystyrene has a high affinity for the uranyl ion from a matrix of artificial seawater. The saturation capacity is 14.8 mg U / $g_{polymer}$ compared to 2.34 mg U / $g_{polymer}$ for a diamidoxime ligand on a polystyrene support. Secondary and tertiary amines have much lower affinities indicating that steric effects are important to the complexation. The results with polystyrene-bound $–CH_2NH_2$ thus suggest at least a 3-fold increase in uranyl capacity (calculated on a per mole ligand basis (not per gram of polymer in order to make the results independent of the weight of the polymer support)) and a 4-fold increase when ligands with two primary amines per ligand are utilized. An additional advantage of the primary amine over amidoxime is that it is a simpler ligand to prepare. The use of primary amines as ligands is therefore a promising approach for meeting the DOE goal "to double the Japanese sorption capacity in three years."

Background and Significance

The total amount of uranium available in global seawater is estimated to be 4.5 billion tons despite its extremely low concentration of 3.3 ppb [1]. Recovery of this uranium could produce nuclear energy for centuries thus solving the problem of the known low reserves available from terrestrial ores. Because of its rarity in the terrestrial crust (0.91 ppm), uranium recovery from seawater has been considered since the early 1950's as a potential resource. Different solid sorbents have been developed, including various inorganic and organic materials [1].

Since the concentration of uranium is so low within a seawater matrix that is a complex mixture of cations and anions, the ideal material for its recovery must meet a number of criteria. A high affinity for the uranyl cation is important because it is bound to the carbonate ion in seawater. This is a non-trivial target to achieve since it is the carbonate ion that solubilizes the uranium and the tricarbonate complex has a high stability constant [2]. By way of comparison, the complexation of uranyl from nitrate by polystyrene-bound phosphonic acid we prepared has a saturation capacity of 175 mg U / $g_{polymer}$, a much higher amount than possible from seawater [3] (see below). The sorbent must also have high selectivity for uranyl in the presence of calcium, magnesium, and other cations; a high loading capacity; high sorption and desorption rates; low manufacturing cost; and a high chemical stability in the seawater pH range of 7.4 to 9.6 [4]. A high sorption rate is important when considering the possibility of bio-fouling during prolonged exposure to the sea. Stability under sorption-desorption cycling is also required to minimize the cost of the extraction process by increasing the lifetime of the sorbent.

Decades of research in this area has focused on immobilized amidoxime ligands [5][6]. The polymer is often prepared by grafting acrylonitrile to polypropylene fibers and subsequent conversion of the nitrile to amidoxime. It provides the benchmark for loading capacity from seawater, often cited as 4 mg U / $g_{polymer}$. However, the efficiency of amidoximes decreases with sorption-elution cycles for reasons related to the stability of the chemical structures involved but not yet fully understood [5][7]. Moreover, amidoxime synthesis involves multi-step processes thus increasing the total cost of the final extraction.

The approach taken in this first phase of our research was to study polymer-supported amines as sorbents for uranium from seawater. Polyamines are reported to have good affinity for uranium from neutral [8] and acidic solutions [9][10][11][12] as well as seawater conditions [13][14]. High complexation constants of linear polyamine with the uranyl cation have also been reported from aqueous carbonate-free solutions [15] [2] due, most likely, to coordination of the uranyl cation by nitrogen-containing ligands along its equatorial plane [16].

R&D Progress / Status

Figure 1 shows the structures of the amines whose uranyl capacities are being reported. Table 1 gives their nitrogen and acid capacities, and per cent dried mass content. The theoretical nitrogen capacities are calculated on the basis of the structures shown in Fig. 1. Comparing the acid to the nitrogen capacity gives the number of amine sites that are in the HCl form and this is included in calculating the theoretical nitrogen capacity. Amines with more than two nitrogens do not exceed two HCl per ligand.

Comparing the experimental to the theoretical nitrogen capacities shows that pA and pDMA consist only of the expected ligand; pMA crosslinks to the tertiary amine and the remaining amines have various levels of secondary crosslinking since the nitrogen capacities are lower than theoretical. FTIR spectra do not show the CH_2Cl band at 1265 cm^{-1} hence the lower nitrogen capacities are not due to incomplete reaction. The per cent yield indicates the extent to which the non-crosslinked ligand is produced. pA has the lowest dried mass content and so has the highest hydrophilicity which is consistent with it having the fewest carbons at the amine site.

The uranyl capacities were determined by contacting polymer conditioned to the HCl form (50 mg) with successive aliquots of artificial seawater until an equilibrium pH value of 8 was attained, then with a 5 mL aliquot of uranyl in artificial seawater at an initial concentration C_0 of 50 mg U/ L for 72 h at 23^{o}C. The uranyl equilibrium concentration at equilibrium C_{eq} was determined on a Perkin–Elmer Optima 7000 DV inductively coupled plasma—optical emission spectrometer (ICP-OES). The equilibrium pH was also recorded. The saturation capacity was calculated using the formula:

$$Saturation\ capacity = \frac{V(C_0 - C_{eq})}{m}$$

$$m = dry\ mass = (D.M.C.) \cdot wet\ mass$$

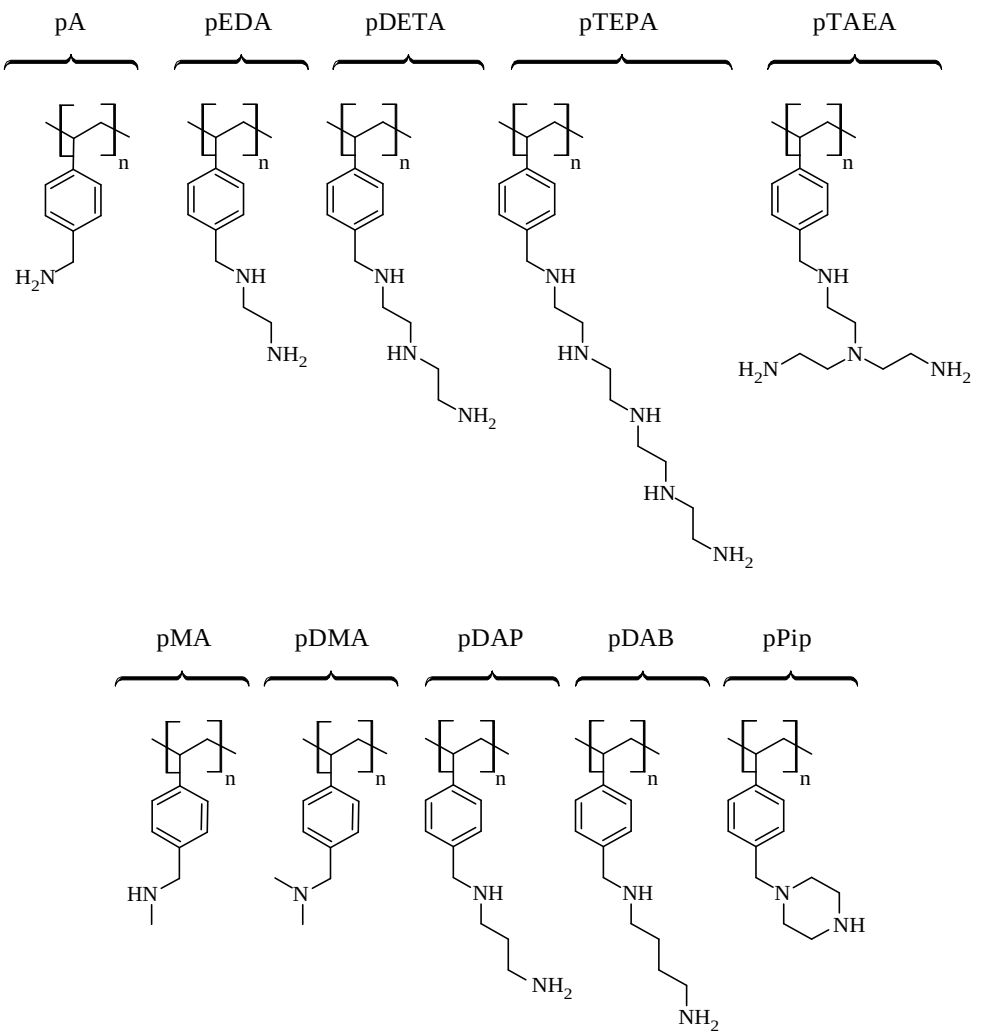

Figure 1. General structures of resin synthesized.

Table 1. Physico-chemical properties of the polymers (nitrogen and acid capacities are to ±0.2 and the dried mass contents are to ±5%).

	N cap.		Yield	Acid cap.	D.M.C.
	mmol N / g		%	mmol H / g	%
polymer	Exp.	Theor.		Exp.	
pVBC	-	0	-	-	100
pA	5.46	5.71	95.6	5.00	18.6
pMA	3.60	5.24	68.7	4.88	49.3
pDMA	4.48	4.87	92.0	4.54	33.0
pDAP	5.56	7.32	76.0	5.50	33.5
pDAB	5.81	6.96	83.5	5.37	34.4
pEDA	6.61	7.74	85.4	6.13	30.0
pDETA	8.43	9.90	85.2	5.96	33.6
pTEPA	8.51	11.6	73.3	5.77	39.6
pPip	5.30	8.06	65.8	3.58	47.2
pTAEA	7.10	11.5	61.7	5.17	41.6

Table 2 compares the uranyl capacities of the polymers. A much higher capacity is evident for pA (14.8 mg U / $g_{polymer}$) than pMA and pDMA (0.14 and 0.09 mg U / $g_{polymer}$, respectively).

Table 2. Uranyl capacities as mg U / $g_{polymer}$ and mmolU / mol_{ligand} (in order of increasing mmol capacity)

Resin	U capacity	N capacity	U capacity
	mg U /$g_{polymer}$	mmol N /$g_{polymer}$	mmol U /mol_{ligand}
pVBC	0	-	0
pDMA	0.09	4.48	0.084
pMA	0.14	3.60	0.165
pPip	0.97	5.30	1.54
pDAP	6.05	5.56	9.14
pDAB	6.62	5.81	9.57
pA	14.8	5.46	11.4
pEDA	10.4	6.61	13.2
pDETA	8.89	8.43	13.3
pTEPA	7.17	8.51	17.7
pTAEA	6.78	7.10	16.0

The primary amine thus has a high affinity for the uranyl ion from seawater and complexation is sensitive to substituents at the amine nitrogen. All polymers with primary amine groups have a significant capacity for uranyl from seawater.

The uranyl capacities for pDAP and pDAB seem lower than for PA, and there seems to be a decrease in capacity along the series pA, pEDA, pDETA, and pTEPA. However, a direct comparison of all polymers on a per gram basis is problematic since the molecular weight of the monomer unit changes as the ligand structure changes. A comparison on the basis of the nitrogen capacity is more useful. Converting mg U / $g_{polymer}$ to mmol U / mol_{ligand} allows for a more meaningful comparison on a molar basis. The results in Table 2 underscore the significance of the primary amine to the removal of uranium from seawater. The pA value is still high (11.4 mmol U / mol_{ligand}) while pDAP and pDAB have comparable and only somewhat lower values (9.14 and 9.57 mmol U / mol_{ligand}, respectively). pEDA and pDETA are now seen to have comparable capacities (13.2 and 13.3 mmol U / mol_{ligand}, respectively). pTEPA has a still higher value (17.7 mmol U / mol_{ligand}) that is almost equivalent to pTAEA (16.0 mmol U / mol_{ligand}). The results are consistent with the primary amine having a high affinity for the uranyl ion from seawater: TEPA immobilization occurs to some extent through one of the interior nitrogens giving two primary amines per ligand while TAEA inevitably gives two primary amines per ligand. (A statistical analysis of the substitution reaction supports this thesis and will be reported in due course.)

It is relevant to compare the results reported in Table 2 with the amidoxime ligand. A value of 4 mg U / $g_{polymer}$ is the highest capacity attained from seawater using polymer prepared from polypropylene fibers [21] but a comparison with pA (14.8 mg U / $g_{polymer}$) is problematic because of the higher monomer molecular weight for the latter and the difference in initial solution uranyl levels (actual seawater in the former, spiked artificial seawater in the latter for analytical purposes). A more valid comparison would be between the values in Table 2 with amidoxime bound to the same polymer support and the same initial solution conditions. While the monoamidoxime is difficult to prepare on polystyrene, the diamidoxime has been prepared (Fig. 2). It has a uranyl capacity is 2.34 mg U / $g_{polymer}$. With a nitrogen capacity of 10.4 mequiv / g, this recalculates to 3.79 mmol U / mol_{ligand}. Since the

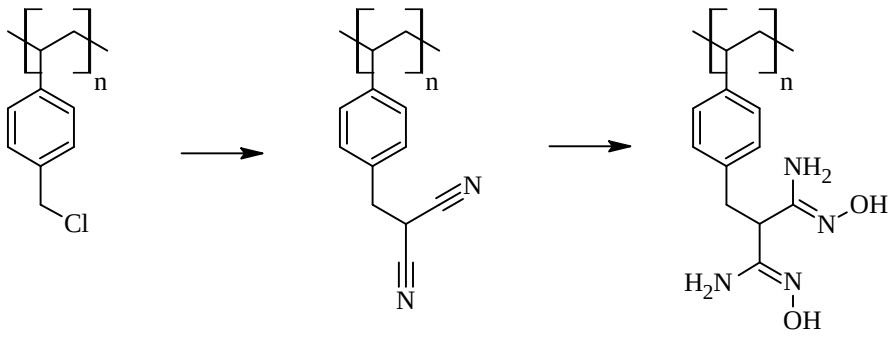

Figure 2. Polystyrene-bound diamidoxime prepared from immobilized malononitrile.

diamidoxime has a higher uranyl affinity than the monoamidoxime [22], the results reported here with pA suggest at least a 3-fold increase in uranyl capacity by the primary amine ligand (calculated on a mole basis) and a 4-fold increase when ligands with two primary amines per ligand are utilized. The use of amines as ligands is therefore a promising approach to meeting the DOE goal "to double the Japanese sorption capacity in three years" and studies are continuing.

Future Work

There are five months remaining to this grant period (June – October 2013). This time will be used to prepare and test polymers along the lines of the first bullet point below. A second set of syntheses will proceed along the lines suggested by the second bullet point below but the details will be developed during the month of June.

* The extent of complex formation is limited by the decreasing probability of formation as molecularity increases. Such a limitation could be overcome by immobilizing ligands with a high density of primary amine sites. Mobility of the primary amine sites also appears crucial to allow the formation of the corresponding complexes around the equatorial plane of the uranyl cation or carbonate complex. Both variables will be addressed by the synthesis of new sorbents involving pentaerythritol as the scaffold. We have published a method for bonding the pentaerythritol to polystyrene then brominating it to bind an amine (see equation below). The dimethylamine whose synthesis was reported cannot be used in the present

work but we will develop a method for binding the primary amine onto the brominated pentaerythritol. Di- and tribromination will provide multi-amine sites whose flexibility may enhance the uranyl affinity.

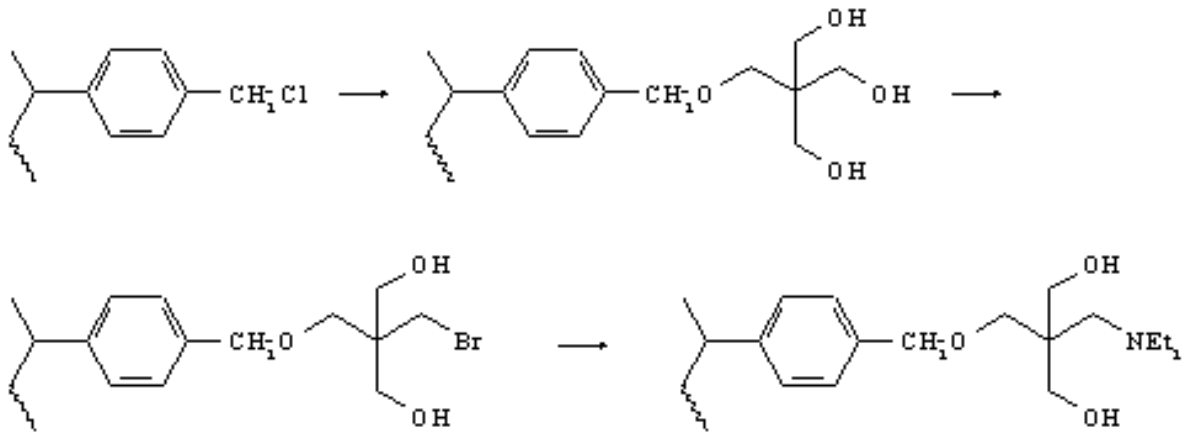

* Since the primary amine has now been found to have an important effect on the sorption of uranyl from seawater, it is reasonable to suggest that the amidoxime affinity may be due to the sum of two elementary coordinative stabilizations, one from the amine and another from the -NHOH. Developing this with new polymers will be the basis of work to the end of this grant period and of a new proposal to be submitted by mid-June.

Acknowledgments

We gratefully acknowledge funding from the U.S. Department of Energy through contract number 120542 from the Nuclear Energy University Program administered by Battelle Energy Alliance, LLC. We thank Ms. Laura A. Oliveira for preparing the polymers with the EDA, DETA and TEPA ligands. We also thank Drs. Ben Hay, Costas Tsouris and Chris Janke at the Oak Ridge National Laboratory for useful discussions.

References

[1] C. K. Gupta and H. Singh, Uranium resource processing : secondary resources, Berlin; New York: Springer, 2003.

[2] S. Berto, F. Crea, P. G. Daniele, A. Gianguzza, A. Pettignano and S. Sammartano, "Advances in the investigation of dioxouranium(VI) complexes of interest for natural fluids," *Coordination Chemistry Reviews,* 256, 63-81, 2012.

[3] X. Zhu and S. D. Alexandratos, *unpublished results*.

[4] G. M. Marion, F. J. Millero, M. F. Camoes, P. Spitzer, R. Feistel and C.-T. A. Chen, "pH of seawater," *Marine Chemistry,* 126, 89-96, 2011.

[5] L. Astheimer, H. J. Schenk, E. G. Witte and K. Schwochau, "Development of sorbers for the recovery of uranium from seawater. 2. The accumulation of uranium from seawater by resins containing amidoxime and imidoxime functional groups," *Separation Science and Technology,* 18, 307-339, 1983.

[6] H. J. Schenk, L. Astheimer, E. G. Witte and K. Schwochau, "Development of sorbers for the recovery of uranium from seawater. 1. Assessment of key parameters and screening studies of sorber materials," *Separation Science and Technology,* 17, 1293-1308, 1982.

[7] S. Vukovic, L. A. Watson, S. O. Kang, R. Custelcean and B. P. Hay, "How Amidoximate Binds the Uranyl Cation," *Inorganic Chemistry,* 51, 3855-3859, 2012.

[8] H. Tbal, J. Morcellet, M. Delporte and M. Morcellet, "Uranium absorption by chelating resins containing amino groups," *Journal of Macromolecular Science, Pure and Applied Chemistry,* A29, 699-710, 1992.

[9] B. L. Rivas, H. A. Maturana, I. M. Perich and U. Angne, "Polyethylenimine supports for resins with retention properties for heavy metals. Part I," *Polymer Bulletin,* 14, 239-243, 1985.

[10] B. L. Rivas, H. A. Maturana, J. Bartulin, R. E. Catalan and I. M. Perich, "Poly(ethylenimine) supports for resins with retention properties for heavy metals. Part 3," *Polymer Bulletin,* 16, 299-303, 1986.

[11] B. L. Rivas, H. A. Maturana, U. Angne, R. E. Catalan and I. M. Perich, "Resins with retention properties for heavy metals. Part 4," *Polymer Bulletin,* 16, 305-309, 1986.

[12] B. L. Rivas, H. A. Maturana, I. M. Perich and U. Angne, "Linear polyethyleneimine supports for resins with retention properties for heavy metals. Part 2," *Polymer Bulletin,*15, 121-125, 1986.

[13] S. Kobayashi, T. Tanabe, T. Saegusa and F. Mashio, "Phosphonomethylated polyethylenimine resin for recovery of uranium from seawater," *Polymer Bulletin,* 15, 7-12, 1986.

[14] S. Kobayashi, M. Tokunoh, T. Saegusa and F. Mashio, "Poly(allylamine). Chelating properties and resins for uranium recovery from seawater," *Macromolecules,* 18, 2357-2361, 1985.

[15] F. Crea, A. Gianguzza, A. Pettignano and S. Sammartano, "Interactions of Dioxouranium(VI) withPolyamines in Aqueous Solution," *Journal of Chemical & Engineering Data,* 55, 3044-3050, 2010.

[16] F. R. Parkin, Comprehensive Coordination Chemistry II, Volume 3: Coordination Chemistry of the s, p, and f Metals, Elsevier Ltd., 2004, p. 629.

[17] Y. Yang and S. D. Alexandratos, "Mechanism of Ionic Recognition by Polymer-Supported

Reagents: Immobilized Tetramethylmalonamide and the Complexation of Lanthanide Ions," *Inorganic Chemistry,* 49, 1008-1016, 2010.

[18] X. Zhu and S. D. Alexandratos, "Polystyrene-Supported Amines: Affinity for Mercury(II) as a Function of the Pendant Groups and the Hg(II) Counterion," *Industrial & Engineering Chemistry Research,* 44, 23, 8605-8610, 2005.

[19] J. J. Vaquero, L. Fuentes, J. C. Del, M. I. Perez, J. L. Garcia and J. L. Soto, "The Reactions of Benzylmalononitriles with Hydrazine and Hydroxylamine. Synthesis of Pyrazoles, Isoxazoles, and Pyrazolo[1,5-a]-pyrimidine Derivatives," *Synthesis,* 1987, 33-35, 1987.

[20] M. Loadman, Analysis of rubber and rubber-like polymers, Dordrecht: Kluwer Academic, 1998.

[21] J. Kim, Y. Oyola, R. Mayes, C. Janke, S. Dai and C. Tsouris, "Testing of Amidoxime-Based Adsorbent for the Recovery of Uranium From Seawater," Am. Inst. Chem. Eng., Annual Meeting, Oct. 28 - Nov. 12, 2012; Abstr. 277098.

[22] P. Kavakli, N. Seko, M. Tamada and O. Goven, "A Highly Efficient Chelating Polymer for the Adsorption of Uranyl and Vanadyl Ions at Low Concentrations," *Adsorption,*10, 4, 309-315, 2005.

Enhancement of the Extraction of Uranium from Seawater

Chanel Tissot – University of Maryland
Aaron Barkatt – The Catholic University of America
Jay LaVerne – University of Notre Dame
Mohammed Adel-Hadadi – The Catholic University of America
Mohamad Al-Sheikhly – University of Maryland: Principal Investigator.*

Known uranium deposits amount to approximately 5.3 Mt of uranium. At present, about 70,000 tons of uranium are consumed every year by the 435 nuclear power plants operating around the globe.[1] Accordingly, known uranium reserves are only sufficient to supply nuclear power plants with enough uranium for approximately 80 years at the current rate of consumption. While exploration can be expected to increase the amount of uranium that can be obtained by locating new deposits and starting to mine them, the costs of exploration and development are expected to be very high.[2] In addition, uranium mining is environmentally harmful and results in the generation of very large volumes of contaminated mill tailings.

Even with an average concentration of only 3.3 ± 0.2 μg/L (or 3.3 ± 0.2 ppb)[1], the world's oceans, are by far the largest uranium resource on earth. The volume of the oceans is $1.3 \cdot 10^{21}$ L, and therefore the amount of uranium that they contain is approximately $4.2 \cdot 10^{3}$ Mt, corresponding to 800 times the known amount of uranium reserves or another 6300 years of reactor operation at the current rate of consumption without using reprocessing techniques or breeder reactors.

Since the inception of research and development aimed at the extraction of uranium from seawater, the requirements and characteristics of the "ideal sorbent" have been defined in an attempt to improve and advance technology. These needs have changed little over time since the 1950's and are still applicable today despite significant advances. Optimization of adsorbents in order to increase the efficiency of the extraction and consequently reduce the costs has to be aimed at the attainment of the following objectives:

- Very high distribution coefficient
- High selectivity for uranium
- High loading capacity
- Rapid loading kinetics
- High capacity for multi-cycle regeneration

In the current project, a new type of adsorbent, based on phosphate functional groups radiation-grafted onto winged fibers™ with ultra-high surface area, has been developed and tested to characterize its adsorption capacity for uranium from real seawater. This adsorbent is fabricated using the 1-9 MeV electron beam linear accelerator or the 100 kCi Co-60 gamma irradiator at the University of Maryland to graft the adsorbing monomer onto the polymeric substrate. Five acrylated phosphate-containing monomers have been grafted onto winged fibers™ of nonwoven nylon-6.

The conditions of grafting were explored in order to obtain high capacities of the grafted adsorbent for sorption of uranium from seawater. The samples were tested for adsorption from Atlantic Ocean seawater collected at 34.7^{o} N, 76.7^{o} W and enriched with uranium by adding a

* To whom correspondence should be addressed

uranyl acetate solution to bring the concentration of U to 10 mg/L (unless otherwise noted). These solutions were analyzed for U before and after rotating 10 mL of test solution with a grafted polymer sample for 1 hour at 30 rpm. The decrease in uranium concentration upon contact with the grafted polymer, normalized to the weight of the adsorbent, was used to calculate the distribution coefficient (K_d, mL/g) of the adsorbent for uranium in a seawater environment. Grafting was performed using the "direct" method, in which the polymeric substrate is irradiated simultaneously with the monomer solution. Experiments with indirect grafting showed significantly lower degrees of grafting and distribution coefficients They also had a higher degree of complexity and required longer processing time.

After verification of uranium adsorption with the monomers adsorbed on activated carbon, the five phosphate-containing monomers were grafted onto winged™ nylon-6. The conditions of grafting and the resulting distribution coefficients are shown in Table 1. The results indicated that bis(2-methacryloxyethyl)phosphate (B2MP) is, by far, the most effective of the five compounds.

Table 1

Distribution Coefficients Obtained for Uranium in Seawater with Nylon Grafted with Various Phosphonate Compounds. Co-60 γ radiation at 5 kGy/hr for one hour, room temperature, direct grafting

Compound	Observed K_d, $mL \cdot g^{-1}$
diethylallylphosphonate	$1.2x10^2$
vinylphosphonic acid	$1.7x10^2$
dimethylvinylphosphonate	$1.8x10^2$
diethylvinylphosphonate	$3.5x10^2$
bis(2-methacryloxyethyl)phosphate (B2MP)	$6.3x10^4$

The high distribution coefficient observed for the adsorbent grafted with B2MP can be attributed to the fact that this compound, unlike the four others, has two, rather than one, double bonds on the two sides of the phosphonate group.

Adsorbents prepared by grafting B2MP onto Winged nylon-6, fibers were found to have much higher K_d values and greater retention of mechanical properties after irradiation than those prepared with conventional nonwoven nylon-6 fibers, poly(tetrafluoroethylene-co-hexafluropropylene) fibers or polypropylene fibers. Both Winged and conventional polypropylene showed very poor radiation resistance, despite favorable degrees of grafting and high distribution coefficients when grafted with B2MP.

Electron paramagnetic resonance (EPR) measurements were performed on irradiated nylon-6 to investigate the behavior of the surface radicals and to determine the radical half-life. **Figure 1** shows the concentration and decay of free radicals produced on Winged nylon under electron beam irradiation at total doses of 150, 200, 250, 300 and 350 kGy (1.9 Gy/3-μs pulse). Irradiations were performed in the absence of oxygen and at room temperature to best simulate the grafting conditions. Radical half-life was determined to be on the order of 10^3 seconds, suggesting that the direct grafting method should be considered.

Figure 1

Radical concentration of irradiated Winged nylon-6. Anaerobic irradiation and measurement at room temperature.

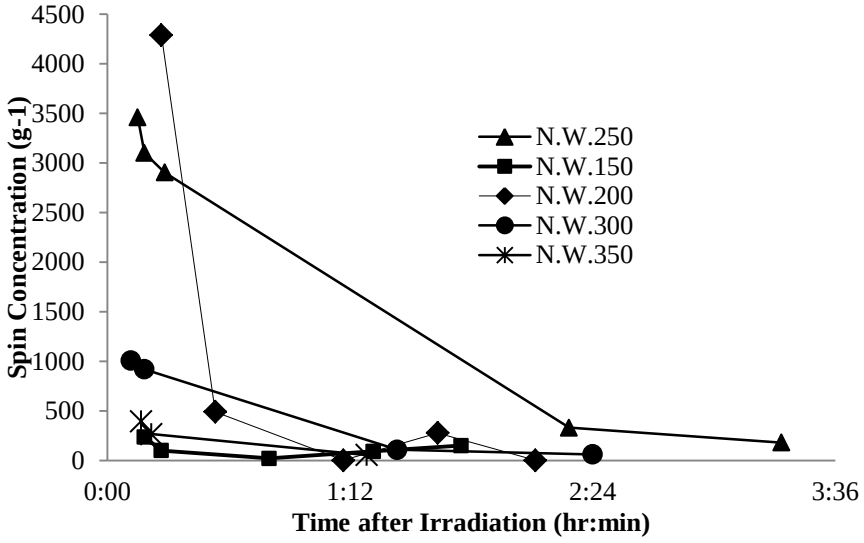

The distribution coefficient of the product is related to the degree of grafting, which is reflected in the weight gain of the substrate upon being subjected to radiation grafting of the phosphate species. In general, distribution coefficients higher than $1x10^4$ $mL \cdot g^{-1}$ were obtained when the grafting density exceeded 80 %. The highest values of k_d were obtained when the grafting densities were in the range of 100-120 %. For degrees of grafting higher than approximately 160%, k_d's were shown to decrease rapidly. This indicates that the number of active sites on the polymer no longer increases, probably due to homopolymerization of the complexing monomer.

After insufficient degrees of grafting were obtained using lower alcohols as solvents during the grafting process, water was selected as solvent despite the low solubility of B2MP in water. The use of water as a solvent is highly desirable, with advantages including the elimination of organic solvents and the production of less hazardous waste. Grafting with B2MP in water produced highly favorable results, even though much of the B2MP was presented in suspension rather than in true solution. Careful control over the conditions of the irradiation was required due to the formation of undesirable homopolyme. **Figure 2** shows the effect of monomer (B2MP) concentration on the percent mass change (degree of grafting) and distribution coefficient for uranium. The rapid rise in percent mass change and associated decrease in distribution coefficient past 100 mg/L B2MP suggest the presence of homopolymer. The presence of homopolymer was also easily observed upon visual inspection of the grafted polymer after drying.

Figure 2

The effect of monomer concentration on percent mass change and the distribution coefficient for uranium in real seawater. Samples irradiated using NIST Co-60 irradiator at 6.53 kGy/hr, 60 kGy.

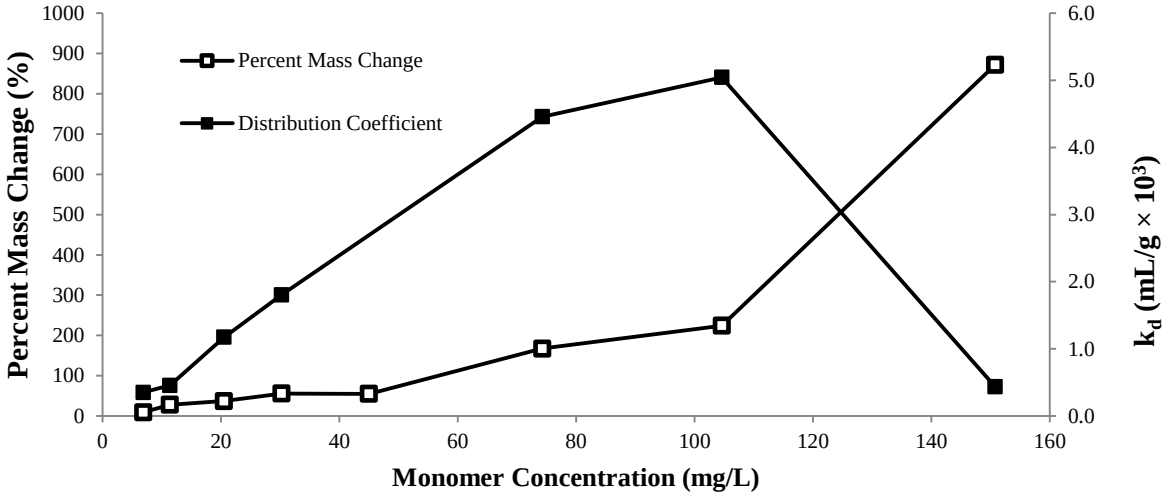

Optimization of irradiation conditions was performed to develop an adsorbent that is both highly effective and practical. The effects of total dose, dose rate and type of radiation on the degree of grafting were determined.

Experiments performed with an electron beam irradiator showed excessive homopolymerization in the monomer emulsion, even at low dose rates. Subsequent experiments with Co-60 gamma radiation showed high uniformity, with much greater control over irradiation conditions.

Distribution coefficients higher than $1x10^4$ $mL \cdot g^{-1}$ were obtained with dose rates in the range of 1-10 $kGy \cdot hr^{-1}$. An intermediate dose rate of 10 kGy/hr was selected for adsorbent fabrication, as higher dose rates produced significant homopolymerization and lower dose rates (<5 kGy/hr) were deemed impractical due to the need to use long irradiation times in order to reach the target total use. **Figure 3** reveals the effect of total dose on the degree of grafting. 40 kGy was selected as the target dose, as only slight increases in degree of grafting were observed after 40 kGy (4 hours irradiation time at 10 kGy/hr).

Distribution coefficients higher than 5×10^3 were shown to correspond to a percent sorption of uranium from seawater (doped to 10 mg-U/L) greater than 97%. Samples grafted at intermediate dose rates (5-10 kGy/hr) and high total doses (>30 kGy/hr) consistently revealed uranium loadings between 6 and 8 mg-U/g-adsorbent after one hour of contact with real seawater doped to 10 mg/L U.

Figure 3

The dependence of degree of grafting on dose rate for a) 4-mg samples irradiated in air, 58 mg/L B2MP; b) 5.6-mg samples irradiated in air, 64 mg/L B2MP.

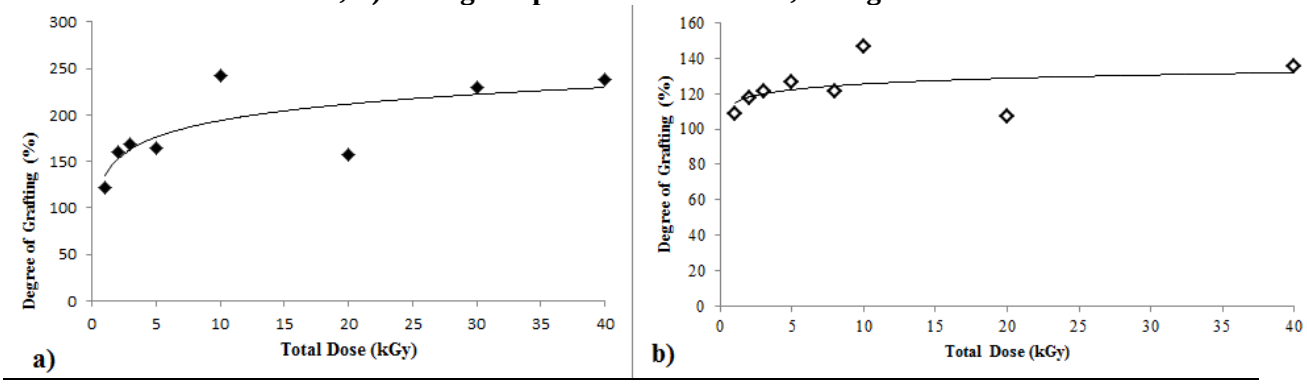

It should be noted that under testing conditions involving a 20-mg adsorbent sample immersed in 10 mL of seawater doped with 20 mg/L U, a distribution coefficient of 1×10^4 mL/g corresponds to a loading of 9.5 mg U/g-adsorbent and to removal of 95% of the uranium.

The loading level of the grafted adsorbents with respect to uranium was characterized by gradually increasing the volume of doped seawater from 10 mL to 100 mL and measuring the extent of removal of uranium from each volume of solution. The increase in loading is shown in **Figure 4**, with loadings of up to 44 mg U/g-adsorbent (4.4%) obtained.

Figure 4

Loading of uranium on adsorbent with increasing mass of uranium in solution for B2MP grafted onto Winged™ nylon, Co-60 irradiation to 40 kGy total dose, 10 kGy/hr dose rate. Testing with 15 mg adsorbent, 10-100 mL of 20 mg/L U in seawater for 24 hours.

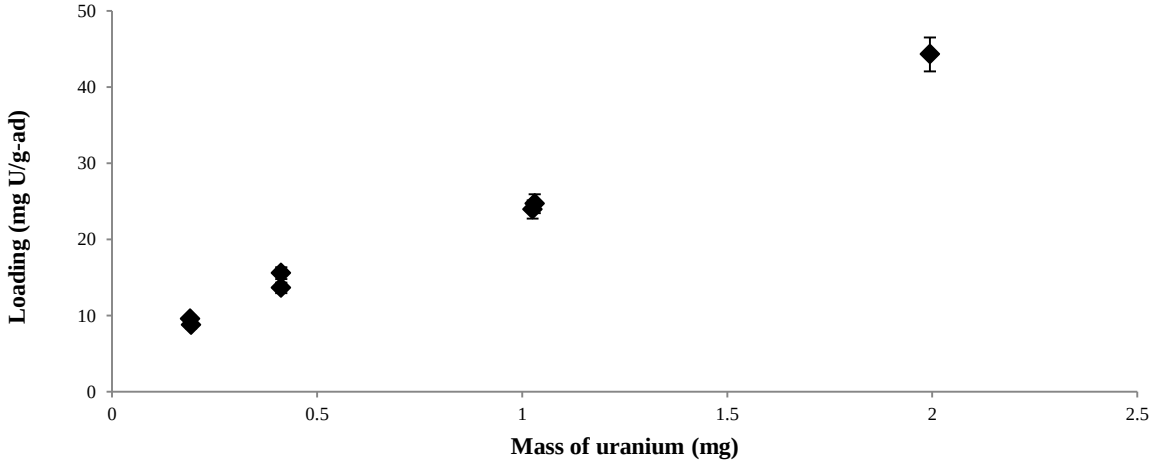

An important feature of the winged-fiber™ nylon adsorbents grafted with B2MP was their high potential for regeneration, i.e., restoration of the capacity for uranium adsorption

following treatment of the loaded adsorbent with an eluent. Adsorbent regeneration has far-reaching implications to its performance under service conditions because successful regeneration greatly enhances the economic feasibility of the process. Traditional, amidoxime-based adsorbents[4] can be regenerated using an acidic eluent (HCl), but the K_d of such adsorbents rapidly falls from one adsorption/elution cycle to the next.

Regeneration of the B2MP-grafted samples following adsorption of uranium was studied using several eluents, including HCl, nitric acid, citric acid, ammonium oxalate, oxalic acid and ethylenediamine. All eluents showed a decrease in adsorption capacity following the first cycle of elution, indicating damage to the eluted adsorbent. However, unlike the other reagents, ammonium oxalate did not exhibit a decrease in performance after the first cycle of regeneration, with distribution coefficients remaining consistent after 156 cycles of re-use. The change in k_d upon consecutive cycles of elution/regeneration followed by uranium adsorption tests is shown in **Figure 5**. We suggest that ammonium oxalate is much less damaging to the adsorbent because the neutral pH of the adsorbent solution does not cause hydrolytic cleavage of the bond between the complexing moiety and the polymeric substrate. It is also possible that the decrease of K_d obtained with the B2MP-doped polymer during the first cycle is due to irreversible removal of some loosely bound B2MP rather than to attack on the strong covalent bonds formed between the B2MP and the polymeric substrate during the grafting process.

Figure 5

Regeneration of grafted adsorbents using 1 M ammonium oxalate for B2MP grafted onto Winged™ nylon, Co-60 irradiation to 60 kGy total dose, 5 kGy/hr dose rate. Testing with 15 mg adsorbent in 10 mL of 10 mg/L U in seawater for 1 hour

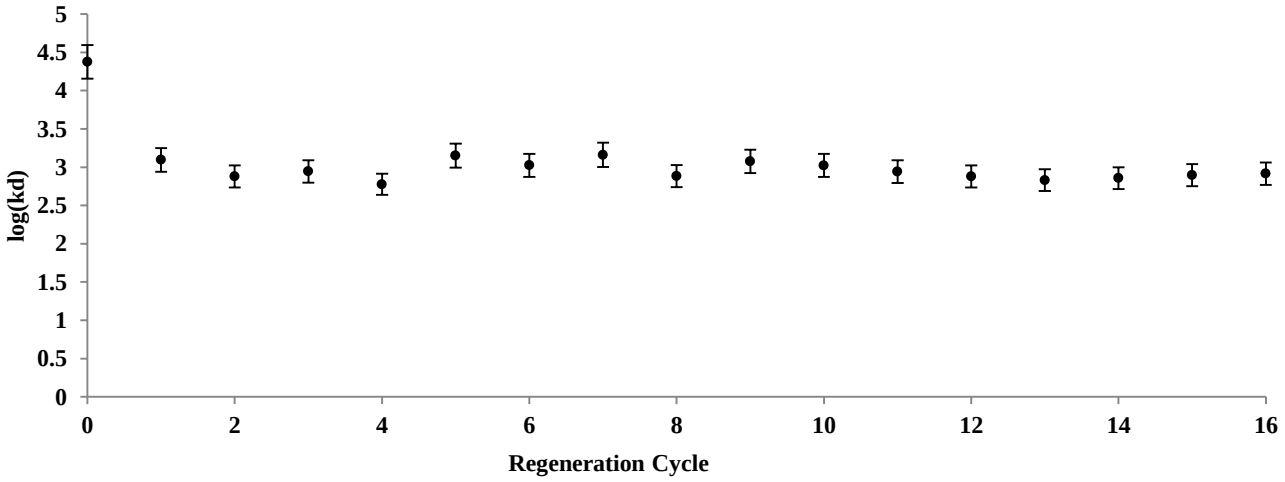

In conclusion, we have demonstrated that effective adsorbents for uranium from seawater can be fabricated through radiation-induced grafting of phosphate-containing monomers onto ultra-high surface area winged fibers™ with ultra-high surface area. Uranium loadings of up to 4.4% and distribution coefficients on the order of 10^4 mL/g have been obtained with grafted adsorbents after contact with real seawater doped with uranium. Adsorbents regenerated with

ammonium oxalate have shown at least sixteen cycles of reusability with negligible degeneration of adsorptive capacity after the first cycle. The present laboratory-scale study has demonstrated the potential for using B2MP-grafted winged fibers™ of nylon 6 to recover uranium from seawater through a simple, effective, and economically friendly process. This process may provide a practical, cost-effective alternative to conventional uranium mining.

[1] World Nuclear Association. World Nuclear Power Reactors and Uranium Requirements (2013).

[2] World Nuclear Association. Supply of Uranium (2012).

[3] Ku, The-Lung; Knauss, K.; Mathieu, G. (1977). Uranium in Open Ocean: Concentration and Isotopic composition. Deep Sea Research, Vol. 24, Issue 11, pp. 1005-1017.

[4] Seko, N.; Katakai, A.; Hasegawa, S.; Tamada, M.; Kasai, N.; Takeda, H.; Sugo, T.; Saito, K. (2002) Aquaculture of Uranium in Seawater by a Fabric-Adsorbed Submerged System. Nuclear Technology, Vol. 144, Issue 2, pp. 274-279.

Project Title: Selectivity in ligand binding to uranyl compounds: A synthetic, structural, thermodynamic and computational study
Contract Number: 119253. **Project Number:** 11-3049
Principal Investigator: John Arnold, Department of Chemistry, University of California, Berkeley, CA 94720-1460

Background and Significance

The uranyl cation (UO_2^{2+}) is the most abundant form of uranium on the planet. It is estimated that 4.5 billion tons of uranium in this form exist in sea water. The ability to bind and extract the uranyl cation from aqueous solution while separating it from other elements would provide a limitless source of nuclear fuel. A large body of research concerns the selective recognition and extraction of uranyl. A stable molecule, the cation has a linear O=U=O geometry. The short U-O bonds (1.78 Å) arise from the combination of uranium 5f/6d and oxygen 2p orbitals. Due to the oxygen moieties being multiply bonded, these sites were not thought to be basic enough for Lewis acidic coordination to be a viable approach to sequestration.

We believe that the goal of developing a practical system for uranium separation from seawater will not be attained without new insights into our existing fundamental knowledge of actinide chemistry. We posit that detailed studies of the kinetic and thermodynamic factors that influence interactions between f-elements and ligands with a range of donor atoms is essential to any major advance in this important area. The goal of this research is thus to broaden the coordination chemistry of the uranyl ion by studying new ligand systems via synthetic, structural, thermodynamic and computational methods. We anticipate that this fundamental science will find use beyond actinide separation technologies in areas such as nuclear waste remediation and nuclear materials.

Most strategies toward uranyl sequestration involve ligands solely bonding to the uranium center equatorially in a planar geometry. Research has shown that when coordinating strong σ and π donating ligands to the equatorial plane, the added electron density softens the U(VI) center giving some Lewis basicity to the axial oxygen atoms as the U-O bond weakens. Several innovative ligand designs dually bond to both the equatorial plane and the axial oxo groups (Figure 1).

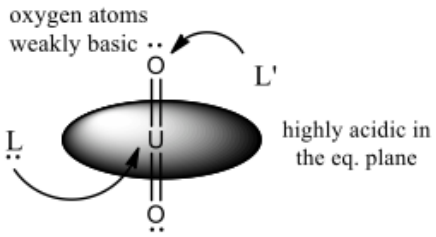

Figure 1. Electron donor ligands (L:) can bind uranyl at the equatorial plane while the axial oxo groups can coordinate Lewis acids (L').

A ligand designed by Raymond and coworkers illustrates this approach by containing carboxylate groups as electron donors to the equatorial plane, while also containing a secondary amine to hydrogen bond with a uranyl oxygen. Such an approach is selective for the target species, as no other present cationic species would have the particular geometry of uranyl. Two reports have shown that the bonding of equatorial NCN ligands to uranyl weakens the U-O stretch frequency. This bond weakening coincides with increased Lewis basicity of the oxo ligands as illustrated by the addition $B(C_6F_5)_3$, yielding the complex $UO\{OB(C_6F_5)_3\}(NCN)_2$. This is the first example of an oxo ligand being functionalized by borane, albeit a highly Lewis acidic one. Additionally several studies report uranyl oxo ligands interacting with transition and alkali metal cations.

The focus of this study is to synthesize uranyl complexes incorporating amidinate and guanidinate ligands. By developing a working methodology for these syntheses, there can be further investigation into more novel ligand coordination. Due to the ability of uranyl to bond with several hard electron rich ligands, it is an academic challenge to develop syntheses limiting this ligation and produce specific complexes with known coordination numbers. In this study, we use both synthetic and computational methods to investigate novel equatorial ligand coordination and how this affects the basicity of the oxo ligands. Such an understanding will later apply to

designing ligands incorporating functionalities that can bind uranyl both equatorially and axially for highly selective sequestration.

Coordination of uranyl with NCN ligands

Due to the limited precedent set forth in literature, we focused on binding the uranyl cation with anionic NCN ligands such as amidinates and guanidinates. These anionic ligands can soften the U(VI) center, affecting the U-O bond length. The pathway chosen for the preparation of uranyl guanidinates was the reaction of a uranyl amide with carbodiimide to undergo a migratory insertion. The uranyl amide $UO_2[N(SiMe_3)_2]_2(thf)_2$ was prepared according to a published procedure by adding two equivalents of $KN(SiMe_3)_2$ to a slurry of $UO_2Cl_2(thf)_2$. The addition of one equivalent of N,N-diisopropylcarbodiimide to $UO_2[N(SiMe_3)_2]_2(thf)_2$ in toluene yields a product coinciding with an immediate color change from orange to red (Scheme 1).

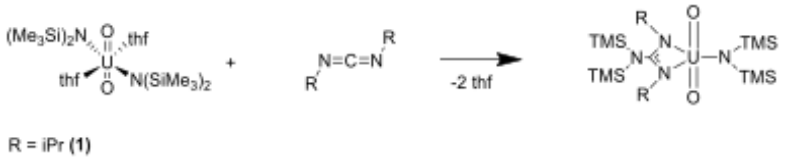

Scheme 1. The preparation of the uranyl monoguanidinate **1.**

The reaction of two equivalents N,N-diisopropylcarbodiimide and $UO_2[N(SiMe_3)_2]_2(thf)_2$ in toluene at 60°C for 24 h afforded the uranyl bis(guanidinate) **2**, isolated as a clean red powder**.** ^{1}H NMR resonances were observed for **2** at δ 5.77, 1.73, and 0.37 with the respective integration ratio 1:6:9. The heptet resonance at 5.77 ppm corresponding to the isopropyl methine nuclei is strikingly downfield and is discussed later on.

Both reactions coincide with color changes similar to those reported for the addition of amidinate ligands to uranyl. Unlike the reported addition of two amidinate ligands onto uranyl, no THF remains coordinated to the uranium in either uranyl guanidinate species **1** or **2.** This suggests some ease in coordinating highly Lewis acidic species to the uranyl oxo ligands, as there are no competitive Lewis bases present in the product.

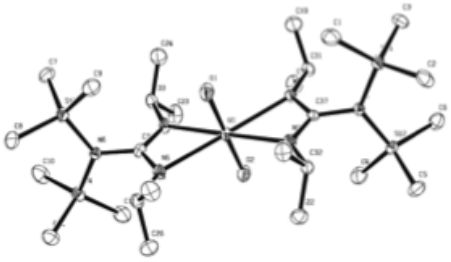

Figure 2. ORTEP diagram of **2**.

Crystals of **2** suitable for X-ray diffraction were grown from ether at -40 °C and confirm the structure analyzed from NMR spectroscopy (Figure 2). The uranyl unit remains almost linear (O1−U1−O2, 179.03°). The U-O bond lengths are typical for neutral complexes (1.769(3) Å and 1.774(3) Å).

Complexes of uranyl amidinates with both planar and non-planar equatorial coordination geometries have been reported. Four equivalents of amidinate salts are added to uranyl chloride to form uranyl bis(amidinate), and as many as three amidinate ligands can bond the uranyl cation with higher equivalent additions of amidinate salt. To further investigate the cause of the interesting ^{1}H NMR resonance of the isopropyl methine proton at 5.77 ppm of the uranyl bis(guanidinate) **2**, we turned to another NCN ligand class, amdinates. We synthesized a series of uranyl bis(amidinate) complexes containing isopropyl groups similar in design to **2**. Complex **4** was synthesized by the salt metathesis of uranyl chloride with a known lithium amidinate (Scheme 2). Although **4** was isolated cleanly, there was a considerable amount of the anionic "ate" complex in the raw product.

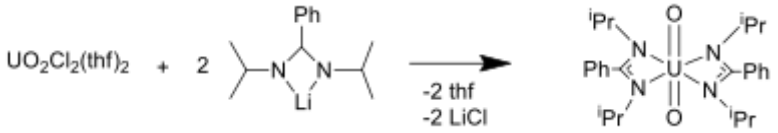

Scheme 2. Salt metathesis reaction to synthesize uranyl bis(amidinate) **4.**

To avoid the evolution of anion "ate" complexes, the uranyl bis(amidinate) compounds **5-7** were targeted by reaction of uranyl bisamide with a series of designed amidines (Scheme 3).

The trifluoromethyl-substituted complex **7** was isolated as a THF-adduct, containing one tetrahydrofuran molecule per complex when solvent was removed under high vacuum as observed by ^{1}H NMR. Both complexes **5** and **6** contained no THF when solvent was removed. Our inability to remove THF from **7** is likely because the trifluoromethyl-substitued amidinate groups do not donate enough electron density to the uranium center for it to release THF. By using electron-withdrawing (EWG) and electron-donating groups (EDG), we hope to tune the electron-donating ability of the amidinate ligands to the uranyl center. Doing this could affect the uranium-oxygen bond distances of uranyl as the uranium receives varying degrees of electron density from its equatorial ligands. Such differences in the U-O bonding would likely lead to differences in binding strength of Lewis acids bonding to the oxo moieties. The O=U=O symmetric stretches of the complexes would provide some basis for comparing how our tuning affects the uranyl oxo basicity. The O=U=O symmetric stretching frequencies of the uranyl bis(amidinate) complexes are higher than that of the uranyl bis(guanidinate). Overall, the stretching frequencies of the different complexes do not vary greatly, and it is likely they all have very similar U-O bond distances.

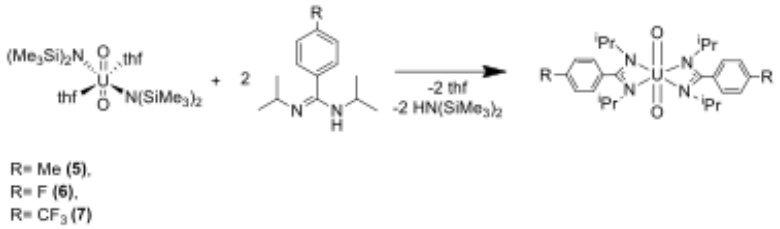

Scheme 3. Synthesis of complexes **5-7.**

Complex	δ (ppm vs. TMS) C*H*(Me)$_2$
Uranyl bis(guanidinate) complex	
2	5.77
Uranyl bis(amidinate) complexes	
5	5.42
4	5.34
6	5.11
7•thf	4.79

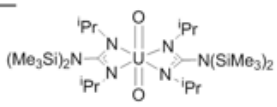

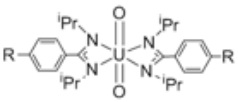

R= H **(4)**, Me **(5)**, F **(6)**, CF_3 **(7)**

Table 1. The ^{i}Pr methine ^{1}H NMR resonances of the uranyl bis(guanidinate) **2** and uranyl bis(amidinate) **4-7** complexes. The uranyl bis(amidinate) complexes are ordered from top to bottom by the decreasing electron-donating ability of their respective amidinate ligands.

Similar to the ^{1}H NMR resonance of the isopropyl methine protons in the uranyl bis(guanidinate), the isopropyl methine protons of the uranyl bis(amidinate) complexes all exhibit particularly downfield ^{1}H NMR resonances (Table 1).

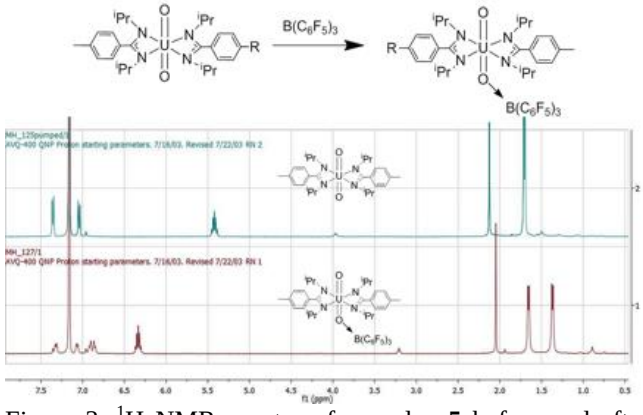

Figure 3. ^{1}H NMR spectra of complex **5** before and after coordination of strong Lewis acid.

The same guanidinate used in our experiment was used as a ligand on ytterbium by Weng et al. The reported resonance of the isopropyl methine proton in their complex Yb(guan)$_3$ was at 2.15 ppm, far upfield to our observed shift, with all other ^{1}H and ^{13}C NMR shifts being similar to our experimental values. Likewise, the lithium amidinate salt used to synthesize complex **4** produced a ^{1}H NMR isopropyl methine resonance at 3.00 ppm, noticeably upfield of that observed in the spectroscopy of **5**. The isopropyl methine

shifts of all our uranyl complexes showed heptets considerably downfield of those of similar compounds, even though the complexes are diamagnetic. It is likely the downfield resonances arise from spin-orbit (SO) effects from the heavy uranium nucleus. Kaupp et al. predicted hydrides bonded to U(VI) as having giant SO effects which were predicted to have ^{1}H NMR shifts as downfield as 146.4 ppm. Although these compounds have hydrogen nuclei directly bonded to uranium, we should and do see lesser spin-orbit coupling at the isopropyl methine protons. Due to a Fermi-contact type mechanism, we see downfield shifts at every atom at odd-numbered positions from the uranium center, and slight upfield shifts at every even-numbered position. Because the hydrogen nuclei are at a third position away from the uranium center, it follows that the isopropyl methine carbon should experience a slight upfield shift (2-4 ppm) as it is two positions from the heavy actinide.

Complex	δ (ppm vs. TMS) $CH(Me)_2$
Uranyl bis(guanidinate) adducts	
2·B(C$_6$F$_5$)$_3$	6.76
Uranyl bis(amidinate) adducts	
5·B(C$_6$F$_5$)$_3$	6.33
4·B(C$_6$F$_5$)$_3$	6.24

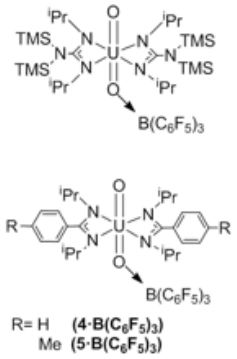

Table 2. The ^{i}Pr methine ^{1}H NMR resonances of uranyl complexes coordinated with B(C$_6$F$_5$)$_3$.

To probe the basicity of the oxo moieties in our uranyl complexes, we monitored their binding of the strongly acidic B(C$_6$F$_5$)$_3$ by ^{1}H NMR. This coordination was observable by ^{1}H and ^{19}F NMR spectroscopy even while the adducts were in benzene solution. Similar to the reaction reported by Sarsfield et al., the formation of the U=O-B bond is indicated by an immediate solution color change from bright red to deep magenta. Figure 3 shows the change in the NMR spectrum as an equimolar amount of B(C$_6$F$_5$)$_3$ is added to complex **5**.

Upon addition of B(C$_6$F$_5$)$_3$, there is a large downfield shift of the isopropyl methine hydrogen nuclei from 5.42 ppm to 6.33 ppm. This same downfield shift is present when other uranyl complexes coordinate with B(C$_6$F$_5$)$_3$ as depicted by Table 2.

The binding of the borane to the oxo moiety pulls electron density away from the uranium center, resulting in a contraction of the U-N bonds in the compounds. This phenomenon was observed by Sarsfield et al. and can be confirmed in the future by X-ray crystallography of the isolated borane adducts. Such a change seems to produce larger spin-orbit coupling of the uranium nucleus with the isopropyl methine hydrogen nuclei. Computed shifts (Peter Hrobárik/Kaupp group) of some of the compounds using PBE and PBE0 exchange-correlation functionals are shown in Table 3 along with their experimental SO coupling contributions.

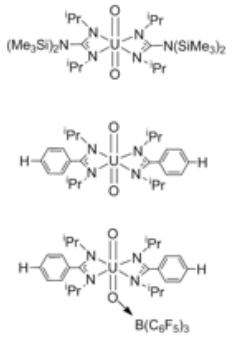

	PBE	PBE0	Expt.
	δ = 6.63 ppm δ_{SO} = 1.83 ppm	δ = 6.05 ppm δ_{SO} = 1.27 ppm	δ = 5.77 ppm
	δ = 6.19 ppm δ_{SO} = 2.20 ppm	δ = 5.21 ppm δ_{SO} = 1.36 ppm	δ = 5.34 ppm
	δ = 6.79 ppm δ_{SO} = 2.82 ppm	δ = 5.84 ppm δ_{SO} = 2.01 ppm	δ = 6.24 ppm

Table 3. Calculated (black) and experimental (green) ^{i}Pr methine ^{1}H NMR shifts (in ppm vs. TMS). The SO coupling contributions to their shift are displayed in red.

The spin-orbit effects on the isopropyl methine resonances are actually predicted computationally as well as their approximate downfield shifts. The computations also exhibit an

increase spin-orbit coupling upon coordination with borane. These relativistic effects are not fully understood, so our synthesized uranyl compounds may help to elucidate some characteristics of spin-orbit effects arising from heavy atoms.

Other Lewis acids could bind to the uranyl oxo much like the very acidic borane. The next compound used for the task was $Al(C_6F_5)_3$, a stronger electrophile than $B(C_6F_5)_3$. Multinuclear NMR spectroscopy (^1H, ^{19}F) indicated the triarylaluminum nucleophile successfully binded to the uranyl bis(amidinate) **5**. Although the same color change to deep magenta was observed, NMR spectroscopy revealed the evolution of minor products likely arising from the aluminum pulling off amidinate ligands. In the ^1H NMR spectrum, a heptet corresponding to the isopropyl methine was observed downfield at 6.48 ppm. It is worth noting that this shift is even further downfield of the isopropyl methine shift of the borane adduct **5·B(C_6F_5)$_3$**. This is likely due to higher SO coupling due to a shorter contraction of the N-U bonds.

Ligand Libraries for Uranyl Recognition (with the Francis Group, UC Berkeley)

In a new sub-project, we began work last fall with Professor Matt Francis to investigate a new means of addressing the concept of selectivity in uranyl binding. Previous reports have shown that near-perfect separation of the lanthanide ions can be achieved using HPLC supports that are chemically modified to display organic ligands. However, these examples have only been demonstrated on small samples (1 - 10 mg) using expensive packing materials and high pressure, preventing their use on industrial process scale. As a low-cost alternative simple cation exchange methods have been used to facilitate large-scale lanthanide purification, but these approaches would clearly benefit from increased resolving power. In the proposed work, we will work with the Francis group to generate efficient and durable chromatography supports for lanthanide separation by (1) identifying robust peptoid-based ligands capable of binding different lanthanides with variable affinities, and (2) developing practical synthetic methods for the attachment of these ligands to Dowex ion exchange resins. The success of these approaches will yield a series of cheap, durable, high-capacity supports capable of separating complex lanthanide mixtures using simple equipment that can be readily adapted from existing water purification technology. To accelerate the discovery process, we will instead prepare small libraries of support ligands and find the structures within it that have the greatest separation potential. The peptoid backbone (Figure 4) has been chosen for the first set of molecules to be evaluated, as these complex structures can be synthesized using efficient and inexpensive chemical strategies. Virtually any carboxylic acid or polyol group can be incorporated into these structures, and they are more resistant to bacterial degradation than natural peptides. The ligands comprising the library will present the uranyl ion with a widely varying collection of multidentate binders.

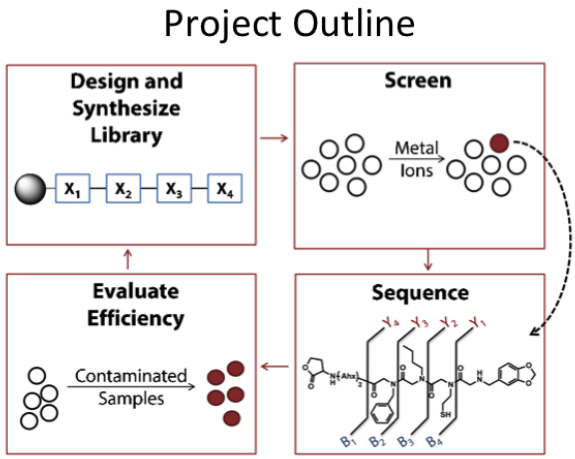

Francis, M. B., Finney, N. S., Jacobsen, E. N., *JACS*, **1996**, 118, 8983-4
Witus, L. S., Moore, T., Thuronyi, B. W., Esser-Kahn, A. P., Scheck, R. A., Iavarone, A. T., Francis, M. B., *JACS*, **2010**, 132, 16812-7

Experiments that have been used for peptoid libraries to bind other metals have been tested and adapted to investigate uranyl binding. Since the uranyl cation is not strongly colored, it is not possible to determine whether binding has occurred simply by visual inspection. We have used a dye, arsenazo III, to qualitatively determine whether uranyl is present within a peptoid bead, which can then be selected for sequencing.

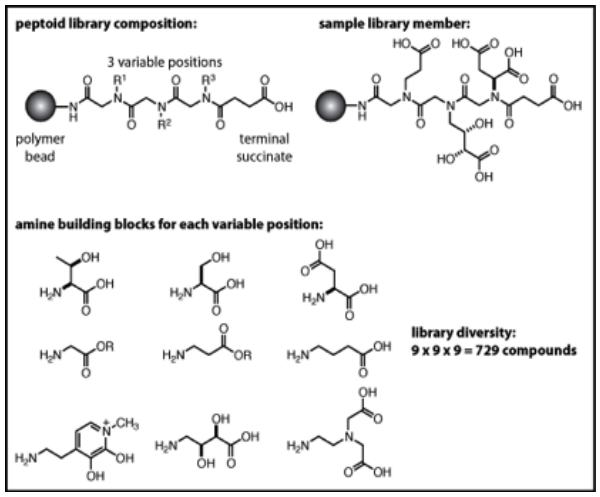

Figure 4. Design of a peptoid-based library of separation supports for lanthanide ions. Through the combination of nine possible amine building blocks in each of three variable positions, a variety of oxygen-rich ligands will be prepared on a solid support. These resins will then be evaluated for their ability to separate a lanthanide ion mixture.

A large library consisting of ten amines that has been tested with other metals has been used to investigate uranyl binding. From this, three hit sequences have been identified: butylamine – β-alanine – glycine – butylamine; piperonylamine – piperonylamine – β-alanine – β-alanine; piperonylamine – β-alanine – β-alanine – β-alanine.

Notably, there are only four amines present in these sequences, only two of which bind to uranyl (β-alanine and glycine; the other two, butylamine and piperonylamine, are just sterics).

The third sequence has been synthesized on a larger scale and cleaved from the polymer bead. The free peptoid will be used to determine binding constants using fluorescence spectrometry, by varying the uranyl concentration in a solution containing the peptoid to determine what fraction is bound. UV-Vis spectrometry has been tested, but it is very difficult to see such low uranyl concentrations due to its weak absorption.

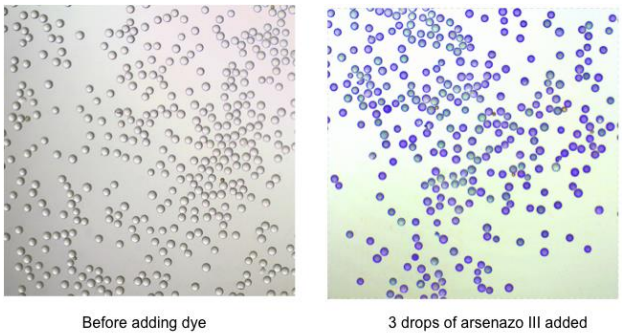

Binding seen in 2 mM uranyl acetate

Using data from the binding experiments as well as molecular modeling, we hope to determine what could improve upon the peptoid sequences and library. Changing the length of the sequence, incorporating different amines, and (possibly) changing the amide backbone length to increase spacing between peptoid amines will be investigated for optimization of the peptoid sequences to attempt binding with lower concentrations of uranyl.

Future Work

Coordination of uranyl with NCN ligands

- Complete Lewis acid binding studies to uranyl amidinates/guanidinates
- Conclude computational studies regarding low-field NMR shifts of amidinate methine signals

Ligand Libraries for Uranyl Recognition

- Initiate modeling studies on first generation of hits
- Scale up of hit molecules for synthesis and characterization of binding mode(s) to uranyl ion
- Expand libraries to new donor sets
- Begin work on transuranics (in collaboration with Seaborg Center, LBNL)

Development of Novel Sorbents for Uranium Extraction from Seawater

Wenbin Lin – University of North Carolina at Chapel Hill

Background and Significance

The oceans contain ~4.5 billion tons of uranium (U) at a concentration of ~3 ppb, which is one thousand times the amount of U in terrestrial ores. Development of technologies to recover the U from seawater would greatly improve the U resource availability, sustaining the fuel supply for nuclear energy. Several methods have been previously evaluated including solvent extraction, ion exchange, flotation, biomass collection, and adsorption; however, none have been found to be suitable for reasons such as cost effectiveness, long term stability, and selectivity. While polymer beads and fibers have been functionalized with amidoxime functional groups to afford U adsorption capacities as high as 1.5 g U/kg, [1] further improvements are needed to make U extraction from seawater economically feasible.

Recent research has focused on amidoximes as promising candidates for U sorption, due in large part to previous screening of numerous polymers functionalized with organic chelating moieties, particularly derivatives of carboxylic acids. [2, 3] Phosphorus-based ligands such as tributyl phosphate and carbamoylmethylphospine oxide (CMPO) are also known to complex strongly to U in decontamination processes, [4-6] but it is not clear to what extent these sorbents were investigated. Furthermore, despite employment of various polymers in the study, there was no discussion of the effect of support matrix on U uptake. [2] Lacking a rigorous, direct comparison of potential sorbent groups on an identical support remains a significant hindrance to the development of efficient uranyl sorbents.

Since the pioneering work of uranyl extraction with amidoxime-containing polymers, there have been many breakthroughs in nanostructured materials. The advances in nanoporous materials present new opportunities in preparing new sorbents for U extraction. The objective of this research is to develop advanced sorbents for U extraction, specifically focused on the development of porous supports with selective binding sites for uranyl ions. Nanostructured porous supports have several key properties making them appealing for use in this area, including large surface areas, high binding site densities, and enhanced mass transport properties. These characteristics will allow for superior uranyl sorption kinetics and extraction capacities, in addition to facilitating uranyl stripping and recovery. [7]

Mesoporous silica nanoparticles (MSNs) and mesoporous carbon nanoparticles (MCNs) have attracted attention due to possessing large surface area, tunable pore volume and size, and facile modification through surface functionalization. These characteristics have made MSNs and MCNs ideal for a variety of applications. [8-21] Despite significant interest, comprehensive studies and direct comparisons of uranyl extraction with organo-functionalized MSNs and MCNs have not been carried out. Furthermore, of the studies available in the literature, the use of different porous supports, unrealistically high U concentrations, an absence of competing ions, and irrelevant pH values are often encountered, yielding unreliable sorption values. MSNs and MCNs can be easily functionalized with a library of organic moieties and tested for uranyl sorption under relevant conditions, providing the much-needed comparison between organic functional groups and establishing a baseline for the development of new generations of sorbents. In-depth characterization will provide insight to the relationships between porosity, saturation capacity, and sorption kinetics, allowing the tuning of mesoporous platforms to optimize uranyl binding.

Though numerous platforms have been functionalized and investigated for uranyl extraction, little attention has been directed to the influence of the support structure on sorption of uranyl with organo-functionalized materials. Polymers, MSNs, and MCNs are poorly ordered with no way of investigating

the uranyl-binding environment, inhibiting detailed investigations of structure-activity relationships. In fact, pre-treatments of amidoxime fibers with KOH solutions are known to enhance extraction of U, presumably due to the formation of an adjacent carboxylic acid, [22-24] but precise knowledge of the binding environment cannot be obtained with poorly-ordered materials. In contrast, metal-organic frameworks (MOFs) are highly porous crystalline materials formed from metal connecting points and organic bridging ligands, allowing precise characterization of binding groups. MOFs provide a readily tunable platform for incorporating desired functionalities, such as organic groups with strong uranyl affinity. Furthermore, by increasing the length of bridging ligands, pore apertures can be adjusted to control access to the sorbent groups inside the MOF channels. MOFs are capable of achieving much higher loading capacities than other functionalized materials as the ligand is part of the structure, rather than merely grafted onto the surface of a heterogeneous support.

Due to their ordered structure and uniform binding environments, MOFs are uniquely suited for investigating the influence of support structure on uranyl extraction. Through ligand synthesis, MOF materials can be designed to afford cooperative interaction between sorbent groups for uranyl binding.

Due to their large surface areas and highly accessible channels, nanomaterials have potential to greatly surpass polymeric braids as the state-of-the-art sorbents. Our objective was to prepare a wide range of nanostructured sorbents including MSNs, MCNs, and MOFs for use in uranyl extraction. These platforms allow rapid screening of ligands on a consistent support, facilitating direct comparison of various organic functional groups under common conditions. Furthermore, using MOFs as model systems, the binding environments for uranyl can be investigated and optimized, providing much needed insight and affording significant advances in developing sorbents with cooperative binding functions.

R&D Progress / Status

Mesoporous Silica Nanoparticles (MSNs)

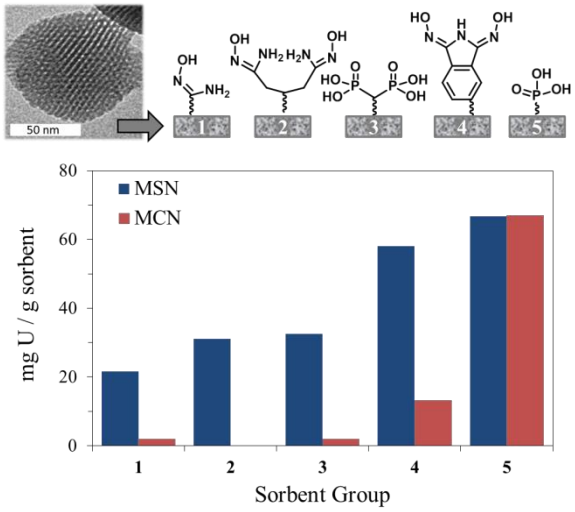

Figure 1: Representative functional groups grafted to MSNs and MCNs using various linkers. Bar graph denotes results of uranyl sorption from seawater simulant for MSN (blue) and MCN (red) materials.

In an effort to provide a scientifically rigorous screening of various ligands for uranyl extraction, a series of amidoxime-, imide dioxime-, phosphonate-, and carboxylate functional groups were grafted onto MSN through condensation with a triethoxysilyl functional group. The library of organic functions was selected based on previous research alluding to their utility in uranyl binding. Previous reports have detailed the capability of amidoxime, [1-3] while recent studies have demonstrated a cyclized imide dioxime to be capable for competing with carbonate for U-binding. [24, 25] Several phosphate-derived ligands were prepared as well, in consideration of their use in complexing actinides for decontamination and reprocessing of nuclear waste streams. [4-6, 26, 27]

The functionalized MSNs were characterized by nitrogen-uptake to determine surface area and pore size distribution, ζ-potential to determine surface charge, and thermogravimetric analysis (TGA) to determine loading of sorbent groups. TGA results

indicate grafting densities of 0.75 to 1.38 mmol/g for the functionalized MSNs, while Brunauer-Emmett-Teller (BET) surface areas range from 186.4 to 526.0 m^2/g, with average pore diameters of 3.8 to 7.8 nm.

Sorption properties of the functionalized MSNs were investigated in water and artificial seawater at pH 8.3. In water, all sorbents showed high uranyl sorption capacity at equilibrium (q_e) ranging from 40 to 50 mg U/g sorbent. However, in artificial seawater the amount of U extracted was reduced at least four-fold, with q_e values between 2 – 13 mg U/g sorbent. A phosphonate-functionalized MSN, MSN-5, exhibits the greatest sorption in seawater, statistically equivalent to amidoxime fibers tested under similar conditions (10.5 mg U/g). While amidoxime-derived MSNs generally performed better than other materials, they did not perform as well as the amidoxime fiber, suggesting simple coordination of uranyl to amidoxime may not be the primary binding mechanism.

For the six materials with highest q_e values, sorption kinetics and sorption isotherms were obtained, with fitting to a Langmuir model allowing calculation of saturation sorption capacity. In water, all materials except MSN-5 had similar saturation capacities. As the unfunctionalized MSN can only extract U by physisorption, it is highly likely nonspecific binding is the primary mode of U extraction for most materials. In contrast, MSN-5 demonstrates a significantly higher saturation capacity than any other sorbent. Isotherms obtained in seawater more closely replicated environmental conditions and also moderated physisorption of U due to competing ions. MSN-5 also had the highest saturation capacity (66.7 mg U/g), followed by the cyclic imide dioxime-functionalized MSN (58.1 mg U/g).

Table 1. Physical Properties and Sorption Capacities for Organo-Functionalized MSN and MCN

	MSN			MCN		
Functional Group	BET Surface Area (m^2/g)	Loading (mmol/g)	$q_{e(max)}$ (mg/g)	BET Surface Area (m^2/g)	Loading (mmol/g)	$q_{e(max)}$ (mg/g)
None	648	---	43.1	189	---	---
1	494	1.09	21.6	109	0.83	2.0
2	526	1.02	31.1	N/A	N/A	N/A
3	253	1.02	32.5	122	0.29	2.0
4	277	1.32	58.1	148	1.82	13.1
5	406	0.82	66.7	154	0.28	67.0

This screening of organo-functionalized MSNs was the first to provide a direct comparison of different sorbent groups on a common support. Sorption isotherms revealed two functional groups to be superior to amidoxime for uranyl sorption in water and seawater. This research suggests organo-functionalized MSNs are promising alternatives for U extraction from seawater, and was recently accepted for publication in *Microporous and Mesoporous Materials*. [28]

Mesoporous Carbon Nanoparticles (MCNs)

MCNs not only possess high surface area and large pore volume, but are also robust under harsh conditions and show negligible background sorption. Surface functionalization of MCNs with organic moieties has been accomplished by inclusion during synthesis [29] or by post-synthesis grafting, where a covalent bond is formed between the MCN and a diazonium generated *in situ*. [30-32] We employed the latter method to graft simple aniline molecules *para*-substituted with amidoxime, phosphoryl, or carboxyl groups onto a commercially available MCN support. Additionally, several materials were prepared possessing two different sorbent groups in an effort to assess if any cooperative effects could be achieved.

The functionalized MCNs were characterized by nitrogen uptake and TGA. TGA profiles reveal loading ranging from 0.13 to 1.82 mmol/g, while nitrogen sorption isotherms yielded BET surface areas ranging from 189 m^2/g to 93 m^2/g. The functionalized MCNs were tested for U sorption from seawater simulant

(pH 8.2) and an aqueous solution representative of acid mine drainage (pH 4). In acidic solution cyclic imide dioxime material absorbed more than the simple amidoxime-functionalized MCN, though co-grafting with carboxyl groups significantly increased sorption of both materials. When loading is considered, the co-grafted materials absorb a greater amount of U per sorbent group than either functional group when grafted in isolation, possibly indicating cooperative binding interactions. Phosphorylation of the starting material produced the material with the greatest sorption capacity, MCN-5, which is particularly remarkable as it also had one of the lowest loadings, with 96% of phosphoryl moieties coordinated by U. In seawater simulant U sorption decreased for all materials. This is expected due to the competition with other ions and the formation of the highly stable uranyl carbonate ion. MCN-5 again had the highest sorption, with 75% of all binding sites occupied, and was further investigated by obtaining the sorption isotherm and investigating sorption kinetics and pH dependence.

Sorption isotherms were obtained in both acidic water and seawater simulant, with data represented well by the Langmuir model. Saturation capacities for the phosphorylate material were 97 mg U/g sorbent and 67 mg U/g sorbent in acidic water and seawater simulant, respectively. Sorption kinetics were investigated under both conditions as well, showing rapid initial uptake with the majority of U absorbed in the first 5 minutes, followed by a slower second step reaching equilibration. These steps could be attributed to sorption at readily available binding sites on or near the surface, with subsequent sorption resulting from diffusion of U through the pores to interior sorbent groups. In acidic water, uranyl sorption was pseudo-first order, while pseudo-second order modeling better fit data from seawater simulant.

These studies indicate phosphorylated MCN materials show great promise as uranyl sorbents, but improvements in binding site density and hydrophilicity are direly needed. A manuscript describing this research is currently in preparation.

Metal-Organic Frameworks (MOFs)

Encouraged by results obtained from bifunctionalized MCN materials, a tunable, ordered system was needed in order to probe cooperative binding effects. As discussed previously, MOFs are crystalline materials with precise structural determination available by x-ray crystallographic techniques. Investigation of known topologies coupled with precise ligand functionalization affords design of MOFs for various applications. To extract uranyl from aqueous media, UiO-68-NH_2, a highly stable MOF with Zr-oxo cluster secondary building units (SBUs) and amino-functionalized triphenyl-dicarboxylate bridging ligands, was selected as the initial scaffold. [33] The single crystal structure of UiO-68-NH_2 revealed a torsional disorder of the central aromatic ring, orienting the orthogonal amino group into adjacent tetrahedron. [34] Upon functionalization with a sorbent moiety, these tetrahedral structures form binding pockets for uranyl extraction.

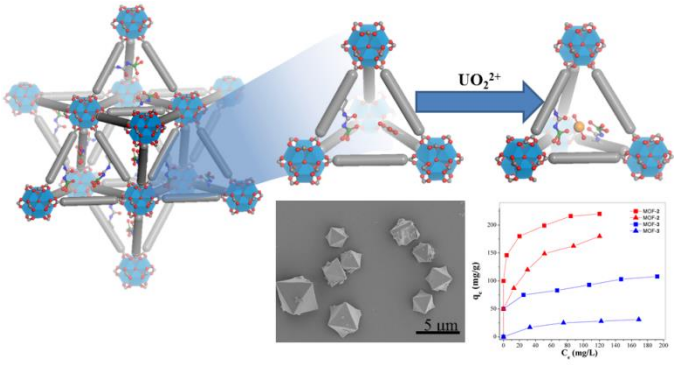

Figure 2: Depiction of observed uranyl-coordinating pocket in MOF tetrahedron. Inset: SEM image of MOF and sorption isotherm in water (squares) and simulated seawater (triangles) for two different functional groups.

The triphenyl bridging ligand was functionalized by condensation with diethoxyphosphinyl isocyanate to form a diethoxy phosphorylurea group orthogonal to the Zr-coordinating carboxylic acids. Similar to the

well-known carbamoylphosphine oxides used to extract actinides in the TRUEX process, the phosphorylurea functional group has been published as capable of complexing actinides and lanthanides. [27] The resulting MOF possessed sorbent groups converging in the tetrahedral cavities to create a binding pocket, allowing cooperative interactions for the extraction of uranyl. Subsequent post-synthetic modification of the functionalized MOF to remove the ethoxy protecting groups yielded a second MOF to investigate for uranyl extraction. The unfunctionalized UiO-68 was also tested as a negative control.

MOFs were characterized by nitrogen adsorption, dye-uptake, TGA, powder x-ray diffractommetry (PXRD), and scanning electron microscopy (SEM). SEM images revealed distinct octahedral crystals for all three MOFs, with dimensions of approximately 2-3μm per side. TGA curves indicated distinct onset temperature for framework decomposition to ZrO_2, consistent with literature values for UiO MOFs. PXRD patterns for all three pristine MOFs as well as MOFs following uranyl sorption studies matched simulated patterns with high angle peaks beyond 2θ of 30°, indicative of highly crystalline structures. The MOFs are highly porous with BET surface areas of up to 2935 m^2/g. Dye uptake with Brilliant Blue and Eosin Y dye unequivocally demonstrated the accessibility of the MOF channels to large molecules.

U sorption experiments were performed at pH 2.5 in water and seawater simulant with U concentrations of 5 ppm and 100 ppm, revealing both functionalized MOFs to have strong affinity for U. The unfunctionalized UiO-NH_2 showed no U uptake. Elution studies with 0.01 M HCl show negligible U is removed from the MOFs, suggestive of specific binding by the organic functions, while amidoxime fiber control samples showed near complete elution.

Sorption isotherms for both ethoxy-protected and deprotected MOFs in water and seawater revealed sorption capacities as high as 217 mg U/g MOF. In comparison, amidoxime-based resin had saturation capacity of 54 mg under similar conditions. [35] Investigation of the possible coordination geometries by Density Functional Theory (DFT) calculations revealed the enthalpically preferred binding motif to be monodentate coordination to two phosphoryl oxygen. Wiberg bond indices were consistent with covalent bonding, and localized MOs clearly display bonding interactions between U and the phosphoryl oxygen. Application of the preferred binding motif to the observed saturation capacity for the MOFs indicates complete saturation for the ethoxy protected MOF, with one U binding to every two sorbent groups. The deprotected MOF showed slightly lower sorption efficiency, one U binding to every 4.5 groups.

This research was recently published in *Chemical Science* [36] and highlighted in *Chemical & Engineering News* [37] as well as the *MIT Technology Review*. [38]

Summary

Over the past 1.5 years of research, our group has made several significant discoveries which have great potential in advancing development of technologies to extract U from seawater. A series of organo-functionalized MSNs, MCNs, and MOFs have been prepared, characterized, and investigated for uranyl sorption. Screening studies with a library of organic functions on the same sorbent platform confirm the suitability of the amidoxime functional group, but also consistently indicate simple phosphoryl groups to be superior. Sorption isotherms, kinetic investigations, and elution studies further reveal physisorption to be a significant contributor for amidoxime fibers and functionalized MSNs, though not for MCNs or MOFs. Investigation of sorption in seawater simulant results in a significant reduction in sorption capacity for all sorbents, though effects for certain functional moieties (cyclic imide dioxime, phosphorylurea, phosphate) are less drastic than for others, indicative of selectivity and strong uranyl coordination. Investigation of a phosphorylated MCN material revealed distinct pH dependence,

correlating with pK_a of phosphoric acid and presumably the isoelectric point of the material. Extrapolation of this finding, particularly in conjunction with known base pre-treatements of amidoxime sorbents, are useful in elucidating the binding mechanism of sorbent groups and the rational design of second-generation functional groups. MOFs were reported as platforms for uranyl sorption for the first time, and used as a model system to investigate the effects of ligand cooperation in uranyl extraction. Crystallographic data revealed the formation of a uranyl-binding pocket with inter-sorbent distances appropriate for cooperative binding, and DFT calculations indicate coordination by two sorbent groups to be enthalpically preferred. The synergistic effects of high surface area coupled with formation of a binding pocket yielded some of the highest saturation capacities reported to date.

Future Work

Year 1:

- Seawater testing of phosphonate-based MCN sorbents
  Tests in seawater simulant indicate the phosphonate-functionalized MCNs to be superior to other reported MCN materials. We intend to collaborate with Pacific Northwest National Lab to design a flow-through sorption apparatus and perform subsequent seawater testing for these nanomaterials.
- DFT screening of phosphonate- and amidoxime-containing bifunctional chelators
  Bifunctional chelators will be designed to encourage cooperative interactions with uranyl. Initial screening will be done by DFT to maximize throughput and minimize cost.
- Synthesis and characterization of promising bifunctional ligands grafted to MSNs
  Facile surface-functionalization of MSN affords rapid experimental screening of ligands identified by DFT as potential sorbents.
- Preparation of MOFs with different metal connecting points and bridging ligands
  Substitution of metal connecting points and bridging ligands affords diverse framework morphologies. Improvements in hydrophilicity and charge density will also be investigated by systematic variation of substituents on bridging ligands.

Year 2:

- Incorporation of bifunctional ligands into MOFs
  Promising bifunctional ligands identified with MSNs will be translated to MOFs to investigate and tune their influence in cooperative binding interactions.
- Investigation of uranyl sorption as a function of MOF physical structure
  Previously prepared MOFs will be functionalized with sorbent groups. Using MOFs with various pore shape and dimensions will elucidate their influence on uranyl affinity and selectivity.
- Seawater testing of MOF-based sorbents
  Preparation of MOFs which are stable under environmental conditions will accommodate seawater testing using the flow-through apparatus used to test MCNs.

Year 3:

- Collaborate with other researchers on nanocomposite processing
  Deployment of nanomaterials remains a challenge for commercialization. Various processing techniques will be investigated to ensure advantages of nanomaterials are maintained.
- Collaborate with other researchers to study uranyl extraction from seawater using nanocomposites
  Incorporation of promising sorbents into nanocomposites will be completed, with nanomaterial monoliths applied to large-scale environmental studies.

[1] M. Tamada, Technology of uranium recovery from seawater, Journal of the Japan Institute of Energy, 88 (2009) 249-253.
[2] H.J. Schenk, L. Astheimer, E.G. Witte, K. Schwochau, Development of Sorbers for the Recovery of Uranium from Seawater. 1. Assessment of Key Parameters and Screening Studies of Sorber Materials, Sep. Sci. Technol., 17 (1982) 1293-1308.
[3] L. Astheimer, H.J. Schenk, E.G. Witte, K. Schwochau, Development of Sorbers for the Recovery of Uranium from Seawater. Part 2. The Accumulation of Uranium from Seawater by Resins Containing Amidoxime and Imidoxime Functional Groups, Sep. Sci. Technol., 18 (1983) 307-339.
[4] K.L. Nash, A Review of the Basic Chemistry and Recent Developoments in Trivalent f-Elements Separations, Solvent Extr. Ion Exch., 11 (1993) 729-768.
[5] G. Ionova, S. Ionov, C. Rabbe, C. Hill, C. Madic, R. Guillaumont, J.C. Krupa, Mechanism of Trivalent Actinide/Lanthanide Separation using Bis(2,2,4-Trimethylpentyl) Dithiophosphinic Acid (Cyanex 301) and Neutral O-Bearing Co-Extractant Synergistic Mixtures, Solvent Extr. Ion Exch., 19 (2001) 391-414.
[6] G.J. Lumetta, A.V. Gelis, G.F. Vandegrift, Review: Solvent Systems Combining Neutral and Acidic Extractants for Separating Trivalent Lanthanides from the Transuranic Elements, Solvent Extr. Ion Exch., 28 (2010) 287-312.
[7] P. Makowski, X. Deschanels, A. Grandjean, D. Meyer, G. Toquer, F. Goettmann, Mesoporous materials in the field of nuclear industry: applications and perspectives, New J. Chem., 36 (2012) 531-541.
[8] G.E. Fryxell, Y. Lin, S. Fiskum, J.C. Birnbaum, H. Wu, K. Kemner, S. Kelly, Actinide Sequestration Using Self-Assembled Monolayers on Mesoporous Supports, Environ. Sci. Technol., 39 (2005) 1324-1331.
[9] H.I. Lee, J.H. Kim, J.M. Kim, S. Kim, J.-N. Park, J.S. Hwang, J.-W. Yeon, Y. Jung, Application of ordered nanoporous silica for removal of uranium ions from aqueous solutions, J. Nanosci. Nanotechnol., 10 (2010) 217-221.
[10] L.-Y. Yuan, Y.-L. Liu, W.-Q. Shi, Y.-L. Lv, J.-H. Lan, Y.-L. Zhao, Z.-F. Chai, High performance of phosphonate-functionalized mesoporous silica for U(VI) sorption from aqueous solution, Dalton Trans., 40 (2011) 7446-7453.
[11] Y. Liu, L. Yuan, Y. Yuan, J. Lan, Z. Li, Y. Feng, Y. Zhao, Z. Chai, W. Shi, A high efficient sorption of U(VI) from aqueous solution using amino-functionalized SBA-15, J. Radioanal. Nucl. Chem., 292 (2012) 803-810.
[12] L.-Y. Yuan, Y.-L. Liu, W.-Q. Shi, Z.-j. Li, J.-H. Lan, Y.-X. Feng, Y.-L. Zhao, Y.-L. Yuan, Z.-F. Chai, A novel mesoporous material for uranium extraction, dihydroimidazole functionalized SBA-15, J. Mater. Chem., 22 (2012) 17019-17026.
[13] J.C. Birnbaum, B. Busche, Y. Lin, W.J. Shaw, G.E. Fryxell, Synthesis of carbamoylphosphonate silanes for the selective sequestration of actinides, Chem. Commun., (2002) 1374-1375.
[14] X. Wang, G. Zhu, F. Guo, Removal of uranium (VI) ion from aqueous solution by SBA-15, Annals of Nuclear Energy, 56 (2013) 151-157.
[15] A. Walcarius, L. Mercier, Mesoporous organosilica adsorbents: nanoengineered materials for removal of organic and inorganic pollutants, J. Mater. Chem., 20 (2010) 4478-4511.
[16] P.J. Lebed, K. de Souza, F. Bilodeau, D. Lariviere, F. Kleitz, Phosphonate-functionalized large pore 3-D cubic mesoporous (KIT-6) hybrid as highly efficient actinide extracting agent, Chem. Commun. (Cambridge, U. K.), 47 (2011) 11525-11527.
[17] P.J. Lebed, J.-D. Savoie, J. Florek, F. Bilodeau, D. Larivière, F. Kleitz, Large Pore Mesostructured Organosilica-Phosphonate Hybrids as Highly Efficient and Regenerable Sorbents for Uranium Sequestration, Chem. Mater., (2012).
[18] R. Ryoo, S.H. Joo, M. Kruk, M. Jaroniec, Ordered mesoporous carbons, Adv. Mater., 13 (2001) 677-681.

[19] G. Tian, J.X. Geng, Y.D. Jin, C.L. Wang, S.Q. Li, Z. Chen, H. Wang, Y.S. Zhao, S.J. Li, Sorption of uranium(VI) using oxime-grafted ordered mesoporous carbon CMK-5, J. Hazard. Mater., 190 (2011) 442-450.
[20] Y.Q. Wang, Z.B. Zhang, Y.H. Liu, X.H. Cao, Y.T. Liu, Q. Li, Adsorption of U(VI) from aqueous solution by the carboxyl-mesoporous carbon, Chem. Eng. J., 198 (2012) 246-253.
[21] J. Gorka, R.T. Mayes, L. Baggetto, G.M. Veith, S. Dai, Sonochemical functionalization of mesoporous carbon for uranium extraction from seawater, Journal of Materials Chemistry A, 1 (2013) 3016-3026.
[22] H. Sodaye, S. Nisan, C. Poletiko, S. Prabhakar, P.K. Tewari, Extraction of uranium from the concentrated brine rejected by integrated nuclear desalination plants, Desalination, 235 (2009) 9-32.
[23] A. Zhang, T. Asakura, G. Uchiyama, The adsorption mechanism of uranium(VI) from seawater on a macroporous fibrous polymeric adsorbent containing amidoxime chelating functional group, React. Funct. Polym., 57 (2003) 67-76.
[24] S.O. Kang, S. Vukovic, R. Custelcean, B.P. Hay, Cyclic Imide Dioximes: Formation and Hydrolytic Stability, Industrial & Engineering Chemistry Research, 51 (2012) 6619-6624.
[25] G. Tian, S. Teat, Z. Zhang, L. Rao, Sequestering uranium from seawater: binding strength and modes of uranyl complexes with glutarimidedioxime, Dalton. Trans., (2012).
[26] M.J. Hudson, L.M. Harwood, D.M. Laventine, F.W. Lewis, Use of Soft Heterocyclic N-Donor Ligands To Separate Actinides and Lanthanides, Inorg. Chem., (2012).
[27] E. Matrosov, E. Goryunov, T. Baulina, I. Goryunova, P. Petrovskii, E. Nifant'ev, First complexes of <i>N -diphenylphosphorylureas with actinides and lanthanides: Synthesis and structure, Doklady Chemistry, 432 (2010) 136-139.
[28] J.L. Vivero-Escoto, M. Carboni, C.W. Abney, K.E. deKrafft, W. Lin, Organo-functionalized Mesoporous Silicas for Efficient Uranium Extraction, Microporous Mesoporous Mater., Accepted (2013).
[29] C.D. Liang, Z.J. Li, S. Dai, Mesoporous carbon materials: Synthesis and modification, Angewandte Chemie-International Edition, 47 (2008) 3696-3717.
[30] A. Stein, Z.Y. Wang, M.A. Fierke, Functionalization of Porous Carbon Materials with Designed Pore Architecture, Adv. Mater., 21 (2009) 265-293.
[31] Z. Li, S. Dai, Surface Functionalization and Pore Size Manipulation for Carbons of Ordered Structure, Chem. Mater., 17 (2005) 1717-1721.
[32] Z.J. Li, W.F. Yan, S. Dai, Surface functionalization of ordered mesoporous carbons - A comparative study, Langmuir, 21 (2005) 11999-12006.
[33] J.H. Cavka, S. Jakobsen, U. Olsbye, N. Guillou, C. Lamberti, S. Bordiga, K.P. Lillerud, A New Zirconium Inorganic Building Brick Forming Metal Organic Frameworks with Exceptional Stability, J. Am. Chem. Soc., 130 (2008) 13850-13851.
[34] A. Schaate, P. Roy, A. Godt, J. Lippke, F. Waltz, M. Wiebcke, P. Behrens, Modulated Synthesis of Zr-Based Metal–Organic Frameworks: From Nano to Single Crystals, Chem. Eur. J., 17 (2011) 6643-6651.
[35] F. Vernon, T.W. Kyffin, Chelating ion-exchangers containing n-substituted hydroxylamine functional groups: Part V. Iron, copper, and uranium separations on Duolite CS-346 resin, Anal. Chim. Acta, 94 (1977) 317-322.
[36] W. Lin, M. Carboni, C. Abney, S. Liu, Highly porous and stable metal-organic frameworks for uranium extraction, Chem. Sci., (2013).
[37] M. Jacoby, Soaking Up Uranium, Chemical & Engineering News, 91 (2013) 8.
[38] M. Orcutt, Novel Material Shows Promise for Extracting Uranium from Seawater, MIT Technology Review, Cambridge, MA, 2013.

Functionalized High Molecular Weight Chitinous Nanofibers from Direct Extraction of Shrimp Shells for Novel Uranium from Seawater Sorbents

PI: Robin D. Rogers
Center for Green Manufacturing and Department of Chemistry
The University of Alabama, Tuscaloosa, AL 35487

Background and Significance:

With the worldwide energy crisis, a great deal of attention is being direct towards extracting uranium from seawater. Though uranium exists in a low 3 ppb concentration, the world's oceans hold almost 1000 times more uranium than that of all known terrestrial reserves.[1,2] With the array of other ions present in seawater, a highly selective extractant is necessary. After several decades of research it was determined that the amidoxime moiety $C(NH_2)(=NOH)$ was the most appropriate for the extraction of uranium from seawater.[3,4] Research has since been primarily aimed at grafting the amidoxime moiety onto polyethylene polymers and refining their properties such as molecular weight, surface area, and degree of functionalization in order to increase their capacity for uranium extraction.[5,6] However, these efforts address neither the environmental effects of using non-biodegradable, plastic fibers nor the energy intensive and expensive process of producing and modifying them. A cost analysis in regards to the latter indicates that the adsorbent comprises 43% of the total cost for extracting uranium from seawater.[7]

In order to make such a process economically and environmentally feasible, the adsorbent must be made of an inexpensive, durable, and renewable material with a high affinity for uranium. One such natural material that has received attention for extraction of uranium from seawater is chitin, a linear amino polysaccharide composed of β (1→4) linked 2-acetamido-2-deoxy-β-D-glucose units (Figure 1) found in the outer skeleton of arthropods and which is the second most plentiful natural polymer after cellulose.[8] Its bioactivity, biocompatibility, and low toxicity, as well as its ability to absorb both metal ions and hydrophobic organic compounds make it useful in waste water processing and other industrial applications.[9] However, due to its high density of hydrogen bonds, it is completely insoluble in water, most organic solvents, and dilute acidic or basic solutions and thus the applications of chitin have not been fully exploited. Various chemical modifications have been applied to make chitin more easily soluble,[10] the most important of which is *N*-deacetylation to form chitosan (Figure 1).

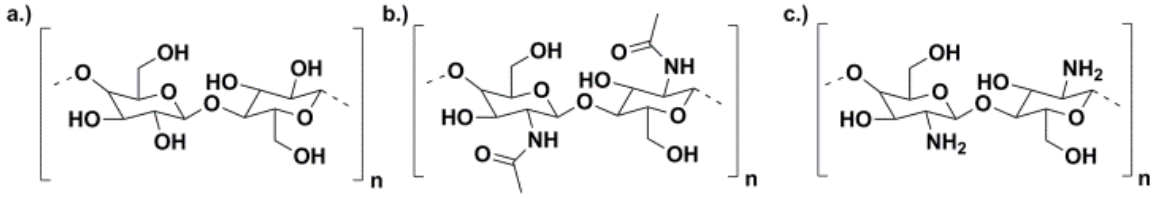

Figure 1 The structures of cellulose (a), chitin (b), and chitosan (c).

Chitin is a very attractive material for the purpose of extracting metal ions, including uranium, for a number of reasons. Materials made from high molecular weight chitin are strong, water insoluble, and microbe-resistant, and *these properties increase with increasing chitin chain length.* From an environmental and energy-conservation standpoint, chitin is almost matchless – it is a renewable resource available from shellfish wastes produced by the seafood industry. The use of a waste product rather than a nonrenewable commodity represents an energy gain and materials from chitin would be expected to have low environmental impact. Chitin can be obtained commercially in pure grade or practical grade (PG-chitin). PG-chitin is primarily produced by a chemical method that involves acid demineralization of the shell, followed by removal of shell proteins by alkali treatment, and then decolorization.[11] It can be further purified by methanesulfonic acid treatment[12] to obtain pure chitin. In those cases where chitin fibers have been produced, commercial chitin powder has been used with solvent systems such as (1) halogenated solvents (e.g., trichloroacetic acid (TCA), dichloroacetic acid (DCA),[13] or formic acid-DCA mixtures,[14] or (2) amide-LiCl systems (e.g., N,N-dimethylacetamide (DMAc)/5% LiCl).[15] Even though the current industrialized chemical process isolates chitin efficiently, the chitin molecular weight (MW) is

reduced during processing.[2] Furthermore, these methods include the use of many chemicals and steps, increasing cost.

In recent years, ionic liquids (ILs), defined as salts that melt at or below 100 °C[16], have been reported to completely dissolve cellulose,[17] lignocellulosic biomass (wood),[18] and many others biopolymers[19 20] s[21 22,23] with high efficiency and no need for extensive processing or harsh-conditions. In 2010, the Rogers Group found that 1-ethyl-3-methylimidazolium acetate ([C_2mim][OAc]) readily dissolves PG-chitin and extracts chitin from raw crustacean shells.[24] The chitin recovered from shells exhibits higher purity and higher MW than chitin obtained from industrial processes. In addition, microwave heating is more efficient than oil bath heating in dissolving chitinous biomass. Using the microwave method at least 94% of the available chitin in shrimp shells can be extracted with total irradiation times measured in minutes. Even more exciting, chitin fibers can be spun directly from the solution prepared with shrimp shells using the same dry-jet wet spinning method successfully employed for producing cellulose fibers from IL solution.[25] Thus, chitin fibers can be spun from shrimp shells in a one-pot process.

The key goal of this research program is to develop an efficient and cost effective chitin-based sorbent for uranium from seawater prepared from shellfish waste. Using the unprecedented control over chitin fiber production made possible by this process, we are grafting uranium selective moieties onto high-surface area chitin fibers. Advantages of this approach include 1) saving energy over the current industrial processes by directly obtaining the chitin from shellfish waste, 2) the potential for continuous processing of high surface area nanofibers in an economical operation, 3) a unique, high molecular weight chitin not available from the current industrial process which may lead to a stronger, more durable adsorbent, and 4) easy chemical modification of the large surface area adsorbent with uranyl selective functionality. The use of a waste product as a feedstock also gives the chitin based sorbent a net economic and energy gain due to offsetting the costs of disposing shellfish waste from the seafood industry and creating a market for crustacean shells.

Three key scientific challenges must be overcome in this effort: obtaining very high uranium selectivity, developing efficient recovery and recycle methods, and preparing chitinous materials that are stable in seawater for extended periods. We have approached them through three tasks: 1) demonstrating continuous extraction processing of chitin, 2) electrospinning chitin nanofibers from a solution of chitin in ionic liquids, and 3) developing the chemistry to modify the fiber surfaces. The key chemical and engineering variables of extraction efficiency, capacity, stripping, fiber cost, and durability must be understood to prove the advantage of a chitin-based sorbent over conventional sorbents.

Research and Development Progress:

Task 1: Extraction of chitin from seafood waste by microwave-assisted dissolution into IL

Our feedstock of shrimp shells was obtained from a recently build seafood waste drying/pulverizing facility in Bayou Le Batre, LA, which was established under the auspices of the Alabama Farmers Market Authority.[26] The facility accepts shellfish waste from local fishermen and processing plants. Shellfish waste is pressed to remove some protein and water and fed through a fluidized bed dryer to obtain the dried crustacean shells used as our starting material. We have measured the chitin content of shrimp shells obtained from this process to be 22.5% by the standard method.[27] Two ionic liquids, 1-ethyl-3-methylimidazolium acetate ([C_2mim][OAc]) and 1,3-diethylimidazolium acetate ([C_2C_2Im][OAc], were found to effectively dissolve PG chitin and shrimp shell using the microwave dissolution method reported by our group. Through the use of a standard domestic microwave we can process up to 18 g shrimp shell waste with 282 g ionic liquid and approximately 4 minutes of microwave heating.

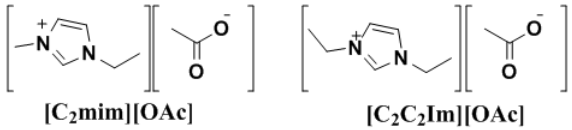

Figure 2 Structures of the ionic liquids used for the dissolution and extraction of chitin from shrimp shells

Scaling our efforts towards a continuous microwave dissolution process, we acquired and setup a high-throughput 2 kW continuous microwave cylindrical heating system from Industrial Microwave Systems, Inc. A trial run at the manufacturer's plant with 10 kg of diethylimidazolium acetate

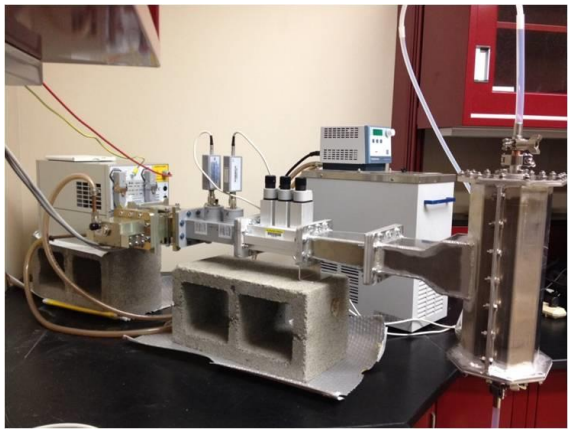

Figure 3 High-throughput microwave for batch and continuous microwave dissolution and extraction of chitin from shrimp shells.

([C_2C_2Im]OAc) indicated that the IL will absorb the microwaves efficiently (99.9%+) and can be run in a continuous fashion. The IL was fed into the unit at a rate of 1 gal/min and using only 23% of the microwave power, a temperature of 82 °C was reached in just 120 sec. This temperature would be sufficient to achieve the dissolution of waste shells, without degrading the IL. To ensure that the IL can be recycled and reused without any major loss, the trial also involved the recirculation of the IL for several cycles, and no obvious degradation was observed.

Using this setup, we were able to successfully extract chitin from up to 30 grams of shrimp shells into ionic liquids in several minutes. An external batch of shrimp shell and ionic liquid was cycled through the setup several times to dissolve the shrimp shells. This indicates that a batch process is viable for large scale extraction of chitin from shrimp shell waste in minimal time using a low energy microwave dissolution process. Adaptation to a continuous process is conceivable by continuously adding shrimp shell and IL to the feed while removing and filtering the IL solution. Continuous processing would utilize different parameters; therefore our goal is for the continuous extraction of chitin from shrimp shell waste. This is critical for the extraction of the raw chitin from waste shells and this microwave is capable of processing approximately 50 L/h of waste shell/IL solution. The continuous microwave system enables the liquid to be uniformly and volumetrically heated on a continuous flow basis, eliminating the problem of hot spots encountered with traditional surface–heating technologies. Since no one has yet used this equipment with ILs and biomass, we are continuing to investigate the appropriate safe conditions for continuous processing.

Task 2: Electrospinning of chitin nanofibers

The electrospinning of chitin into high surface area nanofibers or high porosity nanomaterials is perhaps one of the most exciting new possibilities made available by the dissolution of biomass in ionic liquid.[28,29,30] Electrospinning uses an electric field to pull micron and nano-sized fibers from a polymer solution. A solution containing the polymer is pushed through a charged spinneret where a high electric potential causes the drop of polymer solution to form a Taylor cone. Under the right conditions, a , viscous jet of polymer is then ejected towards a collecting electrode, deforming into a nanoscale-width fiber in the process.[31] The system balances polymer entanglement density, solution viscosity, and surface tension to prevent beads and create smooth, continuous fibers.[32] For solution in volatile solvents, the solvent then evaporates and concentrates the polymer solution which allows for the fibers to form on the electrode. However, the ionic liquids used here are non-volatile. Therefore, a coagulation bath is used for the precipitation of the chitin and the dissolution of the ionic liquid.

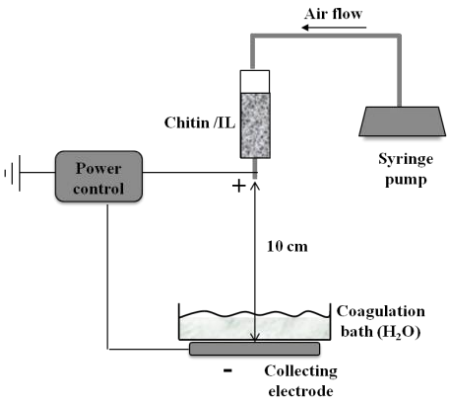

Figure 4 Schematic representation of electrospinning from IL solutions.

Our electrospinning apparatus, shown in Figure 4, consists of a software controlled high-voltage power supply connected to a needle (the spinneret) and an electrode under the coagulation bath (the collector). The needle is attached to a syringe through which the shrimp shell solution is delivered by compression of air pressure from a syringe pump. Water has been used as the coagulation solvent due to its ability to precipitate chitin from the IL During electrospinning, the syringe is loaded with the appropriate solution, the potential is applied, software-controlled, and the flow is controlled by the syringe pump.

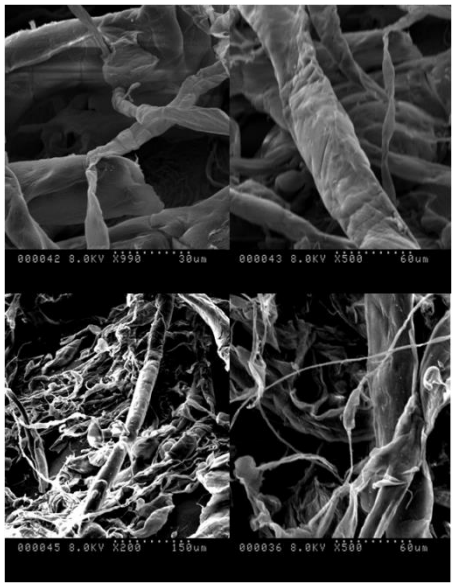

Figure 5 Electrospun nanofibers of PG-chitin from a solution of PG-chitin in $[C_2C_2Im][OAc]$.

The results of our electrospinning experiments with shrimp shell and PG chitin as well as our investigation of the effects of viscosity, concentration, and voltage on electrospinning are reported in "Electrospinning of Chitin Nanofibers Directly from an Ionic Liquid Extract of Shrimp Shells" *Green Chem.* **2013**, *15*, 601–607. Using our apparatus, we were able to electrospun chitin nanofibers from solutions of PG chitin and shrimp shell $C_2C_2Im][OAc]$ and $[C_2mim][OAc]$. This is the *first instance of electrospinning chitin from a high-molecular weight source of chitin*, due to the difficulty in finding an appropriate solvent that will dissolve the biopolymer. We also measured the viscosities of various chitin solutions in IL and determined the optimum viscosity range for electrospinning. Using IR spectroscopy, powder X-ray diffraction, and scanning electron microscopy, it it was determined that a 2 wt % shrimp shell loading in $[C_2mim][OAc]$ produces nanofibers of chitin with the best morphological properties. PG-chitin nanofibers are shown in Figure 5 and nanofibers spun from shrimp shell extract under optimized conditions are shown in Figure 6. .

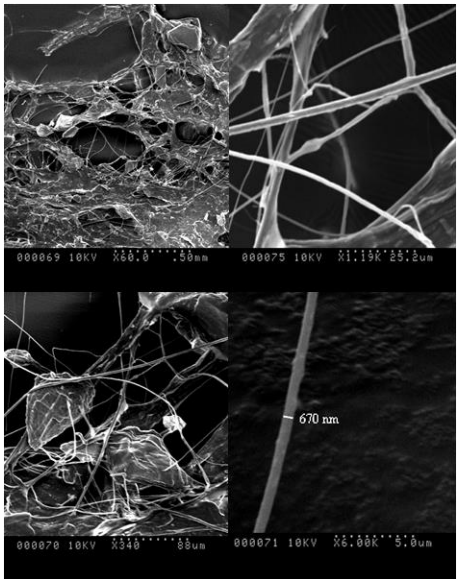

Figure 6 Electrospun nanofibers of chitin from a shrimp shell extract in $[C_2mim][OAc]$.

Task 3: Uranium-selective functionalization of chitin

We sought to investigate the mechanism for the selectivity of amidoxime for uranyl ions in sweater as well as develop methods for chemically modifying chitin with amidoxime groups. We first incorporated an amidoxime coordination site within a hydrophobic IL to directly explore the fundamental aspects of chemical modification as well as the coordination and separation of the uranyl cation. The results of this study are reported in *RSC Adv.* **2012**, *2*, 8526–8530. We prepared two hydrophobic ILs as shown in Figure 7 and, taking advantage of their hydrophobic properties, conducted aqueous extractions to show the selectivity of the ILs for UO_2^{2+}, Eu^{3+}, and Th^{4+}. We found the selectivity for the ILs as UO_2^{2+} > Th^{4+} > Eu^{3+} with separation factors (SF) of $SF_{(UO2/Th)} = 4.6$, $SF_{(UO2/Eu)} = 8.2$, and $SF_{(Th/Eu)} = 1.8$ for $[AO1mim][NTf_2]$ and 11.4, 480, and 42 for $[AO2mim][NTf_2]$. The extraction of the uranyl ion was also studied as a function of nitric acid concentration and sodium nitrate concentrations and indicated that with increasing acid concentration the distribution values decreased significantly, while a change in concentration of the nitrate anion proceeded differently for each IL. This suggested that there was a possible difference in the mechanism between the two similar ILs.

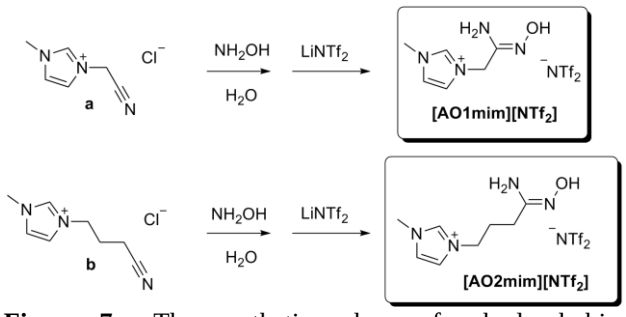

Figure 7 The synthetic scheme for hydrophobic, amidoxime-functionalized ionic liquids.

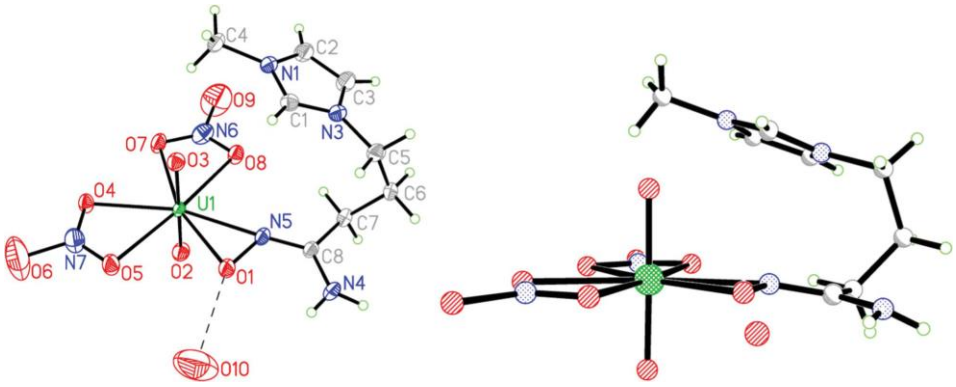

Figure 8 Two views of the hexagonal bipyramidal coordination geometry around uranium in $[UO_2(NO_3)_2$(1-(4-amidoximate)butyl)-3-methylimidazolium$]\cdot H_2O$ (50% probability ellipsoids).

Through reacting these ionic liquids with uranyl nitrate, we were able to isolate single crystals and determine the crystal structure of the complex shown in Figure 8. From this we were able to observe deprotonated amidoximate bonded to the uranyl center in an η^2 coordination mode, as reported by Hay and coworkers.[33] In total, this study verified our approach for grafting amidoxime functional groups onto an amine, showed us the selectivity enhancement of incorporating amidoxime functionality into the receiving phase, and produced evidence for the extraction mechanism of the amidoxime polymers that have been successfully employed in the extraction of uranium from seawater.

We adapted our method for appending the amidoxime moiety onto the imidazolium cation towards modifying the surface of chitin fibers pulled directly from a shrimp shell extract in ILs. The chitin fibers used here were micron-sized fibers pulled using dry-wet jet spinning. The fibers were surface-modified as shown by the scheme in Figure 9. Fibers were first treated with aqueous NaOH to deacetylate the surfaces of the fibers. The deacetylated amino groups were functionalized with nitrile groups which were then converted to amidoximes by reaction with hydroxylamine.

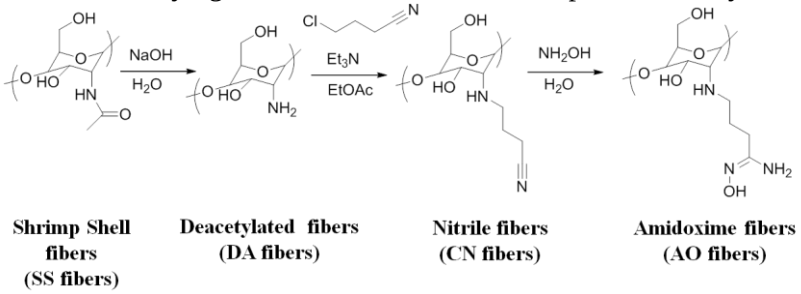

Figure 9 Synthetic scheme for the surface-modification of chitin fibers pulled from a shrimp shell extract in IL.

While IR spectroscopy and PXRD indicated that very little of the fiber had been changed by the treatment, extractions of $^{233}UO_2^{2+}$ at infinite dilution showed dramatic improvements in distribution values for the amidoxime functionalized and the deactylated fibers (shown in Figure 10). This indicated that only the surface of the fibers was modified. Furthermore, chitin fibers and deacetylated chitin (chitosan) prepared from IL extraction showed superior distribution values for UO_2^{2+} compared to commercial PG-chitin and chitosan. These results are currently being written up for publication.

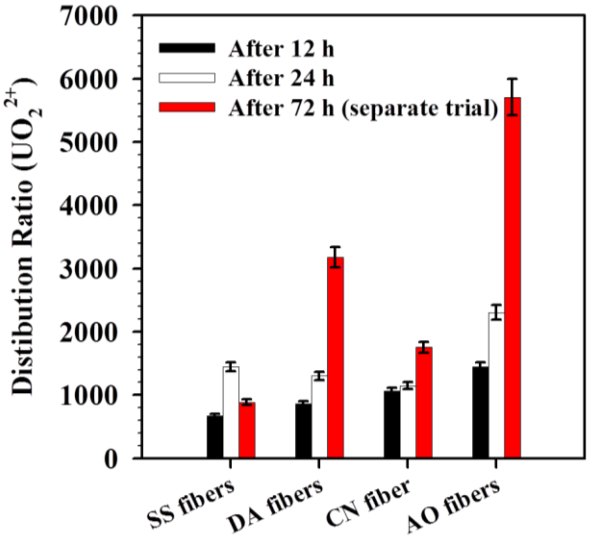

Figure 10 Distribution ratios of UO_2^{2+} for SS, DA, CN, and AO fibers from aqueous solutions.

Future Work:

Having demonstrated the core technologies behind the proposed adsorbent – electrospinning of chitin nanomaterials and uranium-selective functionalization of chitin – our future work will focus on controlling the physicochemical properties of the

renewable chitin based adsorbent and testing its performance.

- By exploiting the solubility of numerous biopolymers in ILs, we will **electrospin homogeneous blends of polymers** in order to control the physical properties of the adsorbent. Specific blends of interest include chitin-cellulose blends to adjust the strength and spinnability of the material and chitin-polydopamine blends for anti-biofouling.
- We will adjust the spinning parameters such as collection method and tip-to-electrode distance to **prepare different fiber architectures** (e.g. nonwoven mats *vs.* aligned fibers *vs.* flocs) and determine which have the best performance for uranium extraction.
- We will **further develop the surface modification chemistry** to control factors such as percentage of functionalized surface area and depth of functionalization into the fiber.
- We will test the performance of the newly developed materials in simulated and actual seawater conditions. Particular emphasis will be placed on **measuring the biodegradation of the adsorbent**. While long term stability is expected to be an issue, the biodegradability of chitin is ultimately an advantage given the large amounts of solid adsorbent that will need to be generated to efficiently extract uranium from seawater. Furthermore, chitin extracted *via* microwave dissolution is expected to be more stable than practical grade chitin due to its higher molecular weight. We will investigate the degradation of chitin-based adsorbents in the presence of chitinases, marine microbes, and in natural seawater.

Publications:

1. Barber, P. S.; Griggs, C. S.; Wallace, S.; Rogers, R. D. Surface Modification of Ionic Liquid Spun Chitin Fibers for the Extraction of Uranium from Seawater, *in preparation.*
2. Barber, P. S.; Shamshina, J. L.; Rogers, R. D. A ' Green ' Industrial Revolution : Using Chitin Towards Transformative Technologies. *Pure and Applied Chemistry* **2013**, *Accepted*.
3. Barber, P. S.; Griggs, C. S.; Bonner, J. R.; Rogers, R. D. Electrospinning of Chitin Nanofibers Directly from an Ionic Liquid Extract of Shrimp Shells. *Green Chem.* **2013**, *15*, 601–607.
4. Barber, P. S.; Kelley, S. P.; Rogers, R. D. Highly selective extraction of the uranyl ion with hydrophobic amidoxime-functionalized ionic liquids via η2 coordination. *RSC Adv.* **2012**, *2*, 8526–8530.

Presentations:

1. "Ionic liquids and strategic metals: Challenges and opportunities" Robin D. Rogers, the 244th American Chemical Society's National Meeting and Exposition (August 21, 2012) in Philadelphia, PA
2. "Extraction of uranium with regenerated chitin from the dissolution of shrimp shells in ionic liquid" Robin D. Rogers, Patrick S. Barber, Chris S. Griggs, Steven P. Kelley, and Gabriela Gurau. Presented before the 244th American Chemical Society's National Meeting and Exposition (August 20, 2012) in Philadelphia, PA
3. "Amidoxime functionalized materials for the selective extraction of the uranium" Patrick S. Barber, Steven P. Kelley, Chris S. Griggs, and Robin D. Rogers. Presented before the 244th American Chemical Society's National Meeting and Exposition (August 21, 2012) in Philadelphia, PA
4. "Electrospun chitin nanofibers for uranyl adsorbant materials" Chris S. Griggs, Patrick S. Barber, Steven P. Kelley, Gabriela Gurau, and Robin D. Rogers. Presented before the 244th American Chemical Society's National Meeting and Exposition (August 21, 2012) in Philadelphia, PA
5. Organization of "Uranium from seawater" session at 244th American Chemical Society's National Meeting and Exposition (August 19-23, 2012) in Philadelphia, PA
6. "Optimization and Evaluation of Uranium Sorptive Bio-materials" Christopher S. Griggs, Steven L. Larson, John H. Ballard, Patrick S. Barber, and Robin D. Rogers, October 24, 2011, The 17th Symposium on Separation Science and Technology, Gatlinburg, TN

7. "Design and Coordination of f-elements with Amidoxime-Functionalized Ionic Liquids" Patrick S. Barber, Steven P. Kelley, and Robin D. Rogers, October 24, 2011, The 17th Symposium on Separation Science and Technology, Gatlinburg, TN

Media:

Audio/Video:

1. "Advances in decades-old dream of mining seawater for uranium," (video) August 21, 2012, ACS Live, http://www.ustream.tv/recorded/24868811
2. Christopher Intagliata, "Nanofibers Extract Uranium from Seawater" (podcast)August 22, 2012, Scientific American Podcast
3. "Harvesting uranium from seawater" (video)The Chicago Tribune, http://www.chicagotribune.com/videogallery/71974432//Harvesting-uranium-from-seawater
4. "Shrimpers And Uranium" (radio) As it Happens with Carol Off and Jeff Douglas, The Wednesday Edition, August 22, 2012, http://www.cbc.ca/asithappens/episode/2012/08/22/the-wednesday-edition-41/

Articles:

1. "Uranium from seawater idea boosted with shrimp shells", August 22, 2012 Science & Environment, BBC, www.bbc.co.uk
2. "The sea is the key to uranium bounty" August 23, 2012, World Nuclear News, www.world-nuclear-news.org
3. *Adrian Bishop, "*Nuclear power from uranium in seawater gets closer" August 21, 2012, The Earth Times, www.earthtimes.org
4. Swagato Chakravorty, "Innovations in Uranium Mining, Extracting Uranium from Seawater" August 23, 2012, Energy and Capital, www.energyandcapital.com
5. Frances White, "Fueling nuclear power with seawater" August 21, 2012, R & D Magazine, www.rdmag.com
6. Mark Prigg, "Are oceans the future of nuclear power? Scientists move closer to extracting uranium from seawater" August 22, 2012, Daily Mail, www.dailymail.co.uk
7. John von Radowitz, "Sea uranium extraction 'close to economic reality" August 21, 2012 The Independent, www.independent.co.uk
8. Pete Sheehan, "Energy from seawater" August 22, 2012 Science and Technology, www.journal-news.net
9. Francie Diep, "Scientists could soon begin extracting nuclear fuel from seawater" August 22, 2012, The Christian Science Monitor, CSMonitor.com
10. "Uranium from seawater said attainable goal" August 21, 2012, United Press International, Inc., www.upi.com
11. "Oceans could be the future of nuclear power: scientists," August 21, 2012, Zany Science, The Hindustan Times, www.hindustantimes.com
12. "Mining' uranium from seawater moves a step closer," August 22, 2012, The Scotsman, www.Scotsman.com

References:

[1] G. Choppin, J. Rydberg and J.-O. Liljenzin, *Radiochemistry and Nuclear Chemistry*, 2nd Ed., Butterworth-Heinemann, Great Britain, 1995, p 107

[2] World Nuclear Organization. Supply of Uranium. http://www.world-nuclear.org/info/inf75.htm (accessed 01/01/11)

[3] H. J. Schenk, L. Astheimer, E. G. Witte, and K. Schwochau, *Separation Science and Technology*, 1982, **17**, 1293.

[4] L. Astheimer, H. J. Schenk, E. G. Witte, and K. Schwochau, *Separation Science and Technology*, 1983, **18**, 307–339.

[5] M. Tamada, Current Status of Technology for Collection of Uranium from Seawater, Japan Atomic Energy Agency, 2009.

[6] L. Rao, *Recent International R & D Activities in the Extraction of Uranium from Seawater; LBNL-4034E*, 2011.

[7] E. Schneider and D. Sachde, *Cost and Uncertainty Analysis of an Adsorbent Braid System for Uranium Recovery from Seawater*, 2011

[8] Bartlett, D. H.; Azam, F. *Science*, **2005**, *310*, 1775.

[9] Kumar, M. N. V. R. *React. Funct. Polym.* **2000**, *46*, 1.

[10] Sashiwa, H.; Shigemasa, Y. *Carbohydrate Polym.* **1999**, *39*, 127.

[11] Percot, A.; Viton, C.; Domard, A. *Biomacromol.* **2003**, *4*, 12.

[12] Hirano, S.; Nagao, N. *Agric. Biol. Chem.* **1988**, *52*, 2111.

[13] Austin, P. R. US patent 3892731, 1975.

[14] Tokura, S.; Nishi, N.; Noguchi, J. *Polym. J.*, **1979**, *11*, 781.

[15] Rutherford, F. A.; Austin, P. R. In Proceedings of the First International Conference on Chitin/Chitosan. Muzzarelli, R.A.A.; Pariser, E.R. Eds., MIT Sea Grant Report, MIT SG 78-7, 1978, 182.

[16] *ILs: Industrial Applications for Green Chemistry*; Rogers, R. D.; Seddon, K.R., Eds.; ACS Symposium Series 818, American Chemical Society: Washington, DC, 2002

[17] Swatloski, R. P.; Spear, S. K.; Holbrey, J. D.; Rogers, R. D. *J. Am. Chem. Soc.* **2002**, *124*, 4974.

[18] Fort, D. A.; Remsing, R. C.; Swatloski, R. P.; Moyna, P.; Moyna, G.; Rogers, R. D. *Green Chem.* **2007**, *9*, 63.

[19] Phillips, D. M.; Drummy, L. F.; Conrady, D. G.; Fox, D. M.; Naik, R. R.; Stone, M. O.; Trulove, P. C.; De Long, H. C.; Mantz, R. A. *J. Am. Chem. Soc.* **2004**, *126*, 14350.

[20] Pu, Y. *J. Wood Chem. Technol*. **2007**, *27*, 23.

[21] Xie, H.; Li, S.; Zhang, S. *Green Chem*. **2005**, *7*, 606.

[22] Xie, H.; Zhang, S.; Li, S. *Green Chem.*, **2006**, *8*, 630.

[23] Wu, Y.; Sasaki, T.; Irie, S.; Sakurai, K. *Polymer* **2008**, *49*, 2321.

[24] Qin, Y. ; Lu, X.; Sun N.; Rogers, R. D. *Green Chem.*, **2010**, *12*, 968.

[25] Sun, N.; Swatloski, R. P.; Maxim, M. L.; Rahman, M.; Harland, A. G.; Haque, A.; Spear, S. K.; Dalyand D. T.; Rogers, R. D. *J. Mater. Chem.* 2008, **18**, 283.

[26] Gulf Coast Agricultural and Seafood Coop Seafood By-Products Processing Facility, EDA Investment No. 04-01-06250. http://blog.al.com/live/2010/05/seafood_waste_recycling_plant.html (Accessed 06/04/10).

[27] Black, M. M.; Schwartz, H. M. *The Analyst* **1950**, *75*, 185.

[28] Meli, L.; Miao, J.; Dordick, J. S.; Linhardt, R. J. *Green Chem.* **2010**, *12*, 1883–1892.

[29] D. Li and Y. Xia, *Advanced Materials*, 2004, **16**, 1151–1170.

[30] J. D. Schiffman and C. L. Schauer, *Polymer Reviews*, 2008, **48**, 317–352.

[31] S. Fridrihk, J. Yu, M. Brenner, and G. Rutledge, *Phys. Rev. Lett.*, 2003, **90**, 144502.

[32] L. Meli, J. Miao, J. S. Dordick, and R. J. Linhardt, *Green Chem*. 2010, **12**, 1883-1892.

[33] Vukovic, S.; Watson, L. A.; Kang, S. O.; Custelcean, R.; Hay, B. P. *Inorg. Chem.* **2012**, *51*, 3855–9.

DOE-NEUP Project Report for DOE Review June 13, 2013

Project Title: Innovative Elution Processes for Recovering Uranium from Seawater

Principal Investigator: Chien M. Wai, Department of Chemistry, University of Idaho, Moscow, Idaho 83844

Introduction

Seawater contains about 3 ppb of uranium. With a total ocean volume of approximately 1.3×10^9 km^3, there is at least 4.5 billion tons of uranium in seawater which is about 1000 times the amount of uranium known to exist in terrestrial ores.[1] Developing efficient, economic, and environmentally sustainable techniques for sequestering uranium from seawater is an active research area currently supported by DOE. Screening studies conducted in 1980s with more than 200 functionalized adsorbents show that the sorbent materials with the amidoxime group $RC(NH_2)(NOH)$ were most effective for uranium adsorption from seawater.[2] Recent research efforts in Japan and in the USA are focused on using amidoxime-based adsorbents for sequestering uranium from seawater.[3] The amidoxime-based fiber can be prepared by a radiation-induced graft polymerization method which involves acrylonitrile grafting onto polyethylene fabrics and chemical conversion of the acrylonitrile to the amidoxime groups as shown in Figure 1. These types of sorbents show good mechanical strength and high capacity for uranium sorption from seawater. If this uranium sequestering technology could be made economically favorable and environmentally sustainable, our ocean would provide virtually an inexhaustible source of uranium for nuclear power production.

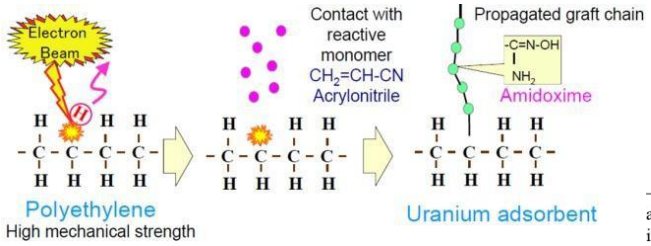

Adsorption of metals on amidoxime fiber from seawater

Metal	Amount adsorbed on amidoxime fiber[a]/μg g^{-1}	Concentration in seawater /μg g^{-1}
U	576	3.3
V	1800	1.5
Co	10.6	0.05
Ni	169	0.5
Fe	401	1.0
Mn	78.0	0.25
Cu	17.7	0.6
Zn	111	4
Ca	12700	4.22×10^5
Mg	13100	1.33×10^6

a. The analysis was carried out for amidoxime fiber, which had been immersed in seawater 6 km off Mutu-Sekine Hama for 30 days.

Figure1. Amidoxime-based sorbent prepared by radiation-induced graft polymerization and adsorption of uranium and other metals on the sorbent from marine experiments.

Uranium collected by the amidoxime-based sorbents is recovered typically by elution with an acid such as 1 M hydrochloric acid (HCl). After acid elution, the sorbent requires a KOH reconditioning process, which involves heating the sorbent in 2.5% KOH solution at 80^{o}C for 3 hrs, to regenerate the active functional groups for repeated use. A serious drawback of the acid elution process is deterioration of the sorbent material caused by acid hydrolysis making its reusability rather limited. This sorbent durability problem limits the economic competitiveness

of the current amidoxime-based sorbent collection system for sequestering uranium from seawater.[3] Another problem is the presence of transition metals including V, Fe, Ni, Zn, Mn, and Cu co-adsorbed with uranium on the sorbent in real seawater experiments, as shown in the table given in Figure 1.[4] For example the amount of the adsorbed vanadium is 3 times more than that of the uranium found in the sorbent in real seawater experiments. Removing the co-adsorbed transition metals is necessary for reuse of the sorbent. Therefore, developing innovative elution processes to improve the elution efficiency of U and other metals and to minimize loss of sorbent capacity are essential in order to make this uranium sequestering technology economically feasible for large-scale industrial applications.

This project has evaluated three different types of elution processes (acid, carbonate, and supercritical fluid) for recovering uranium from an amidoxime-based polymer sorbent prepared by Chris Janke of Oak Ridge Nation Lab (ORNL). The uranium adsorption experiments were performed using simulated seawater which contains Na^+ (10,118 ppm), Cl^- (15,573 ppm), and HCO_3^- (140 ppm) at pH 8.0 similar to the real seawater composition of major ionic species. The simulated seawater was spiked with 9 ppm of uranium $(UO_2)^{2+}$ for our adsorption experiments. Uranium is known to exist in seawater as $[UO_2(CO_3)_3]^{4-}$ which is a very stable uranyl species in aqueous carbonate solutions. It has been shown recently that a cyclic glutarimidedioxime structure (H_2A) formed in the sorbent during the conversion of acrylonitrile to the amidoxime groups (Figure 1) is responsible for sequestering uranium from seawater.[5] The uranium sequestering process may be illustrated by the following reaction

$$[UO_2(CO_3)_3]^{4-} + 2\ H_2A \rightarrow [UO_2(HA)A]^- + 3HCO_3^- \qquad (1)$$

where H_2A is the cyclic glutarimidedioxime structure shown in the figure below. The results of the elution processes investigated by this project are described in the following section.

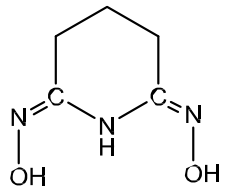

Results and Discussion

1. Hydrochloric Acid Elution of Uranium

Hydrochloric acid (HCl) is quite effective for removing uranium adsorbed on amidoxime-based polymer sorbents in our simulated seawater experiments. Figure 2 shows the rates of uranium removal from the sorbent with different concentrations of HCl solutions at room temperature. According to our experiments, a 0.5 M HCl solution is sufficient for removing uranium quantitatively from the sorbent in 5 minutes.

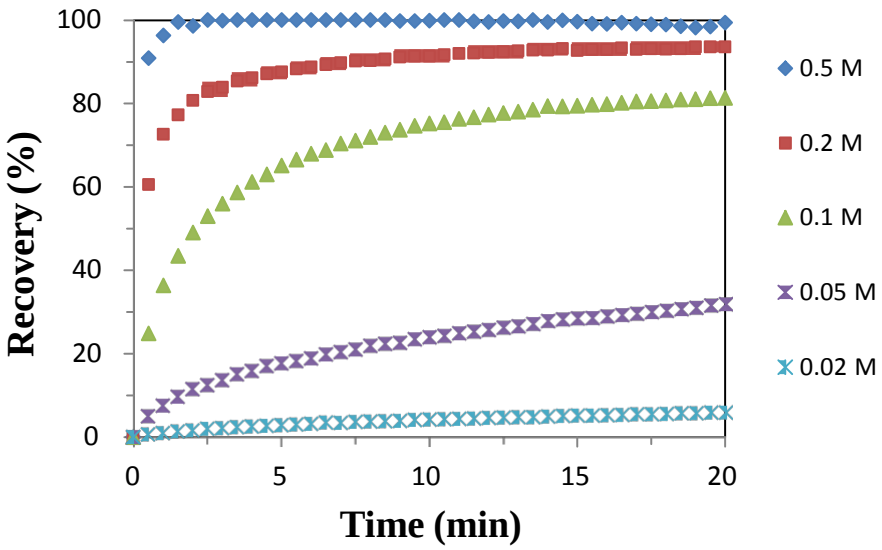

Figure 2. Rate of HCl elution of uranium from amidoxime-based polymer fiber

However, a major problem of HCl leaching of uranium from the sorbent is the damage caused by acid hydrolysis of the amidoxime groups attached to the sorbent. After acid leaching, the amidoxime groups can be regenerated using a KOH reconditioning process (2.5% KOH solution at 80^{o}C for 3 hrs) but the efficiency of the regenerated sorbent for uranium adsorption is decreased by 15-20% in our simulated seawater experiments. Another problem is that vanadium cannot be removed from the sorbent by HCl with less than 3 M concentration. At least 6 M HCl at 50-60^{o}C is required to remove most of the adsorbed vanadium from the sorbent. Leaching at such a high concentration of HCl the sorbent is seriously damaged making it practically useless for re-sequestering uranium. Other transition metals co-adsorbed on the sorbent except iron can be eluded with dilute HCl solutions (0.2-0.5 M).

2. Sodium Carbonate Elution of Uranium

One early study reported that sodium carbonate (Na_2CO_3) is effective for removing uranium from amidoxime-based sorbent because $[UO_2(CO_3)_3]^{4-}$ is a very stable species in aqueous carbonate solutions.[5] The carbonate elution is like a reverse reaction of the uranium adsorption process illustrated in Equation 1. Our results indicate that using 1 M Na_2CO_3 as an eluent, about 70% of the uranium adsorbed on the amidoxime-based polymer fiber in simulated seawater experiments can be eluted at room temperature (Figure 3). After the carbonate leaching, the sorbent can be reused (after rinsing in water) without losing its uranium loading capacity.

One significant discovery made recently in our lab is that when a small amount of hydrogen peroxide (e.g. O.1 M H_2O_2) is added to the carbonate leaching system, the efficiency of uranium elution becomes nearly quantitative (Figure 3). The synergistic elution of uranium by carbonate and H_2O_2 is likely due to formation of an extremely stable uranyl-peroxo-carbonato complex. A recent report actually shows that H_2O_2 can replace one carbonate from $[UO_2(CO_3)_3]^{4-}$ leading to the formation of $[UO_2(O\text{-}O)(CO_3)_2]^{4-}$ complex with an apparent formation constant $10^{4.7}$ greater

than the uranyl tricarbonate species.[6] The carbonate-hydrogen peroxide elution process appears attractive for recovering uranium from the amidoxime-based polymer sorbents. The elution process is simple, rapid and selective for uranium. The sorbent after carbonate leaching does not require any elaborate reconditioning process for its reuse. Rinsing off carbonate with distilled water several times is sufficient to regenerate the sorbent for re-sequestering uranium from simulated seawater. The FTIR spectra shown in Figure 3 indicate that after the carbonate elution, the vibrational features of the sorbent are similar to the original sorbent.

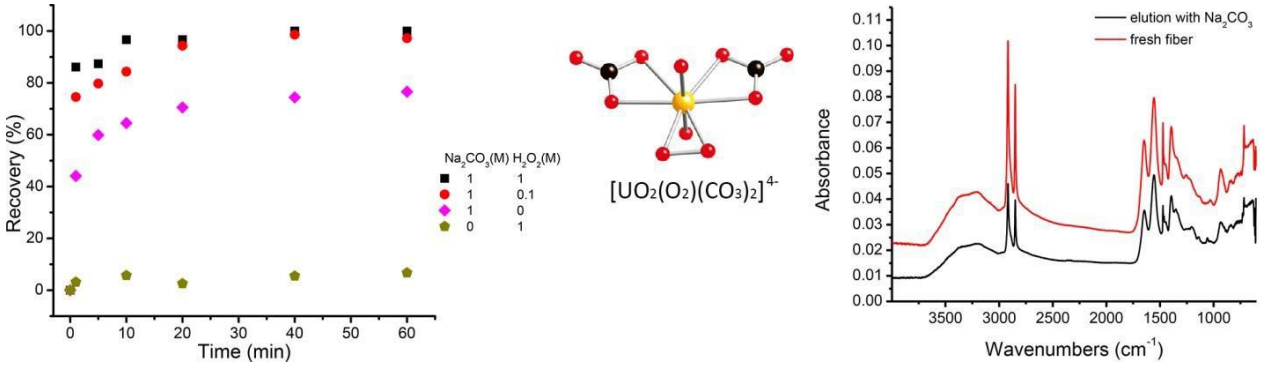

Figure 3. Uranium elution from amidoxime-based fiber using $NaCO_3$ and H_2O_2, the structure of uranyl-peroxo-carbonato complex, and FTIR spectra of the fresh sorbent and the sorbent after carbonate elution.

One unknown factor of this Na_2CO_3-H_2O_2 elution technique is the possible sorbent damage caused by hydrogen peroxide which should depend on the concentration of the peroxide used. Using 1 M sodium carbonate and 0.1 M hydrogen peroxide, the decrease in uranium loading capacity of the recycled sorbent is about 3% in our simulated seawater experiment involving only uranium. The effect of other transition metals on deterioration of the sorbent in the presence of H_2O_2 is unknown. A systematic study of repeated uranium loading-elution experiments using real seawater by varying relative amounts of Na_2CO_3 and H_2O_2 and at different temperatures should enable us to find an optimal condition to achieve a high efficiency of uranium leaching with minimal sorbent damage. Research in this direction is currently in progress.

3. Supercritical Fluid Elution of Uranium

Using supercritical fluid carbon dioxide (sc-CO_2) as a solvent for extraction of uranium from solid materials is a well-established technique in the literature. The advantages of sc-CO_2 extraction compared with conventional solvent extraction processes include its ability to penetrate into solid matrix and its environmental sustainability. Using sc-CO_2 to recover uranium from one type of nuclear waste is already being tested on an industrial scale by AREVA.[7] In this case, a CO_2-soluble extractant such as $TBP(HNO_3)_{1.8}(H_2O)_{0.6}$ is used to convert UO_2 into $UO_2(NO_3)_2(TBP)_2$ which is soluble in CO_2 and thus can be carried out of the extraction system by the fluid phase. Reduction of pressure of the exit fluid would convert the sc-CO_2 to CO_2 gas causing precipitation of the solute from the gas. The CO_2 gas is then recycled and pressurized

again for repeated use. In nuclear waste applications, damage to solid matrix after the sc-CO_2 extraction is not a major concern.

Our supercritical fluid extraction experiments indicate that uranium adsorbed on the amidoxime-based polymer sorbent can be removed by TBP$(HNO_3)_{1.8}(H_2O)_{0.6}$ but the damage to the sorbent is severe, similar to that observed from the high concentration HCl leaching because the extractant contains HNO_3. It is known that uranyl and other metal species present in water and in soil can be extracted by sc-CO_2 with CO_2-soluble ligands which often are phosphorus or fluorine-containing reagents. This extraction approach is based on a ligand exchange mechanism, i.e. a stronger CO_2-soluble ligand is utilized to replace a weaker ligand coordinated with the metal species in water of in solid materials. Supercritical CO_2 elution of uranium from amidoxime sorbent is difficult because uranyl-amidoxime complex is very stable. We have studied one fluorine-containing ligand, hexafluoroacetylaceton (HFA), and one phosphorus-containing ligand, di(2-ethylhexyl)phosphoric acid (D2EHPA), for sc-CO_2 extraction of uranium loaded on the amidoxime-based sorbent in simulated seawater. Both reagents are known to extract uranyl ions from water effectively in solvent extraction and in sc-CO_2 extraction experiments. In the system with uranyl bonded to amidoxime sorbent, our sc-CO_2 extraction experiments with HFA or with D2EHPA result in partial extraction (~60-70%) of uranium from the sorbent at 40^{o}C and 200 atm. Apparently, a stronger CO_2-soluble ligand capable of competing with amidoxime is needed in order to achieve better uranium extraction efficiency from the sorbent in sc-CO_2. We are currently testing other ligands and combination of ligands with the hope of achieving better extraction efficiencies for recovering uranium from the sorbent in sc-CO_2. Another approach under investigation is to add a small amount of a dilute HCl solution (e.g. 0.1 M) to our sc-CO_2 extraction system to facilitate transfer of uranium from the sorbent to the sc-CO_2 phase. These sc-CO_2 extraction experiments are currently in progress.

4. Elution of Vanadium

There is very little information in the literature regarding elution of vanadium from the amidoxime-based sorbents. The high concentrations of vanadium (3 times more than uranium) found in the real seawater experiments suggest that vanadium is competing with uranium for adsorption to the amidoxime-based sorbent. As described in the HCl leaching results, to remove vanadium from the sorbent would require very high concentrations of the acid which would result in severe damage to the sorbent material. We have tested over 25 different reagents for elution of vanadium from the sorbent in aqueous solutions. About a quarter of them including hydrogen peroxide, oxalic acid, catechol, 4,5-dihydroxy-1,3-benzenedisulfonic acid, mercaptosuccinic acid, and nitrilotris(methylene)triphosphonic acid show positive results. Oxalic acid appears to be the most effective eluding agent for vanadium from the sorbent. Using 1 M oxalic acid, about 78% of the adsorbed vanadium can be removed from the sorbent at room temperature in about one hour. Systematic adsorption and elution experiments of vanadium using a combination of different chelating agents are currently in progress.

Conclusion

Based on the results obtained so far, we think to achieve the dual objectives of complete recovery of uranium and effective reuse of the amidoxime-based sorbent, a combination of several elution processes may be necessary. The carbonate-H_2O_2 elution method for selective removal of uranium from the sorbent appears promising. The co-adsorbed transition metals except iron and vanadium may be removed from the sorbent by a dilute HCl leaching. To remove vanadium without causing damage to the sorbent is a challenging problem. Research in supercritical fluid elution including development of effective uranyl complexing agents and utilizing dilute acid-supercritical CO_2 mixed leaching technique may lead to new approaches to replace or to supplement traditional solvent-based elution processes. In summary, further research is needed to achieve the overall goal of recovering uranium without sacrificing durability of the sorbent.

References

1. Davies, R. V.; Kennedy, J.; Hill, K. M.; Mcilroy, R. W.; Spence, R. "Extraction of uranium from seawater", *Nature*, **1964**, *203*, 1110-1115.
2. Schenk, H. J.; Astheimer, L.; Witte, E. G.; Schwochau, K. "Development of sorbers for the recovery of uranium from seawater. 1. Assessment of key parameters and screening studies of sorber materials", *Sep. Sci. Technol*. **1982**, *17*, 1293-1308
3. Rao, L. "Recent international R&D activities in the extraction of uranium from seawater", Lawrence Berkeley National Lab Report LBNL-4034E, March 15, 2010.
4. Suzuki, T.; Saito, K.; Sugo, T.; Ogura, H.; Oguma, K. "Fractional elution and determination of uranium and vanadium adsorbed on amidoxime fiber from seawater", *Anal. Sci*. **2000**, *16*, 429-432; Das, S.; Pandey, A. K.; Athawale, A.; Kumar, V.; Bhardwaj, Y.; Sabharwal, S.; Manchanda, V. K. "Chemical aspects of uranium recovery from seawater by amidoximated electron-beam-grafted polypropylene membranes", *Desalination* **2008**, *232*, 243-253.
5. Tian, G. X.; Teat, S. J.; Zhang, Z. Y.; Rao, L. F. "Sequestering uranium from seawater: binding strength and modes of uranyl complexes with glutarimidedioxime", *Dalton Transactions* **2012,** *41*, 11579-11586.
6. Goff, G.S.; Brodnax, L.F.; Cisneros, M.C.; Peper, S.M.; Field, S.E.; Scott, B.L.; Runde, W.H. "First identification and thermodynamic characterization of the ternary U(VI) species, $UO_2(O_2)(CO_3)_2^{4-}$, in UO_2-H_2O_2-K_2CO_3 solutions", *Inorg. Chem*. **2008**, *47*, 1984-1900
7. Smith, T.; Thomas, J. "Radioactive waste not wasted with new green chemistry technology", *Radwaste Solutions, September/October Issue*, **2008**, p. 32-35.